Integrated Ocean Drilling Program
Expedition 320 Preliminary Report

Pacific Equatorial Age Transect

5 March–4 May 2009

Heiko Pälike, Hiroshi Nishi, Mitch Lyle, Isabella Raffi,
Adam Klaus, Kusali Gamage,
and the Expedition 320/321 Scientists

Disclaimer

July 2009

Expedition 320 participants

Expedition 320 scientists

Heiko Pälike
Co-Chief Scientist
School of Ocean and Earth Science
National Oceanography Centre, Southampton
European Way
Southampton SO14 3ZH
United Kingdom
heiko@noc.soton.ac.uk

Hiroshi Nishi
Co-Chief Scientist
Department of Natural History Sciences
Hokkaido University
Kita-10, Nishi-8, Kita-ku
Sapporo 060-0810
Japan
hnishi@mail.sci.hokudai.ac.jp

Adam Klaus
Expedition Project Manager/Staff Scientist
Integrated Ocean Drilling Program
Texas A&M University
1000 Discovery Drive
College Station TX 77845-9547
USA
aklaus@iodp.tamu.edu

Helen Evans
Logging Staff Scientist
Borehole Research Group
Lamont-Doherty Earth Observatory
   of Columbia University
PO Box 1000, 61 Route 9W
Palisades NY 10964
USA
helen@ldeo.columbia.edu

Trevor Williams
Logging Staff Scientist
Borehole Research Group
Lamont-Doherty Earth Observatory
   of Columbia University
PO Box 1000, 61 Route 9W
Palisades NY 10964
USA
trevor@ldeo.columbia.edu

Gary D. Acton
Paleomagnetist
Department of Geology
University of California, Davis
One Shields Avenue
Davis CA 95616
USA
gdacton@ucdavis.edu

Paul Bown
Paleontologist (nannofossils)
Earth Sciences
University College London
Gower Street
London WC1E 6BT
United Kingdom
p.bown@ucl.ac.uk

Margaret (Peggy) Delaney
Inorganic Geochemist
Ocean Sciences
University of California, Santa Cruz
1156 High Street
Santa Cruz CA 95064
USA
delaney@ucsc.edu

Tom Dunkley Jones
Paleontologist (nannofossils)
Earth Sciences
University College London
Gower Street
London WC1E 6BT
United Kingdom
tom.dunkleyjones@ucl.ac.uk

Kirsty Edgar
Paleontologist (planktonic foraminifers)
School of Ocean and Earth Science
National Oceanography Centre, Southampton
European Way
Southampton SO14 3ZH
United Kingdom
kme@noc.soton.ac.uk

Peter Fitch
Physical Properties/Downhole Tools
  Specialist
Department of Geology
University of Leicester
University Road
Leicester LE1 7RH
United Kingdom
pjf5@le.ac.uk

Nikolaus Gussone
Inorganic Geochemist
Institut für Mineralogie
Westfälische Wilhelms-Universität Münster
Corrensstrasse 24
48149 Muenster
Germany
nikolaus.gussone@uni-muenster.de

Jens Herrle
Sedimentologist
Institute of Geosciences
Goethe University Frankfurt
Altenhoeferallee 1
60438 Frankfurt
Germany
jens.herrle@em.uni-frankfurt.de

Kiseong Hyeong
Sedimentologist
Deep Sea Resources Research Center
Korea Ocean Research and Development
  Institute
ANSAN PO Box 29
Seoul 425-600
Korea
kshyeong@kordi.re.kr

Shin-ichi Kamikuri
Paleontologist (radiolarians)
Graduate School of Science
Hokkaido University
Kita-10, Nishi-8, Kita-ku
Sapporo 060-0810
Japan
kamikuri@geol.tsukuba.ac.jp

Junichiro Kuroda
Sedimentologist
Institute for Frontier Research on Earth
  Evolution (IFREE)
Japan Agency for Marine-Earth Science and
  Technology (JAMSTEC)
2-15 Natsushima-cho
Yokosuka 237-0061
Japan
kurodaj@jamstec.go.jp

Lizette Leon-Rodriguez
Paleontologist (planktonic foraminifers)
Department of Earth Science
Rice University
6100 Main Street, MS-126
Houston TX 77005
USA
lizette@rice.edu

Theodore Moore Jr.
Paleontologist (radiolarians)
Department of Geological Sciences
University of Michigan
1100 North University
Ann Arbor MI 48109-1005
USA
ted.moore@umich.edu

Brandon Murphy
Sedimentologist
Earth and Planetary Sciences
University of California, Santa Cruz
1156 High Street
Santa Cruz CA 95064
USA
bmurphy@es.ucsc.edu

Hideto Nakamura
Sedimentologist
Department of Natural History Sciences
Hokkaido University
Kita-10, Nishi-8, Kita-ku
Sapporo 060-0810
Japan
hideton@mail.sci.hokudai.ac.jp

Christian Ohneiser
Paleomagnetist
Geology Department
University of Otago
Leith Street Central
Dunedin
New Zealand
christian.ohneiser@otago.ac.nz

Carl Richter
Stratigraphic Correlator
Department of Geology and Energy Institute
University of Louisiana
PO Box 44530
Lafayette LA 70504-0002
USA
richter@louisiana.edu

Rebecca Robinson
Sedimentologist
Graduate School of Oceanography
University of Rhode Island
South Ferry Road
Narragansett RI 02882
USA
rebeccar@gso.uri.edu

Ken Sawada
Organic Geochemist
Department of Natural History Sciences
Hokkaido University
Kita-10, Nishi-8, Kita-ku
Sapporo 060-0810
Japan
sawadak@mail.sci.hokudai.ac.jp

Howie Scher
Physical Properties/Downhole Tools
  Specialist
Department of Geological Sciences
University of South Carolina
701 Sumter Street, EWS 617
Columbia SC 29208
USA
hscher@geol.sc.edu

Hiroyuki Takata
Paleontologist (benthic foraminifers)
Research Center for Coastal Lagoon
  Environments
Shimane University
Nishikawatsu 1060
Matsue 690-8504
Japan
yuu@soc.shimane-u.ac.jp

Thomas Westerhold
Stratigraphic Correlator
Center for marine Environmental Sciences
  (MARUM)
University of Bremen
PO Box 330440
28334 Bremen
Germany
tho@uni-bremen.de

Paul A. Wilson
Sedimentologist
School of Ocean and Earth Science
National Oceanography Centre, Southampton
European Way
Southampton SO14 3ZH
United Kingdom
paw1@noc.soton.ac.uk

Yuhji Yamamoto
Paleomagnetist
Marine and Core Research Center
Kochi University
B200 Monobe
Nankoku-City
Kochi 783-8502
Japan
y.yamamoto@kochi-u.ac.jp

Shipboard personnel and technical representatives

Ron Grout
Operations Superintendent

Roy Davis
Laboratory Officer

Tim Bronk
Assistant Laboratory Officer

Lisa Crowder
Assistant Laboratory Officer

Gerald Bode
Curator

William Crawford
Imaging Specialist

Kelly VonDrehle
Publications Specialist

Grant Banta
Marine Computer Specialist

Michael Hodge
Marine Computer Specialist

Randy Gjesvold
Marine Instrumentation Specialist

Alwyn Burger
Marine Instrumentation Specialist

Chris Bennight
Chemistry Laboratory

Yulia Vasilyeva
Chemistry Laboratory

Sarah-Jane Jackett
Core Laboratory

Kazushi Kuroki
Downhole Tools/Thin Section Laboratory

Trevor Cobine
Paleomagnetism Laboratory

Thomas Gorgas
Physical Properties Laboratory

Kristin Hillis
Underway Geophysics Laboratory

Eric Jackson
X-ray/Microbiology Laboratory

Dwight Hornbacher
Applications Developer

Stephanie Zeliadt
Applications Developer

Don Sims Jr.
Database

Leslie Peart
Education/Outreach

Dean Ferrell
Drilling Engineer

Clayton Furman
Schlumberger Logging Engineer

Expedition 321 participants

Expedition 321 scientists

Mitchell W. Lyle
Co-Chief Scientist
Department of Oceanography
Texas A&M University
TAMU 3146
College Station TX 77840-3146
USA
mlyle@ocean.tamu.edu

Isabella Raffi
Co-Chief Scientist
Dipartimento di Geotecnologie per l'Ambi-
    ente e il Territorio
DiGAT—CeRS Geo
Universitá "G. D'Annunzio"
Campus Universitario
via dei Vestini 31
66013 Chieti Scalo
Italy
raffi@unich.it

Kusali Gamage
Expedition Project Manager/Staff Scientist
Integrated Ocean Drilling Program
Texas A&M University
1000 Discovery Drive
College Station TX 77845-9547
USA
gamage@iodp.tamu.edu

Alberto Malinverno
Logging Staff Scientist
Borehole Research Group
Lamont-Doherty Earth Observatory
    of Columbia University
PO Box 1000, 61 Route 9W
Palisades NY 10964
USA
alberto@ldeo.columbia.edu

Louise Anderson
Logging Staff Scientist
Department of Geology
University of Leicester
Leicester LE1 7RH
United Kingdom
lma9@le.ac.uk

Jan Backman
Paleontologist (nannofossils)
Department of Geology and Geochemistry
Stockholm University
SE-10691 Stockholm
Sweden
backman@geo.su.se

Catherine Beltran
Sedimentologist
Laboratoire Biominéralisations et
    Paléoenvironnements (UPMC)
Université Pierre et Marie Curie
Case 116—4 Place Jussieu
75252 Paris
France
catherine.beltran@upmc.fr

William Busch
**Physical Properties/Downhole Tools
    Specialist**
Earth and Environmental Sciences
University of New Orleans
2000 Lakeshore Drive
New Orleans LA 70148
USA
wbusch@uno.edu

James Channell
Paleomagnetist
Department of Geological Sciences
University of Florida
241 Williamson Hall
Gainesville FL 32611-2120
USA
jetc@geology.ufl.edu

Pawan Dewangan
**Physical Properties/Downhole Tools
    Specialist**
National Institute of Oceanography
Dona Paula
Goa 403 004
India
pdewangan@nio.org

Hitoshi Hasegawa
Sedimentologist
Earth and Planetary Science
University of Tokyo
7-3-1 Hongo
Bunkyo-ku
Tokyo 113-0033
Japan
hase@eps.s.u-tokyo.ac.jp

Edmund Hathorne
Inorganic Geochemist
MARUM-Centre for Marine Environmental
    Sciences
University of Bremen
Leobener Strasse
D-28359 Bremen
Germany
ehathorne@marum.de

Hiroki Hayashi
Paleontologist (planktonic foraminifers)
Interdisciplinary Faculty of Science and
    Engineering
Shimane University
1060 Nishikawatsucho
Matsue City
Shimane 690-8504
Japan
hayashi@riko.shimane-u.ac.jp

Ann Holbourn
Paleontologist (benthic foraminifers)
Institut für Geowissenschaften
Christian-Albrechts-Universität zu Kiel
Olhausenstrasse 40
24098 Kiel
Germany
ah@gpi.uni-kiel.de

Steven Hovan
Sedimentologist
Department of Geoscience
Indiana University of Pennsylvania
114 Walsh Hall
Indiana PA 15705
USA
hovan@iup.edu

Koichi Iijima
Physical Properties/Downhole Tools
    Specialist
Institute of Biogeosciences
Japan Agency for Marine-Earth Science and
    Technology
2-15 Natsushima-cho
Yokosuka 237-0061
Japan
kiijima@jamstec.go.jp

Takashi Ito
Sedimentologist
Faculty of Education
Ibaraki University
2-1-1 Bunkyo
Mito
Ibaraki 310-8512
Japan
tito@mx.ibaraki.ac.jp

Katsunori Kimoto
Inorganic Geochemist
Institute of Observational Research for Global
    Change (IORGC)
Japan Agency for Marine-Earth Science and
    Technology
2-15 Natsushima-Cho
Yokosuka 237-0061
Japan
kimopy@jamstec.go.jp

Daniel Murphy
Sedimentologist
Department of Oceanography
Texas A&M University
MS 3146
College Station TX 77845
USA
dmurphy@ocean.tamu.edu

Kaoru Ogane
Paleontologist (radiolarians)
Institute of Geology and Paleontology
Tohoku University
Aoba 6-4
Aramaki, Aoba-ku
Sendai City 980-8578
Japan
ogane@mtc.biglobe.ne.jp

Oscar Romero
Paleontologist (diatoms)
Instituto Andaluz de Ciencias de la Tierra
Universidad de Granada
Campus Fuentenueva
18002 Granada
Spain
oromero@ugr.es

Leah Schneider
Paleontologist (Nannofossils)
Department of Geosciences
Pennsylvania State University
509 Deike Building
University Park PA 16802
USA
lschneid@geosc.psu.edu

Appy Sluijs
Sedimentologist
Palaeoecology, Institute of Environmental
  Biology
Utrecht University
Laboratory of Palaeobotany and Palynology
Budapestlaan 4
3584CD Utrecht
The Netherlands
a.sluijs@uu.nl

Jun Tian
Stratigraphic Correlator
Laboratory of Marine Geology
Tongji University
Siping Road 1239
Shanghai 200092
PR China
tianjun@mail.tongji.edu.cn

Akira Tsujimoto
Sedimentologist
Department of Geosciences
Osaka City University
3-3-138 Sugimoto
Sumiyoshi-ku
Osaka 558-8585
Japan
tujimoto@sci.osaka-cu.ac.jp

Bridget Wade
Paleontologist (planktonic foraminifers)
Department of Geology and Geophysics
Texas A&M University
College Station TX 77843
USA
wade@geo.tamu.edu

Roy Wilkens
Stratigraphic Correlator
Hawaii Institute of Geophysics and
  Planetology
University of Hawaii at Manoa
1680 East West Road
Honolulu HI 96822
USA
rwilkens@hawaii.edu

Shinya Yamamoto
Organic Geochemist
Institute of Low Temperature Science
Hokkaido University
N19W8, Kita-Ku
Sapporo 060-0819
Japan
s.yamamoto@pop.lowtem.hokudai.ac.jp

Toshitsugu Yamazaki
Paleomagnetist
Geological Survey of Japan, AIST
1-1-1 Higashi, Tsukuba
Ibaraki 305-8567
Japan
toshi-yamazaki@aist.go.jp

Shipboard personnel and technical representatives

Heather Barnes
Assistant Laboratory Officer

John Beck
Imaging Specialist

Lisa Brandt
Chemistry Laboratory

Chad Broyles
Curator

Etienne Claassen
Marine Instrumentation Specialist

David Fackler
Applications Developer

Kazuho Fujine
Chemistry Laboratory

Gus Gustafson
Downhole Tools/Thin Section Laboratory

Margaret Hastedt
Paleomagnetism Laboratory

Maarten in 't Hout
Videographer

Jurie Kotze
Marine Instrumentation Specialist

Zenon Mateo
Core Laboratory

Mike Meiring
Engineer

Erik Moortgat
Underway Geophysics Laboratory

Matt Nobles
Marine Computer Specialist

Bob Olivas
X-ray/Microbiology Laboratory

Debbie Partain
Publications Specialist

Chieh Peng
Laboratory Officer

Steve Prinz
Assistant Laboratory Officer

Michael Storms
Operations Superintendent

Kerry Swain
Logging Engineer

Andrew Trefethen
Marine Computer Specialist

Maxim Vasilyev
Petrophysics Laboratory

Hai (James) Zhao
Applications Developer

Abstract

Integrated Ocean Drilling Program Expedition 320/321, "Pacific Equatorial Age Transect" (Sites U1331–U1338), was designed to recover a continuous Cenozoic record of the paleoequatorial Pacific by coring above the paleoposition of the Equator at successive crustal ages on the Pacific plate. These sediments record the evolution of the paleoequatorial climate system throughout the Cenozoic. As we gained more information about the past movement of plates and when in Earth's history "critical" climate events took place, it became possible to drill an age transect ("flow line") along the position of the paleoequator in the Pacific, targeting important time slices where the sedimentary archive allows us to reconstruct past climatic and tectonic conditions. The Pacific Equatorial Age Transect (PEAT) program cored eight sites from the sediment surface to at or near basement, with basalt aged between 53 and 16 Ma, covering the time period following maximum Cenozoic warmth, through initial major glaciations, to today. The PEAT program allows the reconstruction of extreme changes of the calcium carbonate compensation depth (CCD) across major geological boundaries during the last 53 m.y. A very shallow CCD during most of the Paleogene makes it difficult to obtain well-preserved carbonate sediments during these stratigraphic intervals, but we recovered a unique sedimentary biogenic sediment archive for time periods just after the Paleocene/Eocene boundary event, the Eocene cooling, the Eocene–Oligocene transition, the "one cold pole" Oligocene, the Oligocene–Miocene transition, and the middle Miocene cooling. Together with older Deep Sea Drilling Project and Ocean Drilling Program drilling in the equatorial Pacific, we can also delineate the position of the paleoequator and variations in sediment thickness from ~150°W to 110°W longitude.

Scientific objectives, introduction, and background

Scientific objectives

The Pacific Equatorial Age Transect (PEAT) program (Fig. F1) was designed to achieve an age transect along the paleoequatorial Pacific spanning early Eocene through middle Miocene crustal basement ages, with Paleocene/Eocene and late Miocene to recent intervals being covered by previous Ocean Drilling Program (ODP) Legs 138 and 199 (Pisias, Mayer, Janecek, Palmer-Julson, and van Andel, 1995; Lyle, Wilson, Janecek, et al., 2002). Drill sites target specific time slices of interest (Fig. F2) at locations that provide optimum preservation of calcareous sediments (Figs. F1, F3, F4, F5, F6, F7). The

overall aim was to obtain a continuous well-preserved sediment section that addresses the following primary scientific objectives:

1. To detail the nature and changes of the CCD over the Cenozoic in the paleo-equatorial Pacific;

2. To determine the evolution of paleoproductivity of the equatorial Pacific over the Cenozoic;

3. To validate and extend the astronomical calibration of the geological timescale for the Cenozoic, using orbitally forced variations in sediment composition known to occur in the equatorial Pacific, and to provide a fully integrated and astronomically calibrated bio-, chemo-, and magnetostratigraphy at the Equator;

4. To determine temperature (sea surface and bottom water), nutrient profiles, and upper water column gradients;

5. To better constrain Pacific plate tectonic motion and better locate the Cenozoic equatorial region in plate reconstructions; and

6. To make use of the high level of correlation between tropical sedimentary sections and existing seismic stratigraphy to develop a more complete model of equatorial circulation and sedimentation.

Additional objectives include:

7. To provide information about rapid biological evolution and turnover rates during times of climatic stress;

8. To improve our knowledge of the reorganization of water masses as a function of depth and time, as our strategy also implies a paleodepth transect (Fig. **F3**);

9. To develop a limited north–south transect across the paleoequator, caused by the northward offset of the proposed sites by Pacific plate motion, providing additional information about north–south hydrographic and biogeochemical gradients; and

10. To obtain a transect of mid-ocean-ridge basalt (MORB) samples from a fixed location in the absolute mantle reference frame and to use a transect of basalt samples along the flow line that have been erupted in similar formation-water environments to study low-temperature alteration processes by seawater circulation.

Introduction

As the world's largest ocean, the Pacific Ocean is intricately linked to major changes in the global climate system that took place during the Cenozoic. Throughout the Cenozoic, Pacific plate motion has had a northward component. The Pacific Ocean is unique in that the thick sediment bulge of biogenic-rich deposits from the currently narrow equatorial upwelling zone is slowly moving away from the Equator. Hence, older sections are not deeply buried and can be recovered by drilling. Previous Legs 138 and 199 were remarkably successful in giving us new insights into the workings of the climate and carbon system, productivity changes across the zone of divergence, time-dependent calcium carbonate dissolution, an integrated astronomically age-calibrated bio- and magnetostratigraphy, the location of the intertropical convergence zone (ITCZ), and evolutionary patterns for times of climatic change and upheaval. Together with older Deep Sea Drilling Project (DSDP) drilling in the eastern equatorial Pacific, both legs also helped delineate the position of the paleoequator and variations in sediment thickness from ~150°W to 110°W longitude.

Legs 138 and 199 were designed as latitudinal transects across the paleoequator in order to study changing patterns of sediment deposition across equatorial regions at critical time intervals. As we have gained more information about the past movement of plates and when in Earth's history "critical" climate events took place, it became possible to drill an age transect ("flow line") along the position of the paleoequator in the Pacific, targeting important time slices where calcareous sediments have been preserved best and the sedimentary archive in general allows us to reconstruct past climatic and tectonic conditions. Consequentially, the PEAT program will sharpen our understanding of extreme changes of the CCD across major geological boundaries during the last 53 m.y.

During most of the Paleogene the CCD was between 500 and 1300 m shallower than today. Thus, a very shallow CCD makes it difficult to obtain well-preserved sediments during these stratigraphic intervals because initial thermal subsidence of the ridge crest is rapid. Nevertheless, the careful coring and site location strategy of current PEAT Expedition 320/321 allowed us to drill the most promising sites and to obtain a unique sedimentary biogenic sediment archive for time periods just after the Paleocene/Eocene boundary event, the Eocene cooling, the Eocene–Oligocene transition, the "one cold pole" Oligocene, the Oligocene–Miocene transition, and the Miocene. These new cores and data will significantly contribute to the objectives of the IODP

Extreme Climates Initiative and provide material that we were unable to recover during previous legs.

Background

The circulation of the equatorial surface ocean is inescapably linked to the trade wind system. The equatorial Pacific is the classic "world ocean" example of this linkage. It is dominated by wind-driven circulation and is largely unfettered by ocean boundaries. Here, the Equator itself is characterized by a narrow zone of divergence that results from the change in the sign of the Coriolis effect and gives rise to a band of high biologic productivity (Fig. F6). The strength of the equatorial circulation and of this divergence is linked to the strength of the trade winds, which are in turn strongly tied to the global climate system. Variations in global climate, interhemispheric differences in temperature gradients, and marked changes in the ocean boundaries are all imprinted on the biogenic-rich sediments that are accumulating in the equatorial zone. The PEAT program was designed to provide an understanding of equatorial Pacific circulation, carbonate production, deposition, and dissolution for the last ~53 m.y. at a scale where orbital forcing can be resolved. Combined with seismic reflection data (Lyle et al., 2006, 2002) following in the vein of Mitchell et al. (2003) and synthesized with earlier drilling (e.g., Moore et al., 2002, 2004; Lyle et al., 2005; Moore, 2008a), we can reconstruct equatorial Pacific history with high confidence and substantially improve upon work from the early stages of DSDP and recent ODP legs.

Deciphering the sedimentary history of the equatorial Pacific has been greatly simplified by favorable motion of the Pacific plate. Throughout the Cenozoic, the movement of the Pacific plate has had a northward latitudinal component of ~0.25°/m.y. This northward movement transports equatorial sediments gradually out from under the zone of highest sediment delivery, resulting in a broad mound of biogenic sediments (Fig. F8). This transport prevents the older equatorial sections from being buried deeply beneath the younger sections as the crust moves northward. The diminished overburden resulting from this transport allows relatively good preservation of biogenic sediments and minimizes burial diagenesis. In addition, it allows us to core nearly all sections using the advanced piston corer (APC). The northward tectonic displacement, however, is not so large that a traverse of the equatorial zone (within 2° latitude of the Equator) was too rapid to record a reasonable period of equatorial ocean history. Drill sites typically remain within the equatorial zone for 10–20 m.y. before passing beyond the northern edge of high biogenic sedimentation. Older

equatorial sections are thus buried beneath a thin veneer of younger sediments as the crust moves northwestward.

In his summary of DSDP results in the equatorial Pacific, van Andel (1975) gave a general view of the development of the equatorial mound of sediments in the Pacific Ocean, based mostly upon three early DSDP legs (5, 8, and 16). He showed how both temporal and spatial variation in sediment accumulation rates resulted from plate movement, varying biologic productivity at the equatorial divergence and carbonate preservation. The buildup of the Pacific equatorial mound of sediment has been more recently documented and discussed by Mitchell (1998) and Mitchell et al. (2003) (Fig. F8).

Drilling across the Pacific equatorial mound was addressed again some two decades after the van Andel (1975) compilation when an equatorial latitudinal transect along 10 Ma crust was drilled during Leg 138 (Pisias, Mayer, Janecek, Palmer-Julson, and van Andel, 1995) and then again a decade later when a similar transect along 56 Ma crust was conducted during Leg 199 (Lyle, Wilson, Janecek, et al., 2002). The newer drilling, coupled with major advances in geochronology, has documented the remarkable correlation of paleoceanographic events over thousands of kilometers in the equatorial Pacific, caused by the large scale of equatorial Pacific circulation (Fig. F9). It was thus possible during the PEAT program, with the addition of a relatively small number of new sites, to build detailed reconstructions of equatorial Pacific circulation throughout the Cenozoic.

Earlier drilling missed most of this detail because of the lack of important drilling technologies such as APC coring, multisensor track (MST) correlation, and core-log integration that allowed collection of relatively undisturbed sediments, rebuilding of a continuous sediment column from individual cores, and correlation to seismic reflection data. Together with an improved knowledge of the plate tectonic regime, these advances allow us to locate areas of enhanced depositional rates associated with the paleoequator. Combining multiple sites along the Equator will result in a detailed record from the Pleistocene to the Paleocene. These records will be invaluable for the continued development of the Cenozoic timescale as well as for the paleoceanographic information they contain.

Excellent sections were obtained during Legs 138 and 199, on which detailed orbital tuning of the geologic timescale has been carried out. These sections give a much clearer picture of variations in sedimentation rates, isotopic evolution of the oceans,

biologic evolution and zoological provenance, variations in carbonate preservation, and variations in geochemical fluxes that result from paleoceanographic and paleoclimate changes. Parts of the Cenozoic timescale still require further refinement and verification of the proposed orbital tuning. The timescale older than the late Eocene has not yet been calibrated sufficiently, even though evidence of orbital frequencies appears in parts of the records recovered from this older interval (e.g., Norris and Röhl, 1999; Röhl et al., 2001).

To develop a detailed history of the Pacific equatorial current system, the strategy pursued during the most recent ODP legs (138 and 199) was to drill along a line of equal oceanic crustal age, thus obtaining an approximate north–south transect across the major east–west currents during time intervals of particular interest.

During the Paleocene and Eocene, the shallow CCD prevented deposition of carbonate except on crust at relatively shallow depths. Drilling near the paleoposition of the ridge crest at the critical time interval allows the recovery of the shallowest sections available in the pelagic oceans and thereby assures the best possible preservation of the carbonate sediments recovered. As the crust cools and sinks, the seafloor on which the sediments are deposited approaches the lysocline and CCD. Thus, the best preserved part of the sections recovered in such "time line" transects is restricted by the depth at which carbonate dissolution significantly increases, as well as by the northward movement of sediment sections out of the region of high equatorial productivity. This limitation was exemplified by the results from ODP Leg 199, which recovered only limited amounts of carbonate prior to the Eocene/Oligocene boundary (e.g., at ODP Site 1218 on 42 Ma crust).

For the PEAT program, we planned to overcome this limitation of the time line strategy by pursuing an equatorial age transect, or flow line strategy (Figs. F1, F3), to collect well-preserved equatorial sections through the Cenozoic while also making use of the Pacific plate motion to add an oblique latitudinal transect across all time slices.

We drilled a series of sites on the paleoequator at key intervals in the evolution of the Cenozoic climate. These intervals span the extremely warm times of the early Eocene, through the cooling of the late Eocene through Oligocene and the early Miocene time of relatively warm climates (or low ice volume), and into sections deposited during the development of the major Southern and Northern Hemisphere ice sheets (Fig. F2). There are very few previous drill sites that match our site selection criteria. Each site

was selected to be close to the geographic paleoequator and on crust aged slightly older than the age intervals of particular interest.

In this way we will be able to track paleoceanographic conditions at the paleoequator in the best preserved sediments obtainable. We can also make use of the high level of correlation between tropical sediment sections and seismic stratigraphy to develop a more complete model of equatorial productivity and sedimentation.

Understanding the interplay between the CCD, CaCO₃ dissolution, and productivity

The Pacific Ocean, specifically the equatorial upwelling zone, is the largest oceanic source of CO_2 to the atmosphere and controls atmospheric CO_2 levels (Dore et al., 2003). The release and uptake of CO_2 is the direct consequence of calcium carbonate deposition and the interplay between nutrient supply, carbonate dissolution, surface water productivity, and export of biogenic carbonate from surface waters to the sediment pile. Distinguishing between the effects of carbonate dissolution and productivity has been a field of intense study in the past. An important objective of the PEAT program is to address the detailed workings of depth-dependent carbonate dissolution, which is intricately linked to the climate system and paleoceanography. In the standard model for carbonate dissolution, accumulation rates locally decrease linearly from a lysocline down to a CCD, reflecting a linearly increasing rate of dissolution. The depth of both of these mappable surfaces varies spatially and in time as a result of climatic and physical processes. The equatorial Pacific is one of the classic areas where the lysocline-CCD model was first developed, but little subsequent effort had been made to test it—a necessary step, considering that the functional form of dissolution is now known to depend in a more complex way on organic carbon burial and water mass properties. The age transect will provide the necessary additional data with which to test the carbonate paradigm and recover previously unavailable carbonate material from important Paleogene time slices in the Pacific.

Specifically, the recovery of shallowly buried carbonate sediments from near the paleoequatorial upwelling zone will contribute significantly toward separating the various processes that affect carbonate deposition and preservation and will reduce some of the processes that affect climatic proxy records, such as diagenetic recrystallization (Pearson et al., 2001). Neogene productivity has been strongly oriented parallel to the Equator, so differences in carbonate thicknesses at a common latitude but differing depths will permit the effect of dissolution to be isolated (Lyle, 2003; Mitchell et al., 2003; Mitchell and Lyle, 2005). In addition, the strategy adopted in this program will provide new data throughout the Cenozoic with which it will be possible to map the

spatial evolution of the equatorial CCD with time (see **"Results and highlights"**) because the northward component of the Pacific plate movement results in the multiple recovery of the same time slice in different sites but with a slightly different paleolatitude (Fig. **F3**).

Recovering more detailed records from the best possible material will also allow a better understanding of physical processes that might affect or hinder our interpretation of carbonate proxy records, such as the "carbonate ion effect"—an observed and modeled influence of carbonate ion concentration on stable isotope fractionation in carbonate (Spero et al., 1997; Zeebe and Wolf-Gladrow, 2001; Lear et al., 2008).

Preliminary work with seismic data (Mitchell et al., 2003) revealed a surprising lack of correlation between dissolution and depth in the westerly region of this study area. Our aim is to develop a more extensive three-dimensional (3-D) model for the stratigraphy of equatorial Pacific deposits that links all existing core data using a grid of high-resolution seismic reflection profiles, including more recent data from the PEAT site survey AMAT-03 (Lyle et al., 2006). A numerical stratigraphic model will then be used to assess carbonate dissolution and, in particular, the spatial pattern of sharp changes in dissolution, such as the extremely abrupt change in the CCD at the Oligocene/Eocene boundary, which has been linked to a possible abrupt onset of continental weathering. The sediment archive recovered during the PEAT program will allow the application of the substantial array of carbonate-based proxies with which the wider regional seismic study can be constrained and calibrated.

Reconstructing paleoceanographic properties and sea-surface temperature

A large number of paleoceanographic interpretations rely on obtaining proxy data such as stable isotope measurements, elemental ratios such as Mg/Ca, sea-surface temperature estimates from faunal distributions and isotope data, alkenone proxies, TEX_{86}, geochemical productivity, and so on. In turn, a very large number of these measurements rely on the presence of biogenic calcium carbonate. For the Pacific Ocean, the PEAT drilling strategy was designed to recover this important material with the best possible preservation and the least amount of diagenetic effects for long intervals throughout the Cenozoic.

Spatial range considerations

In order to recover the best preserved and most complete carbonate record from the paleoequatorial Pacific, the age transect siting strategy necessarily implies a restricted north–south transect, even though the northward movement of the Pacific plate does

allow us to recover identical time slices multiple times at different paleolatitudes (separated by several degrees). However, we note that the regional seismic study to be developed as part of our site survey work gives us the opportunity to integrate data from older drill sites with new drilling. The site survey linked the new sites to key drill sites from DSDP Legs 9 and 85 and ODP Legs 138 and 199. Combining data from these expeditions and surveys will allow us to construct a site-to-site correlation and, finally, a Pacific "megasplice" of high-resolution data spliced together to cover most of the Cenozoic.

Paleomagnetic objectives

One important aspect of the PEAT program is the recovery of high-quality paleomagnetic data so that attempts to improve existing geological timescales (Gradstein et al., 2004) can be extended further back in time. Results from Leg 199 demonstrate that these records can be recovered from near-equatorial carbonate sediments (e.g., Lanci et al., 2004, 2005). Almost all magnetic reversals from the Paleogene through the present were recovered during Leg 199. However, neither biogenic carbonate sediments through most of the Eocene nor for ages younger than the lower Miocene were recovered during Leg 199. Thus, although the paleomagnetic record during these times was of high quality, global stratigraphic correlation is hindered by the lower mass accumulation rate, the absence of a detailed isotope stratigraphy, and sparser biostratigraphic control. In order to facilitate the development of an integrated magneto- and biostratigraphic framework with a stable isotope stratigraphy (necessary to enable global correlation), recovery of magnetic reversals within carbonate sediment is desirable. In addition, further detailed paleomagnetic, magnetostratigrapic, and magnetic rock fabric data, most importantly from the Eocene, will help resolve the suggestion that the geographic Equator, as determined from the biogenic sediment bulge, might not coincide with the paleoequator position backtracked with a fixed-hotspot reference frame (Moore et al., 2004; Tarduno, 2003; Parés and Moore, 2005).

Ancillary benefits (MORB, basement)

Our drilling aimed to recover basement samples at all sites. A transect of MORB samples from a fixed location in the absolute mantle reference frame is a unique sample suite for mantle geochemists. A transect of basalt samples along the flow line that have erupted in similar environments will be of interest for low-temperature alteration studies (e.g., Elderfield and Schultz, 1996).

Site selection strategy and site targets

The time slices to be drilled during the PEAT program were chosen to cover the overall climatic history of the Cenozoic and target particular times of marked changes in the climatic regime. The spacing of the sites was determined by what we know of the Cenozoic evolution of the lysocline from previous drilling. Where the CCD is particularly shallow, the spacing in time of age transect sites needs to be closer than where the CCD is deep (Fig. F3). As a guide, Site 1218 was drilled on 42 Ma crust during times when the CCD was near 3.3 km. Nannofossil oozes were deposited at this location to ~37 Ma before the crust at this site sank below the CCD. An age separation between drill sites of 2–5 m.y. is a maximum for the shallow CCD of the Eocene; for good preservation of foraminifers even closer spacing should be used. The results of our paleoequator reconstruction and drill site locations are shown in Figure F1.

Site location strategy

In pursuing the history of the equatorial Pacific Ocean through both time line and flow line transects, we have two major advantages over the efforts that took place in the earlier days of scientific ocean drilling. Although previous drill sites targeted the general area, they mostly did not fulfill all of our criteria in terms of (1) a sufficient number of holes to obtain a continuous record, (2) modern coring technology to obtain undisturbed sediments, (3) location inside the paleoequatorial zone, or (4) location on the right crustal age to ensure the presence of calcium carbonate at the targeted time slice. We positioned Sites U1331 through U1338 somewhat south of the estimated paleoequatorial position at their target ages (Fig. F6) to maximize the time that the drill sites remained within the equatorial zone (i.e., ±2° of the equator), to allow for some error in positions (evidence suggests a southward bias of the equatorial sediment mound relative to the hotspot frame of reference [Knappenberger, 2000]), and to place the interval of maximum interest above the basal hydrothermal sediments.

To determine the site and site survey locations, we used the digital age grid of seafloor ages from Müller et al. (1997), heavily modified and improved with additional magnetic anomaly picks from Petronotis (1991) and Petronotis et al. (1994) as well as DSDP/ODP basement ages. For this grid, each point was backrotated in time to zero age, using the fixed-hotspot stage-poles from Koppers et al. (2001) and Engebretson et al. (1985) and the paleopole data from Sager and Pringle (1988). From the backtracked latitudes for each grid point we then obtained the paleoequator at the crustal age by contouring all backrotated latitudinal positions.

Eocene (Sites U1331–U1334)

The Eocene was a time of extremely warm climates that reached a global temperature maximum near 52 Ma, a period around the Early Eocene Climatic Optimum (EECO) (Fig. F2) (Zachos et al., 2001a; Shipboard Scientific Party, 2004). From this maximum there was gradual climatic cooling through the Eocene to the Eocene/Oligocene boundary. There appears to have been a slight reversal to this trend in the middle Eocene near 43 Ma and in the late Eocene at 34–36 Ma, just prior to the pronounced drop in oxygen isotopes that marks the Eocene/Oligocene boundary and one of the most dramatic changes of the CCD (Fig. F3).

Throughout the Eocene, the CCD lay near a depth of 3.2–3.3 km, albeit with potentially significant short-term fluctuations (Lyle et al., 2005). Thus, recovering well-preserved carbonate sediments from the equatorial region is a substantial challenge but not impossible if the depth of the East Pacific Rise lay near the global average of 2.7 km. We presently lack calcareous sediments from the region of the equatorial circulation system during this time of maximum Cenozoic warmth (Zachos et al., 2001a), elevated atmospheric pCO_2 concentrations (Lowenstein and Demicco, 2007), and a shallow early Eocene CCD estimated between 3200 and 3300 m water depth (Lyle, Wilson, Janecek, et al., 2002; Lyle et al., 2005; Rea and Lyle, 2005). The Eocene equatorial upwelling system appears to differ from the modern equatorial upwelling regime by having strong secondary upwelling lobes ~10° in latitude away from the primary equatorial region (Figs. F10, F11). These lobes produced a much broader region of (relatively) high productivity than is present today.

Early and middle Eocene (Sites U1331 and U1332; ~53 and 50 Ma crust)

During Leg 199 a north–south transect was drilled across the equatorial region on ~56 Ma oceanic crust. Sites on this transect had generally drifted below the CCD by 52–53 Ma. Thus, we presently lack calcareous sediments from the region of the equatorial circulation system during the time of maximum Cenozoic warmth. Site U1331 is located on crust with an estimated age of ~53 Ma in order to intercept the interval between 53 and 50 Ma in basal carbonate sediments above the shallow early Eocene CCD (4200–4300 m). This interval was poorly sampled during Leg 199.

Average (noncarbonate) accumulation rates in the early Eocene were moderate, only slightly increasing in some of the more northern sites on the Leg 199 transect (Sites 1215 and 1220). What is particularly interesting in the Leg 199 records is that the very shallow CCD of this early Eocene time appears to deepen to the north, perhaps sug-

gesting a northern source for the bottom waters. Sites targeting this time interval would ideally give us sediments with sufficient carbonate material to better constrain the isotopic and biotic characteristics of the near-surface equatorial waters.

During the early Eocene, a very shallow CCD and typical rapid tectonic plate subsidence of young crust near the shallow ridge crest conspired to make the time window during which carbonate is preserved short (~2–5 m.y.). Thus, although good records of pelagic carbonates during and just after the Paleocene/Eocene Thermal Maximum (PETM) were recovered during Leg 199 (Lyle, Wilson, Janecek, et al., 2002; Nunes and Norris, 2006; Raffi et al., 2005), the time period of the EECO (Zachos et al., 2001a) is not well sampled.

Sites U1331 (53 Ma crust) and U1332 (50 Ma crust) aim to provide the sedimentary archive to address several important questions that relate to causes and responses of the true Cenozoic "Greenhouse" world: the Eocene was a time of extremely warm climates that reached a maximum in temperatures near 52 Ma (Zachos et al., 2001a). From this maximum there was gradual climatic cooling to the Eocene/Oligocene boundary. Good paleomagnetic stratigraphy from Leg 199 sites allowed a much-improved calibration of nannofossil and radiolarian biostratigraphic datums throughout the Eocene. A north–south transect across the equatorial region at ~56 Ma was drilled during Leg 199. Although good records of pelagic carbonates during and just after the PETM were recovered at Leg 199 sites (Lyle, Wilson, Janecek, et al., 2002; Raffi et al., 2005; Nunes and Norris, 2006), the time period of the EECO (Zachos et al., 2001a) and the shallowest CCD is not well sampled.

In combination with Site U1331, which is located on 53 Ma crust, Site U1332 is located on crust with an expected age of ~50 Ma to intercept the interval between 50 and 48 Ma in biogenic sediments above the CCD. Thus, Site U1332 forms the second oldest time slice component of Expedition 320/321.

Middle and late Eocene (Site U1333; 46 Ma crust)

Good paleomagnetic stratigraphy at Leg 199 sites allowed a much improved calibration of nannofossil and radiolarian biostratigraphic datums (Pälike et al., 2005, 2006b; Raffi et al., 2005, 2006; Nigrini et al., 2006). From the combined information, a more detailed picture emerged of temporal variations in sediment accumulation through the middle and upper Eocene of the tropical Pacific. These data showed an increase of a factor of up to 2–3 in accumulation rates of siliceous ooze in the middle Eocene (41–45 Ma).

There are also several notable periods of highly fluctuating CCD associated with intervals in which carbonate is preserved as deep as 4000 m water depth, or ~700 m deeper than the average Eocene CCD (Lyle, Wilson, Janecek, et al., 2002; Lyle et al., 2005; Rea and Lyle, 2005; Bohaty et al., 2009). These fluctuations occur immediately prior to the Middle Eocene Climatic Optimum (MECO), which is associated with CCD shoaling (Bohaty and Zachos, 2003; Bohaty et al., 2009). Such fluctuations in the CCD are similar in magnitude to those at the Eocene/Oligocene boundary (Coxall et al., 2005). High siliceous sedimentation rates occur near an apparent short reversal in the middle Eocene cooling interval. It is difficult to interpret the cause of such a substantial change in silica flux during a very warm climatic regime.

The primary objective of coring at Site U1333 is to recover a complete sequence of carbonate sediments spanning the middle Eocene to Oligocene so we can evaluate changes in temperature and structure of the near-surface ocean, bottom water temperatures, and the evolution of the CCD.

One of the additional objectives of the PEAT program was to provide a depth transect for several Cenozoic key horizons, such as the Eocene–Oligocene transition (Coxall et al., 2005) targeted at Sites U1331–U1334. Site U1333 forms the third deepest paleodepth constraint, with an estimated crustal paleodepth of <4 km and a paleolatitude ~3° north of the paleoequator during the Eocene–Oligocene transition.

Eocene/Oligocene Boundary (Site U1334; 38 Ma crust)

Site U1334 sediments are estimated to have been deposited on top of late middle Eocene crust with an age of ~38 Ma, and this site targets the events bracketing the Eocene–Oligocene transition with the specific aim of recovering carbonate-bearing sediments of latest Eocene age prior to a large deepening of the CCD that occurred during this Greenhouse-to-Icehouse transition (Kennett and Shackleton, 1976; Miller et al., 1991; Zachos et al., 1996; Coxall et al., 2005). The Eocene–Oligocene transition experienced the most dramatic deepening of the Pacific CCD during the Paleogene (van Andel, 1975), which has now been shown by Coxall et al. (2005) to coincide with a rapid stepwise increase in benthic oxygen stable isotope ratios interpreted to reflect a combination of growth of the Antarctic ice sheet and decrease in deepwater temperatures (DeConto et al., 2008; Liu et al., 2009).

So far the most complete Eocene/Oligocene boundary section recovered from the equatorial Pacific has been Site 1218 on 42 Ma crust; however, it is far from pristine. Carbonate percentages drop markedly below the boundary and reach zero near 34 Ma

during a time of apparent global shoaling of the CCD just prior to the Eocene–Oligocene transition and CCD deepening (Bohaty et al., 2008). The absence of carbonate in this interval prevented the recovery of information about paleoceanographic conditions prior to the Eocene–Oligocene transition and also has implications for the interpretation of paleotemperature proxies such as Mg/Ca ratios in foraminifer shells that were bathed in waters with very low carbonate ion concentrations (Lear et al., 2008; Elderfield et al., 2006). The integrated stratigraphy from Site 1218 has been correlated to the planktonic foraminifer marker extinction of the genus *Hantkenina* in exceptionally well preserved shallow clay-rich sediments from Tanzania by Pearson et al. (2008), who demonstrated that the Eocene/Oligocene boundary falls within the middle plateau of the stable isotope double-step described by Coxall et al. (2005) just prior to the base of Chron C13n.

Data from Site 1218 allowed astronomical time calibration of the entire Oligocene (Coxall et al., 2005; Wade and Pälike, 2004; Pälike et al., 2006b), but the lack of carbonate in the uppermost Eocene at this site made the detailed time control now available for the Oligocene much less certain for the late Eocene. Site U1334 is located on crust with a basement age of ~38 Ma and crossed the paleoequator shortly thereafter. It was located to provide the missing information about the crucial chain of events prior to and during the Eocene–Oligocene transition.

Oligocene (Site U1336; ~32 Ma crust)

Site U1336 targets the Oligocene and is located on lower Oligocene crust. This interval of time is noted for its markedly heavy benthic oxygen isotopes (Fig. F2) and its relatively deep CCD (Fig. F3). There was probably ice on Antarctica during this interval, but not the large ice sheets found there later in the middle Miocene. There is no compelling evidence for ice sheets in the Northern Hemisphere during the Oligocene and early Miocene. Thus, there was apparently a time of low global ice volume, cold bottom waters, a cold South Pole, and a relatively warm North Pole. This scenario of a "one cold pole" world has given rise to speculation on the impact of interhemispheric temperature imbalance on pole-to-Equator temperature gradients and on the symmetry of the global wind systems. The extent to which such an imbalance may have affected the trade winds, the position of the ITCZ, and the seasonal shifts in this zone should be seen in the wind-driven currents of the equatorial region.

The older low-resolution DSDP data indicate relatively high but variable sediment accumulation rates during this interval and better carbonate preservation south of the Equator (van Andel, 1975). The highest accumulation rates encountered (>15 m/m.y.)

from the Leg 199 transect occurred in the lower part of the Oligocene, but these were at sites north of the Oligocene Equator or on relatively old (and therefore deep) crust. Thus we expected a better preserved, thicker carbonate section at the Oligocene Equator. Studies of Oligocene sections from Leg 199 and other ODP sites (e.g., Paul et al., 2000; Zachos et al., 2001a; Billups et al., 2004; Pälike et al., 2006a) indicate the presence of strong eccentricity and obliquity cycles in carbonate preservation and suggest a strong (southern) high-latitude influence on the carbonate record. These cycles are leading to the development of an orbitally tuned timescale that reaches back to the base of the Oligocene (Pälike et al., 2006b). Such a timescale will make it possible to develop a detailed picture of equatorial geochemical fluxes and of the degree of variability in the equatorial system of the Oligocene.

Latest Oligocene–earliest Miocene (Site U1335; 26 Ma crust)

Site U1335 was designed to focus on paleoceanographic events in the late Oligocene and into the early and middle Miocene, including the climatically significant Oligocene–Miocene transition and its recovery. In conjunction with Sites U1336 and U1337, Site U1335 was also designed to provide a latitudinal transect for early Miocene age slices. A significant several million year long rise in the oxygen isotope record (Lear et al., 2004; Pälike et al., 2006b) at the end of the Oligocene is closely followed by a relatively short, sharp increase in oxygen isotope values. This increase has been interpreted as a major glacial episode (Mi-1) (Fig. F2) (Paul et al., 2000; Zachos et al. 1997, 2001a, 2001b; Pälike et al., 2006a) and correlated to a pronounced drop in sea level (Miller et al., 1991). The Mi-1 event is very close to the Oligocene/ Miocene boundary and has now been astronomically age calibrated in several ocean basins (Shackleton et al., 2000; Billups et al., 2004). Although there are clear periodic isotopic signals indicating major changes in ice volume, ocean temperatures, and/or ocean structure, this biostratigraphic boundary has always been somewhat of an enigma. Unlike the major changes in the isotopic stratigraphy, the biostratigraphies of the planktonic microfossils show very little change at all across this boundary. In fact, it is one of the most difficult epoch boundaries to pick using solely microfossil biostratigraphy.

At Leg 199 Sites 1218 and 1219 this interval was well recovered; however, carbonate preservation still presented a problem for foraminifer stratigraphy. Both sites were deep and well within the lysocline, making the application of temperature proxies such as Mg/Ca ratios in foraminifer tests more difficult (Lear et al., 2008). At the time Miocene-Oligocene sediments were deposited, Site 1218 already resided on 18 Ma crust and was ~4100 m deep. Site 1219 was on ~34 Ma crust and was ~4500 m deep.

There was a relative increase in the large diatoms near this boundary in the siliceous coarse fraction, suggesting increased productivity; however, detailed high-resolution flux rates across this interval have yet to be determined. A well-recovered section on the latest Oligocene Equator near the late Oligocene ridge crest was targeted at Site U1335 and should provide both the resolution and the preservation required to better describe the changes in the equatorial ocean taking place at this time.

Miocene (Site U1337; 24 Ma crust)

Site U1337 was proposed for drilling to focus on the paleoceanographic events in the early and middle Miocene. The latest Oligocene through the middle Miocene appears to have been a time of relative warmth comparable to the latest Eocene. However, the short-term variability in the isotopic record of the early to middle Miocene is larger than that of the Eocene and may indicate more variability in climate and in global ice volume. The climatic "optimum" at ~15 Ma comes just before the major development of ice sheets on Antarctica and the marked increase in ice-rafted debris in circum-Antarctic sediments. The early Miocene also marked a major evolutionary change from the relatively static Oligocene planktonic biota. In the equatorial Pacific, the early Miocene marked the beginning of abundant diatoms in the stratigraphic record (J. Barron, pers. comm., 2003) and thus may represent a major change in carbon cycling as well.

The only major ocean boundary change proposed for the time near the Oligocene/Miocene boundary was the opening of the Drake Passage to deep flow; however, there is some debate as to the exact timing of this event (Barker, 2001; Pagani et al., 1999; Lawver and Gahagan, 2003; Scher and Martin, 2006; Lyle et al., 2007) and its direct impact on the tropical ocean is uncertain. It may be that, as in the Eocene/Oligocene boundary section, the link lies in the shallow intermediate waters that provide nutrients to lower latitude upwelling regions. For the equatorial region, an even more pertinent question is "What changes were occurring in the Miocene tropical ocean that led to this burst of Miocene evolution?"

Middle Miocene (Site U1338; ~18 Ma crust)

In principle, the age transect strategy of this proposal would not be complete without data from the Pliocene–Pleistocene. However, in addition to limitations of cruise length, near-paleoequatorial records have already been targeted by ODP Legs 138 (Pisias, Mayer, Janecek, Palmer-Julson, and van Andel, 1995) and 202 (Mix, Tiedemann, Blum, et al., 2003); these records provide information about the development of

Northern Hemisphere glaciation. Our last site (U1338) focuses instead on the interesting events following a middle Miocene maximum in deposition (van Andel, 1975).

Site U1338 was proposed for drilling to focus on the paleoceanographic events following a middle Miocene maximum in deposition (van Andel, 1975). In addition, large changes in the state and frequency of continental glaciation have recently been described within the middle Miocene (after 14 Ma) (Holbourn et al., 2005; Abels et al., 2005; Raffi et al., 2006). There is a wide latitude range of $CaCO_3$ deposition during the earliest Neogene, with a relatively sharp transition to a narrower $CaCO_3$ belt after 20 Ma (Lyle, 2003). $CaCO_3$ mass accumulation rates in the central equatorial Pacific recovered from the 18–19 Ma "famine" and in the period between 14 and 16 Ma reached a second maximum in carbonate deposition, which is also evident in the seismic stratigraphy of the equatorial sediment bulge (Knappenberger, 2000; Mitchell et al., 2003). We designed Site U1338 to recover an equatorial record at the early middle Miocene sedimentation maximum.

Results and highlights

During Expedition 320, 16 holes at 6 sites (Holes U1331A–U1331C, U1332A–U1332C, U1333A–U1333C, U1334A–U1334C, U1335A, U1335B, U1336A, and U1336B) (Table **T1**) were cored as part of the PEAT program. By drilling a series of sites that follow the position of the paleoequator and a limited latitudinal and depth transect, as outlined below, we recovered cores that allow us to address the combined PEAT objectives (see **"Scientific objectives"**).

Lithologies recovered and stratigraphic summary

During Expedition 320 sediments similar in lithology to previous DSDP and ODP expeditions to the central equatorial Pacific region were recovered (e.g., Lyle, Wilson, Janecek, et al., 2002). Figure **F12** summarizes the lithostratigraphy of the northwest–southeast transect of sites drilled during Expedition 320 together with the sedimentary sequence from Site 1218, which is included in the PEAT flow line strategy (see **"Scientific objectives, introduction, and background"**). In this figure, the Eocene sequence (green shading) thins from north to south, pinching out between Sites U1335 and U1336 where the basement is of early Oligocene age. In contrast, the Miocene sequence (yellow shading) thins substantially from south to north whereas the Oligocene sequence (blue shading) is thickest in the middle of the transect (Sites

U1334 and U1335) and thins both north and south. Sediments of early Eocene age are only present at Site U1331, and sediments of Pliocene–Pleistocene age are only present at Sites U1331, U1334, and U1335. The thickness of sediments from different parts of the age transect is compatible with that expected from our drilling strategy (see **"Site selection strategy and site targets"**).

Five main lithologies are present in these sites:

1. Surface clays;

2. Nannofossil oozes and chalks;

3. Radiolarian ooze and radiolarite;

4. Porcellanite and chert; and

5. Basal chalks, limestones, and clay.

Surface clays are only present from Site U1334 to the north and in strata of post-Oligocene age. This pattern reflects the accumulation of dominantly aeolian-derived fine-grained sediments below the CCD as the northward motion of the Pacific plate transports the sites out of the equatorial upwelling zone of high production and the underlying crust subsides with age.

Nannofossil oozes and chalks are the main lithology of the Oligocene throughout the Expedition 320 transect. To the south, where Sites U1335 and U1336 have not yet subsided below the present CCD, nannofossil ooze is also the main lithology in strata of Miocene age. North of these two sites, nannofossil ooze is also present but in decreasing importance moving northwestward as basement age becomes progressively older. At the northernmost end of the transect (Site U1331), nannofossil ooze is primarily restricted to a short interval of middle Eocene age and is broadly correlative to carbonate accumulation event (CAE) 3 (Lyle et al., 2005).

Radiolarian ooze is present at all sites (Fig. **F12**) except for Site 1218, but it is a far more abundant lithology in the north (Sites U1331 and U1332), where it is the main lithology of the Eocene, than in the south (Sites U1334–U1336).

Porcellanite and chert are diagenetic in origin, but they are sufficiently regional in extent in the equatorial Pacific to be considered individually. Porcellanite is a major lithology in sediments of early and early middle Eocene age toward the northern end of the Expedition 320 transect (especially Sites U1331 and U1332), where it is associated with thin clay horizons that are interbedded with radiolarian ooze. Chert is a ma-

jor lithology in sediments of early and early late Oligocene age at Site U1336, where it proved a major impediment to recovery of a complete section.

At nearly all sites drilled on the PEAT transect, the recovered basal sediments overlying basalt are calcareous in lithology, indicating that, at the onset of sediment accumulation at these sites, the seafloor lay above the local CCD. This result is in keeping with the Expedition 320 rationale of drilling a flow line of sites on crust of decreasing age (southeast to northwest) to recover stratigraphic "windows" of calcareous sediments overlying contemporaneously young crust prior to its subsidence below the CCD. The only site on the Expedition 320 transect where calcareous sediments were not recovered overlying basement is Site U1332, where the basal sediment unit is primarily zeolite clay of middle Eocene age. This result indicates that the crust at Site U1332 lay below the CCD, even at the point of its formation (~50 Ma), pointing to a very shallow CCD (<2700 m) at this time (see **"Cenozoic CCD in the equatorial Pacific"**).

The combined results of Leg 199 and the PEAT program (Fig. **F13**) will potentially allow us to decipher paleoceanographic and paleoclimatic changes within a latitudinal and depth transect in the equatorial Pacific Ocean. Intervals of interest include the EECO (Zachos et al., 2001a; Lyle, Wilson, Janecek, et al., 2002), the MECO (Bohaty and Zachos, 2003; Bohaty et al., 2009), the middle through late Eocene CAE events (Lyle et al., 2005), the Eocene–Oligocene transition (Coxall et al., 2005), the late Oligocene warming (see supplementary material in Pälike et al., 2006b), the Oligocene–Miocene transition (Zachos et al., 2001b; Pälike et al., 2006a), and the middle Miocene glaciation intensification event (Holbourn et al., 2005).

Sediments of early Eocene age in the Pacific equatorial age transect are characterized by the absence of calcareous sediments and the presence of clay, cherts, and porcellanite. In general, sediments of middle Eocene age from the equatorial Pacific transect are dominated by radiolarian ooze, radiolarite, and clay, but carbonate-rich intervals also occur and appear correlative between Expedition 320 sites and Sites 1218 and 1219, where the CAE events were originally defined. Sediments of middle Eocene age at Site U1333 are carbonate rich compared to those at Site 1218, an observation that cannot be explained by their assumed relative paleodepths during this interval. The Eocene–Oligocene transition is characterized by a major lithologic change from Eocene radiolarian oozes to Oligocene nannofossil oozes at ODP Sites 1218–1221 and Sites U1331–U1333. At Site U1334, sediments of latest Eocene age are more carbonate rich than at any of the other sites.

The Oligocene–Miocene transition occurs within a succession of pale and dark nan-nofossil ooze cycles at all sites where it was recovered except for Site 1220, where it is characterized by a transition from Oligocene radiolarian ooze to Miocene clay. Clay- and diatom-rich sediments characterize the middle to late Miocene interval.

Cenozoic CCD in the equatorial Pacific

One of the primary objectives of the PEAT program was to detail the nature and changes of the CCD throughout the Cenozoic in the paleoequatorial Pacific (Objec-tive 1 in "Scientific objectives"), with potential links to organic matter deposition (Olivarez Lyle and Lyle, 2005). The choice of drilling locations, targeting positions on the paleoequator to track carbonate preservation during crustal subsidence through-out time (Fig. F14), followed the initial work on DSDP sites by van Andel (1975). This first reconstruction of the Cenozoic CCD was augmented by additional results from Leg 199 (Lyle, Wilson, Janecek, et al., 2002; Rea and Lyle, 2005). One of the significant contributions of Leg 199 drilling was the latitudinal mapping of CCD variations with time. During the Eocene, a generally shallow CCD appeared to be deeper outside the zone ±4° from the equator, opposite to the pattern established during the Neogene (Lyle, 2003). The PEAT cores will allow us to refine our knowledge of temporal and spatial variation in sediment accumulation rates resulting from plate movement, varying biologic productivity at the equatorial divergence, and carbonate preserva-tion (Fig. F14). The shipboard sampling program allowed for >1000 determinations of $CaCO_3$ concentrations, approximately one every section from one hole of each site. Shipboard results reveal the carbonate accumulation events of Lyle et al. (2005) as sharp carbonate concentration fluctuations at ~44, 41, 39, and 36 Ma across Sites U1331–U1334 and 1218, followed by a sharp transition into much higher carbonate accumulation rates from the Eocene into the Oligocene. Results from Expedition 320 reveal a complex latitudinal pattern where Sites U1331, U1332, and U1334 track the equatorial CCD that matches well the signal observed from Site 1218, but Site U1333, which is slightly north of the equatorial zone during the Eocene–Oligocene transi-tion, shows significantly more carbonate accumulation.

The early Eocene equatorial CCD is much shallower than previously thought, as shown by results from Site U1332, where we did not recover any carbonate in the basal sediment section above basement, in contrast to Site U1331, which is only ~2 m.y. older. Our estimated CCD at ~49 Ma is only ~3000 m paleodepth. Surprisingly, Expedition 320 results also show a shallower CCD than previously known during the late Oligocene, perhaps 300 m shallower in the time interval between 23 and 27 Ma.

This shallower CCD, at a paleodepth of ~4.5 km, and associated reduced carbonate fluxes to the seafloor could be linked to the gradual late Oligocene cooling, first fully recovered at Site 1218 (supplementary fig. 3 in Pälike et al., 2006b). The design of our drilling locations in combination with existing data will allow us to generate a 3-D view of CCD evolution during the Cenozoic during postcruise research.

Biostratigraphy and preservation

Biostratigraphic integration

A virtually complete composite section with biogenic sediments spanning 51 m.y. from the upper Pleistocene to the lower Eocene was recovered during Expedition 320 (Objectives 2, 3, 4, and 7 in **"Scientific objectives"**). The youngest record during the last 12 m.y. (late middle Miocene to recent) was well preserved at Site U1335 but elsewhere is only present as a thin (5–10 m) section of noncalcareous brown clay. Biostratigraphic records spanning the middle Miocene through lower Eocene are composed of nannofossil and radiolarian oozes as two major biogenic components. At Sites U1331 and U1335 turbidite beds containing reworked microfossils were present, with mixing most obvious at Site U1331. At the shipboard biostratigraphic resolution, all drilled sites contribute apparently continuous successions to this composite section and stratigraphic highlights include multiple recoveries of a complete Eocene–Oligocene transition at Sites U1331–U1334 and Oligocene/Miocene boundaries at Sites U1332–U1336. These sections provide excellent records of biotic response to rapid environmental change in the principal phytoplanktonic and zooplankton groups as well as benthic foraminifers.

Dissolution and microfossil preservation

The preservation of carbonate microfossils varies dramatically throughout the succession as a result of biotic production and export rates, water-column and seafloor dissolution, and other processes. The strength of dissolution reflects the depths of the drilling sites, which are all presently bathed at >4.3 km water depth, whereas the amount of dissolution strongly depends on the paleodepth (subsidence) history at each site and fluctuations of the CCD on a regional and basin-wide scale. The dissolution effect is greatest in the oldest successions at Sites U1331–U1333 (Figs. **F14**, **F15**). The Eocene equatorial CCD has been estimated at a depth shallower than ~3.5 km (Lyle et al. 2005), with short-term CCD fluctuations occurring during the middle to late Eocene based on preservation of calcareous microfossils and calcium carbonate records at Sites U1331–U1334. The most striking CCD change has been recorded close

to the Eocene–Oligocene transition where the sediments change from radiolarian-dominated Eocene sediments to Oligocene nannofossil oozes. The depth transect of these sites indicates a deepening of at least 1 km over this short time interval. The recovery of carbonate-rich Oligocene successions at all sites is evidence for a considerably deeper CCD (>4.5 km water depth) throughout this interval (see Fig. F14).

A compilation of semiquantitative estimates of preservation and abundance of calcareous microfossils reveals a strong coupling of the fossil records with paleodepth history and the CCD at these drilling sites. The carbonate dissolution effect is strikingly different between microfossil groups (Fig. F15). Planktonic foraminifers are the most sensitive to dissolution, and well-preserved specimens were found in sediments if carbonate contents exceeded at least 60%–70%. At the deepest Site U1331, planktonic foraminifers are only present during carbonate maxima in the Oligocene, middle Eocene, and early Eocene ages. At Site U1332 they were present only in the carbonate-rich Oligocene nannofossil oozes (Fig. F15). At Sites U1334 and U1335 high-carbonate sediments (80%–90%) contain abundant and well-preserved planktonic foraminifers.

Calcareous nannofossils and benthic foraminifers are less susceptible to dissolution than planktonic foraminifers and closely track the presence or absence of carbonates in the sediments. The preservation of both groups varies with carbonate content, but the preservation of calcareous nannofossils varies even in sediments with low carbonate content that are barren of planktonic foraminifers. Poor preservation of specimens is observed in sediments of 5%–25% carbonate contents, moderate preservation in sediments of 30%–70%, and good benthic foraminifer and moderate to good nannofossil preservation in sediments with >75% $CaCO_3$.

Within the nannofossil assemblages, however, certain taxa are never present in these sediments, such as holococcoliths. The relatively robust holococcolith *Zygrhablithus bijugatus* was only recorded in one or two samples from Sites U1335 and U1336, and other taxa show distributions that are more similar to those of planktonic foraminifers, such as the long-ranging heterococcolith genus *Helicosphaera* (Fig. F15).

Basal carbonates

Eocene basal carbonate sediments (nannofossil oozes with foraminifers) were recovered on top of basaltic basement at Sites U1331–U1334 (Fig. F16). The existence of carbonates suggests that paleodepths at these sites were maintained at ~2.75 km above the shallow Eocene CCD during the early to middle Eocene. At all four sites

these carbonate intervals are thin and their lower parts are lithified to limestones, probably because of the combined influence of hydrothermal fluid processes and overburden. These sediments contain slightly diagenetically modified calcareous microfossils and are barren of siliceous microfossils. Sites where Eocene sediments were recovered were located within 2° latitude of the paleoequator at the time of first sediment accumulation, so evidence of equatorial upwelling might be expected in the assemblages. The absence of siliceous microfossils is likely a result of dissolution associated with hydrothermal flow of the crust (Moore, 2008a).

Productivity indicators

Shipboard analyses of quantitative microfossil faunal assemblages allow only preliminary speculations on potential microfossil-based productivity indicators; quantitative work will be required to follow up on these initial observations and fully address Objective 2 of the PEAT program (see **"Scientific objectives"**). Calcareous nannofossil assemblages at these lowest stratigraphic levels are not strikingly different from younger examples. At several sites, however, the common presence of taxa that are considered to be higher productivity (or cooler water) indicators is suggestive of an upwelling signal (e.g., common *Chiasmolithus* and small reticulofenestrids [*Reticulofenestra minuta*] at Sites U1333 and U1334). At all sites sphenoliths are also common at these levels, and although some representatives of this group are considered to be oligotrophs (e.g., Gibbs et al., 2004), certain species clearly display more opportunistic behavior, which explains their abundant presence here (e.g., Wade and Bown, 2006; Dunkley Jones et al., 2008).

The absence or relative rarity of the warm-water oligotrophic discoasters in the lowest parts of Sites U1331, U1333, and U1334 is also suggestive of higher productivity surface waters, at least for the sediments immediately overlying basement. Discoasters are actually common in the lowest sediments at Site U1331, and this either represents selective concentration due to the dissolution of less robust taxa or indicates that these species (*Discoaster deflandrei* and *Discoaster lodoensis*) were adapted to more eutrophic paleoenvironments. Planktonic foraminifer assemblages in the basal carbonates at Sites U1333 and U1334 are dominated by relatively robust taxa: subbotinids, parasubbotinids, and paragloborotalids. These genera are thought to occupy a (sub)thermocline habitat (Wade et al., 2007; Sexton et al., 2006) and are often associated with high-productivity environments (Wade et al., 2007), an association consistent with both sites being situated in the equatorial upwelling region. However, planktonic foraminifer assemblages at Sites U1333 and U1334 may also be biased toward these more robust taxa by the effects of dissolution. Detailed assemblage study

is required to elucidate the relative contributions of calcium carbonate dissolution and the true paleocological signal.

Radiolarian stratigraphy

The radiolarian stratigraphy in sediments recovered during Expedition 320 (Table **T2**) span the zones from RN14 (lower Pleistocene) to RP10 (lower middle Eocene) and provide the highest shipboard biostratigraphic resolution for most sections within the Eocene. The preservation of assemblages is generally good with only a few scattered intervals of moderate to poor preservation. Nigrini et al. (2006) took a comprehensive approach toward establishing ages for all radiolarian datums recovered at Leg 199 sites. In so doing, they produced age estimates for >300 radiolarian datums, greatly enhancing our ability to date the Cenozoic section in the tropical Pacific. However, several of these calibrations need to be checked and/or refined. In addition, some of the datums appear to be more reliable than others, and this needs to be further evaluated. In some cases, variation in the levels of first and last appearances of species may be caused by variation in taxonomic interpretation, but more often these variations are due either to real differences in the ranges of species at different locations in the tropical Pacific or to the extremely low abundance of certain species in samples from a given site. Thus, taxonomic difficulty, abundance, and preservation all figure into how well a species serves as a stratigraphic marker.

A few levels were not adequately covered by Leg 199 sites. For the upper Miocene we have relied on the radiolarian studies of Leg 138 in the far eastern tropical Pacific (Moore, 1995). In their studies of Leg 199 sites, Kamikuri et al. (2005) and Funakawa et al. (2006) added substantially to our understanding of the radiolarian assemblage transitions at the Oligocene/Miocene and Eocene/Oligocene boundaries. However, these studies focused on the statistical changes in the faunal assemblages as a whole and made no wholesale attempt to recalibrate first and last appearance datums. During Expedition 320 we have been able to add to the stratigraphic control in the lower part of the middle Eocene collected at Site U1331 and test the usefulness of individual datums at the sites drilled. The full integrated biostratigraphies will address our third objective (see **"Scientific objectives"**).

Diatom distribution from smear slide analysis

One of the great achievements of the PEAT program has been the recovery of all major fossil groups, including diatoms. The diatom biostratigraphy of sediments from Expedition 320 will be conducted postcruise, although initial descriptions of diatom abun-

dance were made during lithostratigraphic smear slide analyses. Sediments from Expedition 320 with diatoms are typically less abundant in smear slides than radio-larians, nannofossils, clay, and foraminifers. Nevertheless, a site-to-site compilation of the smear slide data generated during this expedition and from Site 1218 reveals noticeable stratigraphic changes in diatom abundance relative to these other main lithologic constituents (0%–50%) (Fig. F17). In general, diatoms are quantitatively more important in Miocene sediments than in sediments of Oligocene and Eocene age at these equatorial Pacific sites. Noticeable peaks in diatom abundance occur su-perimposed on this secular pattern, with the most sustained high abundances (up to >25%) observed across the early/middle Miocene boundary (Sites U1335 and U1336). Diatom abundances of up to 25% occur over shorter durations in sediments from the Eocene–early Oligocene (Sites U1332, U1333, and 1218), late Oligocene (Site U1333), early late Miocene (Site U1335), and middle late Pliocene (Site U1336). Sediments of middle Eocene age at these sites are, in comparison with overlying sediments, poor in diatoms with a single minor abundance peak documented in radiolarian Zone RP15 at two sites (U1331 and 1218).

Paleomagnetism

Paleomagnetism and magnetostratigraphic studies are important observations needed to fulfill the expedition objectives of obtaining a well-intercalibrated Ceno-zoic megasplice and constraining the Pacific plate tectonic motion (Objectives 3 and 5 in "Scientific objectives"). Results obtained so far indicate that the sediments re-covered will provide one of Expedition 320's lasting legacies toward addressing these objectives in a comprehensive fashion: shipboard paleomagnetic results were ob-tained from 56,222 intervals measured along ~2000 split-core sections and from de-tailed progressive alternating-field (AF) and thermal demagnetization of 411 small discrete samples (Fig. F18). These data indicate that a useful magnetic signal (charac-teristic remanent magnetization [ChRM]) is preserved in most APC cores after re-moval of the drilling-induced overprint by partial AF demagnetization at 20 mT. Exceptions were mainly limited to intervals affected by reduction diagenesis (70–110 and 210–410 m core depth below seafloor, method A [CSF-A; when using method A, core expansion lengths overlap if longer than 9.5 m and are not scaled], at Site U1335 and 80–160 m CSF-A at Site U1336), which have very low to even negative (diamag-netic) magnetic susceptibilities and retain little or no remanent magnetization.

Cleaned paleomagnetic data were characterized by shallow inclinations, consistent with the sites being near the paleoequator, and by 180° alternations in declinations

downhole, reflecting magnetic polarity zones (magnetozones). These qualities, along with demagnetization results from discrete samples, indicate that the ChRM is the primary depositional magnetization. Magnetostratigraphies at each site were thus constructed by correlating the distinct declination alternations with the geomagnetic polarity timescale (GPTS) (Fig. **F18**).

In total, these magnetostratigraphies yield 803 dates ranging from 51.743 Ma (base of Chron 23n.2n at Site U1331) to the present (Chron C1n; 0–0.783 Ma at Site U1335). In addition, 83 short polarity intervals were observed that might correspond to cryptochrons or geomagnetic excursions. At these short events and at the geomagnetic reversals, magnetization intensities are low, as would be expected if the sediments are accurately recording the past paleomagnetic field intensity. Analysis of paleomagnetic directions over stable polarity intervals (full chrons) indicates the long-term record provides paleolatitude information that will aid in refining the Pacific apparent polar wander path and directional dispersion information for studying geomagnetic secular variation (Objective 5 in **"Scientific objectives"**). Thus, besides providing ages for the six sites, the high-quality paleomagnetic records have the potential to resolve long- and short-term geomagnetic field variability and provide important plate kinematic constraints.

The Cenozoic megasplice and stratigraphic correlation

One of the prime objectives for the PEAT program was a detailed intercalibration of bio-, magneto-, and chemostratigraphic records for the Cenozoic from the early Eocene to the present within an astronomically age-calibrated framework (Objective 3 in **"Scientific objectives"**). The PEAT program was designed to incorporate results from Leg 138 for the younger Neogene part and Leg 199 for time intervals in the Eocene (Pälike et al., 2008) (Fig. **F2**). Expedition 320 shipboard results indicate that we can achieve this objective, based on the observation that even decimeter-scale features in the sedimentary record from the drilled sites can be correlated over large distances across the Pacific seafloor (Fig. **F9**) (Pälike et al., 2005). The PEAT program will leave a long-lasting legacy for the detailed intercalibration of all major fossil groups, a detailed magnetostratigraphy with >800 dated reversals, and sedimentary cycles that can be calibrated across large distances in the Pacific Ocean. Figure **F19** demonstrates that a Cenozoic megasplice can be constructed from the material recovered and spliced onto previous Leg 138 and 199 sites. Physical property data that proxy calcium carbonate oscillations at Sites U1331 and U1332 show a remarkable match with those from Site 1220, which also has an excellent magnetostratigraphy. Simi-

larly, Sites U1333 and U1334 can be spliced to Site 1218, providing a coherent and integrated record of large-scale Pacific sedimentation patterns of biogenic material from the Eocene through the Miocene and younger (Fig. F20). Such stratigraphic correlation makes possible the study of sedimentation patterns and mass accumulation rates at orbital resolution. The material recovered will also allow us to verify existing calibrations (e.g., Pälike et al., 2006b) and further extend these up into the Miocene and down into the Eocene.

We can exemplify the approach toward the Cenozoic by constructing a preliminary multisite splice of gamma ray attenuation (GRA) bulk density (Fig. F21). This record of GRA bulk density from tropical Pacific sediments encompasses a major part of the Cenozoic, stretching from the upper Eocene to the recent, using data from Legs 138 and 199 and the PEAT program.

Sedimentation rates

A study of paleoceanographic processes and variations of mass accumulation rates across the PEAT latitudinal transect and its evolution over time depends on a detailed knowledge of sedimentation rates. The integrated bio- and magnetostratigraphies obtained for all Expedition 320 sites will allow us to fully exploit and understand the complex interplay of productivity, dissolution, and spatial biogenic sedimentation patterns, which leave their imprint in the sedimentation rates recorded at different drill sites. Depending on the crustal subsidence and age for each site, sedimentation rates vary from site to site over time (Figs. F22, F23).

Our results reveal the change in linear sedimentation rates (LSRs) in both the latitudinal and age transect components of the PEAT program. LSRs of the middle Eocene are extremely high, frequently >10 m/m.y. and with a maximum of 18 m/m.y. at Site U1331. Rates at Sites U1332 and U1333 are similar (8–6 m/m.y.). LSRs of the late Eocene decrease to 3.5–6 m/m.y. at Sites U1331–U1333. The highest LSR peaks (>20 m/m.y.) exist in the early to late Oligocene section at Sites U1333 and 1334 and in the early Miocene for Sites U1336 and U1335. LSRs decrease uphole to <10 m/m.y. during the middle to late Miocene. LSRs also increase from the west (Site U1331) to the east (Site U1336), reflecting the relative age, depth, and latitudinal position of the sites. LSRs frequently show high rates >20 m/m.y in the east (Sites U1334–U1336) but rarely exceed 15 m/m.y. in the western sites. The LSRs of Sites 1218 and 1219 are also reflected at Site U1334 but show slightly lower values during the early Miocene (15–20 m.y.). By combining the available data from Leg 199 and Expeditions 320 and 321,

we will obtain a continuous history of sedimentation rates in the equatorial Pacific region for the past 55 m.y.

Middle Eocene Climatic Optimum

A complete downhole transition of the MECO event was recovered at Sites U1331–U1333 (Bohaty and Zachos, 2003; Bohaty et al., 2009) (Fig. F24). Based on bio- and magnetostratigraphic datums, the MECO event (40–41 Ma) occurs between magnetic Chrons C18n.1n and C18r and falls into the radiolarian Zone RP15 to lowermost RP16. Bohaty et al. (2009) revised the position of peak middle Eocene warming at 40.0 Ma in Chron C18n.2n. At Site U1333 the lithostratigraphy of the MECO event is characterized by an alternating sequence of nannofossil ooze and radiolarian nannofossil ooze interrupted by an interval of radiolarian clay as thick as 4.2 m (Fig. F24). The MECO event at Site U1332 is marked by an alternating sequence of nannofossil ooze, radiolarian nannofossil ooze, radiolarian ooze, and clayey radiolarian ooze. Site U1331 lithostratigraphy also shows an alternating sequence of nannofossil radiolarian ooze, radiolarian nannofossil ooze, and nannofossil ooze. However, at Site U1331 the interval is interrupted by coarse-grained gravity flows. These lithostratigraphic results for the MECO event are similar to those obtained from Sites 1219–1221; at Site 1222 the interval is dominated by clay (Lyle, Wilson, Janecek, et al., 2002).

Eocene–Oligocene transition

Lithology

An Eocene–Oligocene transition was recovered at four sites drilled during Expedition 320 (Sites U1331–U1334). The Eocene/Oligocene boundary as formally defined cannot be identified at these sites because of the absence of the planktonic foraminifer biostratigraphic marker *Hantkenina.* Magnetostratigraphy from APC-cored intervals and biostratigraphy (radiolarians and nannofossils) provide excellent age control, however, with the Eocene/Oligocene boundary falling just below the Magnetochron C13n/C13r reversal, near the middle of Biozone NP21, and just above the Biozone RP20/RP19 boundary. (Fig. F25).

Sites U1331–U1334 capture the lithostratigraphy of the Eocene–Oligocene transition in the equatorial Pacific Ocean in a depth transect from ~3600 to 4300 m paleowater depth (~34 Ma) (Fig. F25). At each site, a downhole transition takes place from white to pale brown nannofossil ooze of earliest Oligocene age to much darker brown sediments of Eocene age. At the deep end of the depth transect where the Eocene–Oligo-

cene transition is least expanded (Site U1331), the transition is sharp (over a ~5 cm thick interval) into homogeneous dark brown clayey radiolarian ooze. At the shallow end of the transect (Site U1334), where the correlative section is much more expanded, it is less sharp and takes place through dark clayey nannofossil chalk to alternations of dark nannofossil chalk and even darker clayey nannofossil chalk. At Site U1332 the lithologic transition is through radiolarian nannofossil ooze to radiolarian ooze with clay; at Site U1333 the transition is through radiolarian ooze to alternations of radiolarian nannofossil ooze with clay and clayey radiolarian ooze. At Sites U1332–U1334 prominent ~50 to 100 cm thick beds of particularly dark clays or radiolarian clays are noticeable (Fig. **F25**). At all sites, the line-scan core images reveal stepwise downhole transitions in sediment color (Fig. **F25**). Associated pronounced downhole stepwise increases occur in magnetic susceptibility, a*, and b*, together with pronounced downhole deceases in GRA bulk density, L*, and $CaCO_3$ content.

The lithostratigraphy of the Eocene–Oligocene transition from Expedition 320 sites is remarkably consistent with both the expedition rationale for drilling these sites and Leg 199 results and will allow the study of the early history of Cenozoic glaciation and CCD behavior (see Coxall et al., 2005; Pälike et al., 2006b) across a depth transect. Two major lithostratigraphic results from the Eocene–Oligocene transition from Expedition 320 are unexpected and also demand evaluation:

1. The discovery that the section at Site U1333 (paleowater depth = ~34 Ma; ~4000 m) is more carbonate rich than Site 1218 (paleowater depth = ~34 Ma; ~3850 m), perhaps a paleolatitudinal signal given that this site is at the northern edge of the latitudinal transect of PEAT sites during the Eocene–Oligocene; and

2. The recovery in the most expanded section (Site U1334) of darker more clay rich and yet more calcareous lithologies than at either Site U1333 or 1218 (Figs. **F25, F26**).

The multiplicity of datums throughout a major part of the Cenozoic section provided by the Nigrini et al. (2006) calibration offsets any taxonomic, abundance, or preservation problems that were encountered with a few of the species. One interval, however, has proven to be particularly troublesome: the Eocene/Oligocene boundary. This part of the section not only shows substantial turnover in the radiolarian fauna (Fig. **F27**) (Funakawa et al., 2006), it is often represented by a hiatus and is associated with reworked older Eocene radiolarians being deposited in uppermost Eocene and lower Oligocene sediments. Thus, the upper appearance limit of many Eocene species is problematic. A further complication in establishing the true age of first and last ap-

pearances of these lower Oligocene and upper Eocene species arises from the impact of missing sections on establishing a paleomagnetic stratigraphy. With part of the section missing, chron boundaries can be truncated, giving an inaccurate estimate of the age of the sediment marking that boundary. Finally, the sharp change in the CCD across the Eocene/Oligocene boundary often makes it difficult to correlate the section recovered at one site to that of another site in the same region (Fig. F28). Of all the means of making regional correlations across the Eocene/Oligocene boundary, paleomagnetic chron boundaries appear to be the most reliable (Fig. F28).

Through the many papers on the material collected during Leg 199, we have come to appreciate more fully the true stratigraphic nature of the Eocene/Oligocene boundary. From the study and comparison of these sections we have been able to identify those sites that appear to have the most complete record across this boundary. From Leg 199, Site 1218 appears to provide the most complete stratigraphic record. From this expedition, a complete boundary section appears to have been recovered at Sites U1333 and U1334; however, only Site U1333 has paleomagnetic control.

In an effort to make a detailed correlation of these three sites, we compared their magnetic susceptibility records and, where available, the paleomagnetic stratigraphy (Fig. F28). This comparison is revealing in many ways. Although Site 1218 and U1334 magnetic susceptibility records look quite similar superficially, when compared in detail they are substantially different. The two-step change in magnetic susceptibility (as well as in other geochemical variables) at the base of Chron C13n is common to Sites 1218 and U1334, as well as to Site U1333. This is one of the first indications that the Eocene/Oligocene boundary section at a site is relatively complete (e.g., Coxall et al., 2005). By simple "peak counting," the maximum in magnetic susceptibility at the top of Chron 15n is also fairly easily identifiable at Site U1334 (as well as at Site U1333). However, the broad, major peak in magnetic susceptibility seen at Site 1218 is only partially represented at Site U1334, with only the younger part of this broad maximum seen at Site U1334. It is not seen at all at Site U1333. A sharp minimum in magnetic susceptibility just below the top of Chron C17n.1n at Site 1218 can also be seen, along with similar minima at Sites U1334 and U1333. Finally, the minimum in magnetic susceptibility just below the broad maximum near the top of Chron 18n.1n is associated with the first appearance of *Calocyclas turris* at Site 1218, as well as at Sites U1334 and U1333.

The magnetic susceptibility record from Site U1333 looks very dissimilar to those of the two sites drilled on younger basement (Fig. F28). It looks more similar to those

records from Sites 1219 and 1220 that were drilled on 56 Ma crust (Fig. F29). These differences and similarities exist even though Site U1334 has fairly good preservation of calcium carbonate in the upper Eocene section, whereas at Site 1218 carbonate preservation is relatively poor and at Sites 1219, 1220, and U1333 carbonate is only occasionally present. Thus, it appears that the high-amplitude excursions in magnetic susceptibility records near the top of Chron 16n.1n are found only in sections deposited on crust that is only a few million years older than this chron (~35.5 Ma).

One would hope that the biostratigraphic record of the Eocene/Oligocene boundary region in the more complete sites would reveal a consistent record of faunal turnover. This may be true for the first appearances of species in the lower Oligocene; however, the position of the last occurrences of Eocene species within the uppermost Eocene seem to indicate that the reworking of older fossils into younger sections is common, even if there are no apparent breaks in the sections. For example, the position of the last occurrence of *Cryptocarpium azyx* at Site 1218 is considerably higher in the section than those seen at Sites U1333 and U1334 (Fig. F28). The first appearance of species in these sections is somewhat more reliable (Fig. F28), but it is the very nature of such large faunal turnovers as seen near the Eocene/Oligocene boundary that most of the biostratigraphic datums involve extinctions. Only a very detailed sampling of the section and a more quantitative analysis of the fauna can reveal when the presence of a species in a sample is likely to indicate reworking of older sediments.

Just as the rapid extinction of many Eocene species is a dramatic illustration of the impact of climate change on the planktonic fauna, the recovery from this event is also of interest. A few radiolarian species survived the transition from the warm Eocene to the cooler Oligocene (Funakawa et al., 2006), but the rapid appearance of new species did not occur until several hundred thousand years after the Eocene/Oligocene boundary at 33.7 Ma. Two lower Oligocene marker species (*Lithocyclia crux* and *Theocyrtis tuberosa*) first appear near 33.4 Ma (recalibrated age), followed by *Dorcadospyris pseudopapilio, Dorcadospyris quadripes,* and *Centroboytris gravida* near 33.0 Ma (recalibrated age) (Fig. F27). Abundant diatoms are found in the coarse fraction slides alongside the radiolarians starting in the uppermost Eocene at the same level as the first (older) step in the magnetic susceptibility record (Fig. F27), and the species makeup of this flora changes rapidly upsection. Thus, it appears that there is an increase in the productivity of larger diatoms associated with the Eocene–Oligocene transition and that the changeover of the species makeup of the flora occurs quickly in the diatoms compared to the radiolarians. Radiolarians allow the correlation of Eocene/Oligocene

boundary sections between different sites without relying directly on the lithostratigraphy (Fig. F30).

Oligocene–Miocene transition

At the end of the Oligocene a significant multimillion year–long rise in the oxygen isotope record (Lear et al., 2004) is closely followed by a relatively short, sharp increase in oxygen isotope values that has been interpreted as a major glacial episode (Mi-1) (Zachos et al., 1997, 2001a, 2001b; Pälike et al., 2006a, 2006b) and correlated to a pronounced drop in sea level (Miller et al., 1991). This event is very close to the Oligocene/Miocene boundary and has now been astronomically age calibrated in several ocean basins (Shackleton et al., 2000; Billups et al., 2004; Pälike et al., 2006a). Although there are clear periodic isotopic signals indicating major changes in ice volume, ocean temperatures, and/or ocean structure, this biostratigraphic boundary has always been somewhat of an enigma. Unlike the major changes in the isotopic stratigraphy, the biostratigraphies of the planktonic microfossils show very little change across this boundary. In fact, it is one of the most difficult epoch boundaries to pick using solely microfossil biostratigraphies.

At Sites 1218 and 1219 this interval was well recovered; however, carbonate preservation still presented a problem for foraminifer stratigraphy. Both sites were deep and well within the lysocline, making the application of temperature proxies such as Mg/Ca ratios in foraminifer tests more difficult (Lear et al., 2008). At the time Miocene–Oligocene sediments were deposited, Site 1218 already resided on 18 m.y. old crust and was ~4.1 km deep. Site 1219 was on ~34 Ma crust and was ~4.5 km deep (Lyle, Wilson, Janecek et al., 2002). A relative increase in large diatoms near this boundary in the siliceous coarse fraction suggests increased productivity; however, detailed, high-resolution flux rates across this interval have yet to be determined.

Complete sequences to the biozone and mangetochron level of the Oligocene–Miocene transition were recovered at Sites U1332–U1336 (Fig. F31), providing an excellent integrated stratigraphy. Sites U1332–U1334 display unambiguous magnetostratigraphy coherent with biostratigraphy and a distinct record of alternations in sediment constituents and physical properties. Because of Fe reduction, late Oligocene and early Miocene sediments from Sites U1335 and U1336 do not retain a sufficiently strong magnetic intensity to allow retrieval of a reliable shipboard magnetostratigraphy, but good biostratigraphic control is available. The northwesternmost Site U1331 (Fig. F1) does not record the Oligocene–Miocene transition. The

Oligocene/Miocene boundary is defined by the first occurrence of the planktonic foraminifer *Paragloborotalia kugleri* (23.0 Ma) and is approximated well by the short-lived (~100 k.y.) calcareous nannofossil *Sphenolithus delphix* (23.1–23.2 Ma) just below Chron C6Cn.2n. The Oligocene–Miocene transition in Expedition 320 sediments is characterized by alternations of nannofossil- and radiolarian/clay-dominated intervals upsection of the Oligocene/Miocene boundary at Sites U1332 and U1333 and by subtle light–dark color alternations of nannofossil ooze at Sites U1334 and U1336 (Fig. **F31**).

Miocene

Carbonate-bearing sediments were recovered primarily at Sites U1335 and U1336 during Expedition 320. At Site U1335, the early and middle Miocene are expanded and sedimentation rates are as high as 20–30 m/m.y., allowing us to achieve our Miocene specific objectives (see **"Latest Oligocene–earliest Miocene [Site U1335; 26 Ma crust],"** **"Miocene [Site U1337; 24 Ma crust],"** and **"Middle Miocene [Site U1338; ~18 Ma crust]"**). The Miocene and younger periods form the prime focus for Expedition 321.

Equatorial productivity and redox-related color changes

Relatively white nannofossil oozes are the backdrop for the vivid color changes observed midsection at Sites U1334–U1336. Sediment color shifts from brown/very pale brown to light greenish gray and white. At each of the three sites, the shift in color is illustrated by a steplike drop in b* reflectance (yellow–blue) and a near complete loss of magnetic susceptibility (Fig. **F32**). Dissolved Fe concentrations in pore fluids increase at least sixfold in the zone of greenish gray sediments. Dissolved Mn concentrations increase at least fivefold in peaks just shallower than the dissolved Fe peaks, consistent with less reducing suboxic diagenesis. The link between sediment color and suboxic diagenesis is clearest at Site U1335, where the light greenish gray color is interrupted by a small interval of very pale brown before returning to greenish gray again. That very pale brown interval corresponds to a pronounced dip in dissolved Fe and a small increase in dissolved Mn. Together with the loss of magnetic properties, increases in dissolved Fe concentrations and changes in sediment color indicate intensified microbial Fe reduction, perhaps fueled by higher organic carbon accumulation rates across this interval. The intensification of suboxia at depth is largely controlled by site location with respect to the core of the equatorial upwelling system (Figs. **F6, F32A**). The greenish gray coloration is restricted to the time interval when

each site was located south of 3°N. This pattern of geographic control on organic matter deposition and sediment diagenesis is supported by sediment color change observations in three additional DSDP sites (78, 79, and 574) (Fig. **F32B**). Further postcruise research will establish to what extent geochemical proxies of organic matter productivity, burial, and degradation contribute to the observed patterns, following Olivarez Lyle and Lyle (2005).

Geochemistry

Bulk sediment geochemistry: sedimentary carbon

A high-priority objective of the PEAT program is to reveal the history of CCD fluctuations during the Cenozoic. The findings resulting from >1000 coulometric carbonate measurements (Fig. **F33**) are described in **"Cenozoic CCD in the equatorial Pacific"** (Fig. **F14**). Calcium carbonate, inorganic carbon (IC), and total carbon (TC) concentrations were determined on sediment samples from every hole at Sites U1331–U1335 and Hole U1336A (TC was not determined in Hole U1336A during Expedition 320 and will instead be determined during Expedition 321).

We measured TC and total organic carbon (TOC) at a similar sample resolution and determined very low TOC concentrations, as previously found during Leg 199 (Lyle, Wilson, Janecek, et al., 2002; Olivarez Lyle and Lyle, 2005). TOC concentrations were determined separately by a difference method and by an acidification method for Site U1331. However, we concluded that the TOC concentrations determined by the normal difference method might be overestimates in high-percent $CaCO_3$ and very low percent TOC sediments because they were determined as a small difference between two numbers comparable in magnitude. Therefore, TOC analyses were performed only by the acidification method, in which TOC was determined by using carbonate-free sediments after treatment by acidification for Sites U1332–U1335. Using this acidification technique, we reduced the detection limit for TOC measurements to 0.03 wt%. TOC concentrations in sediments determined by this method are very low throughout the sediment column and near or below the detection limit for samples (below 0.04%) from Sites U1331–U1335 (Figs. **F34, F35**). TOC concentrations tend to be slightly higher at those depths where $CaCO_3$ concentrations are low at Sites U1332–U1335. The maximum TOC value determined is 0.18% in surface sediments from Site U1332. Despite the very low TOC values across the PEAT sediments recovered, postcruise research will be able to measure biomarkers and alkenones from some

of the more organic rich sediments, addressing Objectives 2, 4, and 9 (see **"Scientific objectives"**).

Interstitial water profiles: Si, Sr, and Li

Dissolved silicate increases with depth at each of the Expedition 320 sites to values as high as 1000 µM, at or near saturation with biogenic silica (Fig. **F36**). The increases with depth are generally larger for those sites with larger thermal gradients and higher heat flow, reflecting a temperature dependence of biogenic silica dissolution. In addition, one site shows a pronounced decrease in the depth zone of the Eocene/Oligocene boundary (Site U1332). Although chert was present at some of the sites, no pronounced decreases in dissolved silicate were found.

Interstitial water geochemistry profiles of the different sites drilled during Expedition 320 show considerable differences in respect to dissolved Sr^{2+} concentrations (Fig. **F37**). Whereas Site U1331 shows little variability with depth, Sites U1332–U1336 reveal increasing variability of Sr^{2+} concentrations. At Sites U1331 and U1332, Sr^{2+} shows mainly concentrations around seawater values; Sr^{2+} increases at Sites U1333 and U1334 up to ~110 µM, at Site U1335 up to 250 µM, and at Site U1336 up to 430 µM. Site U1335 is characterized by a pronounced increase in Sr^{2+} with depth followed by a strong decrease toward basement to seawaterlike concentrations. A similar pattern is revealed for Sites 1333 and 1334, but it is considerably less pronounced and developed. This pattern indicates the influence of carbonate diagenesis and or recrystallization, releasing Sr^{2+} to the pore fluid at intermediate depth, and the flow of relatively unaltered seawater through basement and diffusion between end-members. Strontium at Site U1336 is characterized by a steady increase in concentration with depth, indicating, together with the increase in Ca^{2+} and decrease in Mg^{2+}, the influence of a fluid that reacted with the basement. The limited variability of Sr^{2+} at Sites U1331 and U1332 might be related to the relatively thin sediment thickness preventing the establishment of large gradients.

Similar to Sr^{2+}, Li^+ shows considerable differences between the different sites of Expedition 320, with the least variability at Sites U1331–U1333 and increasing depletion of Li^+ in the pore fluid at Sites U1334 (down to 15 µM), U1336 (down to 7 µM), and U1335 (down to 4 µM) at intermediate depth (Fig. **F38**). Near basement, Li^+ increases again toward seawaterlike values. Profiles of Li^+ in the pore fluid indicate diagenetic reactions in the sediments consuming Li, possibly low-temperature clay alteration. Li concentrations similar to seawater values are compatible with observations of Sr, suggesting the flow of relatively unaltered seawater through the oceanic crust.

Seismic stratigraphy and integration

Objective 6 of the PEAT program (see **"Scientific objectives"**) is to establish the age and lithologic origin of the seismic reflections previously identified in the eastern equatorial Pacific and make use of the high level of correlation between tropical sedimentary sections and existing seismic stratigraphy to develop a more complete model of equatorial circulation and sedimentation (Lyle et al., 2002a, 2006). We achieved this objective by calculating synthetic seismograms made from bulk density and sonic velocity data from core material and downhole logs.

The known depths and two-way traveltimes (TWTs) to the seafloor and basement provided an initial depth to TWT model and average sonic velocity for the sediment cover. The depth to TWT model was then adjusted to bring the reflectors in the synthetic seismogram into line with the corresponding reflectors in the seismic section. Typically, only a small number of adjustments were needed to give a good match. An example from Site U1331 is given in Figure **F39.**

Downhole logging at two sites represents the petrographic signals between radiolarian and nannofossil ooze using density, conductivity, and magnetic susceptibility, which are more useful in understanding the lithology in the poor recovery intervals composed of chert and porcellanite. In addition, a hard lithified limestone altered by hydrothermal activity occurred within 10–20 m above basement at most drilling sites. Correlation between seismic profiles and drilling is important in understanding an estimation of basement age and thickness of sedimentary sequences. At Site U1335 the thickness is estimated to be 361 m, but 420 m of sediment was recovered above the basement. Thus, our results contribute to the drilling strategy of the next PEAT Expedition 321 and future drilling in the equatorial Pacific.

MORB age transect

An age transect of sediments on top of basaltic basement in the equatorial Pacific region was recovered during Expedition 320. Basement ages represent eastward younging from Site U1333 to U1336 (Fig. **F16**). Basement basalts are covered by hard lithified limestones spanning from early Eocene through early Miocene age except at Site U1332, where zeolitic clays were recovered above basalt. These clays yielded poorly preserved calcareous nannofossils, and the position of the clays may be due to hydrothermal alteration. At Site U1331, however, a typical calcareous ooze with high carbonate contents containing abundant planktonic foraminifers and calcareous

nannofossils was recovered as observed at Site 1221. Basement basalts are highly altered with a spherulithic texture, whereas ferromagnesian minerals (mainly clinopyroxene) are replaced by chlorite. Thin section analysis indicates a sparsely phyric basalt mainly composed of phenocryst plagioclase.

Chert and porcellanite occurrence

Sites U1331–U1333 and U1336 recovered chert and porcellanite (Fig. F40). Cherts are characterized by their hardness and highly silicified matrix in which sediments are cemented with microcrystalline quartz. Primary pore spaces (e.g., within chambers of foraminifers and radiolarians) are sometimes filled with chalcedony. Porcellanites are silicified to a lesser extent and are richer in clay minerals than the cherts. Porcellanite is much more abundant than chert at Sites U1331–U1333, whereas Site U1336 contains mostly chert. Porcellanite-bearing intervals at Sites U1331–U1333 correspond to a time interval between early Eocene and early middle Eocene (~42 Ma), roughly coincident with the chert-rich intervals at Sites 1220–1222 recovered during Leg 199 (Fig. F40). At Sites U1331 and U1332, porcellanite layers are associated with thin clay horizons interbedded with radiolarian ooze. Oligocene chert layers from Site U1336 show various colors such as greenish gray, dark gray, pink, and black and contain abundant foraminifers that are occasionally replaced with microcrystalline quartz and pyrite.

Porcellanites are interbedded with radiolarian ooze and nannofossil ooze in the early middle Eocene interval at Sites U1332 and U1333 (Fig. F40). Cherts are also interbedded with nannofossil ooze and chalk in the Oligocene interval at Site U1336. In stratigraphic intervals from the early Eocene through earliest middle Eocene at Sites U1331 and U1332, the presence and original structures of porcellanite are not clear because of poor core recovery.

At the base of the sections recovered there was always an interval in which all biogenic silica had been dissolved and which was barren of radiolarians. This "silica free zone" (SFZ) is usually not thick—only 7 to 16 m at most of the sites drilled (Table T2). This is well within the usual 1 to 40 m thickness of the SFZ described by Moore (2008a) for Pacific open-ocean sections recovered by scientific ocean drilling. Moore (2008a) associated this dissolution zone with the circulation of hydrothermal waters in the upper oceanic crust and related the silica removed by this process to the ultimate formation of cherts. Thus, the final site drilled, Site U1336, stands out as very unusual. It has a SFZ of almost 130 m, with abundant chert stringers and lithified sed-

iments below ~170 m in the section. This suggests that hydrothermal waters may actually invade well up into the section near this site, possibly along more permeable, small-offset faults.

Heat flow measurements

Geothermal gradient and heat flow values were determined at Sites U1331–U1335 from in situ temperature measurements made using the advanced piston corer temperature tool (APCT-3). At least four APCT-3 deployments were made per site, to a maximum depth of 106 m. Bottom water temperature was also determined for each site, with values ranging from 1.44° to 1.47°C. Linear geothermal gradients obtained from these data ranged widely from 7.4°C/km at Site U1335 to 75.0°C/km at Site U1332.

Heat flow was calculated according to the Bullard method, to be consistent with the Leg 199 analyses and the synthesis of ODP heat flow data by Pribnow et al. (2000). Similar to the geothermal gradients, Site U1335 had the lowest heat flow, 6.9 mW/m², and Site U1332 the highest, 70.7 mW/m² (Fig. F41). These heat flows are within the range of values in the eastern equatorial Pacific heat flow data set maintained by the International Heat Flow Commission (Pollack et al., 1993).

The wide range of values emphasizes the possibility that local crustal hydrothermal circulation is strongly influencing heat flow values. Results from the PEAT expeditions will also provide heat flow information in an area of the Pacific Ocean that has only a sparse existing heat flow data set.

Gravity flow deposits

Throughout the sedimentary section drilled at Sites U1331 and U1335, sharp irregular contacts are present between lithologies (Fig. F42). Many are recognizable by distinct changes in color. Sharp contacts, occasionally associated with an erosional basis, are often overlain by coarser grained, more carbonate rich (including planktonic and benthic foraminifers), and/or opaque-coated sediments than those below the contact. At Site U1335 angular basalt fragments, pyritized foraminifers and/or radiolarians, and fish teeth are often present at the base of the gravity flows. The overlying sediments fine uphole and in some cases show cross or parallel laminations in the middle of the bed. These features indicate that the erosional contacts and their overlying coarse sediments at both Sites U1331 and U1335 are the product of mass flow events,

typically turbidity currents. Commonly, turbidite thickness is between 2 and 25 cm, with the maximum thickness of 176 cm found at Site U1335. The total thickness of the identified turbidites at Site U1335 occupies at least 2% of the recovered sediment. The provenance of the inferred turbidites observed at Site U1331 is unknown, but their typically calcareous composition points to a source that lay above the CCD at the time that the reworked sediments were originally deposited, possibly a seamount lying a few kilometers south of the drilled location. A similar provenance of turbidites is proposed for Site U1335, where two seamounts lie ~15–20 km to the northeast and southeast of the drilled location.

Site U1331

Three holes were cored at Site U1331 (12°04.088′N, 142°09.708′W; 5116 m water depth), which is the northwesternmost site drilled during the PEAT program (Fig. **F43**). At Site U1331, Eocene age seafloor basalt is overlain by 187.2 m of pelagic sediment, comprising radiolarian and nannofossil ooze with varying amounts of clay. For detailed coring activities, see **"Site U1331"** in "Operations."

The sediment column at Site U1331 has a strong resemblance to that of Site 1220 (Fig. **F44**) (Lyle, Wilson, Janecek, et al., 2002) but with noteworthy sharp erosive contacts concentrated within the upper two-thirds of the section (Fig. **F45**). A total of 7 m of Pleistocene–Pliocene clay overlies lower Oligocene to early Eocene alternations of nannofossil ooze, radiolarian nannofossil ooze, and radiolarian oozes of varying clay and calcium carbonate content, with a sharp lithologic change at the Eocene–Oligocene transition (~26 m CSF-A). The lowermost target interval is characterized by a ~20 m thick radiolarian ooze and porcellanite layer from 157 to 177 m CSF-A, overlying a sometimes clayey radiolarian ooze and zeolitic clays with hydrothermal red staining from 177 to 187.5 m CSF-A, deposited on top of a thin (187.6–188.5 m CSF-A in Hole U1331C) layer of calcareous ooze and zeolitic clay above the basalt. Some of the fine-grained basaltic fragments show fresh glassy chilled margins.

Carbonate content approaches 80% in the Oligocene nannofossil oozes in the upper part of the site and cycles between 0% and 40% in the middle Eocene section. There is a concentration of sharp erosive contacts in the interval between 80 and 120 m CSF-A, with calcareous material dominating the basal portion of these contacts and then fining upward in grain size into radiolarian oozes. Rarely, the sediment above a sharp contact contains well-rounded clasts up to 1 cm in diameter (interval 320-U1331B-10H-6, 117–130 cm). The lithologic and stratigraphic characteristics of these sedi-

ments have been interpreted as gravity-driven deposits, possibly from nearby sea-mounts ~10 km to the south (Fig. **F43B**). Between ~177 and 188.5 m CSF-A, Cores 320-U1331A-22X, 320-U1331C-16H, and 17H achieved our site objective of recovering carbonate-bearing material from the time interval just following 52 Ma.

All major microfossil groups were found in sediments from Site U1331, and they provide a consistent and coherent biostratigraphic succession from basement to below the surficial clay layer. Nannofossils are common in the Oligocene and lower Eocene but sporadic in sediments from the upper Eocene, probably because of dissolution. Middle Eocene sediments commonly contain calcareous nannofossils punctuated by several barren intervals, notably below Zone NP21 (radiolarian Zone RP19 equivalent), below NP17, and between NP15 and NP13 (radiolarian Zones RP12–RP8 equivalent). Radiolarians are common to abundant throughout the section. Radiolarian and nannofossil datums and their age determinations agree and range from nanno-fossil Zone NP12 in the basal sediment section (~51–53 m.y. before present) to NP23/24 and radiolarian Zones RP8 just above basement through RP21 (late Oligocene, older than 25 Ma) in the uppermost section, below the Pleistocene clays. Both radio-larian and nannofossil assemblages contain reworked, older components (deeper than ~50 m CSF-A) but within a coherent and ordered stratigraphy. Planktonic fora-minifers are generally absent, except for sporadic samples often associated with sediment just above sharp lithologic contacts and also in the basal carbonate section (provisionally Zones E4/E5). Benthic foraminifers are generally rare and indicate lower bathyal to upper abyssal paleodepths. They are also frequently found in the graded coarse sediment above the base of sharp contacts but suggest there is no apparent difference in the depth habitat between benthic foraminifers from just above sharp contacts and other parts of the section. Diatoms are observed throughout the column and, once analyzed by specialists not onboard during Expedition 320, will contribute to the stratigraphic integration of the PEAT program.

Apparent sedimentation rates, as implied by the biostratigraphic age determinations and aided by magnetostratigraphic polarity interpretations, vary throughout the section. The radiolarian-rich section below ~80 m CSF-A and basement was deposited at an average rate of 10 m/m.y., whereas the late middle Eocene to Oligocene section was deposited at a rate of ~4 m/m.y., with an apparent inflection between 60–80 m CSF-A. The porcellanite horizon spans a time interval of ~2–3 m.y. The presence of all major fossil groups as well as a detailed magnetostratigraphy will allow us to achieve one of the main PEAT objectives to arrive at an integrated Cenozoic stratigraphy and age calibration (e.g., Pälike et al., 2006b).

A full physical property program was run on cores from all three holes, comprising Whole-Round Multisensor Logger (WRMSL) measurements of magnetic susceptibility, bulk density, *P*-wave velocity, noncontact resistivity, and natural gamma radiation (NGR), followed by discrete measurements of color reflectance, index moisture and density properties, sound velocities, and thermal conductivity. Bulk density measurements show a marked increase in the carbonate-rich Oligocene section. Magnetic susceptibility measurements are variable throughout the section, allowing a detailed correlation between different holes and picking out sharp contacts and clay layers by increased susceptibilities. NGR measurements are elevated by an order of magnitude in the surficial clay layer and reach 130 counts per second (cps) at the seafloor, dropping to <5 cps below 30 m CSF-A. Porosity values are generally high in radiolarian-rich sediments (80%) and decrease within the Oligocene carbonate section. Carbonate content is positively correlated with thermal conductivity. Discrete physical property measurements will prove useful to calibrate WRMSL velocity and density estimates and generally agree with WRMSL estimates, once appropriate correction factors are included for the core liner. Discrete velocities are significantly higher (50–100 m/s) than track measurements in the direction perpendicular to the split plane of the core section (*x*-axis), which is likely an artefact.

Using whole-round magnetic susceptibility measurements, Holes U1331A–U1331C can be spliced to form a continuous section to at least 140 m CSF-A or 150 m core composite depth, method A (CCSF-A; when using method A, core expansion lengths are appended if longer than 9.5 m), with no apparent gaps. Core expansion is ~15%. It is possible that Hole U1331C cores can provide an additional spliced section to the top of the porcellanite interval at ~157 m CSF-A. Below 149 m CCSF-A, it was only possible to tentatively correlate features in the track data down to Core 320-U1331A-17X for a total composite section of ~172 m CCSF-A.

A full range of paleomagnetic analyses was conducted on cores and samples from Site U1331. Our aims are to determine the magnetostratigraphy and study geomagnetic field behavior, environmental magnetism, and Pacific plate paleogeography. Shipboard analyses conducted so far suggest that a useful magnetic signal is preserved in almost all APC-cored intervals. Preliminary comparison of biostratigraphic data and changes in magnetic paleodeclinations suggest the recovery of Oligocene magnetochrons to the base of the middle Eocene (Chron C21n; ~47 Ma). Paleomagnetic directions from discrete samples agree well with those from split-core results.

A standard shipboard suite of geochemical analysis of pore water and organic and inorganic properties was conducted on sediments from Site U1331, including a pilot study of high-resolution "Rhizon" pore water sampling, which does not require the cutting of core whole rounds for squeezing. Carbonate coulometry yielded carbonate concentrations of ~80% in the Oligocene nannofossil ooze and sporadic horizons with up to 40% $CaCO_3$ in the middle Eocene radiolarian-rich oozes. Preliminary calcium carbonate determinations from the white, hydrothermally stained sediments just above basement (whole-round Sample 320-U1331C-17H-4, 83–84 cm) yielded low values of only 2%–3% $CaCO_3$. Alkalinity values range between 2.5 and 3 mM throughout the section. Additional ephemeral samples were taken for shore-based microbiology and permeability studies.

Wireline logging provided valuable information to constrain the interval of chert or porcellanite formation within the borehole, and further analysis will aid in interpretations of carbonate content and lithologies. Integration with the seismic data will allow further improvements with the regional seismic interpretations. Data from Site U1331 indicate that the top of seismic Horizon "P2" (Lyle et al., 2002a) correlates with the top of the chert section. Downhole temperature measurements with the APCT-3 tool, when combined with the thermal conductivity values obtained from the cores, indicate that Site U1331 had a heat flow of ~10.4 mW/m² and a thermal gradient of 13.4°C/km. This is within the range of the lower values in the global heat flow data set for the eastern Pacific but significantly lower than values obtained for Sites 1218 and 1219.

Highlights

Carbonate ooze in basal section

At Site U1331 we recovered a 1.2 m thick interval (lithologic Unit IV) of calcareous ooze with concretions and reddish color streaks, achieving one of the objectives for this site. The nannofossil ooze recovered in Section 320-U1331A-22X-CC contains a moderately to poorly preserved assemblage of early Eocene planktonic foraminifers (planktonic foraminifer Zone E5). This moderately preserved assemblage was also observed in the basal section of Hole U1331C.

Stratigraphic integration

One of the primary objectives of the PEAT science program is the integration of different stratigraphic methodologies and tools. Site U1331 contains almost all major fossil groups (nannofossils, radiolarians, foraminifers, and diatoms), as well as an ex-

cellent magnetostratigraphy. The possibility of a cycle-by-cycle match between Sites U1331 and 1220 has been demonstrated using magnetic susceptibility and bulk density data, providing additional stratigraphic tie points and verification of the completeness of the stratigraphic section on a regional scale. Thus, Site U1331 will help us to achieve an integrated stratigraphy for the Cenozoic Pacific Ocean.

Eocene–Oligocene transition and depth transect

Site U1331 forms the oldest and deepest component of the PEAT depth transect, which will allow the study of critical intervals (such as the Eocene–Oligocene transition; see Coxall et al., 2005) and variations of the equatorial CCD. Site U1331 is estimated to have been ~4.2 km deep during the Eocene–Oligocene transition, ~800 m shallower than today. Sediments rapidly change from radiolarian ooze below the transition to nannofossil oozes above and will provide a tie point for calcium carbonate burial at ~5° paleolatitude.

Variations in the CCD

Site U1331 will provide important constraints for variations and depth of the CCD from the early Eocene to the late Oligocene. This site shows increased carbonate content and much increased mass accumulation rates approximately from the middle of Magnetochron C18r to the base of C19r during the middle Eocene and can be correlated to an interval of enhanced carbonate burial that was previously documented by Lyle et al. (2005) at Leg 199 cores.

Age transect of seafloor basalt

At Site U1331 we recovered what appear to be fresh fragments of seafloor basalt, aged between 52 and 53 Ma. This material will, when combined with other PEAT basalt samples, provide important sample material for the study of, for example, seawater alteration of basalt and paleomagnetic studies.

Site U1332

Three holes were cored at Site U1332 (11°54.722′N, 141°02.743′W; 4924 m water depth) (Fig. F46), which is the second northwesternmost site drilled during the PEAT program. At Site U1332 Eocene age seafloor basalt is overlain by 150.4 m of pelagic sediment, comprising radiolarian and nannofossil ooze with varying amounts of clay and zeolitic clay. Hole U1332A provided high-quality and high-recovery APC-cored sediments from the mudline to 125.9 meters below seafloor (mbsf) (Core 320-U1332-

14H), where we encountered chert and after which we switched to the extended core barrel (XCB) cutting shoe. XCB coring advanced to 152.4 m drilling depth below seafloor (DSF) through a ~10 m thick porcellanite-rich interval with reduced recovery. In the basal section, we recovered a short, ~3.8 m long interval of barren very dense and stiff clay above basalt, ~10 m shallower than predicted from the seismic profile, in Core 320-U1332A-18X. Basement was reached at 152.4 m CSF-A. For detailed coring activities, see **"Site U1332"** in "Operations."

The sediment column at Site U1332 has a strong resemblance to that of Site 1220 (Lyle, Wilson, Janecek, et al., 2002). The uppermost 17.7 m of section is a late Miocene to Pleistocene–Pliocene clay, with varying amounts of radiolarians and zeolite minerals, overlying ~130 m of Oligocene to middle Eocene nannofossil and radiolarian ooze with porcellanite deep in the section. A thin ~3 m thick unit of middle Eocene zeolite clay bearing small chert nodules was recovered at the base of the sedimentary sequence, above basaltic basement. The sedimentary sequence at Site U1332 was divided into five major lithologies (Fig. **F47**).

The upper stratigraphy at Site U1332 has a strong resemblance to that of Site U1331, but without the sharp erosive contacts described at Site U1331. Several meters of white to beige-colored Pleistocene–Pleiocene clay (lithologic Unit I) overlie lower Miocene to lowermost Oligocene nannofossil ooze (Units II and III). There is a sharp lithologic change at the Eocene–Oligocene transition (multiple recovery due to slumping within Cores 320-U1332A-8H, 9H, 320-U1332B-9H, and 320-U1332C-9H) to alternating radiolarian ooze with nannofossils and nannofossil ooze (Subunit IVa). The lithology then gradationally changes downhole into radiolarian ooze with nannofossils and clay intercalated with the sporadic presence of chert (Subunit IVb) and a basal cherty interval (Subunit IVc, down to at least 138 m CSF-A). Lithologic Unit V, below the chert horizon and between ~138 to at least ~147 m CSF-A, is composed of very dark grayish brown to black clay, very dark grayish brown to black zeolite clay, and chert. The sediments directly above basaltic basement are partially lithified. Basalt is designated as lithologic Unit VI, at ~150 m CSF-A.

Carbonate content approaches 85% in Unit III within the Oligocene nannofossil oozes and cycles between 0% and 40%–60% in the middle Eocene section (Unit IV) (Fig. **F48**). All major microfossil groups were found in sediments from Site U1332 and provide a consistent, coherent, and high-resolution biostratigraphic succession from basement to the top of Unit II. Calcareous nannofossils are abundant and moderately well preserved in the Oligocene and poor to moderately well preserved in the Mio-

cene and Eocene. Most of middle Eocene sediments commonly contain nannofossils, with several barren intervals. Radiolarians are common to abundant throughout most of the section, apart from the lowermost sediment section above basalt, and are well preserved in the Eocene. Radiolarian and nannofossil datums and zonal determinations agree, ranging from nannofossil Zone NP13/14 in the basal dark clay section (~48.4–50.7 m.y. before present, Ma) to NN1 and radiolarian Zones RP13 above basement through RN1 (lowermost Miocene, ~22.3 Ma) below the upper Pliocene–Pleistocene clay cover in Core 320-U1332A-3H (Fig. F48). Planktonic foraminifers are generally rare throughout the Oligocene but are absent in the Miocene and Eocene. Benthic foraminifers are present through most of the section but are rare in Miocene and Eocene sediments. They indicate lower bathyal to abyssal paleodepths. Diatoms were observed throughout the column but will have to await analysis by specialists not onboard Expedition 320. Apparent sedimentation rates, as implied by biostratigraphic age determinations, vary throughout the section and are ~5 m/m.y. in the Eocene section and ~2.5 m/m.y. in the Oligocene, with two prominent hiatuses in the Miocene and between the Miocene and younger sediments. The presence of all major fossil groups as well as a detailed and well-resolved magnetostratigraphy will allow us to achieve one of the main PEAT objectives, to arrive at an integrated Cenozoic stratigraphy and age calibration (e.g., Pälike et al., 2006b) for major parts of the Oligocene and Eocene.

Magnetostratigraphic studies as well as high-resolution biostratigraphy and stratigraphic correlation determined that a ~4 m interval from the base of Core 320-U1332A-8H was repeated in the top of Core 320-U1332A-9H, which comprises Magnetochron C13n, and the lowermost Oligocene. This repetition also occurs in Cores 320-U1332B-8H and 9H and within Core 320-U1334C-9H. The lithologic succession from the lower occurrence of Chron C13n downhole as well as from the upper occurrence of Chron C13n uphole both appear complete and continuous, and hence Site U1332 achieved the fortuitous feat of recovering the complete Eocene–Oligocene transition four times and the upper part of Magnetochron C13n five times at a triple-cored site.

A full physical property program was run on cores from all three holes, comprising WRMSL measurements of magnetic susceptibility, bulk density, *P*-wave velocity, non-contact resistivity, and NGR, followed by discrete measurements of color reflectance, index moisture and density properties, sound velocities, and thermal conductivity. Bulk density measurements show a marked increase in the carbonate-rich Oligocene section, as well as in carbonate-bearing horizons in the Eocene (CAE cycles; Lyle et al.,

2005). Magnetic susceptibility measurements are variable throughout the section, allowing a detailed correlation between holes. NGR measurements are elevated by an order of magnitude in the surficial clay layer. Porosity values are generally high in the radiolarian-rich sediments (85%) and decrease in the Oligocene and Eocene carbonate section, which also shows higher thermal conductivity values of ~0.9 to 1.2 W/(m·K), compared with ~0.8 W/(m·K) in the radiolarian oozes and surficial clay.

Stratigraphic correlation allowed us to obtain a composite section to ~125.5 m CSF-A near the top of the cherty interval in Hole U1332A, equivalent to a composite depth of ~140 m CCSF-A. The overall core expansion (growth factor), which is caused by core expansion and calculated by the ratio between the CCSF-A and CSF-A (formerly meters composite depth [mcd] and mbsf) depth scales, is ~10%. The tops of APC cores were often affected by ~3 m heave that occurred during operations at Site U1332. Stratigraphic correlation supports the biostratigraphic, paleomagnetic, and sedimentologic description of a repeated sequence, possibly due to slumping, spanning the Eocene–Oligocene transition.

A full range of paleomagnetic analyses was conducted on cores and samples from Site U1332 and resulted in a spectacularly well resolved magnetostratigraphy. Shipboard analyses suggest that a useful magnetic signal is preserved in all APC-cored intervals and that it was possible to remove the drilling-induced steep inclination overprint after demagnetization. Comparison of biostratigraphic data and changes in magnetic paleodeclinations suggests the recovery of magnetic reversals C1n/C1r.1r to C2An.3n/C2Ar above a hiatus and then a continuous sequence of magnetic reversals from C5En/C5Er (18.52 Ma) in the Miocene at ~12.95 m CSF-A (interval 320-U1332C-2H-4, 95 cm) to C19r/C20n (42.54 Ma) at interval 320-U1332A-14H-5, 80 cm. Magnetostratigraphic interpretation supports the presence of a slump through multiple recovery (five times) of parts of Chron C13n in a triple-cored sequence. Paleomagnetic directions from discrete samples agree well with those from split-core results.

A standard shipboard suite of geochemical analysis of pore water and organic and inorganic properties was conducted on sediments from Site U1332. Alkalinity values increase from ~2.2 to 3.4 mM downsection, and Sr^{2+} increases from ~80 to ~110 µM. H_4SiO_4 remains relatively stable between 400 and 600 µM above 90 m depth in the Oligocene nannofossil oozes but increases to 800–1000 µM in the Eocene silica-rich radiolarian oozes, approaching opal solubility values. Carbonate coulometry yielded carbonate concentrations of ~85% in the Oligocene nannofossil ooze and horizons with up to 60% $CaCO_3$ in the middle Eocene radiolarian-rich oozes. TOC concentra-

tions were measured both by difference between TC and total IC as well as by using an acidification method. Using the acidification method, TOC values were <0.3% for all measured samples. The top ~5 m shows values of 0.2% TOC. Between ~40 and 70 m CSF-A the measurements indicate TOC below the detection limit of 0.03%. Between ~90 and 150 m CSF-A three peaks reach ~0.2% to 0.27% TOC. We conducted a high-resolution Rhizon pore water experiment across the prominent alkalinity trough around 40 m CSF-A, which highlighted differences between squeezed and Rhizon-sampled pore waters. Additional ephemeral samples were taken for shore-based microbiology and permeability studies.

Wireline logging provided valuable information to constrain the interval of chert formation within the borehole. Downhole NGR, density, and magnetic susceptibility logs provide important constraints on the poorly recovered lithologies below and between cherty horizons. The logging data document the presence of two thin chert or porcellanite horizons at ~126 and 130 m wireline log depth below seafloor (WSF) and an ~14 m thick interval of increased magnetic susceptibility, reduced conductivity, and enhanced density and photoelectric factor that appears to be the dark and dense clays and zeolitic clays above basement, rather than carbonate. Integration with the seismic data will allow further improvements with the regional seismic interpretations. Data from Site U1332 indicate that the top of seismic Horizon P2 (Lyle et al., 2002a) correlates with the top of the chert section, just as it did for Site U1331. No Formation MicroScanner (FMS) data were collected, as it was not possible to retrieve the "Paleo-" triple-combo tool string back into the bottom-hole assembly. Eight downhole temperature measurements were conducted in Holes U1332B and U1332C with the APCT-3 tool. Three of these yielded good data; the other measurements were impaired by strong, sometimes >3 m heave during operations in Hole U1332B.

Downhole temperature measurements, when combined with the thermal conductivity values obtained from the cores, indicate that Site U1332 had a heat flow of ~70.6 mW/m^2 and a thermal gradient of 75.6°C/km. This is significantly higher than the values obtained for Site U1331 but comparable to values obtained for Sites 1218 and 1219.

Highlights

Shallow early Eocene CCD

Coring at Site U1332 was designed to capture a very short period of time (~2 m.y.) at ~50 Ma during which this site was thought to be located above the very shallow Eo-

cene CCD (~3.3 km) (Lyle, Wilson, Janecek, et al., 2002; Rea and Lyle, 2005) just after the EECO (Zachos et al., 2001a). Unlike Site U1331, at Site U1332 we cored a ~10 m thick section of dense and dark brown clays, zeolite clays, and chert above basement. This finding will provide important new constraints on the depth of the CCD at ~48–50 Ma at the paleoequator, indicating that the CCD was shallower than previously thought.

Stratigraphic integration

One of the primary objectives of the PEAT science program is the integration of different stratigraphic methodologies and tools. Site U1332 contains all major fossil groups (nannofossils, radiolarians, foraminifers, and diatoms), as well as an excellent magnetostratigraphy and composite depth correlation, which can be tied to nearby Leg 199 sites (e.g., Site 1220) by way of physical property variations. The possibility of a cycle-by-cycle match between Sites U1332 and 1220 has been demonstrated using magnetic susceptibility and bulk density data, providing additional stratigraphic tie points and a verification of the completeness of the stratigraphic section on a regional scale. Thus, Site U1332 will help us to achieve an integrated stratigraphy for the Cenozoic Pacific Ocean, ranging from the Miocene to the middle Eocene.

Eocene–Oligocene and Oligocene–Miocene transitions and depth transects

Site U1332 forms the second oldest and deepest component of the PEAT depth transect, which will allow the study of critical intervals (such as the Eocene–Oligocene transition; see Coxall et al., 2005) and variations of the equatorial CCD. Site U1332 is estimated to have been ~4 km deep during the Eocene–Oligocene transition, ~1 km shallower than today and 200 m shallower at that time than Site U1331. Sediments rapidly change from radiolarian ooze below the transition into nannofossil oozes above, and unlike Site U1331, Site U1332 also contains carbonate-bearing sediments across the Oligocene–Miocene transition (e.g., Zachos et al., 2001b). For the Eocene–Oligocene transition, Site U1332 will provide a tie point for calcium carbonate burial at ~4° to 5° paleolatitude.

Variations in the CCD

Site U1332 has provided important constraints for variations and depth of the CCD from the early Eocene to the late Miocene. This site shows increased carbonate content and much increased mass accumulation rates approaching 200 mg $CaCO_3$/cm²/k.y. around the middle of Magnetochron C18r to the base of C19r during the middle Eocene and can be correlated to an interval of enhanced carbonate burial that was

previously documented by Lyle et al. (2005) at Site 199 cores. The high early Oligocene $CaCO_3$ concentrations decrease significantly in sediments younger than ~27 Ma. By ~22 Ma, in the early Miocene, carbonate was no longer preserved. This is presumably related to Site U1332 sinking below the prevalent CCD and coincides with a CCD shoaling event between ~20 and 15.5 Ma described by Lyle (2003).

Formation of porcellanite

Together with Site U1331, Site U1332 provides important new information on the formation of porcellanite and chert. Coring has shown that the top of the porcellanite-rich interval is mapped by seismic Horizon P2 (Lyle et al., 2002a). In lithologic Subunit IVc, layers and pebbles of very dark brown partially to well-lithified mudstones, often layered or even laminated, are observed within alternating sequences of nannofossil ooze and radiolarian ooze of late to late middle Eocene age. In hand-specimen, the partially lithified mudstones are particularly rich in clay and show evidence of partial secondary silicification. Pieces of porcellanite contain clay minerals, microcrystalline quartz, opaques, and calcite, as well as biogenic shells and fragments from radiolarians and foraminifers. Sediments from Sites U1331 and U1332 appear to document the silicification process in clay-rich horizons near basement, which will likely extend the findings of Moore (2008b).

Age transect of seafloor basalt

At Site U1332 we recovered what appear to be fresh fragments of seafloor basalt, aged between 49 and 50 Ma. This material will, when combined with other PEAT basalt samples, provide important sample material for the study of seawater alteration of basalt.

Site U1333

Three holes were cored at Site U1333 (10°30.996′N, 138°25.159′W; 4853 m water depth) (Fig. **F49**). At Site U1333, Eocene age seafloor basalt is overlain by ~183 m of pelagic sediment, dominated by nannofossil and radiolarian ooze with varying amounts of clay (Fig. **F50**).

In Hole U1333A, APC-cored sediments were recovered from ~3 m below the mudline (~4850 m water depth) to 95 m CSF-A (Core 320-U1333A-10H). XCB coring advanced to 184.1 m DSF through an ~60 m thick sequence of lowermost Oligocene carbonate oozes and nannofossil-bearing Eocene sediments. Near the basal section, we recov-

ered a 30 cm long interval of lithified carbonate in Core 320-U1333A-20X. The following Core 21X contained a dolostone basalt breccia. A 6 cm piece of basalt was recovered in Core 320-U1333A-22X.

Coring in Hole U1333B started 5 m shallower than in Hole U1333A to recover the mudline and to span the core gaps from the first hole. A total of 7.73 m of carbonate-bearing ooze overlain by a few meters of clay were recovered in Core 320-U1333B-1H. Because the cores recovered from Hole U1333A showed no significant porcellanite or chert layers, we used the APC drillover strategy in Hole U1333B to obtain APC cores across and below the Eocene–Oligocene transition to 162.7 m CSF-A. We then XCB cored to basement and a total depth of 180.3 m CSF-A.

Hole U1333C was designed to provide stratigraphic overlap and confirm stratigraphic correlations made between Holes U1333A and U1333B. APC coring in Hole U1333C started 2.75 m shallower than Hole U1333B and reached to 163.2 m CSF-A before we had to switch to XCB coring. No downhole logging was conducted at Site U1333.

The sediment column at Site U1333 has a strong resemblance to that of Site 1218 (Lyle, Wilson, Janecek, et al., 2002) but with notably more carbonate-bearing sediments in the Eocene portion. The ~183 m of pelagic sediments has been divided into four major lithologic units (Fig. F51). Unit I is ~7 m thick and contains an alternating sequence of clay, clayey radiolarian ooze, radiolarian clay, clayey nannofossil ooze, and nannofossil ooze from the early Miocene period. Unit II is ~112 m thick and composed of alternating very pale brown nannofossil ooze and yellowish brown nannofossil ooze with radiolarians of early Miocene to latest Eocene age. Unit III is ~60 m thick and composed of Eocene biogenic sediments comprising clayey nannofossil ooze, nannofossil radiolarian ooze, nannofossil ooze, radiolarian nannofossil ooze, and porcellanite of latest Eocene to middle Eocene age (Unit III). Unit III is divided into two subunits, based on the absence (Subunit IIIa) or presence (Subunit IIIb) of porcellanite. Porcellanite is a third lithology in Unit III between ~168 and 174 m CSF-A. Unit IV is a ~3.3 m thin unit of lithified carbonate (partly dolostone) and dolomitized nannofossil ooze, overlying basalt of Eocene age (Unit V).

All major microfossil groups were found in sediments from Site U1333 and provide a consistent, coherent, and high-resolution biostratigraphic succession from basement to the top of lithologic Unit II. Shipboard biostratigraphy indicates that sediments recovered at Site U1333 span a near-continuous succession from around the lower Miocene boundary to the middle Eocene. Radiolarians are common and well preserved in

the Eocene succession but less well preserved in the Oligocene sediments. A complete sequence of radiolarian zones from RN2 to RP14 (middle Eocene) was described. Initial assessment of the radiolarian assemblages across the Eocene/Oligocene boundary interval indicates a significant loss of diversity through this apparently complete succession. Although a few species from the Eocene carry through to the Oligocene, only one stratigraphic marker species (*Lithocyclia angusta*) first appears near the Eocene/Oligocene boundary. Calcareous nannofossils are present and moderately to well preserved through most of the succession, although there are some short barren intervals in the middle to upper Eocene. The succession spans a complete sequence of nannofossil zones from lower Miocene Zone NN1 to middle Eocene Zone NP15. The Oligocene/Miocene boundary is bracketed by the base of *Sphenolithus disbelemnos* in Sample 320-U1333A-2H-5, 70 cm (16.20 m CSF-A), and the presence of rare *S. delphix* in Section 320-U1332A-2H-CC (9.57 m CSF-A). Discoasters are very rare in basal assemblages, indicative of a eutrophic environment and consistent with the paleolatitude of this site in the early middle Eocene within the equatorial upwelling zone. Planktonic foraminifers are relatively abundant and well preserved from the lowest part of the Miocene to the lower Oligocene. Oligocene fauna is characterized by the common presence of *Catapsydrax* spp., *Dentoglobigerina* spp., and *Paragloborotalia* spp. In contrast, upper Eocene sediments contain poorly preserved specimens or are barren of planktonic foraminifers. Preservation and abundance slightly increased in some intervals of the middle Eocene, which is recognized by the presence of acarininids and clavigerinellids. The absence of the genera *Globigerinatheka* and *Morozovella* makes precise age determination of individual samples problematic. The high abundance of *Clavigerinella* spp. has been linked to high-productivity environments, consistent with the paleogeographic location of this site. Benthic foraminifers were almost continuously present and indicate lower bathyal to abyssal depths. Oligocene fauna is characterized by calcareous hyaline forms, such as *Nuttallides umbonifer, Oridorsalis umbonatus,* and *Cibicidoides mundulus. Nuttallides truempyi* and *O. umbonatus* often dominate the Eocene fauna. Benthic foraminifers are present through most of the section apart from an interval in the middle Eocene equivalent to radiolarian Zone RP16. They indicate lower bathyal to abyssal paleodepths. Diatoms were observed throughout the column but will have to await analysis by specialists not onboard Expedition 320.

Sedimentation rates at Site U1333 are ~6 m/m.y. in the upper sediment column from the early Miocene to the late Oligocene. In the early Oligocene, linear sedimentation rates increased to ~12 m/m.y. Between ~31 Ma (earliest Oligocene) and the earliest

late Eocene they are ~4 m/m.y., increasing slightly in the middle Eocene section (~39–45 Ma) to ~5 m/m.y.

Paleomagnetic results from measurements made along split-core sections and on small discrete samples from Site U1333 provide a well-resolved magnetostratigraphy. Shipboard analyses suggest that a useful magnetic signal is preserved in most APC-cored intervals after removal of the drilling-induced overprint by partial AF demagnetization at 20 mT. The overprint was nearly absent in those cores collected in non-magnetic core barrels at Site U1333, whereas it was quite prominent for cores recovered in standard steel core barrels. Paleomagnetic directions from discrete samples agree well with those from split cores, confirming that AF demagnetization at 20 mT is generally sufficient to resolve the primary paleomagnetic direction regardless of which type of core barrel was used. Cleaned paleomagnetic data provide a series of distinct ~180° alternations in the declination and subtle changes in inclination, which, when combined with biostratigraphic age constraints, allow a continuous magnetostratigraphy to be constructed that correlates well with the geomagnetic polarity timescale. The magnetostratigraphic record extends from the base of Chron C6n (19.722 Ma) at 1.7 m CSF-A in Hole U1333C to the top of Chron C20r (43.789 Ma) at 161.6 m CSF-A in Hole U1333C. Highlights include very high quality paleomagnetic data across Chrons C13r and C13n, which span the latest Eocene and earliest Oligocene, and a newly recognized cryptochron within Chron 18n.1n.

Geochemistry results indicate that samples from the uppermost ~4 m of Site U1333 have modest $CaCO_3$ concentrations of 26%–69% with frequent variations between 58% and up to 93% in the interval between 4 and 35 m CSF-A. Carbonate concentrations are consistently high (75.5%–96%) from 35 to 111 m CSF-A, whereas in the Eocene (between 111 and 171 m CSF-A) $CaCO_3$ concentrations vary rapidly between <1% and 74%. The lowermost lithified carbonate rocks between 173 and 180 m CSF-A have high $CaCO_3$ concentrations between 76% and 90%. TOC concentrations, as determined using an acidification method, are generally very low or below the detection limit (<0.1%, apart from samples in the top most 5 m, which reached ~0.17%). Pore water alkalinity values are never elevated, but alkalinity and dissolved strontium values are somewhat higher near the Eocene–Oligocene transition; these are generally consistent with carbonate dissolution or recrystallization processes. Dissolved silica increases with depth, with values always <1000 µM.

A full physical property program was run on cores from Holes U1333A–U1333C comprising WRMSL measurements of magnetic susceptibility, bulk density, *P*-wave veloc-

ity, noncontact resistivity, NGR, and measurements of color reflectance, followed by discrete measurements of moisture and density properties, sound velocities, and thermal conductivity on Hole U1333A cores only. All track data show variability throughout the section, allowing a detailed correlation between holes primarily using magnetic susceptibility and density (magnetic susceptibility varies around 24×10^{-5} SI in radiolarian ooze–dominated sections and ~3×10^{-5} SI in more carbonate rich intervals). Magnetic susceptibility values gradually increase uphole. NGR measurements are elevated by an order of magnitude in the uppermost clays and increase near the lower Oligocene at ~115 m CSF-A (from 5 to 8 cps). *P*-wave velocity gradually increases downhole as we move from carbonate- to radiolarian-dominated successions. *P*-wave velocity generally varies between 1490 and 1560 m/s depending on lithology, with lower velocities corresponding more to carbonate-rich sections. Bulk density and grain density show a marked decrease at ~112 m CSF-A (~1.704 to 1.313 g/cm^3 in bulk density), where carbonate content decreases rapidly. Porosity values are generally high in the radiolarian-rich sediments (80%) and decrease in the carbonate-rich section (~60%). Thermal conductivity measurements are increased in carbonate-rich intervals and range from ~0.8 W/(m·K) in lithologic Unit I to 1.2–1.3 W/(m·K) in lithologic Unit II.

Stratigraphic correlation indicated that a composite section was recovered to ~130 m CSF-A in the upper Eocene, equivalent to a composite depth of ~150 m CCSF-A. For Site U1333, a growth factor of 15% is estimated from the ratio between the CCSF-A and CSF-A (formerly mcd and mbsf) depth scales. Stratigraphic correlation with Site 1218 suggests a complete stratigraphic section in the Oligocene to uppermost Eocene interval.

Five formation temperature measurements were conducted in Hole U1333B with the APCT-3 tool. These temperature measurements, when combined with thermal conductivity values obtained from the cores, indicate that Site U1333 has a heat flow of ~42.3 mW/m^2 and a thermal gradient of 37.9°C/km.

Highlights

High carbonate fluctuations in middle Eocene sediments

Coring at Site U1333 was designed to capture a time period when the CCD was slightly deeper within the middle Eocene interval that showed prominent fluctuations of carbonate content (Lyle et al., 2005). This interval occurs during the cooling that took place after the EECO (Zachos et al. 2001a) and before the Eocene–Oligocene

transition (e.g., Coxall et al., 2005). Unlike Site 1218, Site U1333 sediments show carbonate concentrations >75% in this interval at a deeper water depth and apparently coeval with the CCD cycles described by Lyle et al. (2005). Basal lithologic Unit IV recovered partially lithified carbonates.

MECO, Eocene–Oligocene and Oligocene–Miocene transitions, and depth transects

Site U1333 forms the third oldest and deepest component of the PEAT depth transect and can be directly compared with Site 1218, which will allow the study of critical intervals (such as the Eocene–Oligocene transition; see Coxall et al., 2005) and variations of the equatorial CCD. Site U1333 is estimated to have been ~3.8 km deep during the Eocene–Oligocene transition, ~1 km shallower than today and 200 m shallower at that time than Site U1332. Carbonate content in these sediments does not change as rapidly as at the deeper and older Sites U1332 and U1333. Some of these sediments appear to be Eocene–Oligocene transition sediments that are suitable for paleoceanographic studies using carbonate-based geochemical proxies and thus are an improvement over Site 1218. Of note, Site U1333 also contains high carbonate content–bearing sediments around the MECO event (Bohaty and Zachos, 2003; Bohaty et al., 2009), allowing a detailed study of the sequence of events linking carbonate preservation cycles (Lyle et al., 2005) with climatic oscillations.

Carbonate-bearing sediments across the Oligocene–Miocene transition were also recovered at Site U1333 (e.g., Zachos et al., 2001b), adding important data to the study of this time interval in the context of the PEAT Oligocene/Miocene depth transect.

Age transect of seafloor basalt

At Site U1333 we recovered what appear to be fresh fragments of seafloor basalt, aged between 45 and 46 Ma. This material will, when combined with other PEAT basalt samples, provide important sample material for the study of seawater alteration of basalt.

Site U1334

Three holes were cored at Site U1334 (7°59.998′N, 131°58.408′W; 4799 m water depth; Fig. **F52**), targeting the events bracketing the Eocene–Oligocene transition as part of an investigation of the wider Cenozoic climatic evolution (e.g., Zachos et al., 2001a) and providing data toward a depth transect across the Oligocene (see **"Eocene/Oligocene Boundary [Site U1334; 38 Ma crust]"**) that will allow exploitation

and verification of a previous astronomical age calibration from Site 1218 (Pälike et al., 2006b).

Site U1334 is in the center of the PEAT program, ~100 km north of the Clipperton Fracture Zone and ~380 km southeast of the previously drilled Site 1218. At Site U1334, late middle Eocene age (38 Ma) seafloor basalt is overlain by ~285 m of pelagic sediment.

The topmost ~47 m thick lithologic Unit I comprises a 15 m thick interval of brown radiolarian clay overlying ~32 m of alternating radiolarian clay and nannofossil ooze. The uppermost section (320-U1334A-1H-CC) is of late Miocene age (radiolarian Zone RN7; ~8.5 Ma). Below, Unit II comprises a ~200 m thick succession of upper Miocene to Oligocene nannofossil ooze and chalk above a ~35 m thick sequence of late Eocene age nannofossil chalk, radiolarite, and claystone (Unit III). Basal lithologic Unit IV (~1 m CSF-A) consists of middle Eocene intercalated micritic chalk and limestone on basalt (Figs. **F53, F54**).

Holes U1334A–U1334C provided high-quality APC-cored sediments from the mudline to ~210 m CSF-A (Cores 320-U1334A-22H, 320-U1334B-22H, and 320-U1334C-22H). Below this depth we encountered increasingly stiffer and harder sediment, after which we switched to the XCB cutting shoe. XCB coring advanced to 288.5 m DSF through lower Oligocene and Eocene sediments with high recovery. In the basal section, an intercalated unit of basalt and hard micritic chalk and limestone below a 10–20 m thick basal section of nannofossil ooze and chalk was recovered in Core 320-U1334A-32X. For detailed coring activities, see **"Site U1334"** in "Operations."

The sediment column at Site U1334 has a strong resemblance to that of Site 1218 (Lyle, Wilson, Janecek, et al., 2002) but with a thinner uppermost clay layer and higher Oligocene and Eocene sedimentation rates, as well as higher carbonate content in the middle and late Eocene sections, as was planned for this site.

Carbonate content exceeds 92% in the upper lower Miocene section below Section 320-U1334A-5H-3 and remains high throughout the Oligocene. Eocene sediments still contain considerable amounts of carbonate, and nannofossil ooze and chalk are dominant lithologies apart from several short less carbonate rich intervals (e.g., Section 320-U1334A-28X-3). In the middle Eocene section, carbonate content cycles between ~40% and 85% (Fig. **F55**), with higher values encountered toward the basal part of the Eocene section. Two short intervals in the late Eocene (~249 to ~257 m CSF-A) exhibit carbonate content of <20%.

A series of middle Oligocene cores (Cores 320-U1334A-16H through 21H) were recovered that had very distinct colors ranging from light grayish green to light blue. These uniquely colored carbonate oozes exhibit extremely low magnetic susceptibilities that complicated a confident stratigraphic correlation. These colored oozes lost almost their entire magnetic susceptibility signal from ~145 to ~215 m CSF-A (Figs. F54, F56). Similar colored cores have previously been described for DSDP Sites 78 and 79 (Hays et al., 1972).

The Eocene–Oligocene transition at Site U1334 is much more expanded than at Sites U1331–U1333 and even Site 1218. The Eocene–Oligocene transition was encountered at ~250 m CSF-A and fully recovered in Cores 320-U1334A-27X and 320-U1334B-26X; Hole U1334C was used to fill small stratigraphic gaps. The Oligocene–Miocene transition was fully recovered in all three holes in Cores 320-U1334A-10H (based on magnetostratigraphy, the boundary is at interval 320-U1334A-10H-6, 98 cm), 320-U1334B-10H (top of Section 2), and 320-U1334C-10H.

All major microfossil groups were found in sediments from Site U1334 and provide a consistent, coherent, and high-resolution biostratigraphic succession spanning a near-continuous sequence from the middle Miocene to the uppermost middle Eocene. The uppermost 12 m of radiolarian clay is barren of calcareous microfossils but contain radiolarians of middle Miocene age, similar to the site survey piston Core RR0306-08JC (Lyle et al., 2006). Nannofossil ooze and radiolarian clays are present in the Miocene and Eocene parts of the section, with nannofossil ooze dominant in the thick Oligocene section. Radiolarians are present through most of the section, apart from the lowermost cores, and are well preserved in the Eocene. They provide a coherent, high-resolution biochronology and indicate a complete sequence of radiolarian zones from RN7 (upper Miocene) to RP17 (uppermost middle Eocene). Calcareous nannofossils are present and moderately to well preserved through most of the succession, and there appears to be a complete sequence of nannofossil zones from NN6 (middle Miocene) to NP17 (uppermost middle Eocene), providing a minimum age estimate for basaltic basement of 37 Ma. In the Eocene, the base of *Chiasmolithus oamaruensis* is determined in Sample 320-U1334A-30X-1, 66 cm, and the top of *Chiasmolithus grandis* in Sample 320-U1334-30X-2, 74 cm. Intriguingly, both species are mid- to high-latitude taxa (Wei and Wise, 1989) and are present only rarely and sporadically at Site U1334. Planktonic foraminifers are present through most of the succession and are relatively abundant and well preserved from the lower Miocene to the lower Oligocene. The lower Miocene is characterized by the presence of *Dentoglobigerina* spp., *Paragloborotalia siakensis–mayeri, P. kugleri,* and *Paragloborotalia pseudoku-*

gleri. Oligocene sediments contain *Catapsydrax* spp., *Paragloborotalia opima-nana,* and characteristic *Dentoglobigerina* spp. The preservation and abundance of planktonic foraminifers is more variable in the middle Miocene and upper Eocene/lowermost Oligocene. No Eocene/Oligocene boundary marker hantkeninids were identified. Benthic foraminifers are present through most of the section and indicate lower bathyal to abyssal paleodepths.

Apparent sedimentation rates, as implied by magneto- and biostratigraphic age determinations, vary throughout the section and are ~4 m/m.y. in the topmost sediment cover, vary between ~12 and 14 m/m.y. in the early Miocene through late early Oligocene section, increase to ~24 m/m.y. in the early Oligocene, and are ~8 m/m.y. in the late Eocene. There is no apparent hiatus at the shipboard biostratigraphic resolution. The presence of all major fossil groups as well as a detailed and well-resolved magnetostratigraphy will allow us to achieve one of the main PEAT objectives of arriving at an integrated Cenozoic stratigraphy and age calibration for major parts of the Miocene, Oligocene, and Eocene.

A full physical property program was run on cores from Site U1334C. This program comprises WRMSL measurements of magnetic susceptibility, bulk density, *P*-wave velocity, noncontact resistivity, NGR, and measurements of color reflectance, followed by discrete measurements of moisture and density properties, sound velocities, and thermal conductivity on Hole U1334A. All track data are variable throughout the section, allowing a detailed correlation between different holes, with the exception of a very low susceptibility signal within an interval extending slightly above and below the light greenish gray tinted cores of Unit II, between ~140 and 210 m CSF-A. Magnetic susceptibility varies between 10×10^{-5} and 40×10^{-5} SI in Unit I, oscillates around 5×10^{-5} to 10×10^{-5} SI above the colored sediments, and then drops to near zero and negative values, returning to values around 10×10^{-5} SI in the lower part of Unit II and Subunit IIIa. NGR slightly increases at the Eocene/Oligocene boundary at ~246 m CSF-A (from 4 to 7 cps). *P*-wave velocity remains continuous through the upper 150 m of sediment (varying around 1500 m/s) but increases rapidly below the ooze/chalk boundary to ~1600 m/s. This explains the slightly thicker sediment section than was expected from seismic data prior to coring (~20 m thicker). For Hole U1334B, no *P*-wave velocity WRMSL data were collected between ~125 and 240 m CSF-A to allow for a more timely stratigraphic correlation of cores within the iron reduction–dominated colored cores with the GRA instrument. Bulk density and grain density increase gradually with carbonate content to ~204 m CSF-A to a maximum of ~1.8 g/cm³ and then show stepped decreases in the lower part of this succession.

Ephemeral whole-round samples were collected at ~50 and ~165 m for shore-based studies of sediment permeability.

WRMSL data were used to achieve stratigraphic correlation between holes at Site U1334. Magnetic susceptibility was initially the main parameter used for real-time correlation, as a second loop of the susceptibility meter is mounted on the Special Task Multisensor Logger (STMSL); the second bulk density instrument on this track was not working. In the very low (negative) susceptibility interval between ~145 and ~198 m CSF-A (Cores 320-U1334A-16H through 21H), the magnetic signal was not useful for correlation, and we measured the corresponding cores from Hole U1334B out of sequence to establish the amount of core overlap using bulk density. The coring effort in Hole U1334C was successful at covering gaps between cores at this site to ~111 m CCSF-A, as well as from 250 to 335 m CCSF-A, almost to the bottom of the section. The correlation was challenging between the three holes at Site U1334 in the greenish–light gray interval (Cores 320-U1334A-15H through 22H, 320-U1334B-14B through 22H, and 320-U1334C-14H through 22H) and in the bottom 80 m of the section, where XCB coring compromised the GRA density variations that would otherwise help stratigraphic correlation. Visual inspection, comparison with core imagery, and biostratigraphic datums were used to establish and verify hole-to-hole correlation where track data lacked clearly identifiable features. Stratigraphic correlation between individual holes indicates a growth factor (ratio between the CCSF-A and CSF-A depth scales) of ~16%. Stratigraphic correlation resulted in a complete splice through the Eocene–Oligocene transition almost to basement (~38 Ma).

A full range of paleomagnetic analyses was conducted on 66 APC cores and 188 discrete paleomagnetic samples from Site U1334 for the APC-cored section of Site U1334 (upper ~209 m). Unlike Sites U1331 and U1332, the drilling overprint was generally weak for Site U1334 cores, but only for those collected with the nonmagnetic core barrel (Cores 320-U1334A-1H through 16H, 320-U1334B-1H through 15H, and 320-U1334C-1H through 15H). In contrast, those cores collected with the steel core barrels are highly overprinted to the extent that the overprint is so severe that even demagnetization at 20 mT is only partially able to remove it. This extreme overprint notably degrades the paleomagnetic declination data as can be noted by their higher variability, which makes polarity determination much more difficult in the intervals collected with steel core barrels. The problem is exacerbated by the decay in the intensity (and susceptibility), which occurs at ~135 m CSF-A in all three holes as a result of apparent reduction diagenesis. Even within the highly reduced interval, an interpretable signal was present prior to switching to steel core barrels. Susceptibility in the

upper 45 m of Hole U1334A averages ~18 × 10^{-5} SI (volume normalized) and decreases to a mean of 6 × 10^{-5} SI from 45 to 135 m CSF-A. A notable low occurs from ~142 to 204 m CSF-A, where the average susceptibility is 0.6 × 10^{-5} SI. This low interval is associated with a change in sediment color from yellowish tan to very light green, blue, and gray at ~140 m CSF-A and another abrupt change to reddish brown tones at ~205 m CSF-A, which corresponds to middle early Oligocene (~30 Ma). Just below 205 m susceptibility steps up to an average of 5 × 10^{-5} SI and then increases again across the Eocene/Oligocene boundary (~245 m) to an average of 18 × 10^{-5} SI. The magnetostratigraphy in Hole U1334A has been interpreted from the top of Chron 11r (29.957 Ma), which occurs ~55 cm below the top of Section 320-U1334C-21H-4 (~195 m CSF-A), through the base of C3n.4n (5.235 Ma) in Core 320-U1334A-1H. Magnetic reversals have also been interpreted from C1n through C2r.1r in the upper ~2 m of Core 320-U1334A-1H.

A standard shipboard suite of geochemical analysis of pore water and organic and inorganic properties was undertaken on sediments from Site U1334. We also conducted a high-resolution (1 per section) Rhizon pore water investigation across the interval's middle Oligocene cores (320-U1334A-16H through 21H) that exhibited colored sediments. Site U1334A is marked by alkalinities between 3 and 4 mM throughout. The most striking features in the interstitial water geochemistry are a dissolved manganese peak from ~20 to ~240 m CSF-A with a maximum of ~6 μM at ~110 m CSF-A and a dissolved iron peak as high as >15 μM centered at 165 m CSF-A. The depth range of the dissolved iron peak, indicative of iron oxide reduction, coincides with the colorful interval seen in the lithology and with the interval of low magnetic susceptibilities (~140–205 m CSF-A). Sulfate results indicate limited sulfate reduction. Calcium carbonate contents are low in the uppermost ~35 m of Site U1334, and initial results indicate high calcium carbonate contents below the uppermost clay layer.

Wireline logging was attempted in Hole U1334C with a redesigned tool string configuration after the loss of equipment at Site U1332. However, this attempt had to be abandoned after the logging winch failed when the tool was on its way down the drill pipe.

Five downhole temperature measurements were conducted in Hole U1334B with the APCT-3 tool and reveal a thermal gradient of 33°C/km. Temperature data combined with whole-round core temperature conductivity measurements indicate the heat flow is 31.6 mW/m² at this site. This is somewhat lower than values obtained for the nearest site (1218). Seafloor temperature is ~1.5°C.

Highlights

Eocene–Oligocene and Oligocene–Miocene transitions and depth transects

Site U1334 was planned as the youngest and shallowest component of the PEAT Eocene–Oligocene depth transect, which will allow the study of critical intervals (such as the Eocene–Oligocene transition; see Coxall et al., 2005) and variations of the equatorial CCD. Site U1334 is estimated to have been ~3.5 km deep during the Eocene–Oligocene transition, ~1.3 km shallower than today and 800 m shallower at that time than Site U1333. Unlike previously drilled sites, the dominant lithology is still nannofossil ooze and chalk below the Eocene–Oligocene transition, with significant amounts of carbonate present, which will allow us to achieve the prime objective for this site. The Eocene–Oligocene transition, which was cored multiple times at Site U1334, has much higher sedimentation rates than Site 1218. The remaining Oligocene is also much more expanded than at Site 1218, with better preservation of planktonic foraminifers over a longer time interval, allowing a more detailed study of the Oligocene climate system. Site U1334 also contains carbonate-bearing sediments across the Oligocene–Miocene transition (e.g., Zachos et al., 2001b; Pälike et al., 2006a). Physical property data from Site U1334 can be correlated cycle by cycle to Site 1218, allowing correlation to a previously astronomically calibrated site for the Oligocene.

Geochemical front

At Site U1334 we recovered a ~50 m thick interval of multicolored carbonates that show a distinct Mn increase and elevated Fe pore water concentrations, characteristic of a geochemical alteration front. A detailed Rhizon pore water sampling program will provide insights into limited sulfate reduction processes. A similar but much thicker alteration zone is also observed at Site U1335 and provides the opportunity to study organic matter degradation while these sites migrate from south to north through the equatorial belts of high productivity.

Age transect of seafloor basalt

At Site U1334 we recovered what appear to be fresh fragments of seafloor basalt, aged ~38 Ma. This material will, when combined with other PEAT basalt samples, provide important sample material for the study of seawater alteration of basalt.

Site U1335

Two holes were cored at Site U1335 (5°18.735′N, 126°17.002′W; 4327.5 m water depth) (Fig. **F57**), targeting paleoceanographic events in the late Oligocene and into the early and middle Miocene, including and focusing on the climatically significant Oligocene–Miocene transition and the recovery from the Mi-1 glaciation event (Zachos et al., 2001b; Pälike et al., 2006a) and the expansion of the East Antarctic cryosphere (Holbourn et al., 2005). Site U1335 also provides data toward a depth transect across the latest Oligocene and Miocene (see **"Latest Oligocene–earliest Miocene [Site U1335; 26 Ma crust]"**) that will allow exploitation and verification of a previous astronomical age calibration from Site 1218 (Pälike et al., 2006b).

Site U1335 (~26 Ma crust) is situated halfway between Site U1336 ~340 km toward the northwest and Site U1337 ~390 km toward the southeast, ~250 km south of the Clipperton Fracture Zone (Lyle et al., 2006). At Site U1335, late Oligocene age (26 Ma) seafloor basalt is overlain by ~420 m of pelagic sediment.

The sedimentary sequence at Site U1335 is divided into two major lithologic units. The topmost ~64 m thick lithologic Unit I comprises an alternating sequence of earliest late Miocene to Pleistocene calcareous nannofossils, diatoms, radiolarians, and foraminifer oozes. The topmost sediment of Unit I is younger than the Pleistocene/Pliocene boundary as recognized by the top of planktonic foraminifer *Globigerinoides fistulosus* (between Section 320-U1335A-1H-CC and interval 320-U1335A-2H-2, 104–106 cm) and then follows a continuous biostratigraphic succession to the early late Miocene. Below, lithologic Unit II comprises a ~350 m thick succession of late Miocene to late Oligocene (calcareous nannofossil Zone NP25) nannofossil ooze and chalk overlying basalt (lithologic Unit III) (Figs. **F58, F59**). One of the prominent features of Unit II is the presence of at least 49 described beds (2–176 cm thickness) of nannofossil foraminifer ooze that have sharp basal boundaries, many of which are irregular and some of which are inclined, interpreted as gravity flow deposits from the nearby seamounts and representing ~2% of the total sediment recovered.

Holes U1335A and U1335B provided high-quality APC-cored sediments from the mudline to ~341 and 378 m CSF-A, respectively (Cores 320-U1335A-36H and 320-U1335B-41H). The APC-cored interval from Hole U1335B represents the second deepest APC-cored depth in ODP and IODP history. Below this depth we encountered stiffer and harder sediment, after which we switched to the XCB cutting shoe. XCB coring advanced to ~420 m DSF through early Miocene and late Oligocene sediments

with high recovery. In the basal section, Core 320-U1335B-46X recovered pieces of basalt up to 10 cm in length with a glassy rim and overlain by nannofossil chalks of Unit II. For detailed coring activities, see **"Site U1335"** in "Operations."

The sediment column at Site U1335 represents the youngest end-member drilled during Expedition 320 and provides one of the most stratigraphically complete and expanded early Miocene sections from the equatorial Pacific to date (~320 m cored depth from the earliest to latest Miocene).

At Site U1335 carbonate content fluctuates between 12% and 87% within Unit I (Fig. **F60**), presumably reflecting the close proximity of the seafloor to the lysocline. With the exception of the depth interval from 140 to 220 m CSF-A, the remainder of Unit II exhibits uniformly high calcium carbonate content between 80% and 90%. From ~150 to 210 m CSF-A (approximately equivalent to Cores 320-U1335A-16H through 22H), carbonate content cycles between ~50% and 90% and corresponds to a change in dominant sediment color from light greenish gray to tan, displaying higher magnetic susceptibility values up to 25×10^{-5} SI.

A series of late Oligocene through late middle Miocene cores (320-U1335A-8H through 40X) were recovered with distinct colors ranging from light grayish green to light blue, similar but much thicker in total stratigraphic thickness (~70–170 m and ~200–350 m) than those observed at Site U1334. The uniquely colored carbonate oozes exhibit extremely low magnetic susceptibilities that complicated a confident stratigraphic correlation. These colored oozes lost almost their entire magnetic susceptibility signal from ~70 to ~105 m CSF-A and below ~210 m CSF-A (Figs. **F59, F61, F62**). Similar colored cores have previously been described for Sites 78 and 79 (Hays et al., 1972).

All major microfossil groups were found in sediments from Site U1335, representing a complete biostratigraphic succession at the shipboard sample resolution level of Pleistocene to latest Oligocene sediments, including a thick sequence of lower Miocene nannofossil ooze and chalk. Radiolarians are present through most of the section apart from the basal 3 m of nannofossil chalk. They provide a coherent high-resolution biochronology through a complete sequence of radiolarian zones from RN14 (Pleistocene) to RP21 (upper Oligocene). Calcareous nannofossils are present and moderately to well preserved through most of the succession, representing the complete sequence from NP25 (upper Oligocene) above basaltic basement through NN20 (Pleistocene). Planktonic foraminifers are present throughout the succession

and are moderately to well preserved. Recognized planktonic foraminifer zones range from PT1a (Pleistocene) to O6 (upper Oligocene). Nannofossil, radiolarian, and planktonic foraminifer datums are in good agreement. Benthic foraminifers are present through most of the section and indicate lower bathyal to abyssal paleodepths. The Oligocene–Miocene transition at Site U1335 was encountered at ~350 m and fully recovered in Cores 320-U1335A-37X and 320-U1335B-38H as defined by the planktonic foraminifer datum base of *P. kugleri* between Samples 320-U1335A-37X-4, 136–138 cm, and 37X-CC (midpoint = 348.6 m CSF-A), in good agreement with the calcareous nannofossil event top of *S. delphix* at 349.7 m CSF-A between Sample 320-U1335A-37X-6, 50 cm, and Section 37X-CC. The oldest sediment overlying seafloor basalt has been zoned within calcareous nannofossil Zone NP25 (24.4–26.8 Ma).

Apparent sedimentation rates, as implied by the magneto- and biostratigraphic age determinations, vary throughout the section and are ~6 m/m.y. in the late to middle Miocene to recent sediment cover, ~17 m/m.y. in the middle early Miocene, and as high as ~25 m/m.y. throughout the late Oligocene and early Miocene. There is no apparent hiatus at the shipboard biostratigraphic resolution, although some condensed horizons are apparent (e.g., near the early/middle Miocene boundary and in the early late Miocene). The presence of all major fossil groups as well as a detailed and well-resolved magnetostratigraphy will allow us to achieve one of the main PEAT objectives of arriving at an integrated Cenozoic stratigraphy and age calibration for the Miocene and late Oligocene.

A full physical property program was run on cores from Site U1335. This program comprises WRMSL measurements of magnetic susceptibility, bulk density, *P*-wave velocity, NGR, and measurements of color reflectance, followed by discrete measurements of moisture and density properties, sound velocities, and thermal conductivity on Hole U1335A. All track data are variable throughout the section, allowing a detailed correlation between different holes, with the exception of a low susceptibility signal within an interval extending slightly above and below the light greenish gray tinted cores of Unit II, between ~70 and 110 and ~200 and ~380 m CSF-A. Magnetic susceptibility varies between 5×10^{-5} and 20×10^{-5} SI in the upper parts of Unit I and then increases to ~25×10^{-5} SI toward the lower portion of Unit I, coinciding with the presence of clayey radiolarian ooze within the major lithology of nannofossil ooze. Magnetic susceptibility values decrease at the top of Unit II (~64 m CSF-A) and then fall to values around -1×10^{-5} SI near 70 m CSF-A. Between ~110 and 150 m CSF-A, magnetic susceptibility values increase slightly and become highly variable (0 to 10×10^{-5} SI). Magnetic susceptibility values are higher in the interval from 160 to 200 m

CSF-A, coinciding with an observed decrease in Fe reduction. Below 200 m CSF-A, the magnetic susceptibility signature is largely diamagnetic, with values close to zero. Magnetic susceptibility values slightly increase again in the basal 20 m of Unit II (below ~400 m CSF-A). NGR is elevated at the surface sediment (~73 cps) but low throughout the rest of the sedimentary column. *P*-wave velocities from the WRMSL agree with discrete velocity measurements and reflect key lithologic transitions, particularly the ooze to chalk transition near ~220 m CSF-A. *P*-wave velocities are between 1460 and 1490 m/s in Unit I and the upper portion of Unit II and then increase to >1500 m/s. Slightly below the ooze–chalk transition near 345 m CSF-A, velocities increase significantly, reaching 1600–1750 m/s at the bottom of Unit II. This partly explains the thicker sediment section than expected from seismic data prior to coring (~60 m thicker). Bulk density and grain density increase with depth, with a decrease in wet bulk density from 1.2–1.6 g/cm³ in Unit I to ~1.7 g/cm³ at the top of Unit II and ~1.8 g/cm³ in the basal part of the section. Sediment porosity ranges from 70%–90% in Unit I to 50%–60% at ~300 m CSF-A in Unit II. Ephemeral whole-round samples were collected at ~96, ~196, and ~305 m CSF-A for shore-based studies of sediment permeability.

The coring effort in Holes U1335A and U1335B was successful at covering stratigraphic gaps between cores at this site from the surface throughout most of the APC-cored section, with the exception of a gap (~1 m) at the bottom of Core 320-U1335A-16H due to flow-in (~146.40–151.46 m CSF-A). Features in magnetic susceptibility and GRA density are well aligned down to a depth of 337 m CSF-A (Hole 1335A) and 344 m CSF-A (Hole U1335B), corresponding to ~398 m CCSF-A. Between ~230 and ~398 m CCSF-A, GRA density data allowed confident alignment of cores despite very low magnetic susceptibility values. The section below ~398 m CCSF-A was mostly XCB cores, lacked clearly identifiable features, and therefore had to be appended to the splice. A single spliced record was assembled for the aligned cores down to Section 320-U1335B-37H-6 (343.76 m CSF-A; 398.15 m CCSF-A). Stratigraphic correlation between individual holes indicates a growth factor (ratio between the CCSF-A and CSF-A depth scales) of ~16%. Stratigraphic correlation resulted in a complete splice through the Eocene–Oligocene transition almost to basement (~38 Ma).

A full range of paleomagnetic analyses was conducted on 78 archive halves and 257 discrete paleomagnetic samples from Site U1335 for the APC-cored section (upper ~378 m). The most prominent feature of the records is the magnetic intensity and susceptibility low that occurs between ~70 and 110 m CSF-A and below ~210 m CSF-A. We could not obtain any reliable paleomagnetic directions from this interval because

the magnetic intensity after 20 mT AF demagnetization is in the order of 10^{-5} A/m, which is comparable to the noise level of the superconducting rock magnetometer. Except for these low magnetic intensity intervals, we found distinct declination reversals at 20 mT demagnetizations. The drilling overprint was generally weak when nonmagnetic core barrels were used (Cores 320-U1335A-1H through 16H and 320-U1335B-1H through 19H). In contrast, those cores collected with the steel core barrels are highly overprinted. Except for the low magnetic intensity interval, the cleaned paleomagnetic data provide a series of distinct ~180° alternations in the declination. When combined with biostratigraphic age constraints, the data allow a continuous magnetostratigraphy from Chron C1n (0–0.781 Ma) to C5n.2n (9.987–11.040 Ma) from 0 to 65.95 m CSF-A in Hole U1335A and from Chron C1n to C5r.1n (11.118–11.154 Ma) from 0 to 66.225 m CSF-A in Hole U1335B. Below the bottom of the first magnetic low zone (~70–110 m CSF-A), magnetostratigraphy is again interpretable downhole: from Chron C5Br (15.160–15.974 Ma) to C6n (18.748–19.722 Ma) from 155.35 to 208.40 m CSF-A in Hole U1335A and from Chron C5AAn (13.015–13.183 Ma) to C5Er (18.524–18.748 Ma) from 107.95 to 202.60 m CSF-A in Hole U1335B. The highlights of the magnetostratigraphy at Site U1335 are the identifications of (1) a previously observed cryptochron (C5Dr-1n) in two holes and (2) 40 potential geomagnetic excursions (10 of which are recorded in both holes).

A standard shipboard suite of geochemical analysis of pore water and organic and inorganic properties was undertaken on sediments from Site U1335. Site U1335 is marked by alkalinities between 2.5 and 4.3 mM throughout, sulfate concentrations between 23 and 28 mM, and dissolved phosphate concentrations of ~2 µM in the shallowest sample, decreasing to ~0.5 µM in the uppermost ~50 m. The most striking features in the interstitial water geochemistry are three dissolved manganese peaks with concentrations of up to 44, 13, and 5 µM at ~0–40, 50–80, and 150–210 m CSF-A, respectively. Dissolved iron also shows three peaks, with concentrations up to 6 µM at ~6 m CSF-A, between 90 and 170 m CSF-A, and between 190 and 370 m CSF-A. Minima in dissolved Fe correspond to elevated Mn concentrations. The alternating pattern of dissolved Mn and Fe correspond well to apparent color changes in the sediment column. Lithium concentrations decrease from ~26 µM at the sediment surface to 5 µM at ~300 m CSF-A, below which Li concentrations increase strongly to ~32 µM. The Sr concentration profile mirrors that of Li, with concentrations ranging between 82 and 250 µM. Sr values increase from the top to 200 m CSF-A, followed by a decrease toward basement. Calcium carbonate, IC, and TC concentrations were determined on sediment samples from Hole U1335A (Fig. **F60**). $CaCO_3$ concentrations ranged between 13% and 96%. In the uppermost ~67 m, carbonate concentration

ranges from 12% to 87%, and concentrations are then consistently high (~72%–96%) between 67 and 157 m CSF-A and below 222 m CSF-A. Concentrations vary more widely (between 37% and 89%) from 157 to 222 m CSF-A. TOC concentrations were determined by acidification, with a range from below the detection limit to 0.08%. TOC is significantly higher in the uppermost ~57 m and at ~220 m CSF-A (0.08% and 0.04%, respectively), corresponding to intervals with lower carbonate concentrations.

Wireline logging was not conducted at Site U1335. Five downhole temperature measurements were conducted in Hole U1335B with the APCT-3 tool and reveal a thermal gradient of 7.5°C/km. Temperature data combined with whole-round core temperature conductivity measurements indicate the heat flow is 7 mW/m² at this site. This is much lower than values obtained for any of the other Expedition 320 sites and would suggest recirculation of seawater through basement, consistent with some of the interstitial pore water results.

Highlights

Highly expanded Miocene sedimentary section

One of the highlights from Site U1335 is the recovery of a very thick Miocene carbonate-dominated section from the central equatorial Pacific, one of the high-priority objectives of the PEAT program. The early Miocene (~7 m.y. duration) is captured in ~190 m of sediment, corresponding to a sedimentation rate of 27 m/m.y. The middle Miocene (4.5 m.y. duration) is recovered in ~95 m sediment, with a sedimentation rate of ~21 m/m.y. The sedimentation rate from the late Oligocene into the Miocene is just under 20 m/m.y. These high sedimentation rates will facilitate the study of paleoceanographic processes at unprecedented resolution for the equatorial Pacific.

Oligocene–Miocene transition and depth transects

Site U1335 was planned as the youngest and shallowest component of the PEAT Oligocene–Miocene depth transect, which will allow the study of critical intervals (such as the Mi-1 glacial inception; see Zachos et al., 2001b; Pälike et al., 2006a) and variations of the equatorial CCD throughout this transition as well as the latest Oligocene and early Miocene. Site U1335 is estimated to have been ~3.3 km deep during the Oligocene–Miocene transition, ~1.5 km shallower than today. The dominant lithologies are nannofossil ooze and chalk, with better preservation of calcareous microfossils than any other site drilled during Expedition 320, which will allow us to achieve the prime objective for this coring site. Physical property data from Site U1335 provide an important contribution toward the Cenozoic megasplice, connecting with

younger sediments from Leg 138 (e.g., ODP Site 850) and older sediments from Leg 199 (Site 1218), allowing the generation of astronomically calibrated datums and isotope stratigraphies from the Miocene into the Eocene.

Geochemical front

At Site U1335 we recovered an interval of multicolored carbonates that show a distinct Mn increase and elevated Fe pore water concentrations, characteristic of a geochemical alteration front. At Site U1335, this zone is similar but much thicker in total stratigraphic thickness (~70–170 and ~200–350 m CSF-A) than that observed at Site U1334 (~50 m). Although the paleomagnetic signal was lost in most parts of this section, sediments recovered will provide the opportunity to study organic matter degradation while these sites migrated from south to north through the equatorial belts of high productivity. Paleolatitudinal reconstructions show that these characteristic geochemical alteration fronts can be mapped to similar equatorial positions between Sites U1334 and U1335, roughly between the Equator and ~2°N. One feature of interest at Site U1335 is the observation that the multicolored interval of sediments is interrupted between ~170 and 200 m CSF-A (Cores 320-U1335A-18H through 20H), again showing higher magnetic susceptibility values. It remains to be established whether this interruption in the geochemical alteration front is related to the shape and position of the equatorial high-productivity zone or instead is the result of reduced sedimentation rates during this time (late early Miocene). Interstitial pore water profiles provide additional important information about the redox chemical processes operating in this zone, which have also been observed at DSDP Sites 78, 79, and 574 (e.g., Hays et al., 1972).

Gravity flow deposits

One of the prominent features of Unit II is the presence of at least 49 described beds (2–176 cm thickness) of nannofossil foraminifer ooze that have sharp basal boundaries, many of which are irregular and some of which are inclined, interpreted as gravity flow deposits from the nearby seamounts and representing ~2% of the total sediment recovered. Their grain size fines upward from medium sand to silt and they are often darker colored than immediately overlying deposits and instantly recognizable by their coarser texture. Angular basalt fragments (<1 mm), fish teeth, and pyritized foraminifers and radiolarians were also found within the basal parts of these beds, of which at least three show parallel or cross laminations in their upper or middle part. These beds, interpreted as gravity flow deposits, are present with an approximate frequency of one or two beds per core. The abundance and thickness of these beds is

highest within Cores 320-U1335-21H through 37X (189.4–350.1 m CSF-A). No gravity flow deposits were observed in Cores 320-U1335A-3H through 8H. The provenance of these deposits, as indicated by the observed basalt fragments, is inferred to be the nearby seamounts (Fig. F57B) situated ~15–20 km toward the northeast and southeast of Site U1335, with a present summit water depth that is 400–600 m shallower than Site U1335. Initial indications are that these gravity flow deposits, unlike those observed at Site U1331, might not be very erosive and therefore essentially add to the sediment column rather than removing large sections of geological time. The high sedimentation rates at Site U1335 will allow paleoceanographic studies to avoid the generally thin layers of gravity flows.

Age transect of seafloor basalt

At Site U1335 we recovered what appear to be fresh fragments of seafloor basalt with an age of ~26 Ma, as inferred by the oldest biostratigraphic datums from the sediment above. This material will, when combined with other PEAT basalt samples, provide important sample material for the study of seawater alteration of basalt.

Site U1336

Two holes were cored at Site U1336 (7°42.067′N, 128°15.253′W; 4286 m water depth) (Fig. F63), targeting paleoceanographic events in the late Oligocene and into the Miocene, including a focus on the Oligocene–Miocene transition and the recovery of the Mi-1 glaciation event (Zachos et al., 2001b; Pälike et al., 2006a). In conjunction with Sites U1335 and U1337 it was also designed to provide a latitudinal transect for early Miocene age slices. Site U1336 provides data toward a depth transect across the late Oligocene and Miocene (see "Oligocene [Site U1336; ~32 Ma crust]") that allow us to verify and apply a previous astronomical age calibration from Site 1218 (Pälike et al., 2006b).

At Site U1336, APC cores were taken from the mudline to 184.8 m CSF-A (Cores 320-U1336A-1H through 21H) and 173.6 m CSF-A (Cores 320-U1336B-1H through 20H). Nonmagnetic core barrels were used for Cores 320-U1336A-1H through 16H and 320-U1336B-1H through 16H, and steel barrels were used for all other cores. A hard layer at 120–140 m CSF-A prevented us from achieving a full stroke during coring (Cores 320-1336A-14H and 320-1336B-16H). XCB cores (320-U1336A-22X through 35X) were taken from 184.8 to 302.9 m CSF-A in Hole U1336A. We stopped coring before reaching the basement objective because of the decreasing rates of penetration, the

relatively low recovery, and the possibility of obtaining a stratigraphically complete Miocene section.

The sedimentary section at Site U1336 is composed of an ~300 m thick nannofossil ooze and chalks of middle Miocene through early Oligocene age. They are divided into three lithologic units (Figs. F64, F65). Unit I (0–74.54 m CSF-A) consists of Miocene nannofossil ooze with varying amounts of radiolarians, foraminifers, diatoms, and clay as minor constituents. Physical properties, including magnetic susceptibility, b* and L* reflectance, and GRA bulk density, all represent higher amplitude variability throughout Unit I. $CaCO_3$ contents are also variable, ranging between 48% and 90% (Fig. F65).

Unit II (74.50–189.50 m CSF-A) is dominated by nannofossil ooze. Sediment color changes occur downhole from pale yellow to light greenish gray at 92 m CSF-A. Below this boundary, the color of Unit II alternates between light greenish gray and white to 184.80 m CSF-A. Greenish gray millimeter-scale color bands are present below 120.86 m CSF-A. $CaCO_3$ contents are relatively constant in Unit II and typically >85%.

The dominant lithologies of Unit III (189.5–299.6 m CSF-A) are light greenish gray and white nannofossil chalk with light greenish gray millimeter-scale color banding and chert layers. The chert shows many different colors including black, dark greenish gray, very dark greenish gray, dark gray, olive-yellow, dark brown, and pink. The Unit II–III transition is identified by the uppermost common occurrence of chert. Below 289 m CSF-A nannofossil chalk contains increasing amounts of micrite and the cherts vary in color. The lowermost cherts are olive-yellow, then pink, and finally dark brown at the base. The chalk changes color to white below 298.54 m CSF. $CaCO_3$ contents remain >88% in the chalk layers. Igneous basement was not recovered at Site U1336. Lithologic descriptions of this site are based only on sediments recovered in Hole U1336A. A second hole (U1336B) was cored to 174.01 m CSF-A at this site during Expedition 320. Cores from Hole U1336B were left onboard to be split and described during Expedition 321.

Light–dark cycles in the nannofossil oozes of Unit I are associated with variations in the relative amounts of accessory lithologic components within the nannofossil oozes, including clay, radiolarians, and diatoms (Fig. F64) along with higher amplitude variations in the physical properties, including L*, b*, magnetic susceptibility, and GRA bulk density.

Light greenish gray sediments were recovered just as they were at Sites U1334 and U1335 and persist for ~250 m before shifting to white and pink. Magnetic susceptibility drops to near zero throughout the light greenish gray interval. Unlike other sites drilled during Expedition 320, discrete millimeter- to centimeter-scale color bands frequently occur within the interval where Fe reduction has occurred in Units II and III.

All major microfossil groups were found in sediments from Site U1336, representing a complete biostratigraphic succession at the shipboard sample resolution level of middle Miocene to early Oligocene sediments. They provide a coherent high-resolution biochronology through a complete sequence. Calcareous nannofossils are moderately well preserved throughout the succession, and there appears to be a complete sequence of nannofossil zones from NN6 (middle Miocene) to NP22 (lower Oligocene). Planktonic foraminifers are present throughout the succession, ranging from Zones M9 through O1. They are abundant and well preserved in the Miocene and less well preserved in the Oligocene. The radiolarian biostratigraphy at Site U1336 spans the interval from just above the RN6/RN5 boundary (middle Miocene) in Core 320-U1336A-1H to the uppermost part of RP22 (upper Oligocene) in Core 320-U1336A-19H (Section 320U1335-19H-CC; ~170.3 m CSF-A). Below this level the sediments are barren of radiolarians. Above this level the assemblages tend to have moderate preservation, with intermittent intervals of good preservation in RN3 and RN4 (lower to middle Miocene). This downsection decrease in preservation and ultimate disappearance of the radiolarians below ~170 m CSF-A appears to be associated with the dissolution of biogenic silica. However, the nannofossil, radiolarian, and planktonic foraminifer datums are in good agreement except for the dissolution interval of radiolarians. Benthic foraminifers are present through most of the section and indicate lower bathyal to abyssal paleodepths.

The Oligocene/Miocene boundary marker of the base of *P. kugleri* (23.0 Ma) occurs between Section 320-U1336A-16H-CC and Sample 320-U1336A-17H-2, 38–40 cm (142.96 m CSF-A), whereas calcareous nannofossil event top of *S. delphix* is recognized at 145.9 m CSF-A between Samples 320-U1336A-17X-2, 90 cm, and 17X-4, 90 cm.

Paleomagnetic measurements were conducted on archive-half sections of 21 APC cores from Hole U1336A and the magnetic susceptibilities and masses of 138 discrete samples. NRM measurements above ~80 m CSF-A in Hole U1336A indicate moderate magnetization (1×10^{-3} A/m) with a patchy but generally weak viscous isothermal remanent magnetic (IRM) coring overprint. Between ~80 and ~160 m CSF-A is a zone

of diagenetic alteration within the greenish gray core interval in which sediments effectively have no remanence or have been entirely overprinted during the coring process. Below ~160 m CSF-A polarity reversals are present, but the inclinations are steep (up to 80°), indicating that the drilling overprint was not effectively removed during demagnetization.

The magnetozones in the upper ~80 m CSF-A correlate well with the biostratigraphic framework. At the top of Hole U1336A, magnetozones in Cores 320-U1336A-1H and 2H tentatively correlate with the interval from the base of Chron C5Ar.3r to the base of C5ABn. Core 320-U1336A-3H contains one polarity interval, corresponding to polarity Chrons C5ACn and C5ADn, but Chron C5ACr was not identified. Core 320-U1336A-4H includes Chrons C5ADr and C5Bn, and the top of Chron C5Br occurs at the base of Core 320-U1336A-4H and terminates at the base of Core 5H. Below Chron C5Br the correlation with the GPTS is relatively unambiguous through Core 320-U1336A-9H, which contains the upper portions of Chron C6n. Between ~80 and ~160 m CSF-A the magnetization of the sediment deteriorates below analytical noise level within the greenish gray core interval as observed at Site U1335. Below ~160 m CSF-A a reversal pattern is discernible and tentatively correlates with Chrons C6Cr through C7An.

Biostratigraphic datums and magnetostratigraphy results allow the calculation of average LSRs that are 9 m/m.y. for the upper 74 m of the section on the corrected CCSF-A depth scale. Site U1336 LSRs increase from 12 m/m.y. in the lower Miocene to 15 m/m.y. in the Oligocene. There are no apparent hiatuses in the shipboard biostratigraphic resolution.

A complete physical property program was conducted on whole cores, split cores, and discrete samples. Hole U1336B was analyzed only using the WRMSL and NGR detector. Physical property data for Hole U1336B have not been filtered for drilling disturbances.

Magnetic susceptibility measurements correlate well with the major differences in lithology of Site U1336. Magnetic susceptibility values are highest in Unit I with high amplitude and frequency variations from 5×10^{-5} to 30×10^{-5} SI. In Unit II, they decrease from ~10×10^{-5} to near 0 SI. There is a slight increase in the amplitude and frequency of the variation in Unit III. The highest NGRs are present at the seafloor (~56 cps), rapidly decrease with depth in Unit I, and then are very low (2 cps) in Unit II.

Velocities are between 1480 and 1500 m/s in Unit I and between 1480 and 1530 m/s in Unit II. At ~176 m CSF-A velocities begin to increase rapidly into Unit III, from 1530 to ~1960 m/s at 208 m CSF-A. The remainder of Unit III shows high-frequency and high-amplitude variation averaging 1910 m/s in this more lithified interval.

Wet bulk density is lowest in Unit I (1.4–1.7 g/cm³), which contains a large amount of clay, radiolarians, and diatoms, and then increases slightly and is more uniform (~1.7 g/cm³) in Unit II. In Unit III wet bulk density becomes variable deeper than 180 m CSF-A, averaging 1.9 g/cm³. Grain density variations match changes in lithology. At the top of the section, grain density is 3.0 g/cm³ and falls rapidly, reflecting clay-rich sediments that grade rapidly into nannofossil ooze. Grain density averages 2.7 g/cm³ for most of the succession (varying from 2.6 to 3.0 g/cm³); this reflects the dominance of carbonate material through the succession (grain density of calcite = 2.70 g/cm³). Porosity is highest in Unit I, varying from 65% to 80%, and decreases gradually toward the base of Unit II to 55%–60% at ~184 m CSF-A. In Unit III, porosity ranges from 45% to 60%.

Thermal conductivity decreases from 1.2 to 1 W/(m·K) through Unit I, with a minimum conductivity of 0.91 W/(m·K) at 31 m CSF-A. Units II and III values increase from 1 to 1.4 W/(m·K). Below 183 m CSF-A thermal conductivity decreases because of increased core disturbance by XCB coring.

Spectral reflectance corresponds to pronounced lithologic and diagenetic changes. In Unit I, L* values are lowest (50%–80%) and display high-amplitude variations because of minor lithologic changes. Unit II values are higher and more uniform, and Unit III values are slightly lower and more variable. Variations in b* (blue–yellow) decrease abruptly below 92 m CSF-A.

Hole U1336B cores were not split during Expedition 320; the position of coring disturbances is unknown and the construction of a spliced section for sampling purposes had to be postponed. Magnetic susceptibility and GRA density were used for correlating Holes U1336A and U1336B. Features in these data are well aligned between Holes U1336A (84 m CSF-A) and U1336B (84 m CSF-A) to a depth of ~94 m CCSF-A. Below 94 m CCSF-A the correlation between the two holes becomes challenging without additional split-core data, and a single spliced record was not assembled at this point. A growth factor of 1.13 is calculated by linear regression for the top 94 m CCSF-A of Site U1336, indicating a 13% increase in CCSF-A relative to CSF-A depth.

A standard geochemical analysis of pore water and organic and inorganic properties was undertaken on sediments from Site U1336. A total of 22 whole-round interstitial water samples from Hole U1336B were analyzed. Chlorinity values show a distinct increase from ~555 to ~570 mM in the uppermost 40 m CSF-A, potentially reflecting the boundary condition change from the more saline ocean at the Last Glacial Maximum to the present. Alkalinity is relatively constant at values >2.5 mM in the upper 110 m, with a pronounced decline to 1 mM at 170 m CSF-A. Sulfate concentrations decrease with depth to values as low as 22 mM. Dissolved phosphate concentrations are ~5 μM at ~9 m CSF-A, decreasing to ~1 μM at ~15 m CSF-A. Dissolved manganese and iron have broad peaks in the depth range from ~25 to 120 m CSF-A and below 100 m CSF-A. An increase of iron mirrors a decrease in manganese. Concentrations of dissolved silicate increase with depth from <400 to 800 μM but do not reach saturation with biogenic opal.

Highlights

Miocene sedimentary section and cyclic sedimentations

One of the highlights from Site U1336 is the recovery of a very thick Miocene carbonate section from the central equatorial Pacific, one of the high-priority objectives of the PEAT program. We recovered the complete early Miocene sequence (~9 m.y. duration) in a ~110 m thick section with a sedimentation rate of 12 m/m.y. and the middle Miocene sequence (4.5 m.y. duration) in a ~45 m thick with a sedimentation rate of ~21 m/m.y. These high sedimentation rates will facilitate the study of paleoceanographic processes at unprecedented resolution for the equatorial Pacific.

The obvious variations of both color and biogenic composition within nannofossil oozes represent cyclically changing fluctuations of CCD and upwelling intensity during the middle Miocene through early Miocene. The variable lithology also results in variations of many petrophysical signals of physical properties including L*, b*, magnetic susceptibility, and GRA bulk density. These high sedimentation rate and cyclic sediments will facilitate the study of paleoceanographic processes at unprecedented resolution for the equatorial Pacific.

Oligocene–Miocene transition and depth transects

Site U1336 was planned as a latitudinal transect for early Miocene age slices and the PEAT Oligocene–Miocene depth transect in conjunction with Sites U1335 and U1337. The Miocene sequence at these sites includes the critical intervals of the Mi-1 glaciation and middle Miocene ice sheet expansion (Holbourn et al., 2005; Zachos et al.,

2001b; Pälike et al., 2006a). The dominant lithologies of nannofossil ooze and chalk at Sites U1336 and U1335, with better preservation of calcareous microfossils than any other site drilled during Expedition 320, will allow us to achieve the prime objective for this coring site.

The Oligocene–Miocene transition in Hole U1336A occurs in very homogeneous nannofossil ooze within the alternations of white and light greenish gray ooze. The same alternating sequence is observed above the Oligocene–Miocene transition at Site U1334 (see **"Site U1334"**). The biostratigraphy reveals that the Oligocene/Miocene boundary exists between 142.96 and 145.9 m CSF-A at Site U1336; that will allow high-resolution study of this critical interval.

Geochemical front

At Site U1336 we recovered an interval of greenish gray carbonates that show a distinct Mn increase and elevated Fe pore water concentrations with characteristics similar to geochemical alteration fronts at Sites U1334 and U1335. At Site U1336, this zone is ~200 m thick. The paleomagnetic signal was very weak in most parts of this section (80–160 m CSF-A). High Fe and Mn pore water concentrations may be related to changes in the oxidation state in the sediments. The oxidation-reduction reactions are likely fueled by the enhanced availability of organic carbon overlying and underlying the sediment zone. This site may provide the opportunity to study organic matter degradation.

Site U1336 migrated from south to north through the equatorial belt of high productivity. Based on paleolatitudinal reconstructions, these geochemical alteration fronts can be mapped to similar equatorial positions between Sites U1334 and U1335, roughly between the Equator and ~4°N.

Chert formation in the early Oligocene

The sequence at Site U1336 includes barren intervals of radiolarian fossils and many thin intercalated chert layers and fragments. Radiolarians decrease in preservation downsection and disappear below Core 320-U1336A-19H. Instead, the sediments contain several chert fragments. Some inferred chert layers are present at ~120–140 m CSF-A and prevented the APC penetration. Below ~190 m CSF-A, various colored chert layers and fragments are present in the cores. The chert frequently contains foraminifer tests, reflecting the diagenetic process of dissolution and reprecipitation of the biogenic silica.

The dissolution of biogenic silica is the source of porcellanite and chert, and on crust <65 Ma in age almost all cherts in the Pacific lie <150 m above basement. Although we have not recovered basement rocks at this site, the sediments became hard, lithified limestones and the drilled section is probably close to basement. The dissolution of silica in the basal sedimentary section is likely associated with the circulation of warm hydrothermal waters in the upper oceanic crust that extends into the lower sediments where they are cut by fractures and faults (Moore, 2008a, 2008b). This site will provide information on chert formation in the equatorial Pacific regions.

Operations

Expedition 320 was the first of two expeditions that comprise the PEAT science program. Expedition 320 began in Honolulu, Hawaii, and drilled 16 holes at 6 sites (Sites U1331–U1336; Table T1) before returning to Honolulu.

Unless otherwise noted, times in this operations section are given in local ship time, which was Hawaii Standard Time (UTC − 10 h) for Sites U1331–U1333. During the transit to Site U1334, shipboard clocks were advanced 1 h, resetting local ship time to UTC − 9 h. Shipboard clocks were returned to Hawaii Standard Time (UTC − 10 h) during the transit from our last site (U1336) back to Honolulu.

Honolulu port call

Expedition 320 officially began when the first line was passed ashore to Pier 29 of Honolulu harbor at 1042 on 5 March 2009. Following the routine U.S. customs and immigration formalities, port call activities were initiated with the changing and crossover of Overseas Drilling Limited (ODL) and IODP personnel. Expedition scientists boarded the ship on 6 March.

During the ~5 day port call, the usual food stocks and provisions were loaded and offgoing freight disembarked. Items of note that were loaded in Honolulu included ~707 MT of marine gasoil, 147 short tons of bulk attapulgite, 7 joints of 20 inch casing, 16 joints of 16 inch casing, and 46 joints of 10¾ inch casing. Other significant items were two boxes of core liners and two reentry cone assemblies.

In accordance with the port call plan, customer service representatives came on the vessel to perform maintenance and repair on the ship's elevator and the HVAC system. A Siemens engineer also performed upgrades to the throttle system program.

A number of shipboard tours were conducted for the IODP Science and Technology Panel (STP), several classes from the University of Hawaii (USA), and National Science Foundation (NSF) visitors. Of the unplanned events, a replacement refrigerated food container had to be leased at the last moment because the 10 ft auxiliary unit located on the accommodation roof could not be repaired in the time available. The U.S. Coast Guard interrupted the loading of compressed gas cylinders on 9 March for nearly an hour to address concerns relating to the handling of these items at this facility.

Following the release of the last line from the pier at 1500 h on 10 March, the *JOIDES Resolution* exited the harbor. Outside the harbor, a small vessel came alongside to deliver a radioactive source and two neutron tools required for the logging effort. The vessel then departed at full speed to the first site (U1331) with an expected arrival the evening of 14 March.

Transit to Site U1331

The transit to the first site of Expedition 320 was made through generally moderate seas and swell with predominantly overcast skies and occasional showers signifying that we were under the influence of the ITCZ. We began positioning over Site U1331 at 2330 h on 14 March 2009. The 1081 nmi voyage from Honolulu was accomplished at an average speed of 10.4 kt.

The 4 day voyage was almost without incident. The zero-speed module which monitors shaft speed and direction failed 1 h out of port, and the breaker supplying power to starboard shaft Motor 17A and port shaft Motor 14B tripped offline 2 h before arriving on the location.

Site U1331 (PEAT-1C)

Hole U1331A

Once the vessel was positioning over Site U1331 (PEAT-1C), an operational test of the dynamic positioning (DP) system was undertaken. Concurrent with the DP testing, the making up of the bottom-hole assembly and spacing out of the core barrel and colletted delivery system was accomplished. As the drill string was deployed, each joint of pipe was measured and the internal clearance of each tubular inspected in accordance with routine practices.

Because the precision depth recorder (PDR) was inoperative, the driller carefully extended the bit and tagged the seafloor. Using the passive heave compensator, the bit was pulled back 10 m from this depth. Hole U1331A was spudded with the APC at 0750 h on 16 March, 2009. The depth calculated from the recovery of the first core was established at 5127.3 m DRF (5116.2 meters below sealevel [mbsl]). The offset of the rig floor was 11.1 m, so the water depth as determined by drill string length was 5116.2 m. Prior to spud-in, the drill string was flushed and cleaned of rust particles by pumping down a clean-out plug and two round trips of an XCB core barrel. Depths reported in this operations section are based on the measurements using the length of the drill string and are either drilling depth below rig floor (DRF) or DSF.

Piston coring advanced the hole to 138.2 m DSF just above the chert layer suggested by the seismic record. To avoid damaging the APC, operations were then conservatively switched to the XCB corer. We cored to 138.2 m DSF with APC Cores 320-U1331A-1H through 15H and recovered 141.3 m of core (102%). Cores 1H through 11H were oriented with the FlexIt tools.

Cores 12H through 15H were not oriented because the FlexIt tool was not deployed in anticipation of having to drill over stuck core barrels. The pullout force to recover the core barrels from the sediment was gradually increasing with depth and then decreased; it was anticipated that the drillover technique to free stuck core barrels might have to be employed. We switched to the standard, more durable steel core barrels starting with Core 12H instead of the nonmagnetic core barrels.

XCB coring advanced the hole from 138.2 m DSF to basement at ~190.6 m DSF. We cored to 52.4 m with Cores 15X to 21X and recovered 13.6 m (26%). From Core 18X to 22X (157.3–190.6 m DSF), recovery was negatively impacted by the presence of chert. We did manage to recover a short (0.42 m) section of the basal carbonate section in the last core, and bottomed out with a small sample of basalt. The total average recovery of APC/XCB coring in Hole U1331A was 81%.

Upon completion of the coring program, we conducted downhole logging. Downhole logging completed one run to a total depth of the borehole with the "paleo"-combo tool string (NGR, GRA density, and magnetic susceptibility). The data were used to guide the coring strategy in subsequent holes at this site. The planned second run with the FMS-sonic tool was aborted because of problems with the logging winch.

Hole U1331B

After the bit was pulled above the seafloor at 0820 h on 18 March 2009, the vessel was offset 20 m to the west of Hole U1331A. Hole U1331B was spudded with the APC, and the recovery of the first core was used to calculate the seafloor depth at 5127.4 m DRF (5116.3 mbsl). The vertical offset to Hole 1331A was 5 m deeper to cover gaps between cores in the first hole. APC Cores 320-U1331B-1H through 17H advanced from 0 to 156.6 m DSF; we cored 156.5 m and recovered 163.13 m (104%). Five formation temperature measurements were made with the APCT-3 in Cores 320-U1331B-2H, 3H, 5H, 7H, and 10H (19.6, 29.1, 48.1, 67.1, and 95.6 m DSF, respectively).

We switched to XCB coring for Core 18X (156.6–166.3 m DSF) but did not recover any core. Based on the drill, log, and core data from the first hole, we decided to drill with a center bit (without coring) through the chert interval (166.3–177.0 m DSF) and then attempt a single APC core in the sediment section below. APC Core 20H was attempted below the chert in the early Eocene basal carbonate section, but the corer was not able to penetrate the formation. We drilled ahead again without coring to 179.0 m DSF and one more XCB core was taken from 179.0–188.5 m DSF, but it did not recover any material. From 156.6 to 188.5 m DSF, we XCB cored 19.2 m but did not recover any material. An additional 12.7 m was drilled without coring. The bit was pulled free of the seafloor at 2220 h on 19 March, and the vessel was offset 20 m west of Hole U1331B.

Hole U1331C

The program for the third hole of the site was to spot core and fill in gaps in the sedimentary record from the first two holes and to obtain any core from below the chert. Hole U1331C was spudded with the APC at 0155 h on 20 March 2009. The recovery of the first core was used to calculate the seafloor depth of 5128.0 m DRF (5116.9 mbsl). Cores 320-U1331C-1H through 4H penetrated to 38.0 m DSF, and we recovered 39.2 m (103%). The interval from 38.0 to 59.0 m DSF was then drilled without coring, and Core 6H was taken from 59.0 to 68.5 m DSF (9.99 m recovered; 105%). We then drilled without coring from 68.5 to 92.5 m DSF and took APC Core 8H (92.5–102.0 m DSF; recovery = 9.21 m, 97%).

A short interval of 0.5 m was drilled to 102.5 m DSF, and Core 10H was taken from 102.5 to 112.0 m DSF; we recovered 8.48 m (89%). The interval from 112.0 to 129.0 m DSF was drilled without coring, and Cores 2H through 14H were obtained from 129.0 to 157.5 m DSF (29.1 m recovered; 102%). Following a drilled interval of 19.5

m through a chert sequence (157.5–177.0 m DSF), a third attempt to core the short interval below the chert and above the top of basaltic oceanic crust was attempted.

This early Eocene section was one of the highest priority sections at this site and was poorly recovered in the previous two holes. This time the drillers successfully obtained this interval in APC Cores 17H and 18H (177.0–189.0 m DSF), coring 12.0 m and recovering 14.0 m (117%). Judging by the deformation of the cutting shoe and a bent 15 ft section of core barrel, it was surmised that Core 18H had more than vigorously encountered basement.

During the spot coring in Hole U1331C, all piston cores up to and including Core 14H employed nonmagnetic core barrels and were oriented with the FlexIt tool. Standard steel barrels were used to obtain Cores 16H and 17H and did not use the orientation tool to avoid damaging it. We recovered 109.5 m (102%) in the cored interval of 107.0 m. An additional 82.0 m was drilled without coring. With the recovery of Core 17H, the decision was made to end coring on this site and to proceed to Site U1332.

After the drill string was pulled free of the seafloor at 1300 h on 21 March, the pipe trip was temporarily suspended for 1.5 h to accomplish the slipping and cutting of 115 ft of drilling line. Once drilling line maintenance was completed, tripping was resumed. The beacon was retrieved at 1500 h while the drill string was being recovered. At 0500 h on 22 March the drilling equipment was secured and the vessel departed for the second site of Expedition 320.

Transit to Site U1332

Following completion of Site U1331, we started heading east to Site U1332. The vessel made slow progress into a 20 kt wind and against a strong current with moderate pitching and rolling into a 6–8 ft swell with spray occasionally over the bow. These elements conspired to reduce the average speed of the 66.1 nmi voyage to Site U1332 to a lethargic 7.1 kt.

Site U1332 (PEAT-2C)

Hole U1332A

After the 9.25 h transit, we began positioning over the site at 1445 h on 22 March 2009. We assembled the bottom-hole assembly, and spaceout of the colletted delivery system was verified. Because the PDR was not working, it was necessary for the driller

to carefully lower the bit and tag the seafloor to verify the exact depth. As the driller was preparing to spud the hole, the display that indicates coring line position relative to the rig floor failed. Because it is imperative for the core winch operator to know where the coring line is at all times, operations had to be suspended for 3 h while the defective unit was replaced.

Hole U1332A was spudded with the APC at 1050 h on 23 March. The water depth calculated from the recovery of the first core was established at 4935.1 m DRF (4923.9 mbsl). APC Cores 320-U1332A-1H through 14H penetrated from 0 to 125.9 m DSF, and we recovered 131.9 m (104%). All piston cores were oriented with the FlexIt tool. Because of the potential presence of chert horizons, no downhole temperature measurements were attempted in the initial hole of this site. We switched to XCB coring after Core 14H, which required 70,000 lb of overpull to extract the core barrel from the sediment.

We recovered 13.8 m (51%) in XCB Cores 15X through 18X (125.9 to 152.4 m DSF). Coring was terminated when Core 18X was recovered with a piece of basaltic basement. Hole U1332A was cored to 152.4 m, and we recovered 145.6 m (96%).

After coring was finished, we prepared the hole for logging by flushing it with 65 bbl of attapulgite mud and then dropping a go-devil to open the lockable float valve (LFV). We then displaced the hole with 80 bbl of attapulgite mud and raised the bit to 78 m DSF.

We then deployed a tool string consisting of the magnetic susceptibility, GRA density, and NGR tools. This tool string acquired good logs over the entire open hole interval. Unfortunately, the tool string parted from the logging wireline when attempting to recover the tool and the tool string was lost in the hole.

We spent ~ 18 h conducting three unsuccessful coring line fishing attempts to recover the logging tool string. After acknowledging that spending more time fishing for the tool string would not be productive, the decision was made to seal Hole U1332A with 15 bbl of cement above the lost logging tool, extending from 125 to 90 m DSF. Deploying the cement had to be delayed for 4 h while the cement pumps were repaired.

After the cementing operations were completed, the bit was pulled free of the seafloor at 0800 h on 26 March and the vessel was offset 20 m north of Hole U1332A. Before coring could resume, the drill string was flushed with seawater to remove any cement from the tubulars and bit nozzles.

Hole U1332B

Hole U1332B was spudded at 1230 h on 26 March 2009. We started coring Hole U1332B with the bit offset 5 m deeper than the seafloor depth established for Hole U1332A but only penetrated to 2.1 m CSF-A below the mudline. We recovered 118.4 m (107%) in APC Cores 320-U1332B-1H through 13H (0–110.1 m DSF). In an attempt to maintain an offset with the first hole, there were short advances with Core 3H (8.0 m) and 11H (5.0 m). The APCT-3 was deployed while taking cores at six different depths: 11.6, 19.6, 38.6, 57.6, 76.6, and 100.6 m DSF (Cores 2H, 3H, 5H, 7H, 9H, and 12H, respectively). Nonmagnetic core barrels were used on all cores except 13H.

We then switched to the XCB and took Cores 14X to 18X from 110.1 to 148.6 m DSF and recovered 23.4 m (61%). Coring was terminated when we recovered ~2.4 m of dark brown sediment above several small pieces of oceanic basalt in Core 18X.

At Hole U1332B we cored a total of 148.6 m and recovered 141.8 m (95%). The drill string was pulled out of the hole and the bit cleared the seafloor at 2230 h on 27 March.

Hole U1332C

Hole U1331C was designed to provide stratigraphic overlap and confirm stratigraphic correlations with Holes U1332A and U1332B. After the vessel was offset 30 m north of Hole U1332B, Hole U1332C was spudded at 0105 h on 28 March 2009. The seafloor depth calculated from the recovery of the first core was 4934.0 m DRF (4922.8 mbsl). Piston coring then routinely proceeded to 85.0 m DSF, during which the advances of Cores 320-U1333C-6H (4.0 m advance) and 8H (7.0 m advance) were adjusted to maintain overlap with previous holes. At ~1330 h on 28 March, while retrieving Core 10H, an electrical transient attributed to the rotating condenser caused two of the three main generators to trip off the main bus and resulted in a load shedding sequence to various systems on the vessel, which included loss of control voltage to all Thyrig bays for ~10 min. The consequence of the loss of Thyrig control voltage was a short-term loss of power to thrusters, propulsion, and drilling motors. During this short event, the DP 3% watch circle (percentage of water depth or ~150 m off the hole) was not exceeded. The main breakers quickly reset and power was restored to all main systems by 1341 h. We think the switching circuit for removing the rotating condenser from the main bus may be defective.

Because of the power loss, the coring line parted while attempting to recover Core 10H, and we had to make two fishing trips with the coring line to recover the sinker bars and the full core barrel. Unfortunately, this APC core was near the Eocene/Oligocene boundary and was very disturbed. APC coring continued to 113.5 m DSF where coring was switched to the XCB. All the APC cores were obtained with nonmagnetic core barrels and with the FlexIt core orientation tool except Core 13H, for which we used standard steel core barrels. APCT-3 formation temperature measurements were made at 36.0 m DSF (Core 4H) and 75.5 m DSF (Core 9H). APC Cores 1H through 13H extended from 0 to 113.5 m DSF, and we recovered 122.04 m (108%). XCB Cores 14X through 18X extended from 113.5 to 155.5 m DSF, where basement was encountered, and we recovered 26.02 m (62%). The total core interval with both coring systems was 155.5 m with 148.1 m recovered (95%).

Once the final core was on deck, we started recovering the drill string. The seafloor beacon was successfully recovered on deck at 1202 h on 29 March. At 1930 h on 29 March, the drilling equipment had been secured and we departed for Site U1333.

Transit to Site U1333

The 176 nmi voyage to Site U1333 took 18.3 h and was accomplished at an average speed of 9.6 kt. The journey required a little more than the allotted time because the speed was adversely affected by having to sail into a 22–26 kt wind and a strong current.

Site U1333 (PEAT-3C)

Hole U1333A

At 1400 h on 30 March, the vessel began positioning over the site in DP mode. Once the drilling assembly was deployed, the driller carefully lowered the bit and tagged the seafloor at ~4875 m DRF. The bit was raised 10 m, and Hole U1333A was spudded at 1225 h on 31 March 2009. The seafloor depth calculated from the recovery of the first core was 4865.0 m DRF (4853.7 mbsl); however, this depth measurement is questionable because the recovery was a full core (10.05 m).

APC Cores 320-U1333C-1H through 10H were taken from 0 to 95.0 m DSF, and we recovered 104 m (109%). We switched to XCB coring after the core barrel for Core 10H had to be drilled over to free the fully stroked core barrel from the sediment. All

APC cores were obtained with nonmagnetic core barrels; the FlexIt orientation tool was not deployed since there were questions about its data reliability.

XCB Cores 11X through 22X penetrated from 95.0 to 184.1 m DSF, and we recovered 77.0 m (87%). Coring ended when we recovered basalt in Core 22X. The drill string was pulled out of the hole and cleared the seafloor at 1155 h on 1 April.

Hole U1333B

The vessel was offset 25 m east of Hole U1333A, and APC coring in Hole U1333B started at 1305 h on 1 April 2009 with the bit 5 m shallower than the first hole. We recovered 7.7 m in Core 320-U1333B-1H, so the seafloor was established at 4861.8 mbsf (4850.5 mbsl).

Based on the drilling and coring data from the first hole, the drillers were confident that by drilling over stuck core barrels, the APC could safely be pushed deeper than the 95.0 m penetration that was realized in the first hole. This confidence was justified when APC Cores 1H through 18H were advanced to 162.7 m DSF and we recovered 166.4 m (102%). Nonmagnetic core barrels were used on Cores 1H through 9H, and standard steel core barrels were deployed on all subsequent piston cores. Formation temperature measurements were made with the APCT-3 tool at 26.7, 45.7, 64.7, and 83.7 m DSF (Cores 3H, 5H, 7H, and 9H, respectively). The FlexIt orientation tool was not used. Three stuck core barrels (Cores 13H, 16H, and 17H) required drilling over when they could not be released from the sediment despite 70,000 lb of overpull. Core 18H failed to achieve a full stroke of the core barrel, and no further APC coring was conducted.

Two XCB cores advanced the hole from 162.7 to the final depth of 180.3 m DSF, and we recovered 13.44 m (76%). Coring ended when we recovered basalt in Core 20X. The drill string was pulled out of the hole and cleared the seafloor at 1845 h on 2 April.

Hole U1333C

Hole U1333C was started 25 m east of and 2.75 m shallower than Hole U1333B. Core 320-U1333C-1H was shot at 2000 h on 2 April 2009, and we recovered 1.65 m, so the water depth for this hole is 4865.1 m DRF (4853.8 mbsl).

Cores 1H through 21H penetrated from 0 to 163.2 m DSF, and we recovered 176.1 m (108%). Seven core barrels (Cores 13H through 19H) required drilling over to release

the barrels from the sediment when the application of 70,000 lb of overpull was not successful. Nonmagnetic core barrels were used on Cores 1H through 13H. Standard steel core barrels were used on all subsequent APC cores. The advancement of four cores was adjusted to maintain the overlap with previous holes: Cores 11H (6.0 m advance), 12H (5.0 m advance), 16H (4.5 m advance), and 19H (4.0 m advance). All other cores advanced the full 9.5 m except for Core 21H, which did not penetrate into the formation at all—so we switched to XCB coring.

XCB Cores 22X through 24X penetrated from 163.0 to 177.0 m DSF, and we recovered 0.87 m (6%). Coring in this hole ended when we recovered basaltic basement in the last core.

Once the seafloor beacon was recovered on board, the drill string recovered on the rig floor, the thrusters raised, and the drilling equipment secured, the vessel departed for the Site U1334 at 1815 h on 4 April.

Transit to Site U1334

The 410 nmi voyage from Site U1333 to Site U1334 took 40.8 h and was accomplished at an average speed of 10.1 kt. During the transit the ship's clocks were advanced 1 h, resetting local ship time to more closely follow the earlier rising sun as we migrated eastward to each site. Unless otherwise noted, times for Sites U1334 are given in ship local time (UTC – 9 h).

Site U1334 (PEAT-4C)

Hole U1334A

Once the vessel approached the coordinates of the new location, the captain slowed the vessel and maneuvered the vessel over the site. We were positioning over the new location by 1222 h on 6 April 2009. After assembling the drill string and lowering it to the seafloor, we attempted to spud the new site with the bit positioned 10 m shallower than the corrected depth of 4798.4 m DRF (4787.0 mbsl) from the PDR. We recovered only water, so the bit was lowered to 4798 m DRF for a second attempt. This was successful, and Hole U1334A was spudded with the APC at 0030 h on 7 April. The mudline recovered in Core 320-U1334A-1H was used to establish the seafloor depth at 4799.3 m DRF (4787.9 mbsl). This depth was within 1 m of the corrected PDR depth.

APC Cores 1H through 22H were taken from 0 to 206.9 m DSF, and we recovered 212.39 m (103%). APC coring was terminated when Core 22H did not stroke fully and required 80,000 lb to release it from the formation. Nonmagnetic core barrels were used on Cores 1H through 16H; standard steel core barrels were used on Cores 17H through 22H.

XCB Cores 23X through 32X were taken from 206.9 to 285.5 m DSF, and we recovered 77.99 m (99%). Coring was terminated when we recovered a sample of basalt in Core 32X. The total cored interval for Hole U1334A was 285.5 m, and we recovered 209.4 m (102%). The drill string was pulled out of the hole and cleared the seafloor at 2150 h on 8 April.

Hole U1334B

The ship was offset 25 m west of Hole U1334A, and we spudded Hole U1334B at 2330 h on 8 April 2009 with the bit 5 m deeper than at the first hole. APC Cores 320-U1334B-1H through 22H were taken from 3.7 to 210.7 m DSF, and we recovered 218.43 m (105%). Nonmagnetic core barrels were used on Cores 1H through 15H; standard steel barrels were used on Cores 16H through 22H. Downhole temperature measurements were obtained at 32.2, 49.2, 68.2, 87.2, and 106.2 m DSF (Cores 3H, 5H, 7H, 9H, and 11H, respectively). Core U1334B-5H was advanced 7.5 m to maintain an ~5 m vertical offset with Hole U1334A.

XCB Cores 23X through 31X were taken from 207.0 to 281.7 m DSF, and we recovered 76.84 m (103%). We stopped coring when we recovered basalt in Core 31X. We pulled the drill string out of the hole and the bit cleared the seafloor at 1840 h on 10 April.

Hole U1333C

After the ship was offset 25 m west of Hole U1334B, Hole U1334C was spudded at 2020 h on 10 April 2009 with the bit 3 m deeper than Hole U1334A. APC Cores 320-U1334C-1H through 22H penetrated from 0 to 209.0 m DSF, and we recovered 213.0 m (102%). Nonmagnetic core barrels were used on Cores 1H through 15H; Cores 16H through 22H used the standard steel barrels. We had to drill over Cores 19H, 21H, and 22H to release them from the formation. We then switched to XCB coring. Cores 23X through 33X were taken from 209.0 to 280.7 m DSF, and we recovered 72.9 m (102%). Core 26 was advanced by 6 m to maintain stratigraphic overlap with the first two holes. Coring finished when limestone including basalt clasts was recovered in the last core. Cores from Hole U1334C successfully covered the stratigraphic gaps in the first two holes.

Our final operations planned for Hole U1334C were to conduct two downhole logging runs. We circulated the hole with 50 bbl of attapulgite mud and then displaced the hole with 100 bbl of attapulgite mud. We raised the bit up to 95 m DSF and rigged up for logging. The first tool string was assembled and deployed into the pipe at 1930 h on 12 April. While lowering the logging tool string into the hole, the transmission on the logging winch failed when the tool was ~1700 m below the rig floor. We started to manually retrieve the tool string using T-bar clamps, air tuggers, and the starboard crane. After recovering ~550 m of wireline and spooling it back onto the logging winch drum, we decided to retrieve the remaining logging wireline by spooling the logging wireline onto the core winch drum. The logging tool was back on the rig floor at ~1200 h on 13 April. No more logging could be conducted during Expedition 320.

We started pulling the drill string out of the hole and the bit cleared the seafloor at 1225 h on 13 April. After the drill string was recovered and the thrusters retracted, we began the transit for Site U1335 at 2200 h on 13 April.

Transit to Site U1335

The 375 nmi voyage from Site U1334 to Site U1335 took 42.3 h at an average speed of 8.9 kt. Shortly after departing Site U1334, propulsion Motor 16A on the port propeller shaft had to be taken offline because of defective field coils. This was the second propulsion motor to exhibit the same problem this expedition. Propulsion Motor 15A on the starboard shaft had to be removed from the grid shortly after leaving Honolulu. It is expected that these units will be repaired during the port call in Honolulu. The rest of the voyage was made with reduced revolutions on both shafts (120 rpm instead of 140 rpm). Although capable of higher shaft revolutions, the lower shaft power was necessary to keep the ambient temperature in the propulsion room from moving into a critically high range.

Site U1335 (PEAT-6C)

Hole U1335A

The ship slowed and was in DP mode over Hole U1335A at 1630 h on 15 April 2009. We assembled the drill string, lowered it to the seafloor, and started coring Hole U1335A at 0355 h on 16 April. The estimated water depth based on the recovery of the first core was 4339.0 m DRF (4327.5 mbsl).

Cores 320-U1335A-1H through 36H were taken from 0 to 341.4 m DSF, and we recovered 354.7 m (104%). APC piston coring to this depth is an operational highlight for this site. Nonmagnetic core barrels were used for Cores 1H through 16H; steel barrels were used for all other cores. Nine core barrels required drilling over to release them from the formation (Cores 19H through 22H, 26H, 27H, and 34H through 36H) and Cores 16H and 36H only partially stroked.

We then switched to XCB coring and took Cores 37X through 45X from 341.4 to 421.1 m DSF and recovered 67.9 m (85%). We retrieved Core 45X after taking ~1 h to advance only 3 m. When retrieving this core, it apparently became stuck in the drill string just above the bottom-hole assembly. We attempted to free the stuck core barrel with the wireline jars by alternating the tension on the coring line for ~1 h when the overshot shear pin parted. Once we recovered the sinker bars and wireline jars, we pumped another core barrel down on top of it and this succeeded in dislodging the stuck core, which dropped back down to the bit. When Core 45X was recovered, it contained hard limestone and the XCB bit was very worn down, so we decided it was best to stop coring in this hole. The basement depth is deeper than anticipated and suggests higher seismic velocities in the sediment column from Site U1335 than those from the nearest site (ODP Site 574). Once Hole U1335A was completed, the bit was pulled free of the seafloor at 1725 h on 18 April and the vessel offset 25 m west.

Hole U1335B

We started coring Hole U1335B at 1955 h on 18 April 2009 with the bit 5 m deeper than at Hole U1335A. The seafloor depth based on the recovery of the first core was 4339.6 m DRF (4328.1 mbsl).

APC Cores 320-U1335B-1H through 41H were taken from 0 to 378.2 m DSF, and we recovered 392.7 m (104%). This is the second deepest APC penetration in the history of ocean drilling. Nonmagnetic core barrels were used on Cores 1H through 19H, and steel barrels were used on all remaining cores. Formation temperature measurements were made with the APCT-3 at 22.3, 41.3, 60.3, 79.3, and 98.3 m DSF (Cores 3H, 5H, 7H, 9H, and 11H, respectively). Twelve core barrels had to be drilled over to release them from the formation (Cores 19H, 20H, and 35H through 41H). Cores 37H through 41H did not achieve a full stroke and were advanced by recovery.

After switching to XCB coring, we took Cores 42X through 46X from 378.2 to 417.5 m DSF and recovered 36.0 m (92%). Coring was terminated when basement was reached.

Originally we had planned three holes at Site U1335. However, after recovering a continuous Miocene section with nearly complete recovery and overlap between the two holes, we decided to not core a third hole at Site U1335. The fact that the cores contained frequent turbidites and a very weak magnetic signal in the interval with the distinctly colored sediment also contributed to this decision. Instead we decided to use our remaining time to core at Site U1336 to provide the second PEAT expedition more information for optimizing their operations plan.

We pulled the drill string out of the hole and the bit cleared the seafloor at 1215 h on 21 April. Before the drill string was recovered, we spent 1 h to slip and cut 115 ft of drill line. Once the drilling line maintenance was completed, the drill string was recovered, the beacon retrieved, and the drilling equipment secured for transit. The vessel departed for the Site U1336 at 2145 h on 21 April.

Transit to Site U1336

The 185 nmi transit from Site U1335 to Site U1336 took 17.8 h at an average speed of 10.4 kt. Unless otherwise noted, times for Site U1336 are given in ship local time (UTC – 9 h).

Site U1336 (PEAT-5C)

Hole U1336A

The ship slowed as it approached Hole U1336A and was in DP mode at 1545 h on 22 April 2009. Once the ship was stabilized over the new site, the drill string was deployed and the bit positioned 5 m shallower than the corrected PDR depth of 4300.4 m DRF. Hole U1336A was spudded with the APC at 0135 h on 23 April. The seafloor depth estimated from the recovery in the first core was 4296.9 m DRF (4285.3 mbsl).

APC Cores 320-U1336A-1H through 21H were taken from 0 to 184.8 m DSF, and we recovered 190.2 m (103%). Nonmagnetic core barrels were used to obtain Cores 1H through 16H; steel barrels were used for all other cores. Three cores (14H, 16H, and 21H) only partially stroked and we advanced by recovery. A hard layer at ~124 m DSF prevented Core 14H from achieving a full stroke; the layer was ~0.5 ft thick and was not recovered; based on how it drilled, we inferred it may have been chert. The last piston core (21H) required drilling over to free the barrel from the formation.

Cores 22X through 35X were taken from 184.8 to 302.9 m DSF, and we recovered 69.0 m (58%). We stopped coring before reaching the basement objective because of the decreasing rates of penetration (as low as ~4 m/h for Cores 34X and 35X), the relatively low recovery, and the possibility of obtaining a stratigraphically complete Miocene section by coring in a second hole. We pulled out of the hole and the bit cleared the seafloor at 0400 h on 25 April. We offset the ship 25 m to the south of Hole U1336A.

Hole U1336B

After positioning the bit at 4284 m DRF (5 m shallower than in Hole U1336A), we started coring in Hole U1336B at 0540 h on 25 April 2009. Based on the recovery in the first core, the seafloor depth was 4298.1 m DRF (4286.5 mbsl). Cores 320-U1336B-1H through 20H were taken from 0 to 173.9 m DSF, and we recovered 179.6 m (103%). Nonmagnetic core barrels were used for Cores 1H through 16H; steel barrels were used for the others. Core 16H only achieved a partial stroke and was advanced by recovery. Once coring was completed, the drill string was pulled out of the hole with the bit clearing the seafloor at 0400 h on 26 April. Once all the drilling equipment was secured, the vessel departed for Honolulu, Hawaii, at 1315 h on 26 April.

Transit to Honolulu, Hawaii

The 1954 nmi transit from Site U1336 to Honolulu, Hawaii, took 7.8 days at an average speed of 10.5 kt. At 2400 on 27 April, the shipboard clocks were set back 1 h so ship local time was now UTC – 10 h. Expedition 320 concluded with the first line ashore at 0700 h on 4 May 2009.

References

Abels, H.A., Hilgen, F.J., Krijgsman, W., Kruk, R.W., Raffi, I., Turco, E., and Zachariasse, W.J., 2005. Long-period orbital control on middle Miocene global cooling: integrated stratigraphy and astronomical tuning of the Blue Clay Formation on Malta. *Paleoceanography,* 20(4):PA4012. **doi:10.1029/2004PA001129**

Amante, C., and Eakins, B.W., 2008. *ETOPO1 1 Arc-Minute Global Relief Model: Procedures, Data Sources and Analysis:* Washington, DC (DOC/NOAA/NESDIS/NGDC).

Barker, P.F., 2001. Scotia Sea regional tectonic evolution: implications for mantle flow and palaeocirculation. *Earth-Sci. Rev.,* 55(1–2):1–39. **doi:10.1016/S0012-8252(01)00055-1**

Billups, K., Pälike, H., Channell, J.E.T., Zachos, J.C., and Shackleton, N.J., 2004. Astronomic calibration of the late Oligocene through early Miocene geomagnetic polarity time scale. *Earth Planet. Sci. Lett.,* 224(1–2):33–44. **doi:10.1016/j.epsl.2004.05.004**

Bohaty, S.M., Pälike, H., Ridgwell, A., Zachos, J.C., and Lear, C.H., 2008. Timing and significance of a global deep-sea dissolution event during the Eocene–Oligocene transition. *Eos, Trans. Am. Geophys. Union,* 89(53)(Suppl.):PP41D-1487. (Abstract) **http://www.agu.org/meetings/fm08/waisfm08.html**

Bohaty, S.M., and Zachos, J.C., 2003. Significant Southern Ocean warming event in the late middle Eocene. *Geology,* 31(11):1017–1020. **doi:10.1130/G19800.1**

Bohaty, S.M., Zachos, J.C., Florindo, F., and Delaney, M.L., 2009. Coupled greenhouse warming and deep-sea acidification in the middle Eocene. *Paleoceanography,* 24(2):PA2207. **doi:10.1029/2008PA001676**

Coxall, H.K., Wilson, P.A., Pälike, H., Lear, C.H., and Backman, J., 2005. Rapid stepwise onset of Antarctic glaciation and deeper calcite compensation in the Pacific Ocean. *Nature (London, U. K.),* 433(7021):53–57. **doi:10.1038/nature03135**

DeConto, R.M., Pollard, D., Wilson, P.A., Palike, H., Lear, C.H., and Pagani, M., 2008. Thresholds for Cenozoic bipolar glaciation. *Nature (London, U. K.),* 455(7213):652–656. **doi:10.1038/nature07337**

Dore, J.E., Lukas, R., Sadler, D.W., and Karl, D.M., 2003. Climate-driven changes to the atmospheric CO_2 sink in the subtropical North Pacific Ocean. *Nature (London, U. K.),* 424(6950):754–757. **doi:10.1038/nature01885**

Dunkley Jones, T., Bown, P.R., Pearson, P.N., Wade, B.S., Coxall, H.K., and Lear, C.H. 2008. Major shifts in calcareous phytoplankton assemblages through the Eocene–Oligocene transition of Tanzania and their implications for low-latitude primary production. *Paleoceanography,* 23(4):PA4204. **doi:10.1029/2008PA001640**

Elderfield, H., and Schultz, A., 1996. Mid-ocean ridge hydrothermal fluxes and the chemical composition of the ocean. *Annu. Rev. Earth Planet. Sci.,* 24(1):191–224. **doi:10.1146/annurev.earth.24.1.191**

Elderfield, H., Yu, J., Anand, P., Kiefer, T., and Nyland, B., 2006. Calibrations for benthic foraminiferal Mg/Ca paleothermometry and the carbonate ion hypothesis. *Earth Planet. Sci. Lett.,* 250(3–4):633–649. **doi:10.1016/j.epsl.2006.07.041**

Engebretson, D.C., Cox, A., and Gordon, R.G., 1985. *Relative Motions between Oceanic and Continental Plates in the Pacific Basin.* Spec. Pap.—Geol. Soc. Am., 206.

Funakawa, S., Nishi, H., Moore, T.C., and Nigrini, C.A., 2006. Radiolarian faunal turnover and paleoceanographic change around Eocene/Oligocene boundary in the central equatorial Pacific, ODP Leg 199, Holes 1218A, 1219A, and 1220A. *Palaeogeogr., Palaeoclimatol., Palaeoecol.,* 230(3–4):183–203. **doi:10.1016/j.palaeo.2005.07.014**

Gibbs, S., Shackleton, N.J., and Young, J., 2004. Orbitally forced climate signals in mid-Plio-cene nannofossil assemblages. *Mar. Micropaleontol.,* 51(1–2):39–56. **doi:10.1016/j.marmi-cro.2003.09.002**

Gradstein, F.M., Ogg, J.G., and Smith, A. (Eds.), 2004. *A Geologic Time Scale 2004:* Cambridge (Cambridge Univ. Press). **http://www.stratigraphy.org/**

Hays, J.D., et al., 1972. *Init. Repts. DSDP,* 9: Washington, DC (U.S. Govt. Printing Office). **doi:10.2973/dsdp.proc.9.1972**

Holbourn, A., Kuhnt, W., Schulz, M., and Erlenkeuser, H., 2005. Impacts of orbital forcing and atmospheric carbon dioxide on Miocene ice-sheet expansion. *Nature (London, U. K.),* 438(7067):483–487. **doi:10.1038/nature04123**

Huber, M., 2002. Straw man 1: a preliminary view of the tropical Pacific from a global cou-pled climate model simulation of the early Paleogene. *In* Lyle, M., Wilson, P.A., Janecek, T.R., et al., *Proc. ODP, Init. Repts.,* 199: College Station, TX (Ocean Drilling Program), 1–30. **doi:10.2973/odp.proc.ir.199.103.2002**

Kamikuri, S., Nishi, H., Moore, T.C., Nigrini, C.A., and Motoyama, I., 2005. Radiolarian fau-nal turnover across the Oligocene/Miocene boundary in the equatorial Pacific Ocean. *Mar. Micropaleontol.,* 57(3–4):74–96. **doi:10.1016/j.marmicro.2005.07.004**

Kennett, J.P., and Shackleton, N.J., 1976. Oxygen isotopic evidence for the development of the psychrosphere 38 Myr ago. *Nature (London, U. K.),* 260(5551):513–515. **doi:10.1038/260513a0**

Knappenberger, M., 2000. Sedimentation rates and Pacific plate motion calculated using seis-mic cross sections of the Neogene equatorial sediment bulge [M.Sc. thesis]. Boise State Univ., Idaho.

Koppers, A.A.P., Phipps Morgan, J., Morgan, J.W., and Staudigel, H., 2001. Testing the fixed hotspot hypothesis using $^{40}Ar/^{39}Ar$ age progressions along seamount trails. *Earth Planet. Sci. Lett.,* 185(3–4):237–252. **doi:10.1016/S0012-821X(00)00387-3**

Lanci, L., Parés, J.M., Channell, J.E.T., and Kent, D.V., 2004. Miocene magnetostratigraphy from equatorial Pacific sediments (ODP Site 1218, Leg 199). *Earth Planet. Sci. Lett.,* 226(1–2):207–224. **doi:10.1016/j.epsl.2004.07.025**

Lanci, L., Parés, J.M., Channell, J.E.T., and Kent, D.V., 2005. Oligocene magnetostratigraphy from equatorial Pacific sediments (ODP Sites 1218 and 1219, Leg 199). *Earth Planet. Sci. Lett.,* 237(3–4):617–634. **doi:10.1016/j.epsl.2005.07.004**

Lawver, L.A., and Gahagan, L.M., 2003. Evolution of Cenozoic seaways in the circum-Antarc-tic region. *Palaeogeogr., Palaeoclimatol., Palaeoecol.,* 198(1–2):11–37. **doi:10.1016/S0031-0182(03)00392-4**

Lear, C.H., Bailey, T.R., Pearson, P.N., Coxall, H.K., and Rosenthal, Y., 2008. Cooling and ice growth across the Eocene–Oligocene transition. *Geology,* 36(3):251–254. **doi:10.1130/G24584A.1**

Lear, C.H., Rosenthal, Y., Coxall, H.K., and Wilson, P.A., 2004. Late Eocene to early Miocene ice sheet dynamics and the global carbon cycle. *Paleoceanography,* 19(4):PA4015. **doi:10.1029/2004PA001039**

Liu, Z., Pagani, M., Zinniker, D., DeConto, R., Huber, M., Brinkhuis, H., Shah, S.R., Leckie, R.M., and Pearson, A., 2009. Global cooling during the Eocene–Oligocene climate transi-tion. *Science,* 323(5918):1187–1190. **doi:10.1126/science.1166368**

Lowenstein, T.K., and Demicco, R.V., 2007. Elevated Eocene atmospheric CO_2 and subse-quent decline. *Science,* 313(5795):1928. **doi:10.1126/science.1129555**

Lyle, M., 2003. Neogene carbonate burial in the Pacific Ocean. *Paleoceanography,* 18(3):1059. **doi:10.1029/2002PA000777**

Lyle, M., Gibbs, S., Moore Jr., T.C., and Rea, D.K., 2007. Late Oligocene initiation of the Antarctic Circumpolar Current: evidence from the South Pacific. *Geology,* 35:691–694.

Lyle, M., Liberty, L., Moore, T.C., Jr., and Rea, D.K., 2002. Development of a seismic stratigraphy for the Paleogene sedimentary section, central tropical Pacific Ocean. *In* Lyle, M., Wilson, P.A., Janecek, T.R., et al., *Proc. ODP, Init. Repts.,* 199: College Station, TX (Ocean Drilling Program), 1–21. **doi:10.2973/odp.proc.ir.199.104.2002**

Lyle, M., Olivarez Lyle, A., Backman, J., and Tripati, A., 2005. Biogenic sedimentation in the Eocene equatorial Pacific—the stuttering greenhouse and Eocene carbonate compensation depth. *In* Lyle, M., Wilson, P.A., Janecek, T.R., et al., *Proc. ODP, Init. Repts.,* 199: College Station, TX (Ocean Drilling Program), 1–35. **doi:10.2973/odp.proc.sr.199.219.2005**

Lyle, M., Wilson, P.A., Janecek, T.R., et al., 2002. *Proc. ODP, Init. Repts.,* 199: College Station, TX (Ocean Drilling Program). **doi:10.2973/odp.proc.ir.199.2002**

Lyle, M.W., Pälike, H., Moore, T.C., Mitchell, N., and Backman, J., 2006. *Summary Report of R/V Roger Revelle Site Survey AMAT03 to the IODP Environmental Protection and Safety Panel (EPSP) in Support for Proposal IODP626:* Southampton, U.K. (Univ. Southampton). **http://eprints.soton.ac.uk/45921/**

Miller, K.G., Wright, J.D., and Fairbanks, R.G., 1991. Unlocking the ice house: Oligocene–Miocene oxygen isotopes, eustasy, and margin erosion. *J. Geophys. Res.,* 96(B4):6829–6848. **doi:10.1029/90JB02015**

Mitchell, N.C., 1998. Modeling Cenozoic sedimentation in the central equatorial Pacific and implications for true polar wander. *J. Geophys. Res., [Solid Earth],* 103(B8):17749–17766. **doi:10.1029/98JB01577**

Mitchell, N.C., and Lyle, M.W., 2005. Patchy deposits of Cenozoic pelagic sediments in the central Pacific. *Geology,* 33(1):49–52. **doi:10.1130/G21134.1**

Mitchell, N.C., Lyle, M.W., Knappenberger, M.B., and Liberty, L.M., 2003. Lower Miocene to present stratigraphy of the equatorial Pacific sediment bulge and carbonate dissolution anomalies. *Paleoceanography,* 18(2):1038. **doi:10.1029/2002PA000828**

Mix, A.C., Tiedemann, R., Blum, P., et al., 2003. *Proc. ODP, Init. Repts.,* 202: College Station, TX (Ocean Drilling Program). **doi:10.2973/odp.proc.ir.202.2003**

Moore, T.C., Rea, D.K., Lyle, M., and Liberty, L.M., 2002. Equatorial ocean circulation in an extreme warm climate. *Paleoceanography,* 17(1):1005. **doi:10.1029/2000PA000566**

Moore, T.C., Jr., 1995. Radiolarian stratigraphy, Leg 138. *In* Pisias, N.G., Mayer, L.A., Janecek, T.R., Palmer-Julson, A., and van Andel, T.H. (Eds.), *Proc. ODP, Sci. Results,* 138: College Station, TX (Ocean Drilling Program), 191–232. **doi:10.2973/odp.proc.sr.138.111.1995**

Moore, T.C., Jr., 2008a. Biogenic silica and chert in the Pacific Ocean. *Geology,* 36(12):975–978. **doi:10.1130/G25057A.1**

Moore, T.C., Jr., 2008b. Chert in the Pacific: biogenic silica and hydrothermal circulation. *Palaeogeogr., Palaeoclimatol., Palaeoecol.,* 261(1–2):87–99. **doi:10.1016/j.palaeo.2008.01.009**

Moore, T.C., Jr., Backman, J., Raffi, I., Nigrini, C., Sanfilippo, A., Pälike, H., and Lyle, M., 2004. Paleogene tropical Pacific: clues to circulation, productivity, and plate motion. *Paleoceanography,* 19(3):PA3013. **doi:10.1029/2003PA000998**

Müller, R.D., Roest, W.R., Royer, J.-Y., Gahagan, L.M., and Sclater, J.G., 1997. Digital isochrons of the world's ocean floor. *J. Geophys. Res.,* 102(B2):3211–3214. **doi:10.1029/96JB01781**

Nigrini, C., Sanfilippo, A., and Moore, T.C., Jr., 2006. Cenozoic radiolarian biostratigraphy: a magnetobiostratigraphic chronology of Cenozoic sequences from ODP Sites 1218, 1219, and 1220, equatorial Pacific. *In* Wilson, P.A., Lyle, M., and Firth, J.V. (Eds.), *Proc. ODP, Sci. Results,* 199: College Station, TX (Ocean Drilling Program), 1–76. **doi:10.2973/ odp.proc.sr.199.225.2006**

Norris, R.D., and Röhl, U., 1999. Carbon cycling and chronology of climate warming during the Palaeocene/Eocene transition. *Nature (London, U. K.),* 401(6755):775–778. **doi:10.1038/44545**

Nunes, F., and Norris, R.D., 2006. Abrupt reversal in ocean overturning during the Palaeocene/Eocene warm period. *Nature (London, U. K.),* 439(7072):60–63. **doi:10.1038/ nature04386**

Olivarez Lyle, A., and Lyle, M., 2005. Organic carbon and barium in Eocene sediments: possible controls on nutrient recycling in the Eocene equatorial Pacific Ocean. *In* Wilson, P.A., Lyle, M., and Firth, J.V. (Eds.), *Proc. ODP, Sci. Results,* 199: College Station, TX (Ocean Drilling Program), 1–33. **doi:10.2973/odp.proc.sr.199.222.2005**

Pagani, M., Arthur, M.A., and Freeman, K.H., 1999. Miocene evolution of atmospheric carbon dioxide. *Paleoceanography,* 14(3):273–292. **doi:10.1029/1999PA900006**

Paillard, D., Labeyrie, L., and Yiou, P., 1996. Macintosh program performs time-series analysis. *Eos, Trans. Am. Geophys. Union,* 77(39):379. **doi:10.1029/96EO00259O**

Pälike, H., Lyle, M.W., Ahagon, N., Raffi, I., Gamage, K., and Zarikian, C.A., 2008. Pacific equatorial age transect. *IODP Sci. Prosp.,* 320/321. **doi:10.2204/iodp.sp.320321.2008**

Pälike, H., Frazier, J., and Zachos, J.C., 2006a. Extended orbitally forced palaeoclimatic records from the equatorial Atlantic Ceara Rise. *Quat. Sci. Rev.,* 25(23–24):3138–3149. **doi:10.1016/j.quascirev.2006.02.011**

Pälike, H., Moore, T., Backman, J., Raffi, I., Lanci, L., Parés, J.M., and Janecek, T., 2005. Integrated stratigraphic correlation and improved composite depth scales for ODP Sites 1218 and 1219. *In* Wilson, P.A., Lyle, M., and Firth, J.V. (Eds.), *Proc. ODP, Sci. Results,* 199: College Station, TX (Ocean Drilling Program), 1–41. **doi:10.2973/odp.proc.sr.199.213.2005**

Pälike, H., Norris, R.D., Herrle, J.O., Wilson, P.A., Coxall, H.K., Lear, C.H., Shackleton, N.J., Tripati, A.K., and Wade, B.S., 2006b. The heartbeat of the Oligocene climate system. *Science,* 314(5807):1894–1898. **doi:10.1126/science.1133822**

Parés, J.M., and Moore, T.C., 2005. New evidence for the Hawaiian hotspot plume motion since the Eocene. *Earth Planet. Sci. Lett.,* 237(3–4):951–959. **doi:10.1016/ j.epsl.2005.06.012**

Paul, H.A., Zachos, J.C., Flower, B.P., and Tripati, A., 2000. Orbitally induced climate and geochemical variability across the Oligocene/Miocene boundary. *Paleoceanography,* 15(5):471–485. **doi:10.1029/1999PA000443**

Pearson, P.N., Ditchfield, P.W., Singano, J., Harcourt-Brown, K.G., Nicholas, C.J., Olsson, R.K., Shackleton, N.J., and Hall, M.A., 2001. Warm tropical sea surface temperatures in the Late Cretaceous and Eocene epochs. *Nature (London, U. K.),* 413(6855):481–487. **doi:10.1038/ 35097000**

Pearson, P.N., McMillan, I.K., Wade, B.S., Dunkley Jones, T., Coxall, H.K., Bown, P.R., and Lear, C.H., 2008. Extinction and environmental change across the Eocene–Oligocene boundary in Tanzania. *Geology,* 36(2):179–182. **doi:10.1130/G24308A.1**

Petronotis, K.E., 1991. Paleomagnetic studies of the skewness of Pacific plate marine magnetic anomalies 25–32R: implications for anomalous skewness and the motion of the Pacific plate and hotspots [Ph.D. thesis]. Northwestern Univ., Evanston, IL.

Petronotis, K.E., Gordon, R.G., and Acton, G.D., 1994. A 57 Ma Pacific plate paleomagnetic pole determined from a skewness analysis of crossings of marine magnetic anomaly 25r. *Geophys. J. Int.,* 118(3):529–554. **doi:10.1111/j.1365-246X.1994.tb03983.x**

Pisias, N.G., Mayer, L.A., Janecek, T.R., Palmer-Julson, A., and van Andel, T.H. (Eds.), 1995. *Proc. ODP, Sci Results,* 138: College Station, TX (Ocean Drilling Program). **doi:10.2973/odp.proc.sr.138.1995**

Pollack, H.N., Hurter, S.J., and Johnson, J.R., 1993. Heat flow from the earth's interior: analysis of the global data set. *Rev. Geophys.,* 31(3):267–280. **doi:10.1029/93RG01249**

Pribnow, D.F.C., Kinoshita, M., and Stein, C.A., 2000. *Thermal Data Collection and Heat Flow Recalculations for ODP Legs 101–180:* Hanover, Germany (Inst. Joint Geosci. Res., Inst. Geowiss. Gemeinschaftsauf. [GGA]). **http://www-odp.tamu.edu/publications/heat-flow/ODPReprt.pdf**

Raffi, I., Backman, J., Fornaciari, E., Pälike, H., Rio, D., Lourens, L., and Hilgen, F., 2006. A review of calcareous nannofossil astrobiochronology encompassing the past 25 million years. *Quat. Sci. Rev.,* 25(23–24):3113–3137. **doi:10.1016/j.quascirev.2006.07.007**

Raffi, I., Backman, J., and Pälike, H., 2005. Changes in calcareous nannofossil assemblages across the Paleocene/Eocene transition from the paleo-equatorial Pacific Ocean. *Palaeogeogr., Palaeoclimatol., Palaeoecol.,* 226(1–2):93–126. **doi:10.1016/j.palaeo.2005.05.006**

Rea, D.K., and Lyle, M.W., 2005. Paleogene calcite compensation depth in the eastern subtropical Pacific: answers and questions. *Paleoceanography,* 20(1):PA1012. **doi:10.1029/2004PA001064**

Röhl, U., Ogg, J.G., Geib, T.L., and Wefer, G., 2001. Astronomical calibration of the Danian time scale. *In* Kroon, D., Norris, R.D., and Klaus, A. (Eds.), *Western North Atlantic Paleogene and Cretaceous Paleoceanography.* Geol. Soc. Spec. Publ., 183:163–184.

Sager, W.W., and Pringle, M.S., 1988. Mid-Cretaceous to early Tertiary apparent polar wander path of the Pacific plate. *J. Geophys. Res., [Solid Earth],* 93(B10):11753–11771. **doi:10.1029/JB093iB10p11753**

Scher, H.D., and Martin, E.E., 2006. Timing and climatic consequences of the opening of Drake Passage. *Science,* 312(5772):428–430. **doi:10.1126/science.1120044**

Shackleton, N.J., Hall, M.A., Raffi, I., Tauxe, L., and Zachos, J., 2000. Astronomical calibration age for the Oligocene–Miocene boundary. *Geology,* 28(5):447–450. **doi:10.1130/0091-7613(2000)28<447:ACAFTO>2.0.CO;2**

Sexton, P.F., Wilson, P.A., and Pearson, P.N., 2006. Palaeoecology of late middle Eocene planktic foraminifera and evolutionary implications. *Mar. Micropaleontol.,* 60(1):1–6. **doi:10.1016/j.marmicro.2006.02.006**

Shipboard Scientific Party, 2002. Leg 199 summary. *In* Lyle, M., Wilson, P.A., Janecek, T.R., et al., *Proc. ODP, Init. Repts.,* 199: College Station, TX (Ocean Drilling Program), 1–87. **doi:10.2973/odp.proc.ir.199.101.2002**

Shipboard Scientific Party, 2004. Leg 208 summary. *In* Zachos, J.C., Kroon, D., Blum, P., et al., *Proc. ODP, Init. Repts.,* 208: College Station, TX (Ocean Drilling Program), 1–112. **doi:10.2973/odp.proc.ir.208.101.2004**

Spero, H.J., Bijma, J., Lea, D.W., and Bemis, B.E., 1997. Effect of seawater carbonate concentration on foraminiferal carbon and oxygen isotopes. *Nature (London, U. K.),* 390(6659):497–500. **doi:10.1038/37333**

Steiger, T.H., 2006. Biogenic sedimentology of radiolarian assemblages in a middle Eocene diatom-rich unit from the eastern equatorial Pacific: ODP Leg 199, Site 1219. *In* Wilson, P.A., Lyle, M., and Firth, J.V. (Eds.), *Proc. ODP, Sci. Results,*199: College Station, TX (Ocean Drilling Program), 1–19. **doi:10.2973/odp.proc.sr.199.217.2006**

Tarduno, J.A., Duncan, R.A., Scholl, D.W., Cottrell, R.D., Steinberger, B., Thordarson, T., Kerr, B.C., Neal, C.R., Frey, F.A., Torii, M., and Carvallo, C., 2003. The Emperor Seamounts: southward motion of the Hawaiian hotspot plume in Earth's mantle. *Science,* 301(5636):1064–1069. **doi:10.1126/science.1086442**

van Andel, T.H., 1975. Mesozoic/Cenozoic calcite compensation depth and the global distribution of calcareous sediments. *Earth Planet. Sci. Lett.,* 26(2):187–194. **doi:10.1016/0012-821X(75)90086-2**

Wade, B.S., and Bown, P.R., 2006. Calcareous nannofossils in extreme environments: the Messinian salinity crisis, Polemi Basin, Cyprus. *Palaeogeogr., Palaeoclimatol., Palaeoecol.,* 233(3–4):271–286. **doi:10.1016/j.palaeo.2005.10.007**

Wade, B.S., Berggren, W.A., and Olsson, R.K., 2007. The biostratigraphy and paleobiology of Oligocene planktonic foraminifera from the equatorial Pacific Ocean (ODP Site 1218). *Mar. Micropaleontol.,* 62(3):167–179. **doi:10.1016/j.marmicro.2006.08.005**

Wade, B.S., and Pälike, H., 2004. Oligocene climate dynamics. *Paleoceanography,* 19(4)PA4019. **doi:10.1029/2004PA001042**

Wei, W., and Wise, S.W., Jr., 1989. Paleogene calcareous nannofossil magnetobiochronology: results from South Atlantic DSDP Site 516. *Mar. Micropaleontol.,* 14(1–3):119–152. **doi:10.1016/0377-8398(89)90034-0**

Zachos, J.C., Dickens, G.R., and Zeebe, R.E., 2008. An early Cenozoic perspective on greenhouse warming and carbon-cycle dynamics. *Nature (London, U. K.),* 451(7176):279–283. **doi:10.1038/nature06588**

Zachos, J.C., Flower, B.P., and Paul, H., 1997. Orbitally paced climate oscillations across the Oligocene/Miocene boundary. *Nature (London, U. K.),* 388(6642):567–570. **doi:10.1038/41528**

Zachos, J.C., Pagani, M., Sloan, L., Thomas, E., and Billups, K., 2001a. Trends, rhythms, and aberrations in global climate 65 Ma to present. *Science,* 292(5517):686–693. **doi:10.1126/science.1059412**

Zachos, J.C., Quinn, T.M., and Salamy, K.A., 1996. High-resolution (10^4 years) deep-sea foraminiferal stable isotope records of the Eocene–Oligocene climate transition. *Paleoceanography,* 11(3):251–266. **doi:10.1029/96PA00571**

Zachos, J.C., Shackleton, N.J., Revenaugh, J.S., Pälike, H., and Flower, B.P., 2001b. Climate response to orbital forcing across the Oligocene–Miocene boundary. *Science,* 292(5515):274–278. **doi:10.1126/science.1058288**

Zeebe, R.E., and Wolf-Gladrow, D.A., 2001. *CO_2 in Seawater: Equilibrium, Kinetics, Isotopes:* Amsterdam (Elsevier).

Table T1. Expedition 320 coring summary. (**See table note.**)

Hole	Latitude	Longitude	Seafloor depth DRF (m)	Cores (N)	Cored (m)	Recovered (m)	Recovered (%)	Drilled (m)	Total penetration (m)	Total depth DRF (m)	Time on hole (h)	Time on hole (days)
U1331A	12°04.0884′N	142°09.6961′W	5127.3	22	190.6	155.08	81.4	0.0	190.6	5317.9	80.83	3.4
U1331B	12°04.0877′N	142°09.7085′W	5127.4	20	175.8	163.03	92.7	12.7	188.5	5315.9	38.00	1.6
U1331C	12°04.0892′N	142°09.7201′W	5128.0	12	107.0	109.54	102.4	82.0	189.0	5317.0	54.67	2.3
		Site U1331 totals:		54	473.4	427.65	90.3	94.7	568.1	NA	173.50	7.2
U1332A	11°54.7095′N	141°02.7428′W	4935.1	18	152.4	145.61	95.5	0.0	152.4	5087.5	89.25	3.7
U1332B	11°54.7209′N	141°02.7427′W	4936.9	18	148.6	140.31	94.4	0.0	148.6	5085.5	38.50	1.6
U1332C	11°54.7366′N	141°02.7422′W	4934.0	18	155.5	148.06	95.2	0.0	155.5	5089.5	45.00	1.9
		Site U1332 totals:		54	456.5	433.98	95.1	0.0	456.5	NA	172.75	7.2
U1333A	10° 30.9953′N	138°25.1728′W	4865.0	22	184.1	176.25	95.7	0.0	184.1	5049.1	45.92	1.9
U1333B	10° 30.9960′N	138°25.1597′W	4861.8	20	180.3	178.36	98.9	0.0	180.3	5042.1	30.83	1.3
U1333B	10° 30.9958′N	138°25.1459′W	4865.1	24	177.0	177.04	100.0	0.0	177.0	5042.1	47.50	2.0
		Site U1333 totals:		66	541.4	531.65	98.2	0.0	541.4	NA	124.25	5.2
U1334A	07°59.9980′N	131°58.3937′W	4799.3	32	285.5	288.80	101.2	0.0	285.5	5084.8	57.58	2.4
U1334B	07°59.9979′N	131°58.4071′W	4799.3	31	281.7	294.59	104.6	0.0	281.7	5081.0	44.83	1.9
U1334C	07°59.9979′N	131°58.4219′W	4801.0	33	280.7	285.87	101.8	0.0	280.7	5081.7	75.33	3.1
		Site U1334 totals:		96	847.9	869.26	102.5	0.0	847.9	NA	177.75	7.4
U1335A	05°18.7341′N	126°16.9949′W	4339.0	45	421.1	422.08	100.2	0.0	421.1	4760.1	72.92	3.0
U1335B	05°18.7362′N	126°17.0088′W	4343.4	46	417.5	428.70	102.7	0.0	417.5	4760.9	76.33	3.2
		Site U1335 totals:		91	838.6	850.78	101.5	0.0	838.6	NA	149.25	6.2
U1336A	07°42.0735′N	128°15.2526′W	4296.9	35	302.9	259.12	85.5	0.0	302.9	4599.8	60.25	2.5
U1336B	07°42.0599′N	128°15.2526′W	4298.1	20	173.6	179.59	103.5	0.0	173.6	4471.7	33.25	1.4
		Site U1336 totals:		55	476.5	438.71	85.5	0.0	476.5	NA	93.50	3.9
		Expedition 320 totals:		416	3634.3	3552.03	97.7	94.7	3729.0	NA	891.00	37.1

Note: NA = not applicable.

Table T2. Radiolarian zones present in Expedition 320 sites. (**See table note.**)

Radiolarian zone	Site					
	U1331	U1332	U1333	U1334	U1335	U1336
RN16						
RN15						
RN14					X	
RN13					X	
RN12					X	
RN11					X	
RN10					X	
RN9					X	
RN8					X	
RN7				X	X	
RN6				X	X	X
RN5				X	X	X
RN4				X	X	X
RN3				X	X	X
RN2			X	X	X	X
RN1		X	X	X	X	X
RP22		X	X	X	X	X
RP21	X	X	X	X	X	
RP20	X	X	X	X		
RP19	X	X	X	X		
RP18	X	X	X	X		
RP17	X	X	X			
RP16	X	X	X			
RP15	X	X	X			
RP14	X	X	X			
RP13	X	X	X			
RP12	X					
RP11	X					
RP10	X					
RP9						
RP8						
Total thickness (m):	189	151	182	285	420	298
Thickness of SFZ (m):	15.5	16	12	7	8	128

Note: SFZ = silica-free zone (SFZ).

Figure F1. Location map of sites drilled during Expeditions 320 and 321. Red stars = sites drilled during Expedition 320, red circles = sites drilled during Expedition 321, black circles = previous DSDP and ODP sites. F.Z. = fracture zone. The positions of Honolulu and Papeete are indicated for orientation.
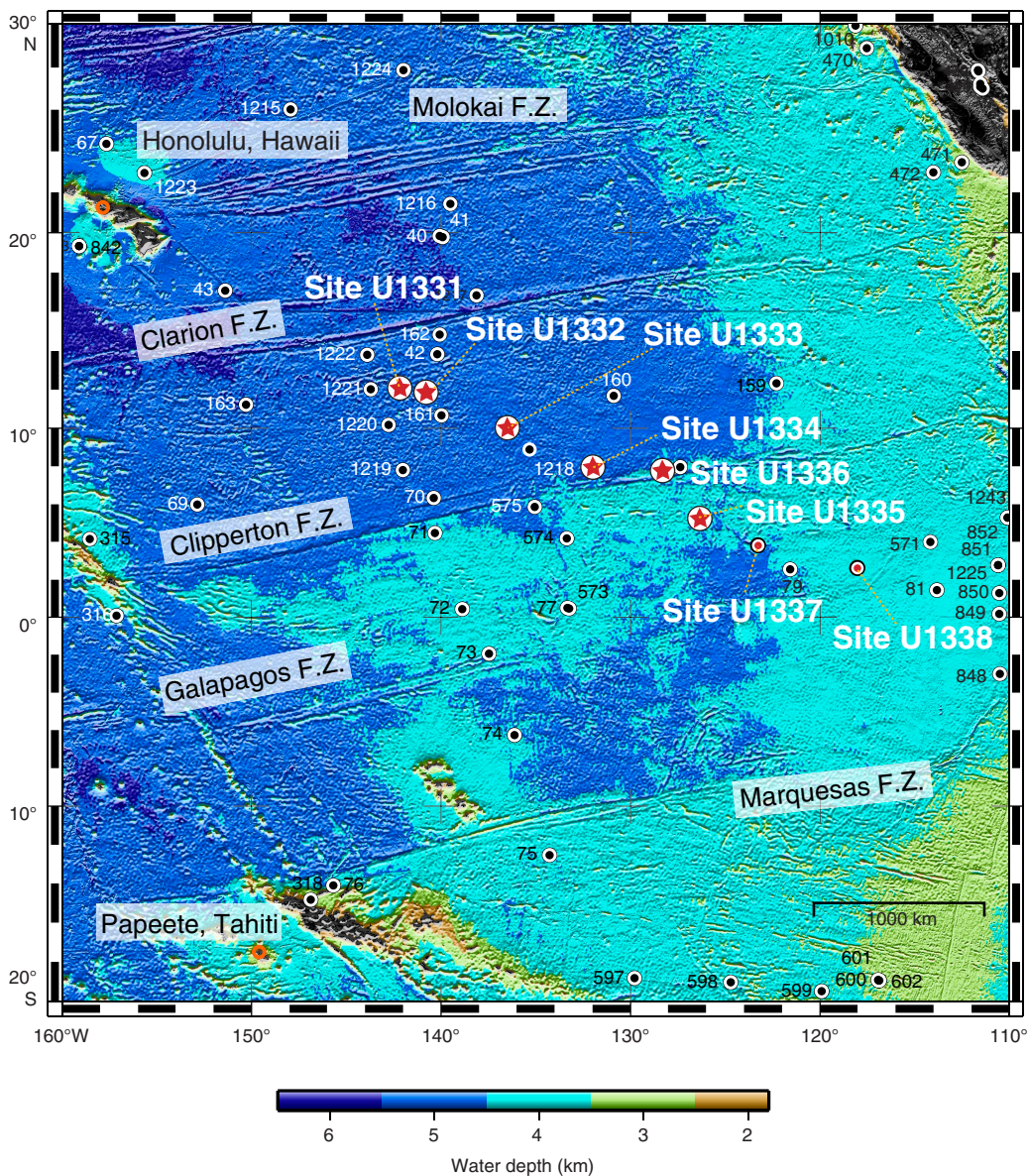
Figure F2. Evolution of oxygen stable isotopes ($\delta^{18}O$) through the Cenozoic and related major phases of climate change (modified from Zachos et al., 2001b, 2008). Yellow boxes = time slices of interest for the PEAT program, green and blue boxes = ODP legs and sites previously drilled in the equatorial Pacific region; these additional sites will be used with the PEAT sites to obtain a nearly continuous Cenozoic record of the equatorial Pacific region. VPDB = Vienna Peedee belemnite. Oi-1 = Oligocene isotopic Event 1, Mi-1 = Miocene isotopic Event 1 (described in Miller et al., 1991). ETM2 = Eocene thermal maximum 2.
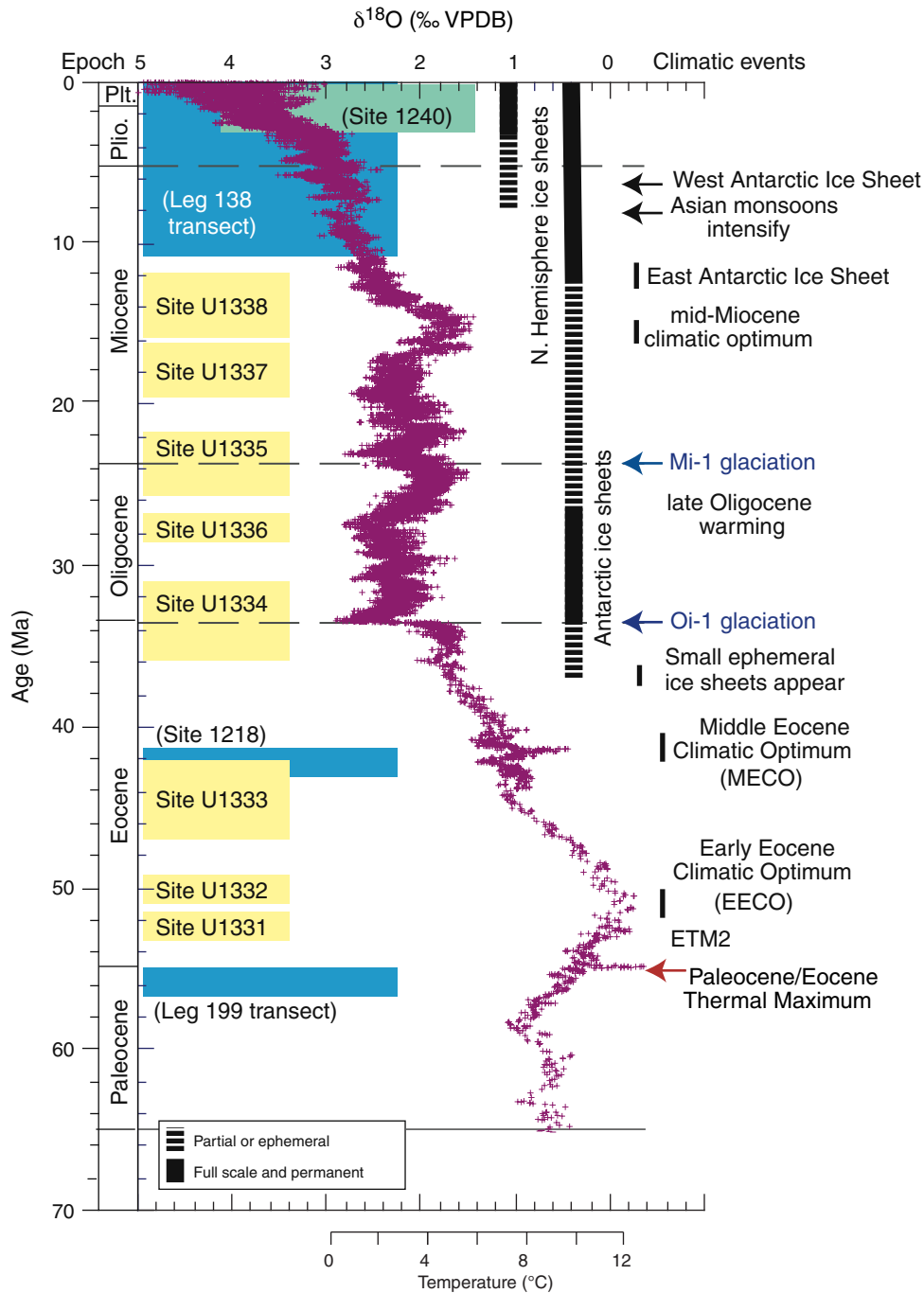
Figure F3. Targeting drill sites based on calcium carbonate compensation depth (CCD) history (van Andel, 1975), with new data from Leg 199 prior to coring. Colored boxes = critical time interval targeted for each site. Colored subsidence lines = time intervals when we expected carbonate to be deposited (i.e., when site is above CCD). Subsidence curves use a subsidence parameter calculated from estimated basement age of PEAT sites and their present-day depth (k = ~0.35). Additional subsidence due to sediment loading was not modeled.
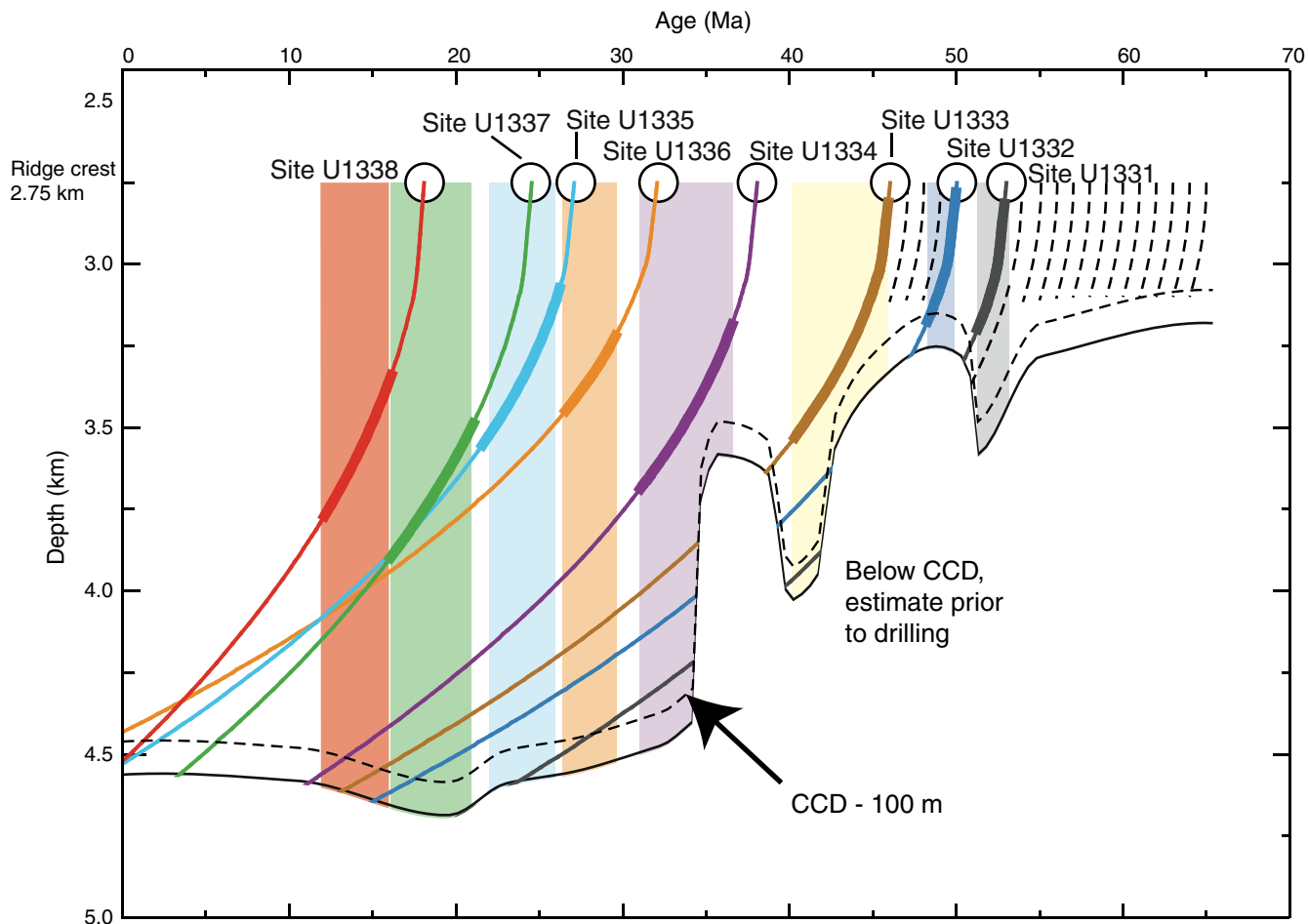
Figure F4. Location map of drill sites with backtracked position of paleoequator, corresponding to time slices targeted. Grayscale = present-day bathymetry (darker = deeper), thin yellow lines = revised magnetic anomaly isochrons (modified with new points from Petronotis, 1991, and Petronotis et al., 1994). Paleoequator position at crustal age obtained by backtracking, using fixed-hotspot stage poles from Koppers et al. (2001; pink) and Engebretson et al. (1985; orange) and paleomagnetic poles from Sager and Pringle (1988; purple). Shaded band lies within 1° north and south of the paleoequator (averaged from fixed-hotspot rotation models). Colored areas = time intervals of interest obtained by intersecting white paleoequator area with younger end of the time interval of interest, which was then backrotated to the older boundary of the time slice. Method requires correction if backtracking occurs across fracture zones. Positions of PEAT sites as plotted are slightly different to final positions. Locations of previous DSDP and ODP sites are also shown.
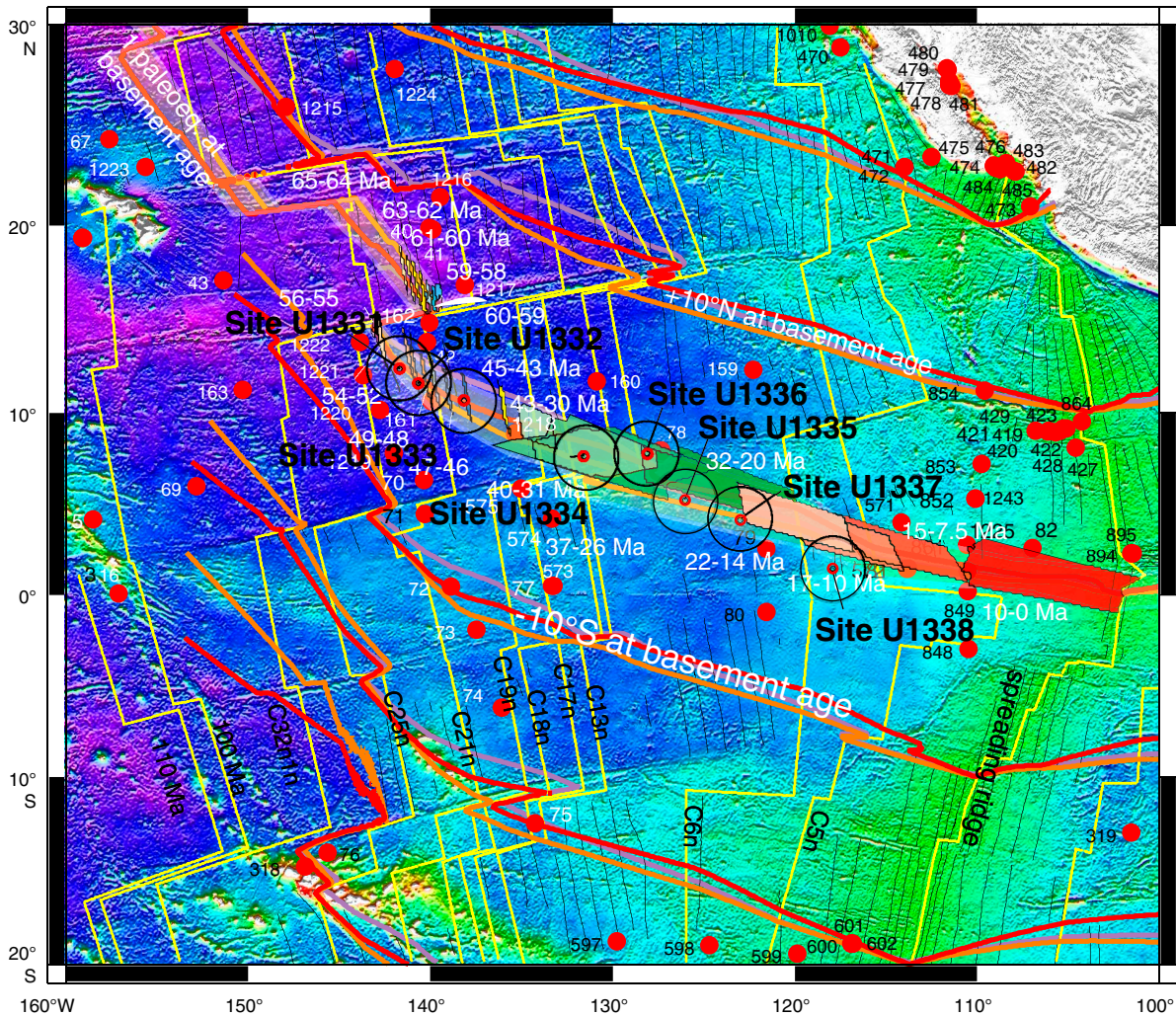
Figure F5. Backtracked latitudinal positions for PEAT sites and selected ODP sites (1218 and 1220) vs. geological age. Sites were backrotated along the flow line using stage poles from Koppers et al. (2001).
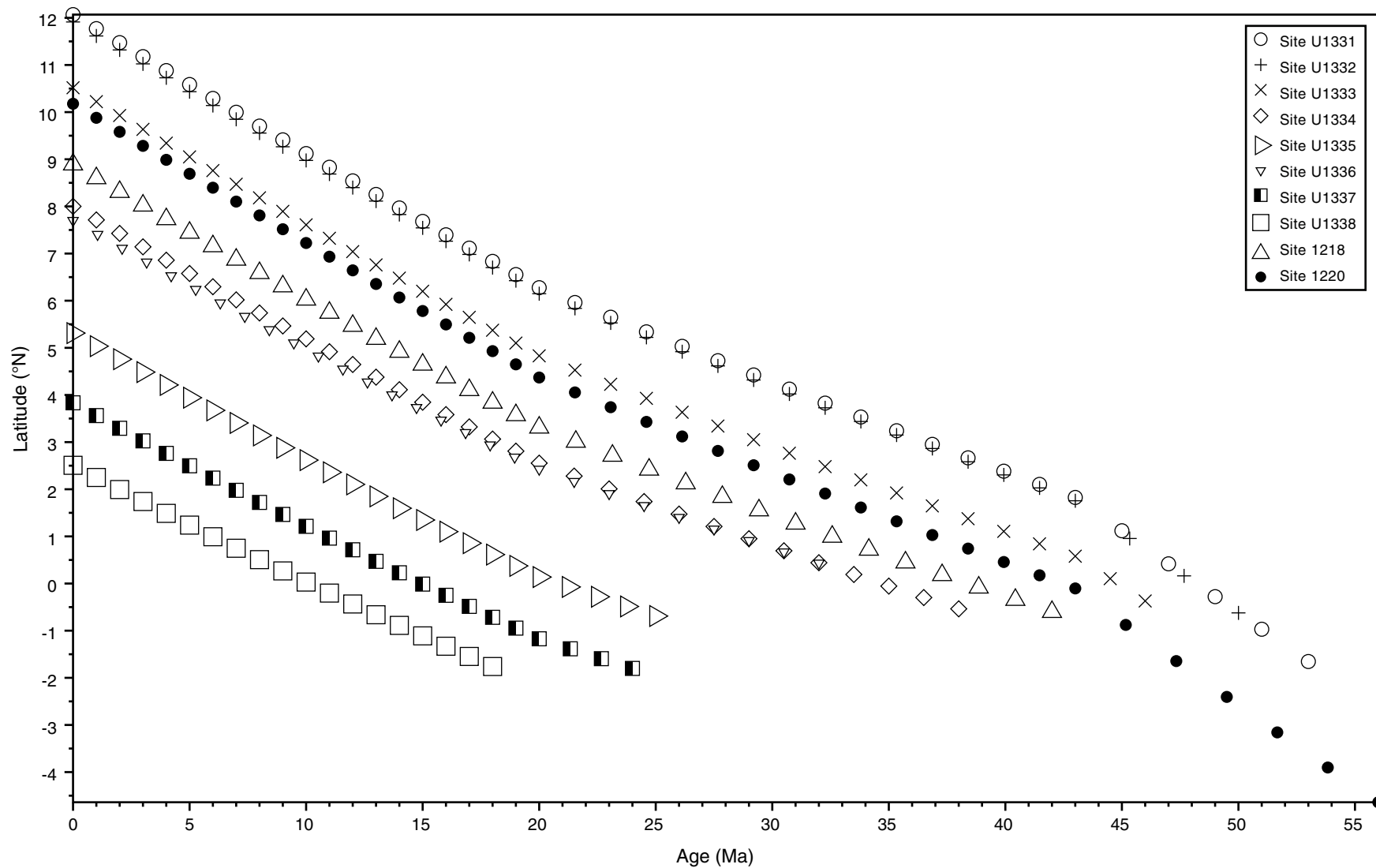
Figure F6. A. Backtracked positions for PEAT sites (red circles), using stage poles from Koppers et al. (2001) superimposed on a satellite-derived (GlobColour) map of present ocean chlorophyll-a concentrations (December 2005 mean monthly). Red = high productivity, blue = low productivity. Solid circles = previous DSDP and ODP sites. **B.** Backtracked positions for PEAT sites, with annotated positions every 10 m.y. back from present. Estimated basement ages for each site while situated at paleo–ridge crest are noted.
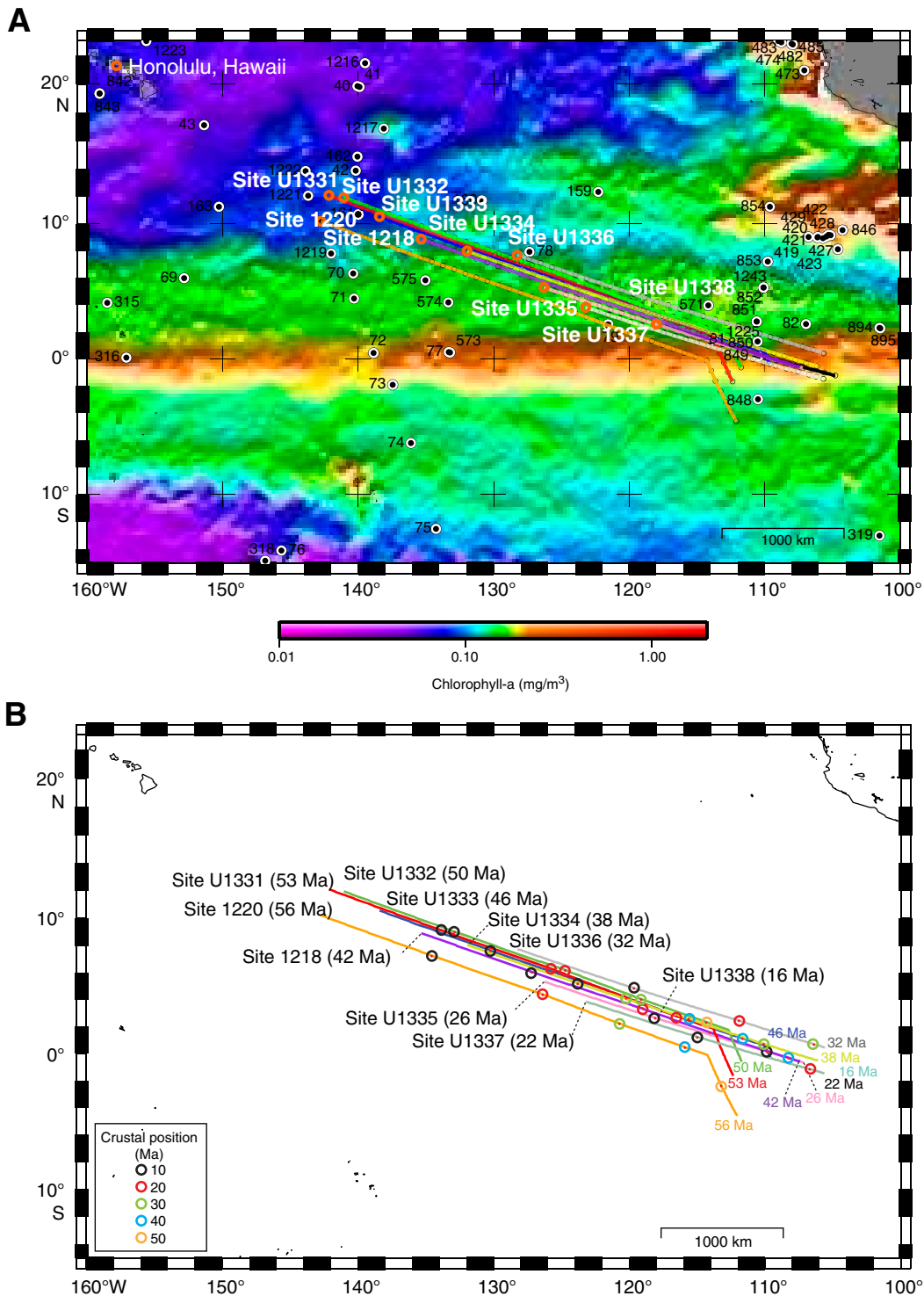
Figure F7. Times when PEAT sites (U1331–U1338) and selected DSDP and ODP sites (574, 572, 849, 851, and 1218) were positioned within paleoequatorial band. Equatorial band is defined as being within 2° latitude of Equator. Lighter shading = calcium compensation depth (CCD) (estimated prior to drilling for PEAT sites). Paleopositions were calculated with a fixed-hotspot model.
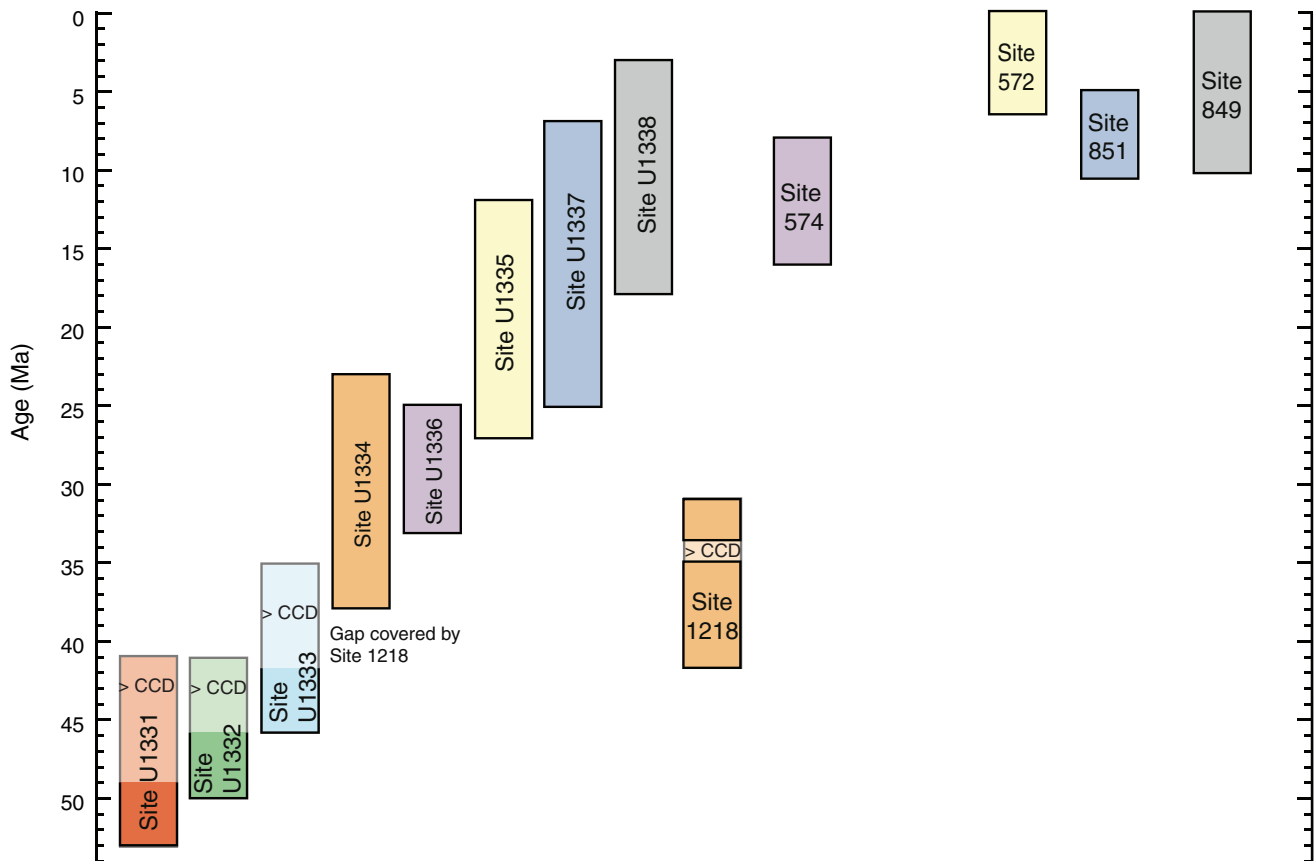
Figure F8. A. Model cross-section of equatorial sediment mound taking into account northward drift of Pacific plate. **B.** Mapped thickness of Pacific equatorial sediment mound. Color code = thickness of mound. (Both modified from Mitchell, 1998; Mitchell et al., 2003.)
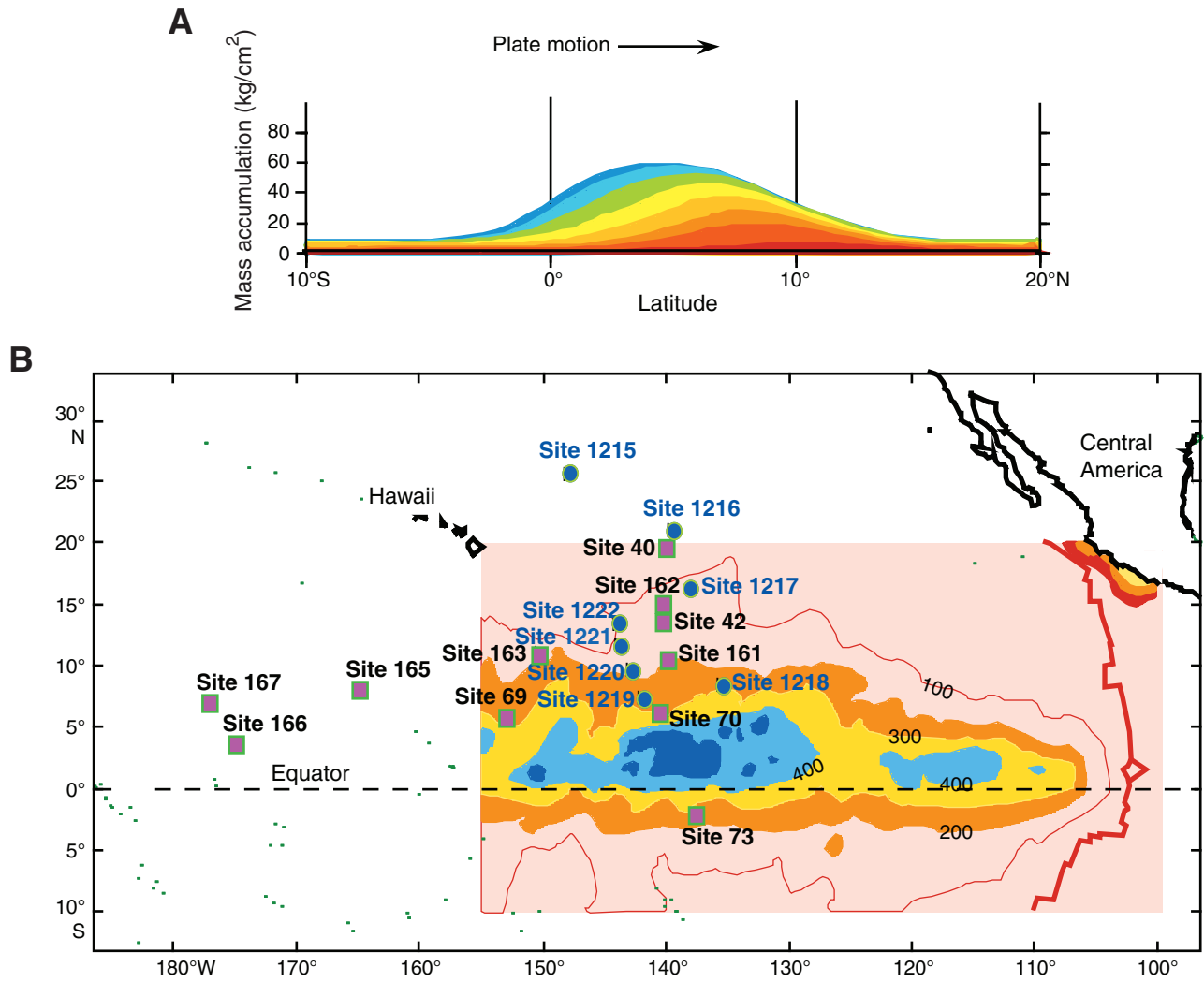
Figure F9. Coherence of sediment properties between widely separated drill sites in the equatorial Pacific is very high, allowing correlation of sediment properties over hundreds of kilometers. Figure shows Sites 1218 and 1219 (Shipboard Scientific Party, 2002), two sites >740 km apart. VGP = virtual geomagnetic pole, GRA = gamma ray attenuation, L* = lightness reflectance value of sediment as defined in the LAB color model. GRA and magnetic susceptibility were completed on board. (**Figure shown on next page.**)

Figure F9 (continued). (Caption shown on previous page.)
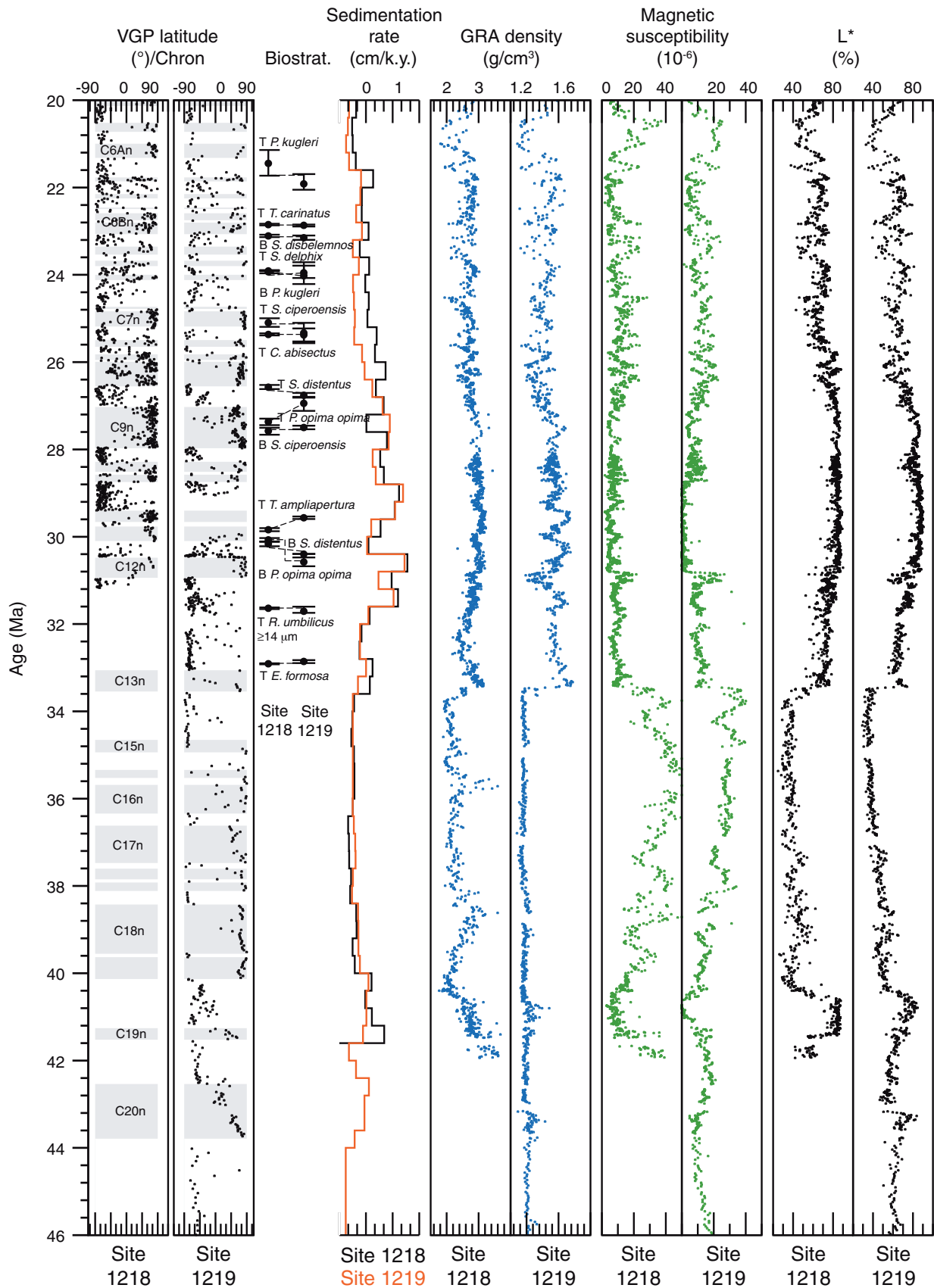
Figure F10. Model of early Eocene equatorial upwelling from Huber (2002), showing global land-sea distribution and annual average upwelling into thermocline (56 Ma sites, fixed-hotspot paleopositions). Red = regions of vigorous upwelling, green to blue = regions of weak upwelling, white = areas of average downwelling. Current streamlines at ~100 m ocean depth are shown for the Pacific Ocean. All map views are projected on a Mollweide projection. Upwelling region in eastern Pacific was broader than that of the modern region, primarily because of secondary upwelling centers on edges of region.
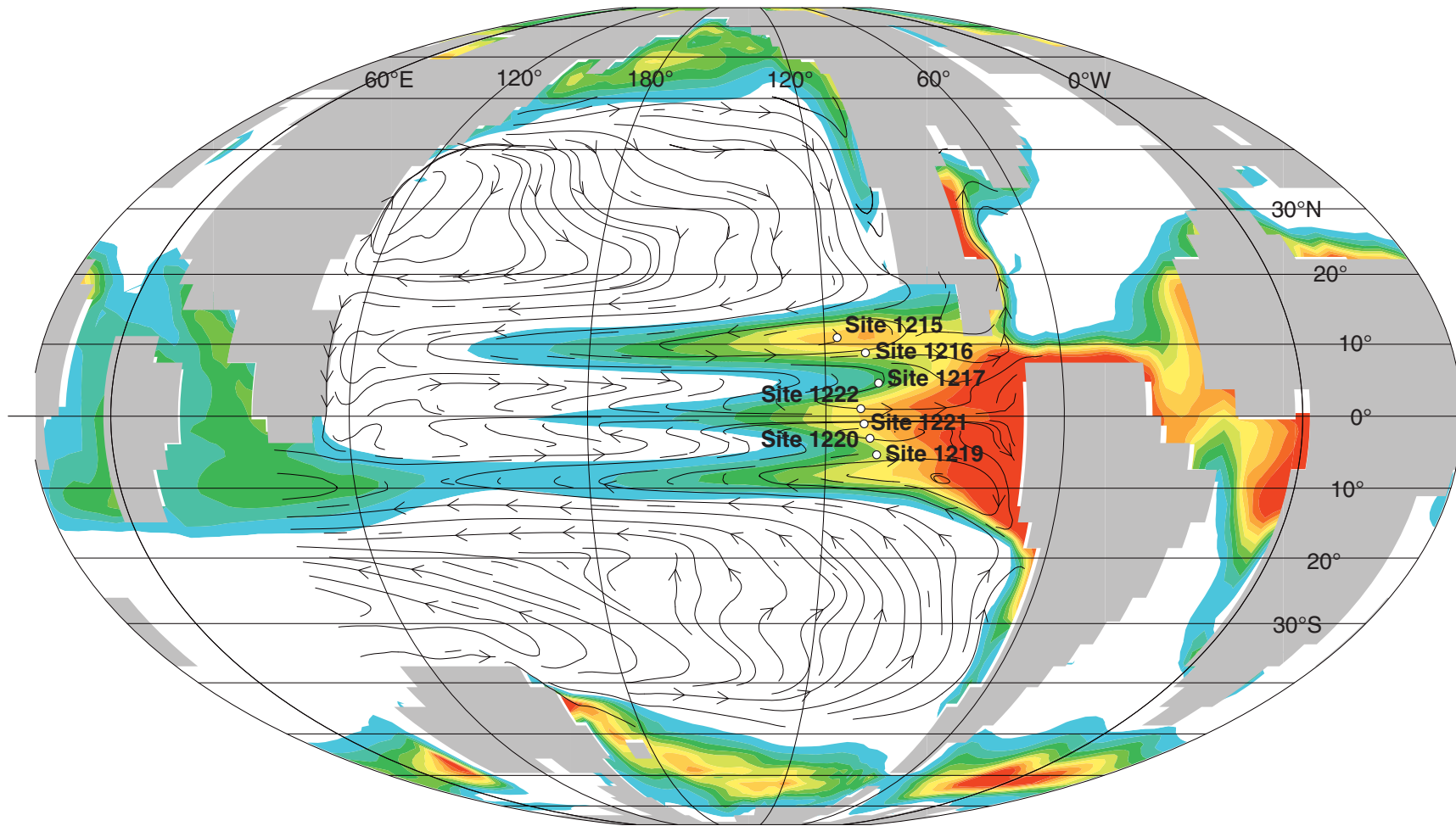
Figure F11. Average sedimentation rate for the interval 40–46 Ma, given in m/m.y. (after Moore et al., 2004). DSDP and ODP site positions are backtracked to their estimated position at 43 Ma. Site locations are colored according to sediment type for the time interval: blue = carbonate, green = siliceous-carbonate, red = siliceous, brown = clay. Contours are at 1, 5, and 10 m/m.y. Red dashed line = approximate geographic paleoequator based on the sediment archive, with a notable difference compared to the fixed-hotspot based rotation. Two regions of relatively high accumulation occur on both sides of the paleoequator in addition to the primary upwelling center.
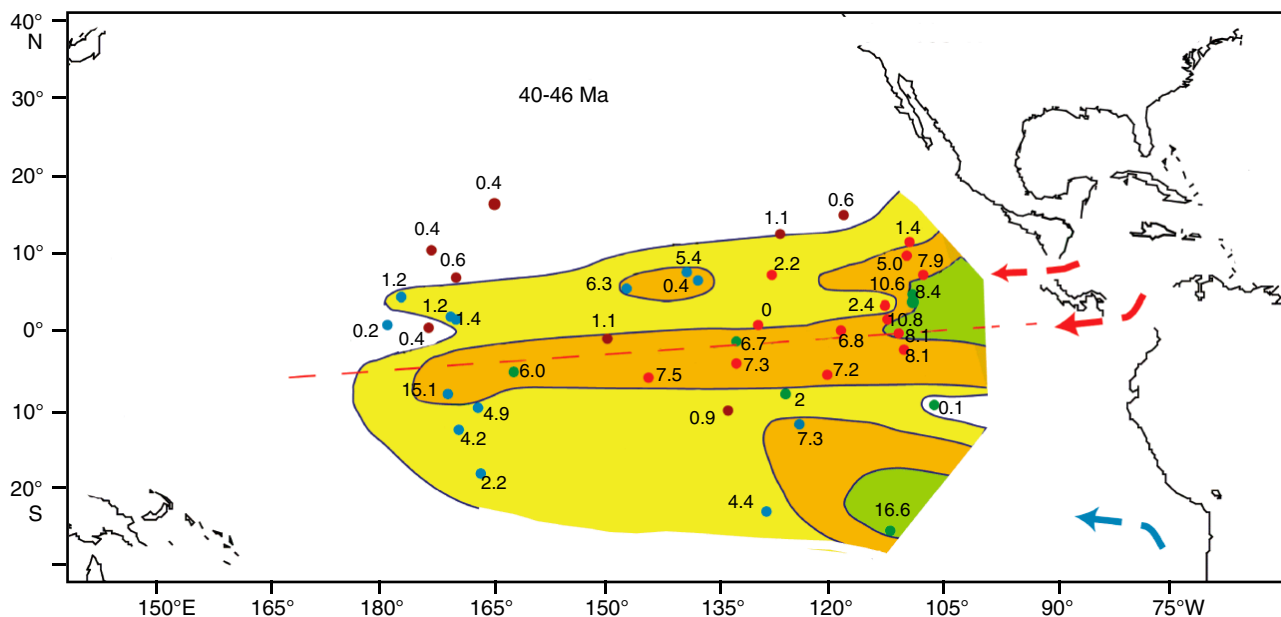
Figure F12. Stratigraphic summary plots, PEAT Sites U1331–U1336 and ODP Site 1218. Planktonic foraminifer Zones O2, O3, O6, and M2 are informally divided into an upper and lower part using the base of *Paragloboro-talia opima* and top of *Subbotina angiporoides* and the base of *Paragloborotalia pseudokugleri* and top of *Globoquadrina binaiensis,* respectively. Green = Eocene, blue = Oligocene, yellow = Miocene. Magnetic stratigraphy data for Site U1335 is from Hole U1335B. See Figure F1 for site locations. CSF-A = core depth below seafloor, method A; DSF = drilling depth below seafloor; mbsf = meters below seafloor.
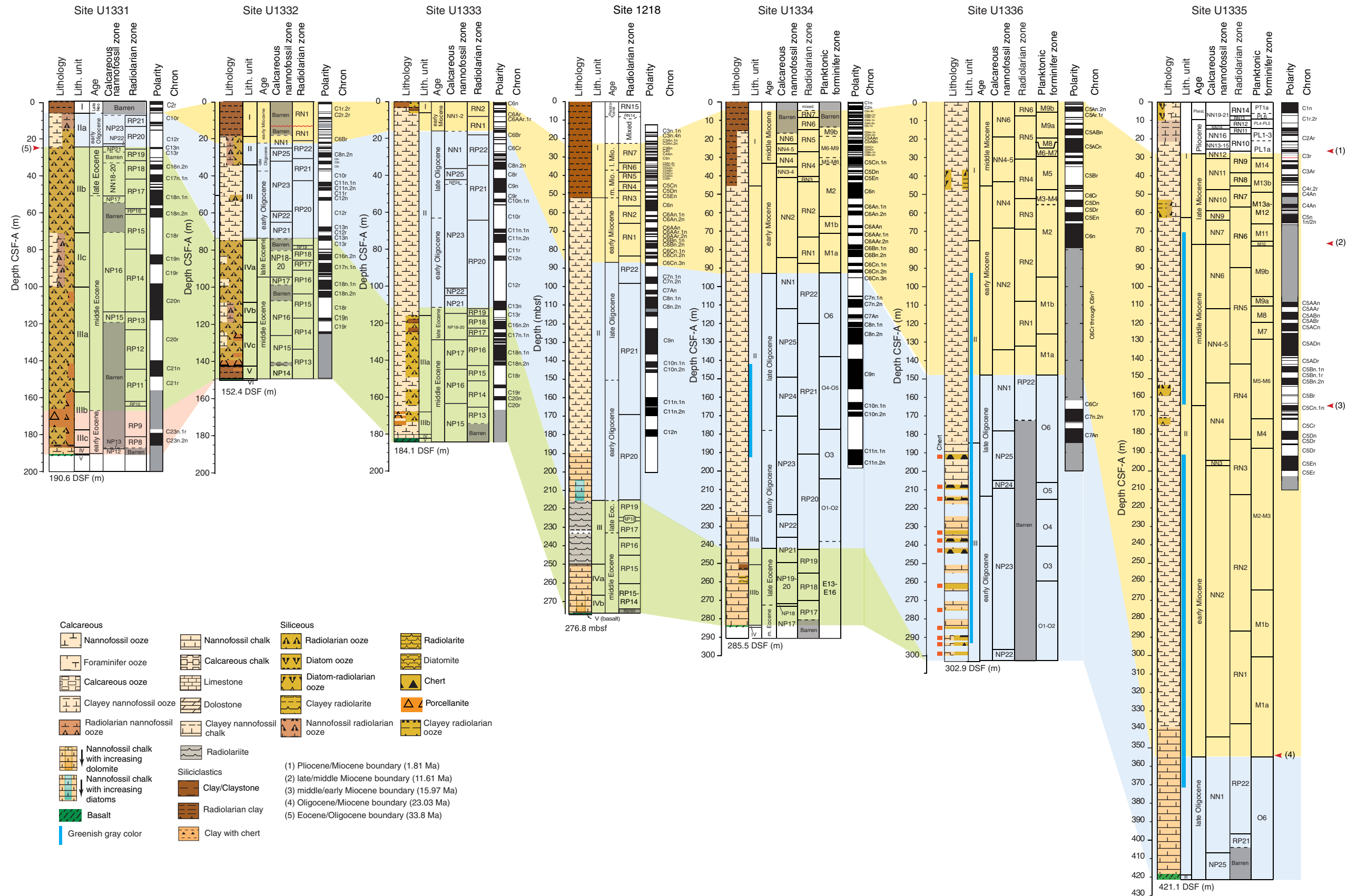
Figure F13. Expedition 320 and selected ODP Leg 199 drill sites plotted against the Pacific Equatorial Age Transect (PEAT) timescale. Sites are plotted approximately ordered by site longitude and basement age, with younger and more eastern sites toward the right. Crustal ages are listed underneath each stratigraphic column. Carbonate accumulation events (CAE) appear as defined by Lyle et al. (2005). MECO = Middle Eocene Climatic Optimum.
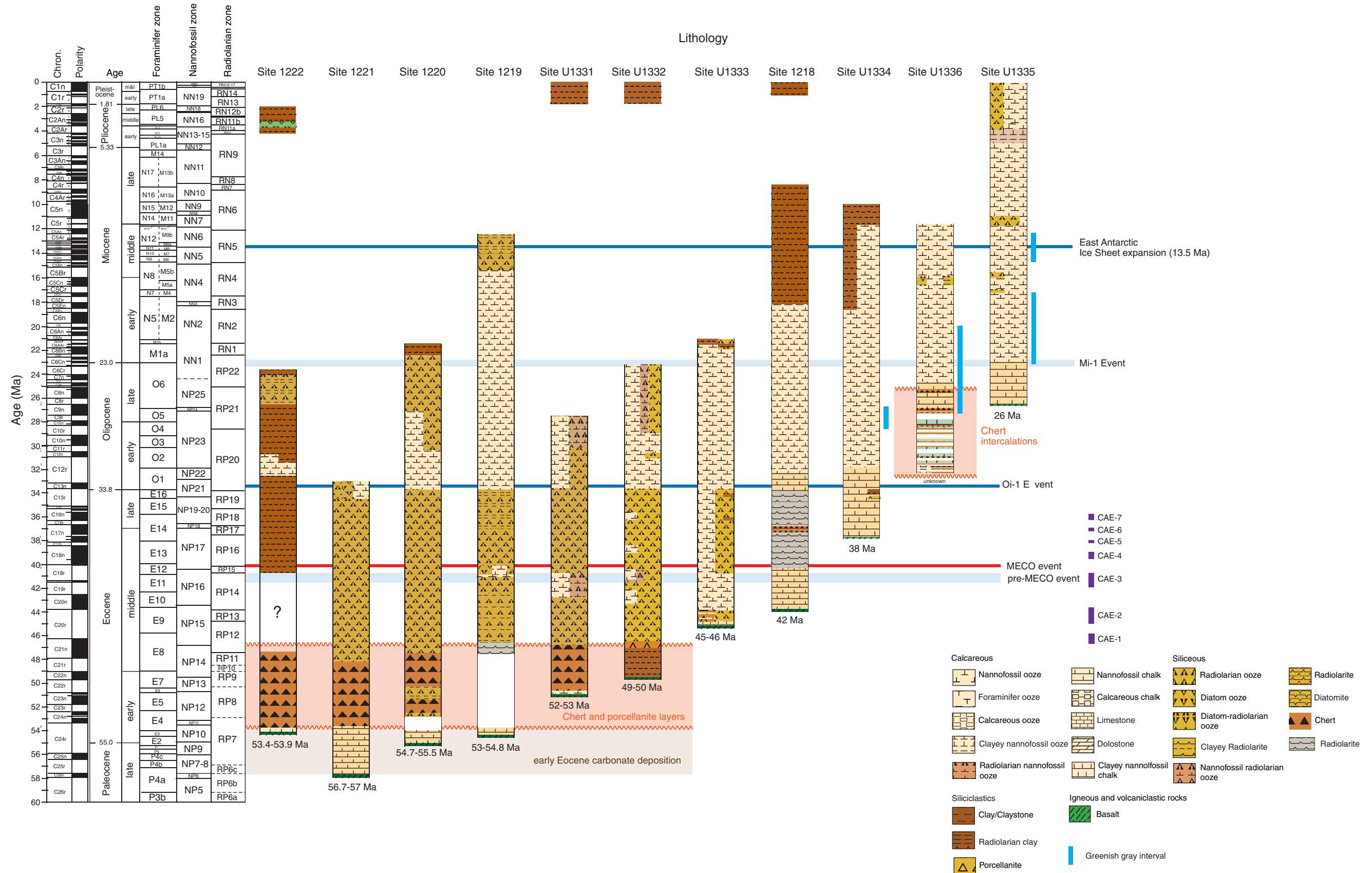
Figure F14. CaCO$_3$ and carbonate mass accumulation rates from Expedition 320 and selected ODP Leg 199 sites (1218, 1220) (Lyle, Wilson, Janecek, et al., 2002). **A.** Weight percentages from shipboard analysis of samples from all Expedition 320 drill sites plotted vs. shipboard PEAT age model for each site and reconstructed paleodepth (see Fig. F3). Bubble area is proportional to CaCO$_3$ wt% measured. Events marked are the Eocene–Oligocene transition (E/O) (e.g., Coxall et al., 2005) and carbonate accumulation events (CAE) of Lyle et al. (2005). Dashed gray line = previous reconstructions of equatorial CCD during the Cenozoic (Lyle 2003; Rea and Lyle, 2005), solid gray line = revised tentative reconstruction based on new data. **B.** As in A, with carbonate mass accumulation rates (CAR) for each site. Calculation uses linear sedimentation rates and dry bulk densities determined on board. Sedimentation rates calculated from data tables, adjusted core composite depth, method A (CCSF-A), depth scales by dividing by the growth factor for each site to convert thicknesses back into in situ sediment thickness. **C.** As in B, plotting carbonate mass accumulation rates (CAR) as a function of age and site paleolatitude, reconstructed using stage poles from Koppers et al. (2001). Note that although the equatorial upwelling zone does result in elevated accumulation rates, the disappearance of carbonate for most sites is primarily a function of paleodepth. (**Continued on next page.**)

Figure F14 (continued). (Caption shown on previous page.)
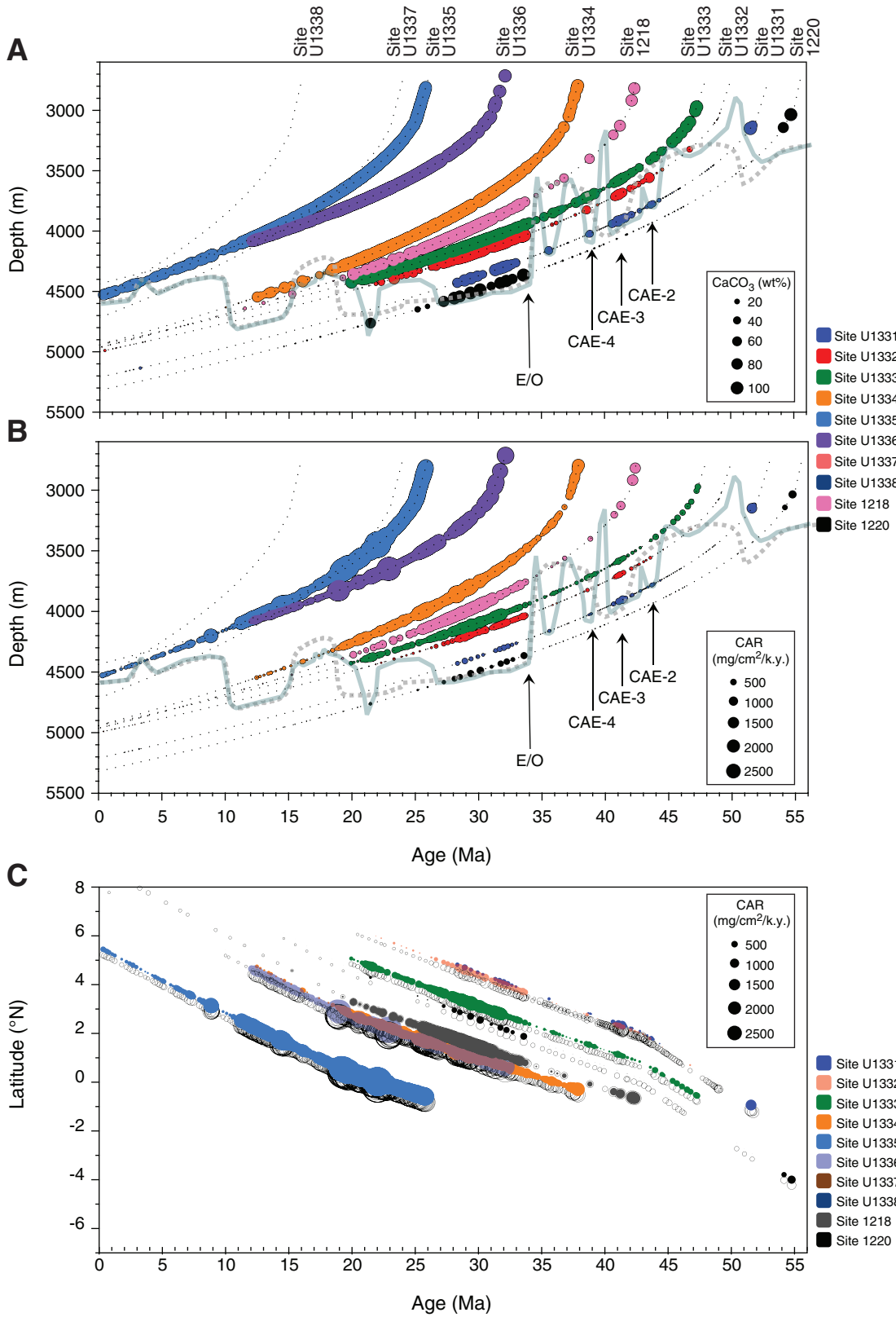
Figure F15. Carbonate content vs. preservation and abundance of calcareous microfossil groups for (**A**) Site U1332 and (**B**) Site U1334. Blue shading = wt% CaCO₃, blue line = nannofossil preservation, purple crosses = abundance of coccolith taxon *Helicosphaera* (all from Hole A). Red shading = semi-quantitative assessment of planktonic foraminifer abundance (percent of planktonics vs. other grains), red line = planktonic foraminifer preservation, orange line = benthic foraminifer preservation (all with compiled data from Holes A, B, and C). Preservation: G = good, M = medium, P = poor. Core composite images are from Hole A. CCSF-A = core composite depth. (**Continued on next page.**)
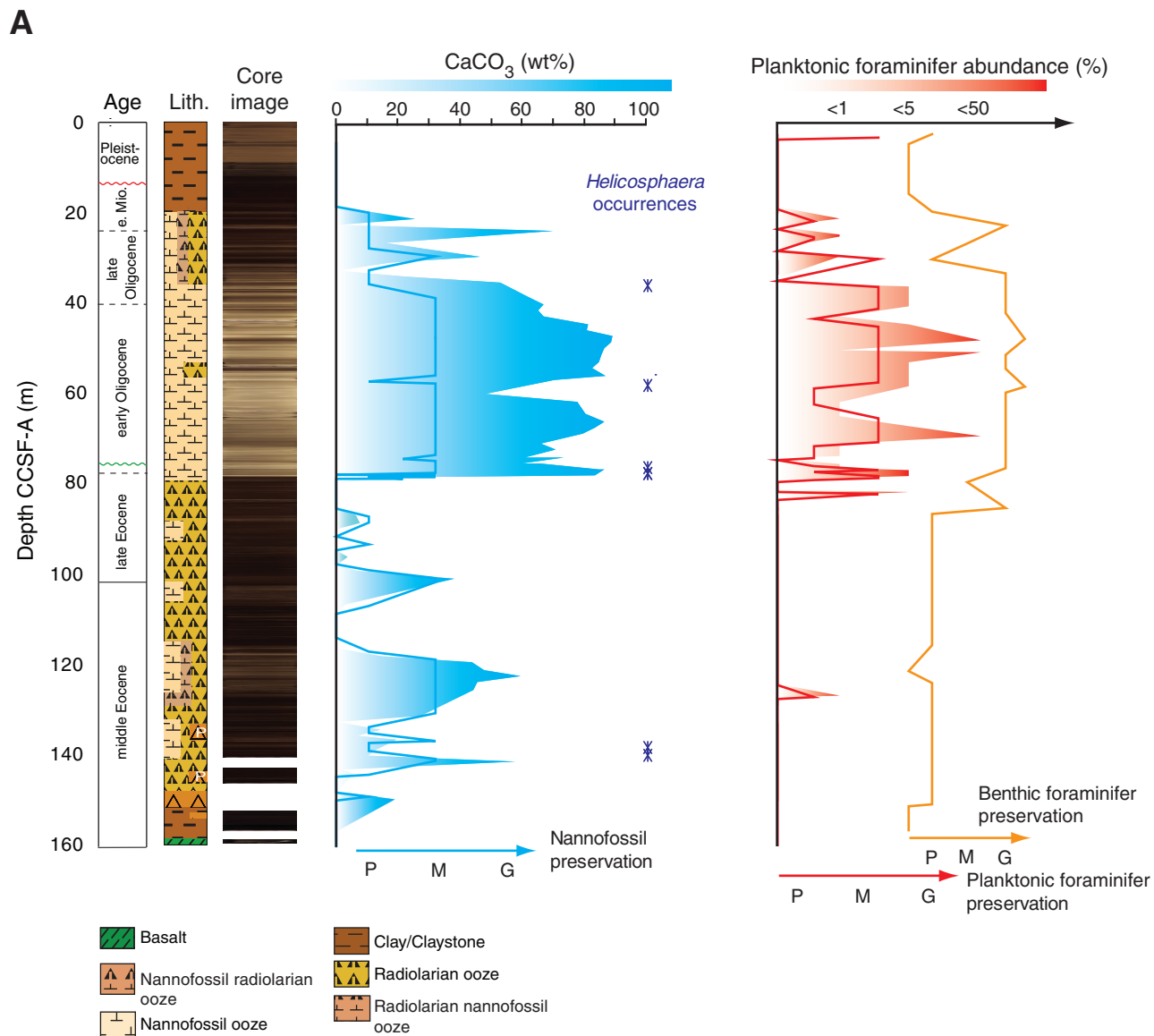
Figure F15 (continued). (Caption shown on previous page.)
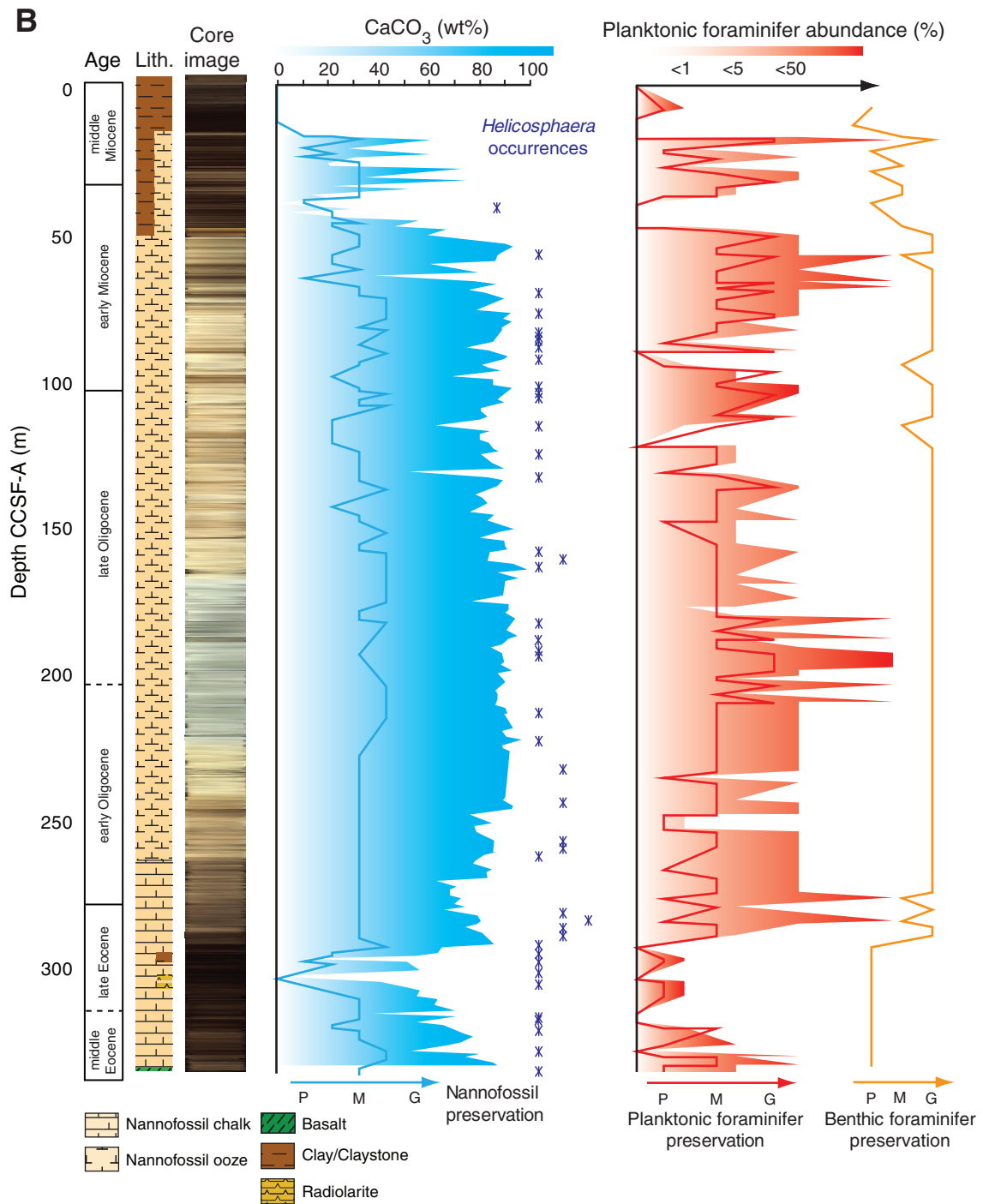
Figure F16. Line scan image compilation of basement basalt fragments recovered during Expedition 320, with overlying sedimentary section.
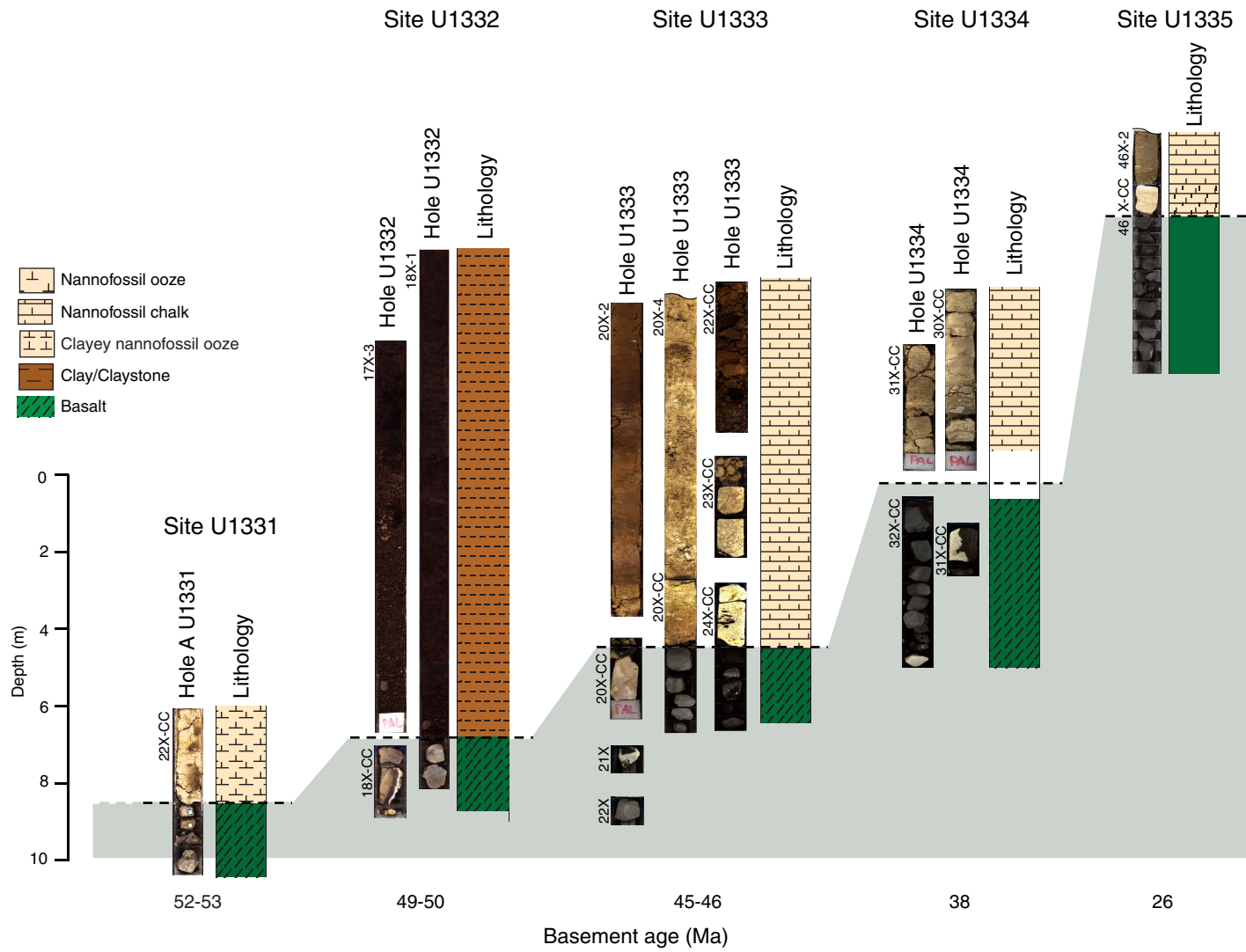
Figure F17. Stratigraphic compilation of diatom abundance in sediments from Expedition 320 and ODP Site 1218. Data for Expedition 320 sites are from shipboard analysis of >1000 smear slides during generation of visual core descriptions. Data from ODP Site 1218 are from Steiger (2006).
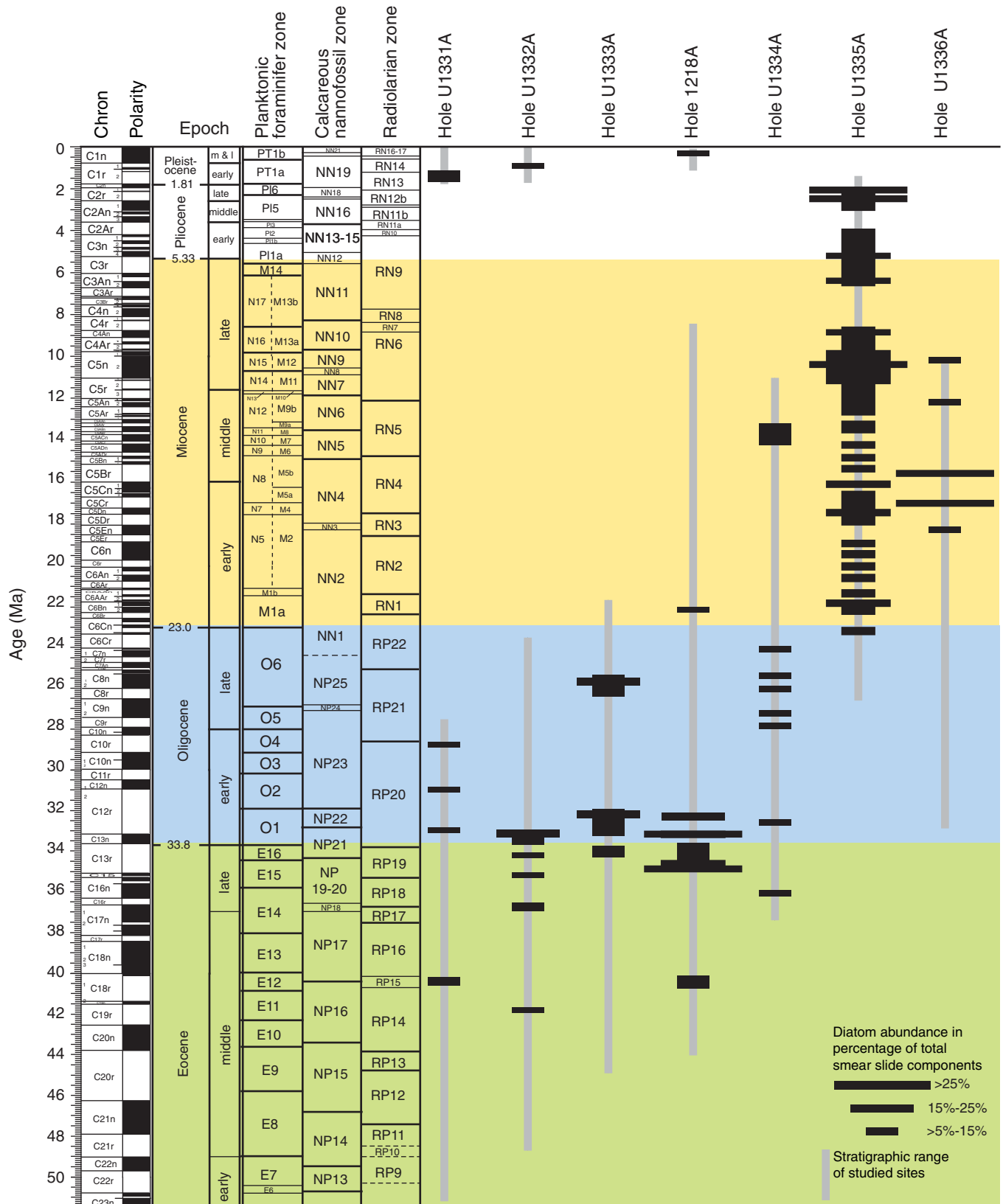
Figure F18. Synthesis for downhole variation of paleomagnetic declination (green curves) along with magnetostratigraphic interpretations for Expedition 320 drill sites. Red bars = possible geomagnetic excursions. CSF-A = core depth below seafloor, method A.
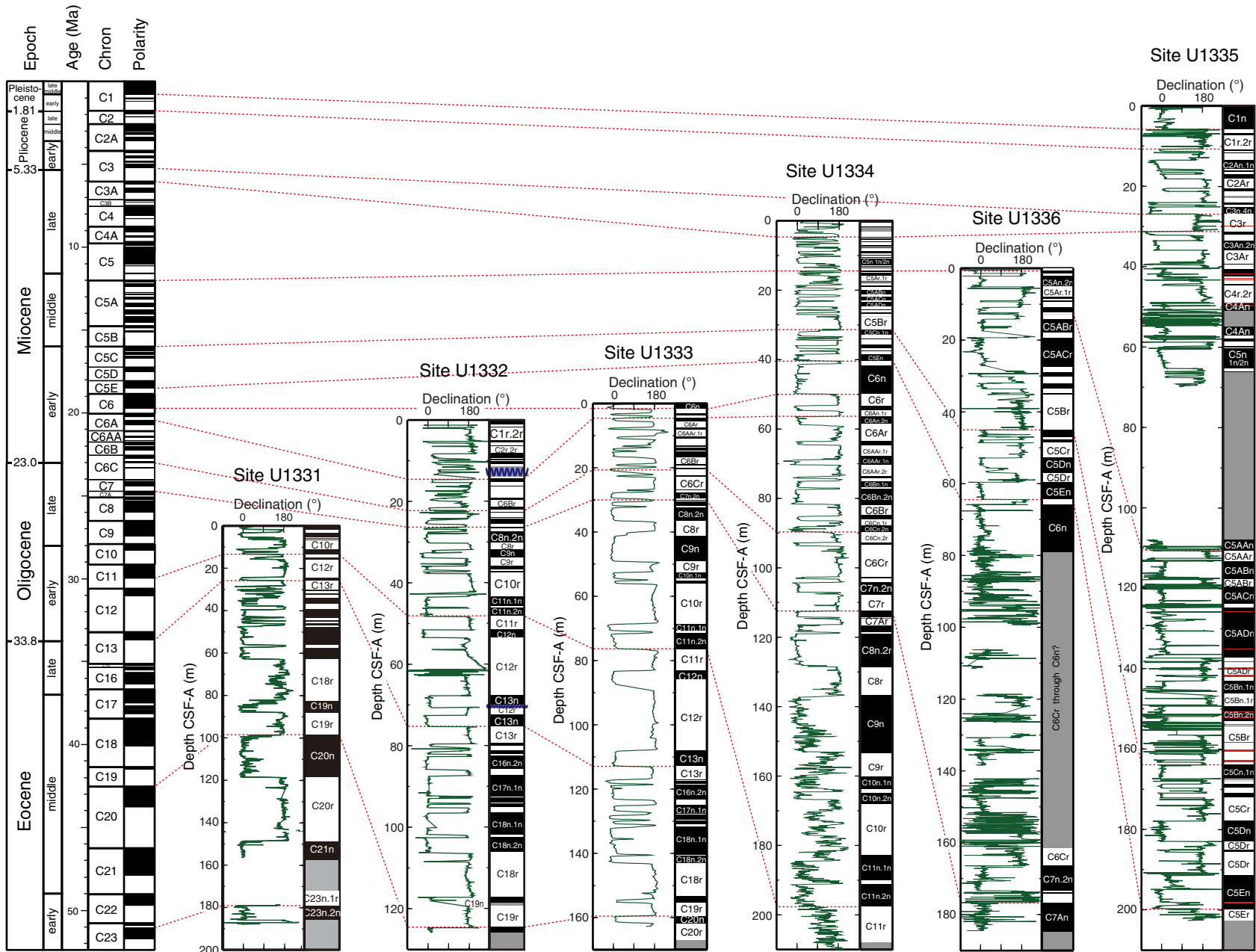
Figure F19. Coherence of sediment properties between widely separated drill sites from ODP Leg 199 and Expedition 320 in the equatorial Pacific is very high, allowing correlation of sediment properties over hundreds of kilometers. ODP Site 1220 and Expedition 320 Sites U1331 and U1332 are compared from 45 to 30 Ma. VGP = virtual geomagnetic pole. GRA density = gamma ray attenuation density (estimated on board).
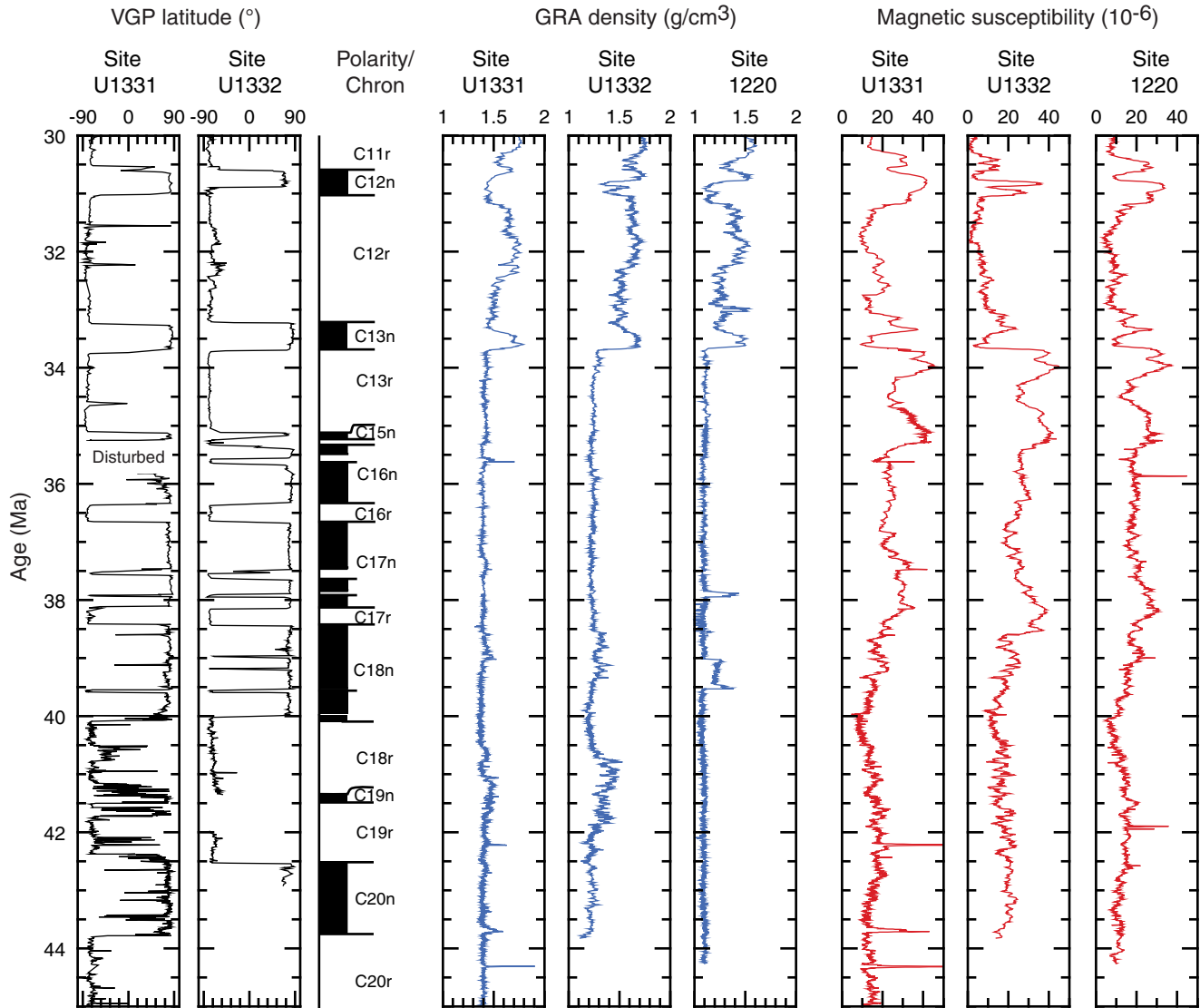
Figure F20. Coherence of sediment properties between widely separated drill sites from ODP Leg 199 and Expedition 320 in the equatorial Pacific is very high, allowing correlation of sediment properties over hundreds of kilometers. ODP Site 1218 and Expedition 320 Sites U1333 and U1334 are compared from 35 to 20 Ma. VGP = virtual geomagnetic pole. GRA density = gamma ray attenuation density (estimated on board).
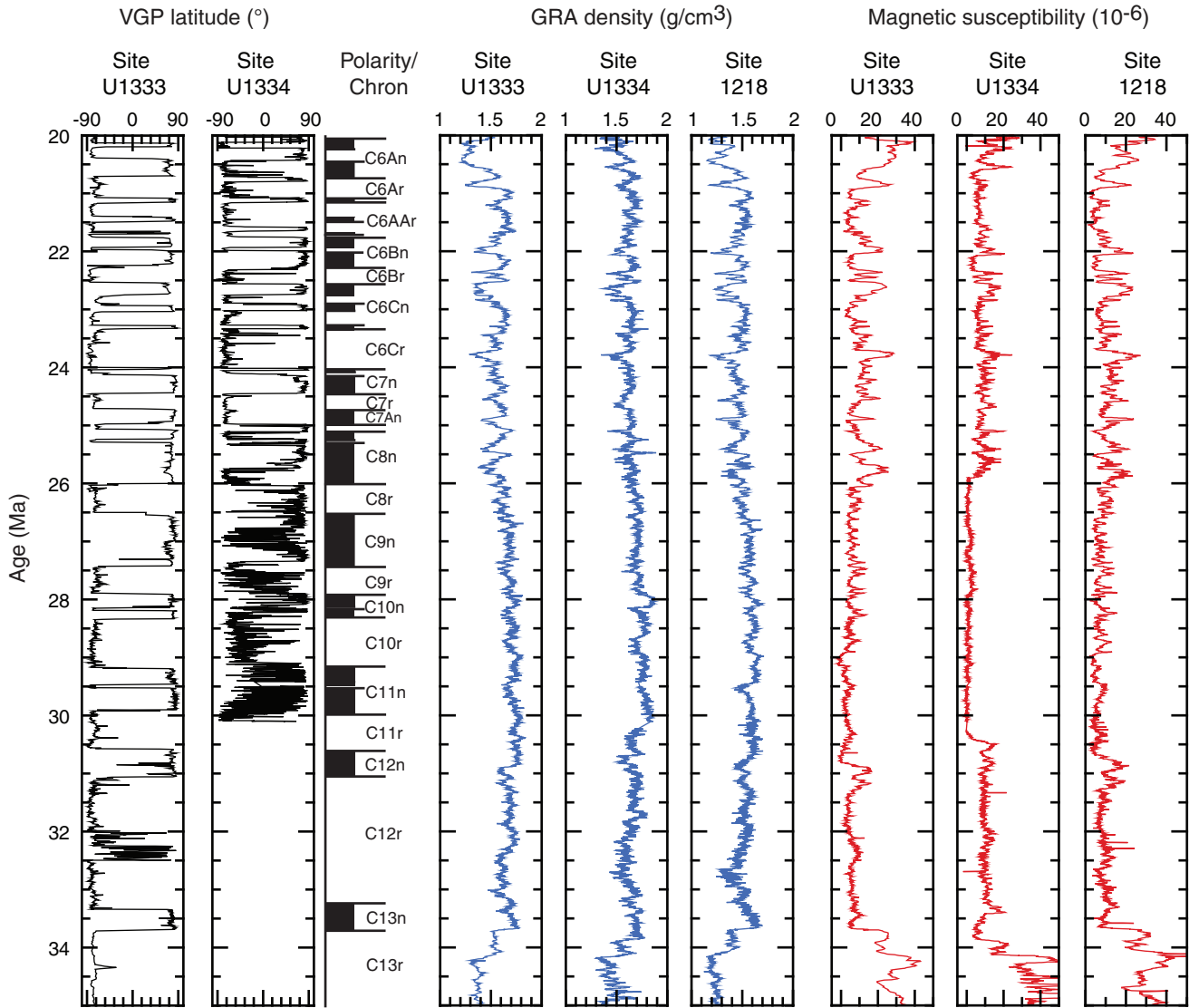
Figure F21. Indicative gamma ray attenuation (GRA) bulk density megasplice constructed from a stack of Leg 138 equatorial Sites 849, 850, and 851. Sites 849 and 851 were correlated to Site 850 using the Analyseries program (Paillard et al., 1996) and biostratigraphic datums to check the similarity in character of the curves. These records were stacked and averaged (three-point smooth), forming the Site 850 composite record. Site 844 was also correlated to the lower part of the Site 850 composite and appended to the bottom of the record in order to extend its range back to the middle Miocene. Expedition 320 Site U1335 (black curve) was correlated to the bottom of this composite record, again using biostratigraphic datums, to check the similarity in character of the two records near the join. This exercise was repeated to join Site U1335 to the Site 1218 record (green curve). Because the base of Site U1335 is several hundred meters below the seafloor, its compacted density was substantially offset from the Site 1218 values. A density offset value of 0.44 was added to all density values of the Site 1218 record. Near the Eocene/Oligocene boundary, the Site 1218 density record was correlated to that of Site 1334 (the site with the highest carbonate content) with an added density offset of 0.22 (purple curve). This completes the megasplice density record back to the top of the middle Eocene. rmcd = revised meters composite depth.
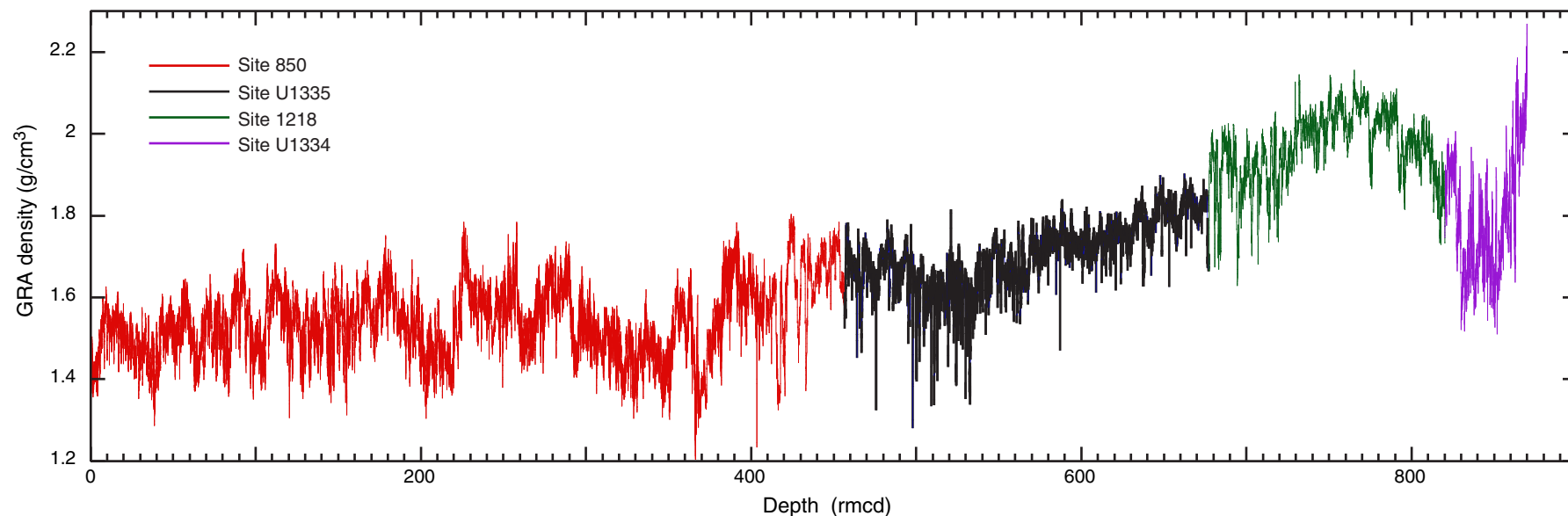
Figure F22. Summary of sedimentation rates derived from age-depth models at each Expedition 320 site.
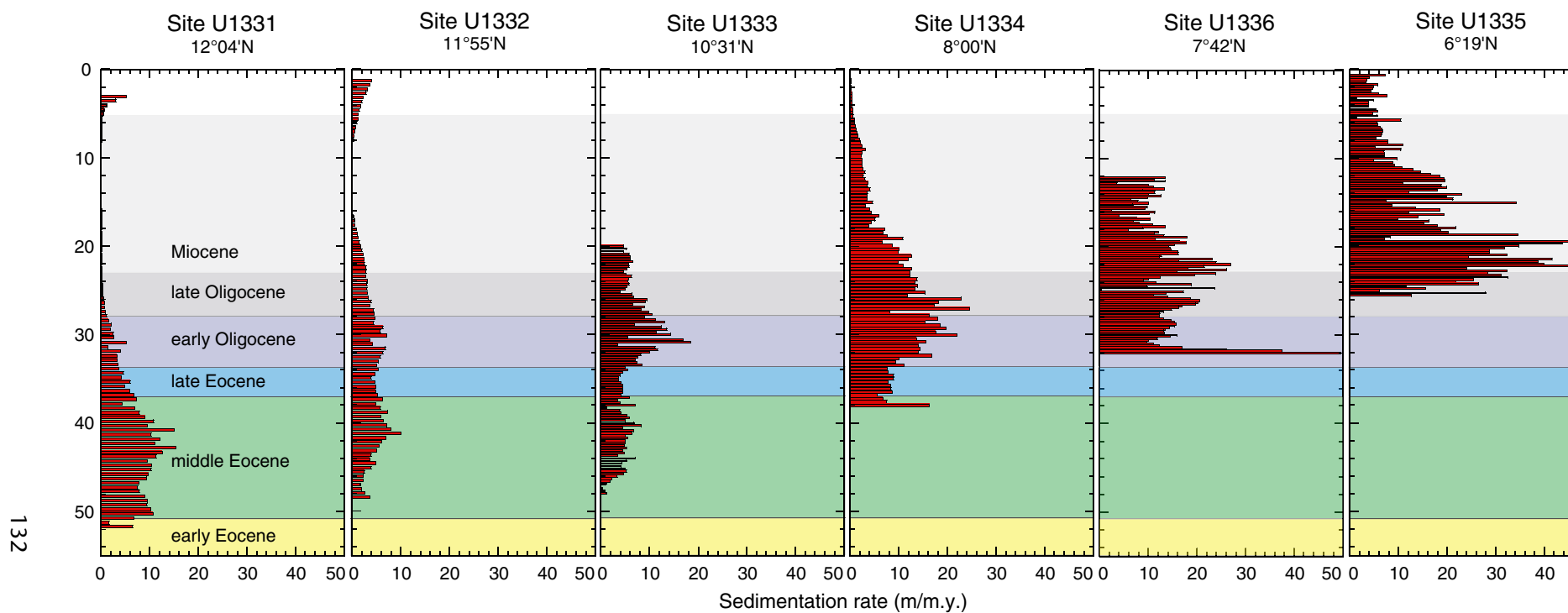
Figure F23. Summary of sedimentation rates derived from age-depth models at each Expedition 320 site plotted vs. corrected core composite depth, method A (CCSF-A).
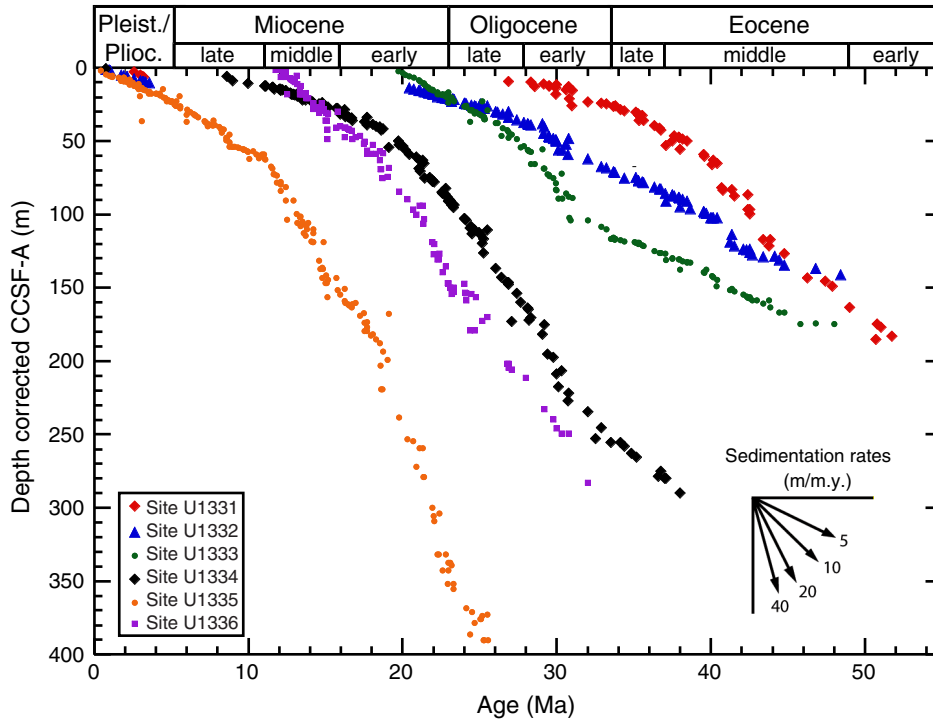
Figure F24. Line scan images of the Middle Eocene Climatic Optimum (MECO) event, Holes U1333A, U1331B, and U1331C. CSF-A = core depth below seafloor, method A.
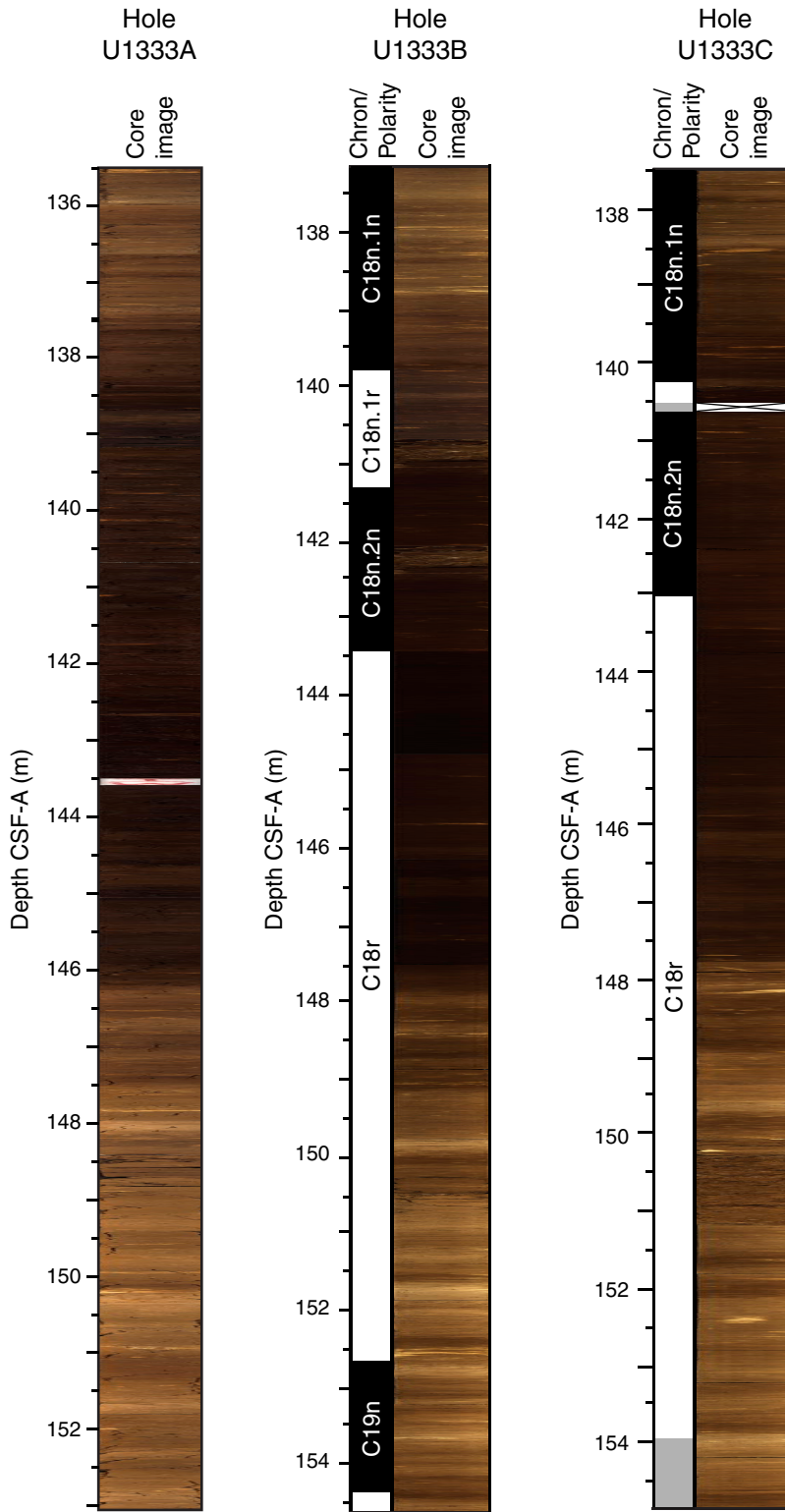
Figure F25. Line scan image compilation of depth transect across Eocene–Oligocene transition captured by Expedition 320 Sites U1331, U1332, U1333, and U1334. Dashed line approximates position of the Eocene/Oligocene boundary, as refined by Pearson et al. (2008).
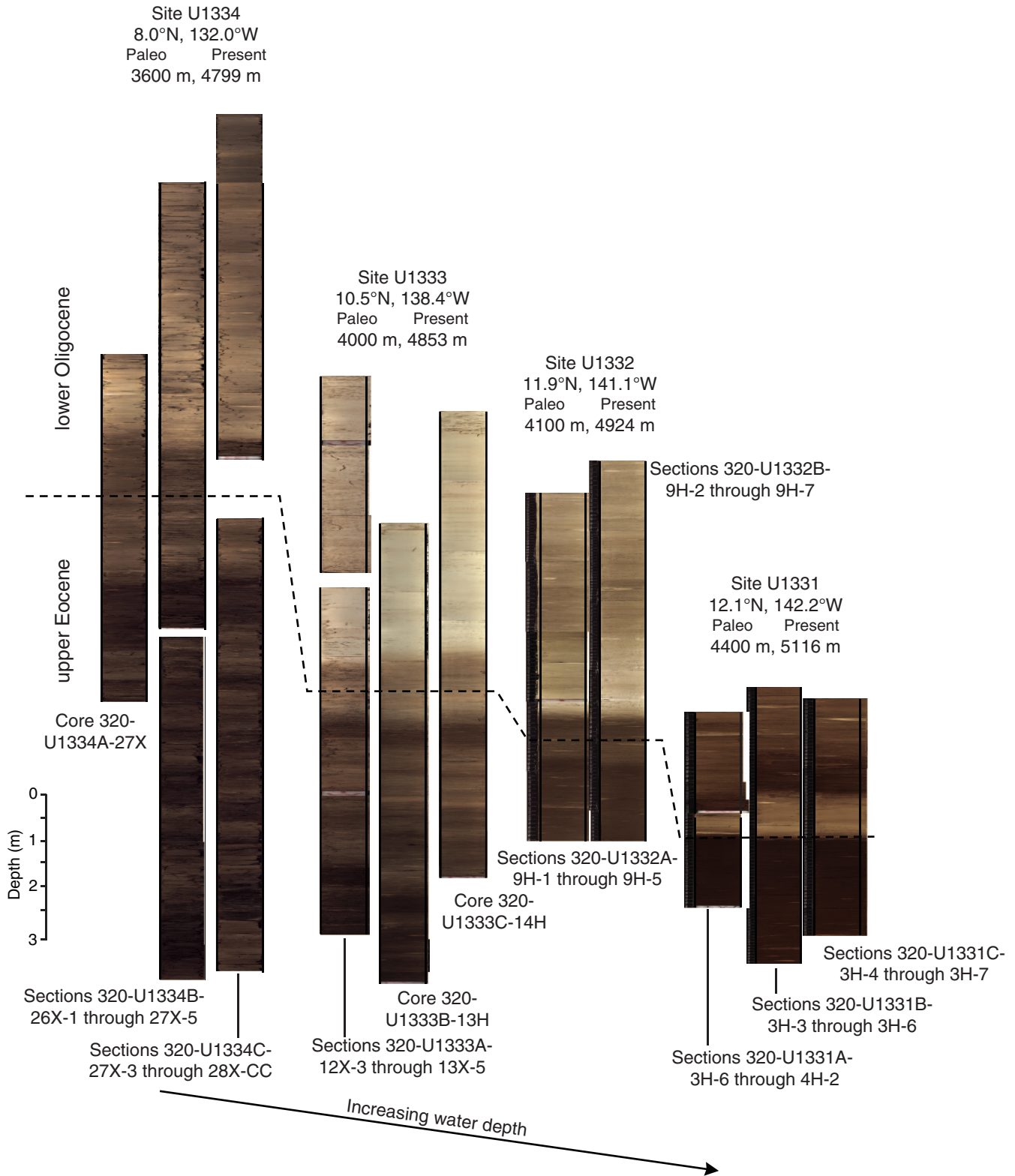
Figure F26. Eocene–Oligocene transition recovered in Holes U1334A, U1334B, and U1334C. Line scan images were manipulated by applying a shadow highlight adjustment to the whole image for better visual inspection of the darker strata. CSF-A = core depth below seafloor, method A. L* = lightness reflectance value of sediment as defined in the LAB color model.
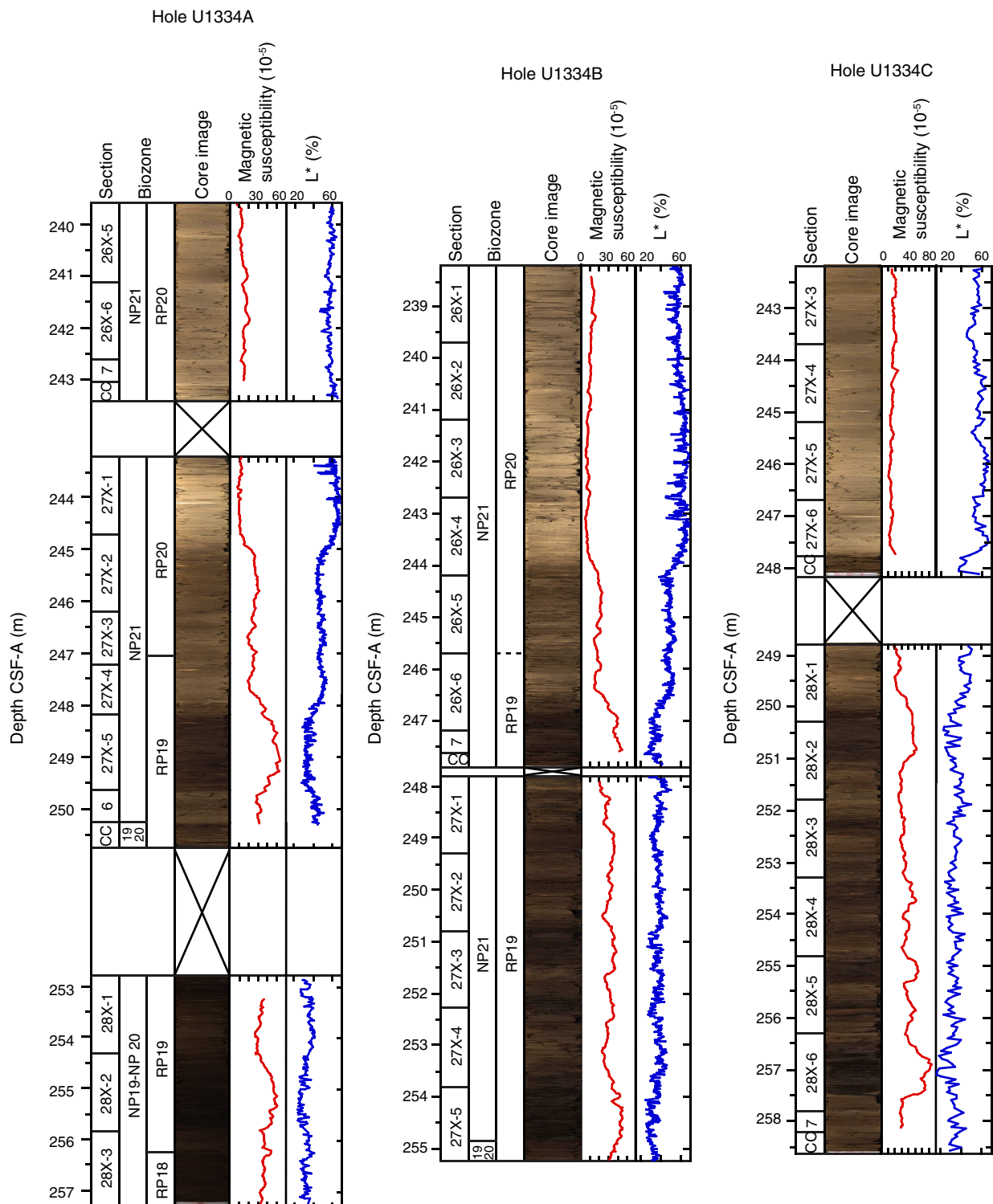
Figure F27. Magnetic susceptibility for each hole drilled at Site U1333. Depths are adjusted in overlapping hole intervals to match corrected core composite depth, method A (CCSF-A). Solid black circle = first appearance of Eocene species, solid black arrowhead = last appearance of Eocene species, open red circle = first appearance of Oligocene species, open red arrowheads = last appearances of Oligocene species. T = top, B = bottom.
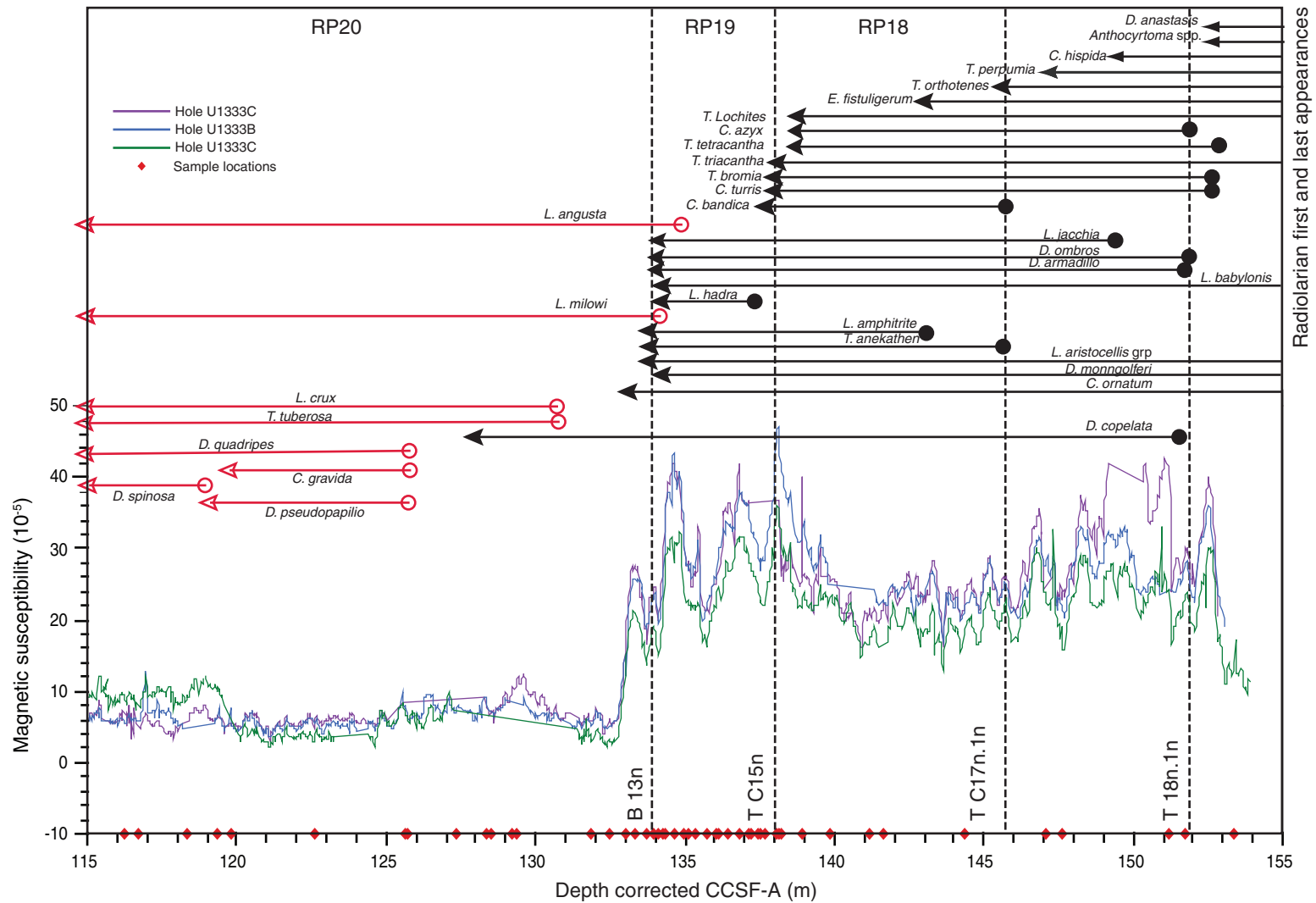
Figure F28. Correlation of magnetic susceptibility records from ODP Site 1218 and Expedition 320 Sites U1334 and U1333 for the upper Eocene and lower Oligocene. Solid and dashed vertical lines = positions of magnetic chron boundaries, solid green and dashed red lines = points of proposed correlation, green stars = species datums used in correlation. mcd = meters composite depth, rmcd = revised meters composite depth. T = top, B = bottom.
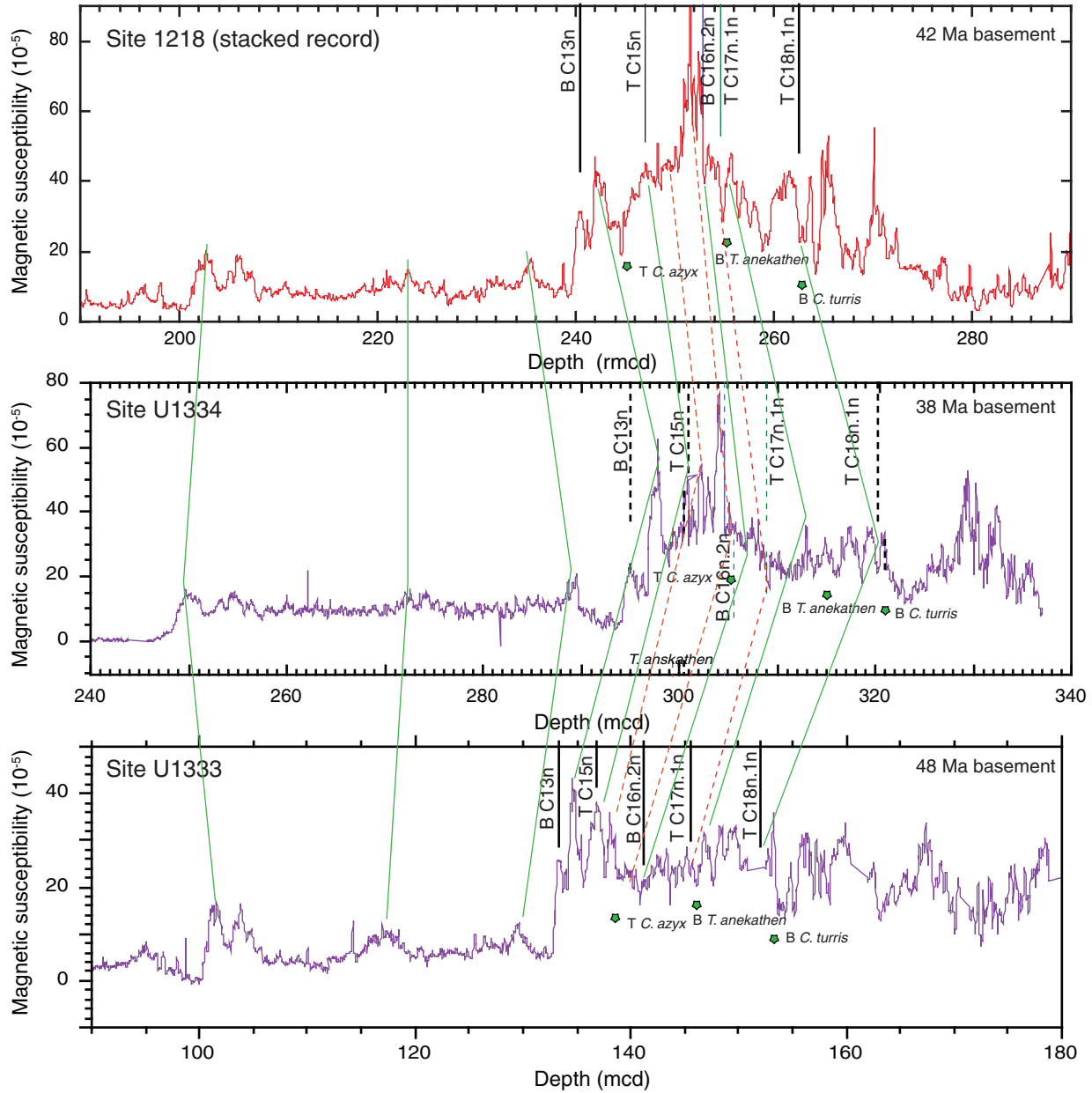
Figure F29. Magnetic susceptibility records for ODP Sites 1218, 1219, and 1220 and Expedition 320 Site U1333 for the upper Eocene. Site 1219 and 1220 depths have been adjusted to match the record of Site 1218. Note that the general character of the record from Site U1333 (located on 48 Ma crust) is more similar to records from Sites 1219 and 1220 (located on 56 Ma crust) than to that of Site 1218 (located on 42 Ma crust). CCSF-A = core composite depth, method A; rmcd = revised meters composite depth.
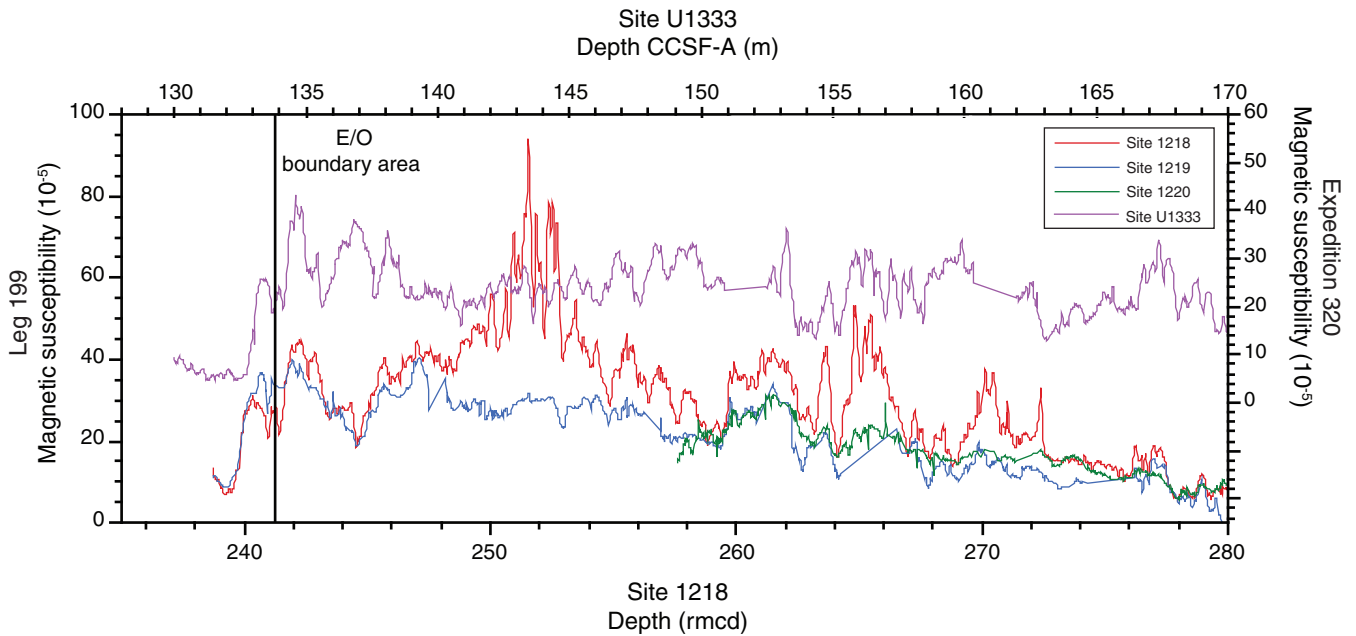
Figure F30. Lowermost Oligocene through upper middle Eocene magnetic susceptibility records, Sites U1331–U1334. Radiolarian datums in this section guide the correlation (red lines) of these records. All records plotted using approximately the same depth scale. Oligocene section is expanded as we move southward toward the early Oligocene paleoequator (Site U1334); Eocene section is expanded at the northern Sites (U1331, U1332) that are closer to the middle Eocene paleoequator. However, the northern sites have the most condensed Eocene/Oligocene boundary interval. The two-step transition from the Eocene to the Oligocene is most pronounced at Sites U1333 and U1334. T = top, B = bottom.
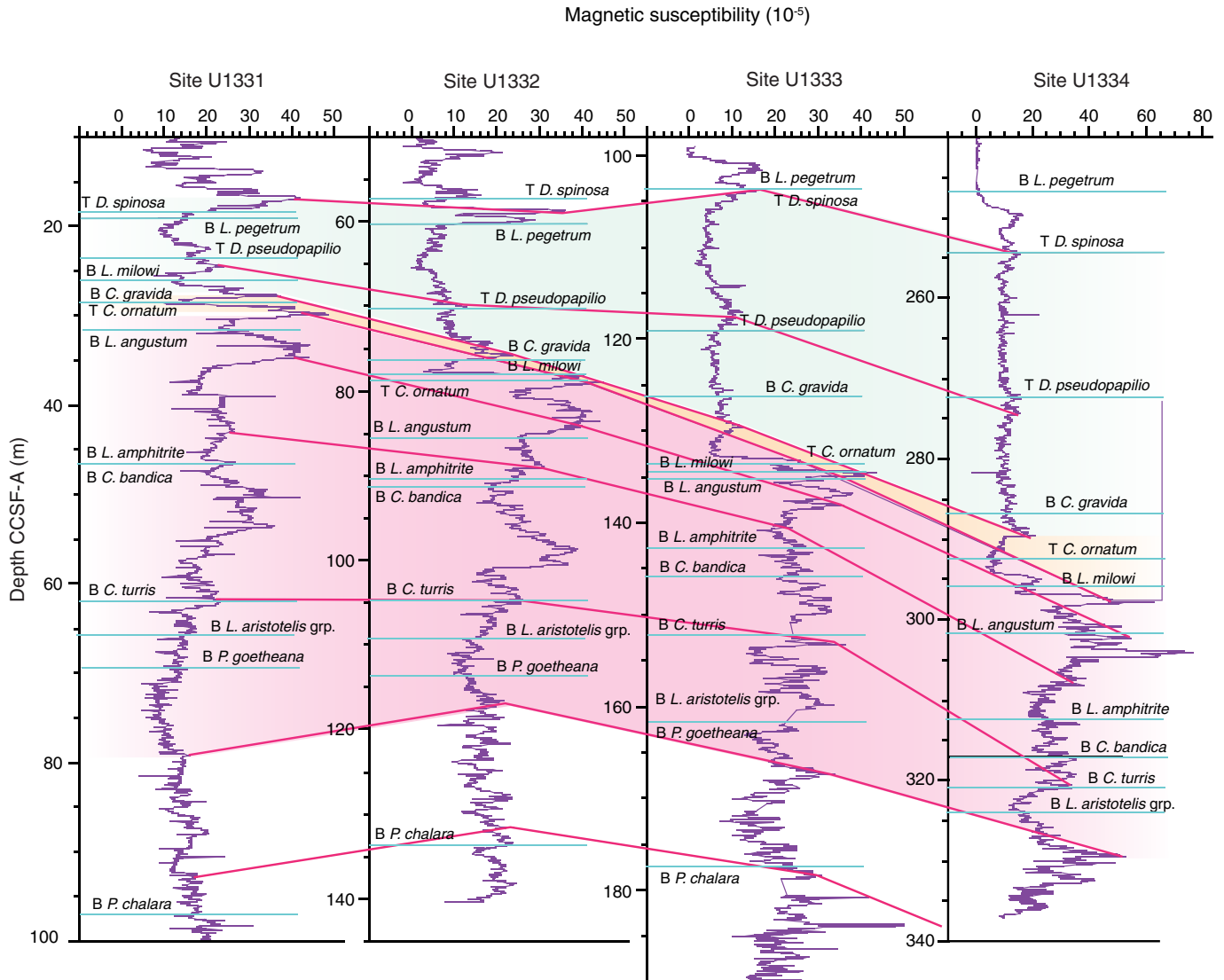
Figure F31. Composite line scan images of cores taken from the Oligocene–Miocene transition, Sites U1332, U1333, U1334, and U1336. The Oligocene/Miocene (O/M) boundary is defined by the M1a/ O6 planktonic foraminifer zone boundary, here approximated at the base of the C6Cn.2n Chron at Sites U1332, U1332, and U1334 and at the lower middle part between the *S. delphix* biozone and the first occurrence (FO) depth of *P. kugleri* at Site U1336, taking account of sedimentation rate and light–dark color alternation pattern. Paleo-water depths estimated at 23 Ma. Note that an O/M boundary was also recovered at Site U1335. However, biostratigraphic control is only available for Hole 1335A where the utility of the core section images is limited by the effect of the core splitting process. These sediments are too consolidated for use of a cheese wire and too soft for use of a saw to cut whole-round core sections. Physical property data did not yet allow correlation between Holes U1335A and U1335B in these intervals. Chron is listed on the left for Sites U1332–U1334. LO = last occurrence.
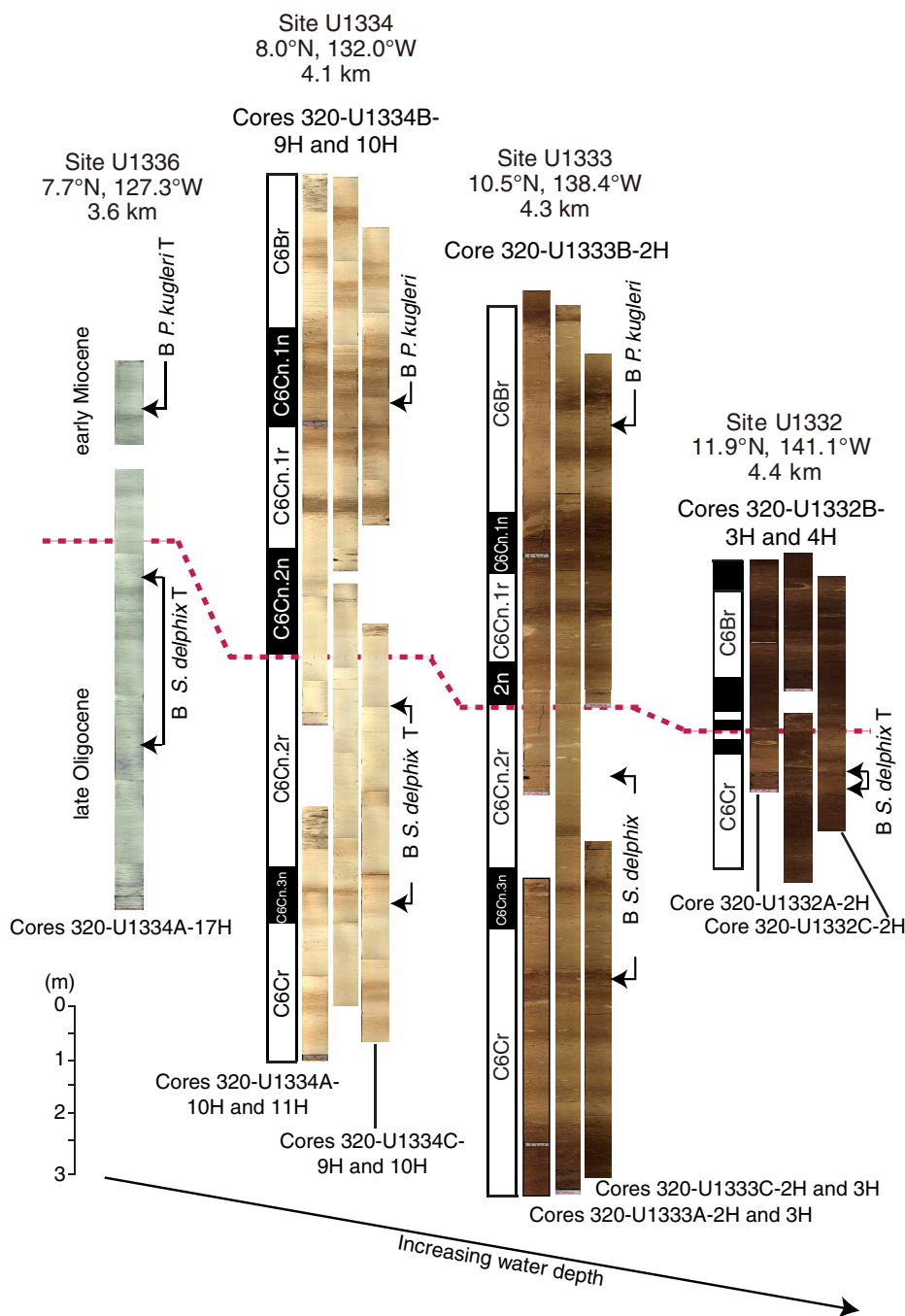
Figure F32. Summary of sediment color and interstitial water chemistry changes. **A.** Geologic series, paleolatitude, stacked line scan core images, b* reflectance, magnetic susceptibility, dissolved Fe, and dissolved Mn concentrations are plotted vs. depth for Sites U1334, U1335, and U1336. **B.** Sediment color changes superimposed on site backtrack curves for Expedition 320 Sites U1334, U1335, and U1336 and DSDP Sites 78, 79, and 574, as interpreted from visual core descriptions.
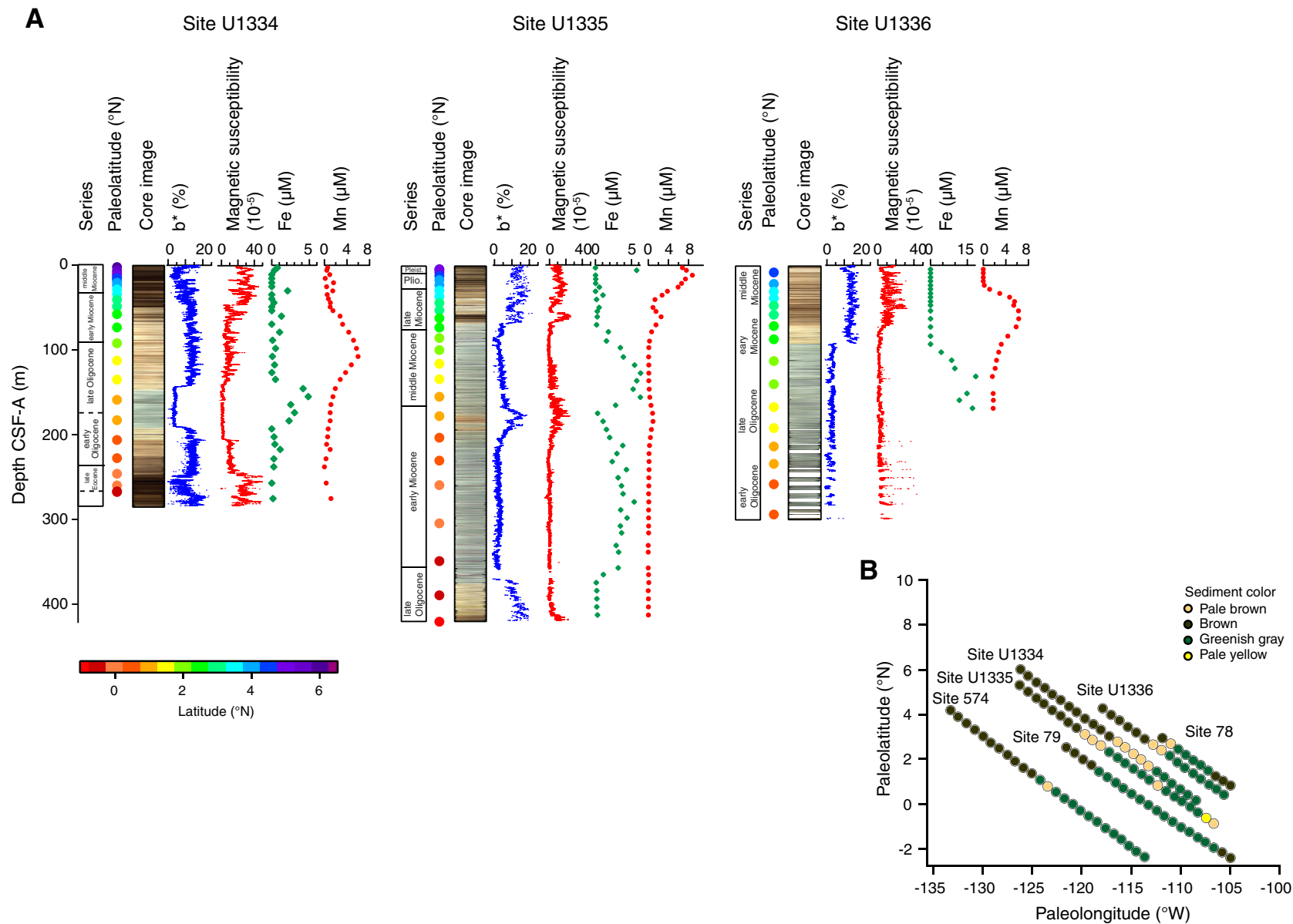
Figure F33. Calcium carbonate (CaCO₃) concentrations in sediments, Holes U1331A, U1332A, U1333A, U1334A, U1335A, and U1336A. CSF-A = core depth below seafloor, method A.
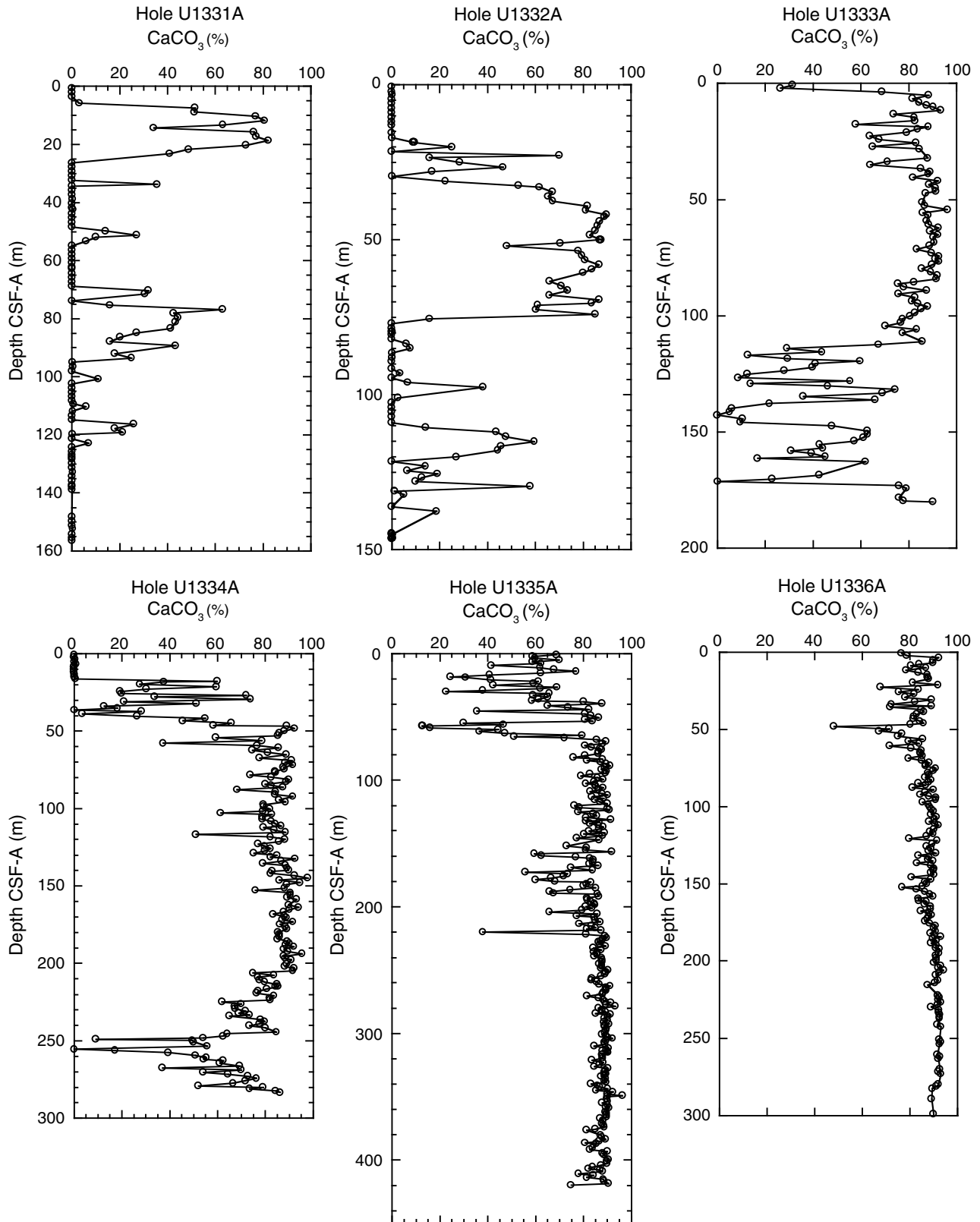
Figure F34. Concentrations of total and inorganic carbon in sediments, Holes U1331A, U1332A, U1333A, U1334A, U1335A, and U1336A. CSF-A = core depth below seafloor, method A.
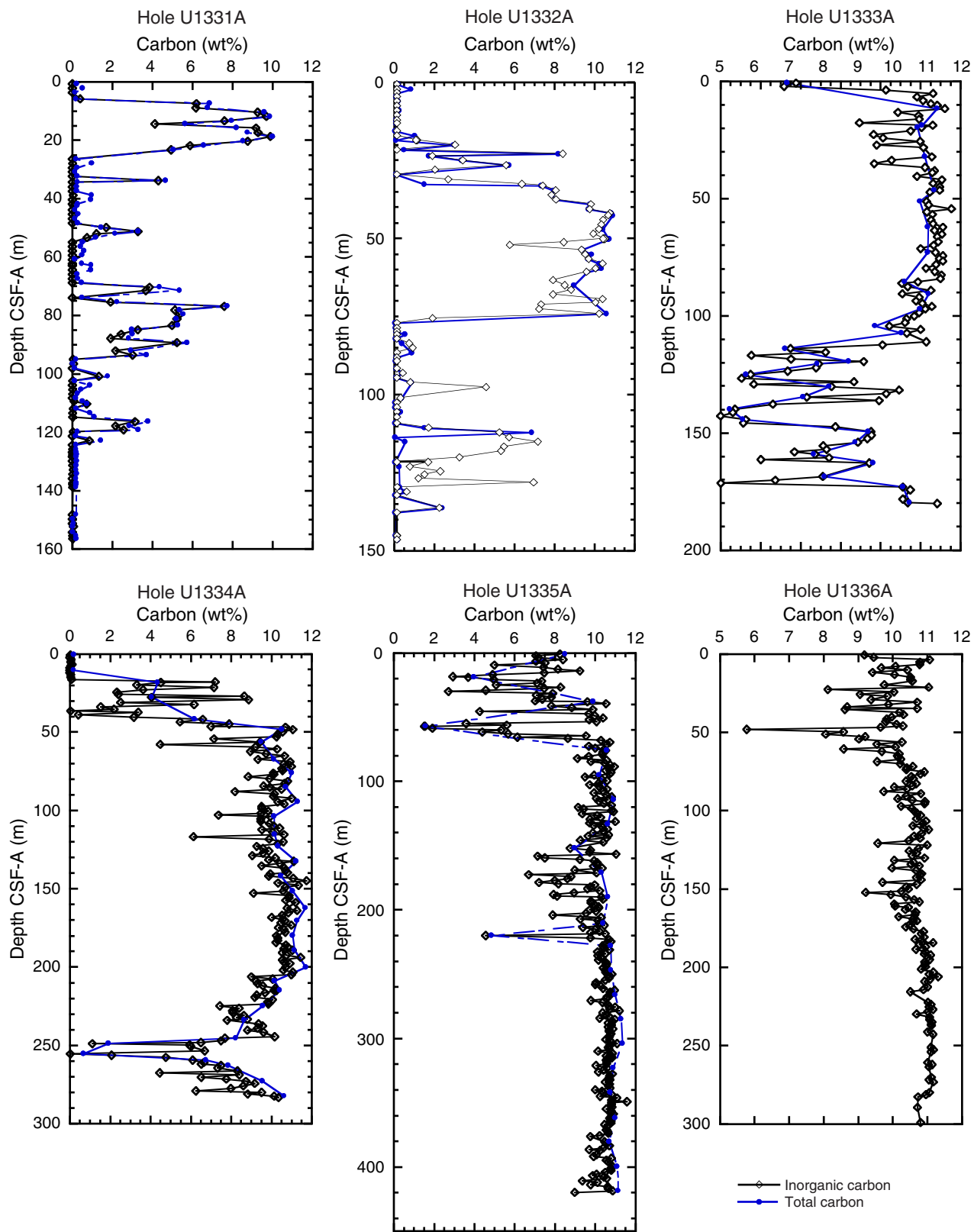
Figure F35. Total organic carbon (TOC) content in sediments determined by acidification method, Holes U1331A, U1332A, U1333A, U1334A, and U1335A. CSF-A = core depth below seafloor, method A.
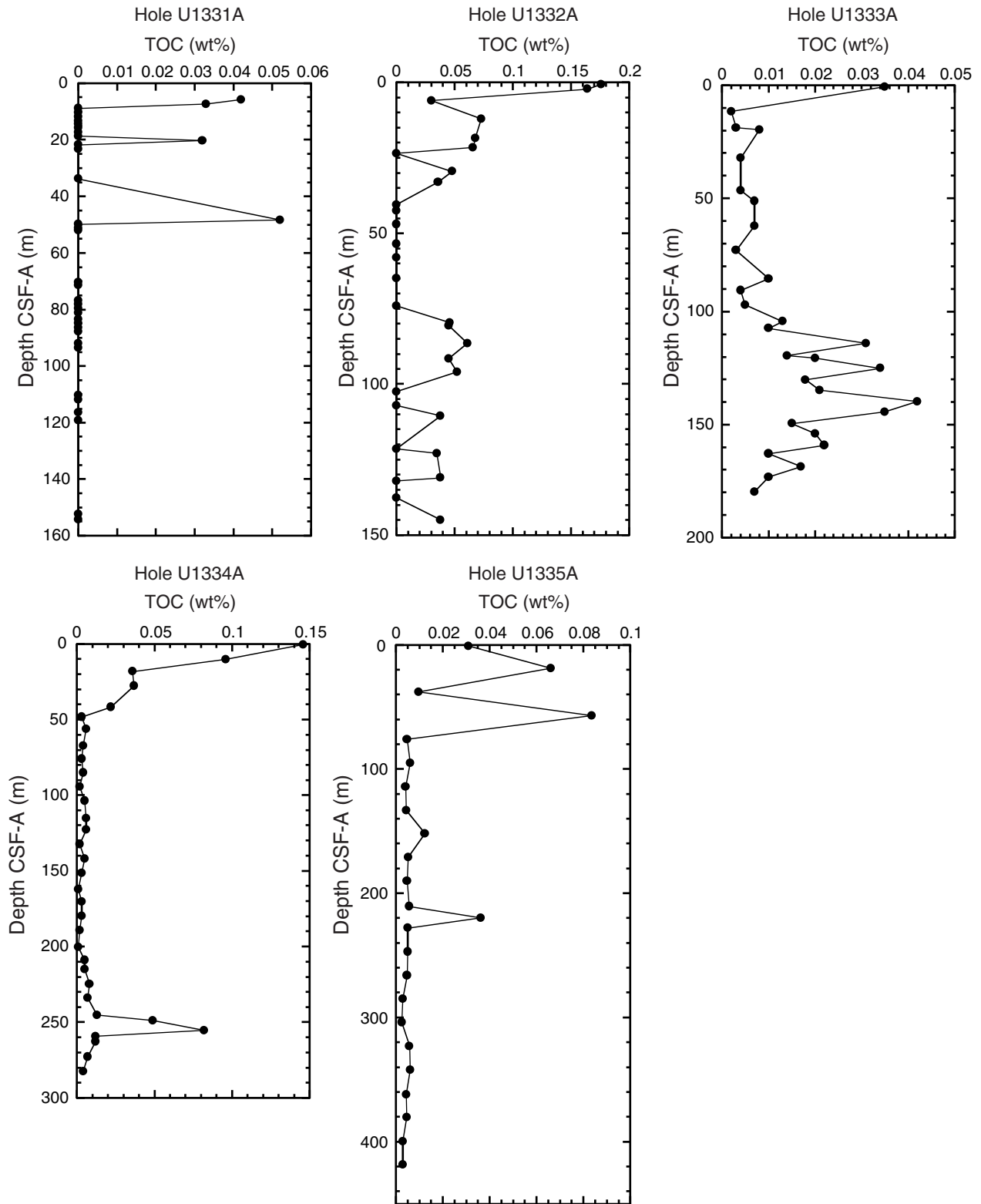
Figure F36. Depth profiles of dissolved silicate in interstitial waters, all Expedition 320 sites. CSF-A = core depth below seafloor, method A.
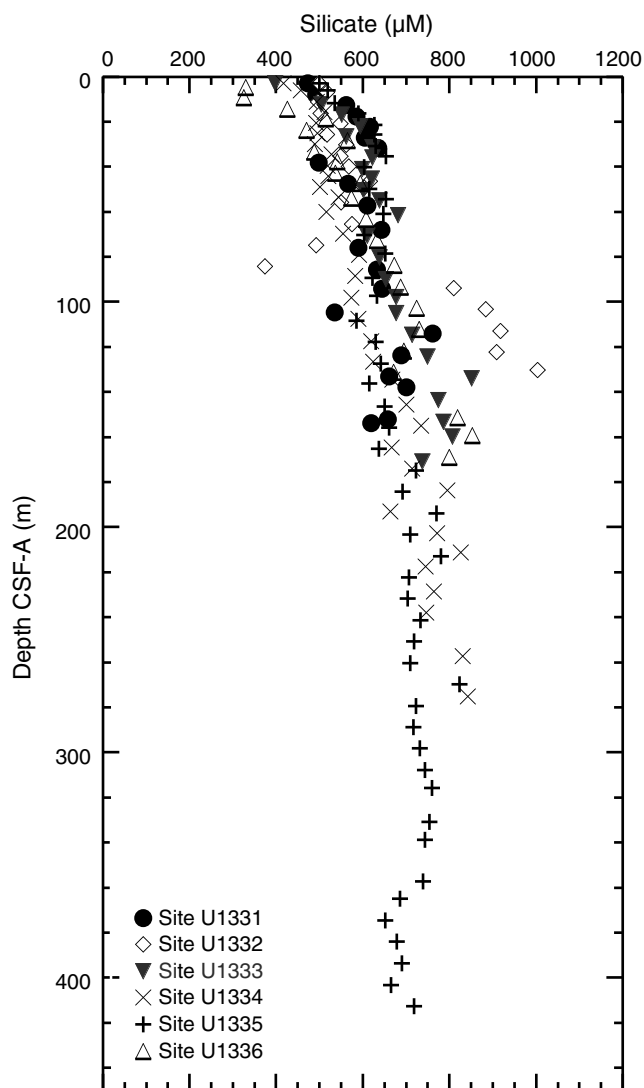
Figure F37. Depth profiles of dissolved strontium concentrations in interstitial waters, all Expedition 320 sites. CSF-A = core depth below seafloor, method A.
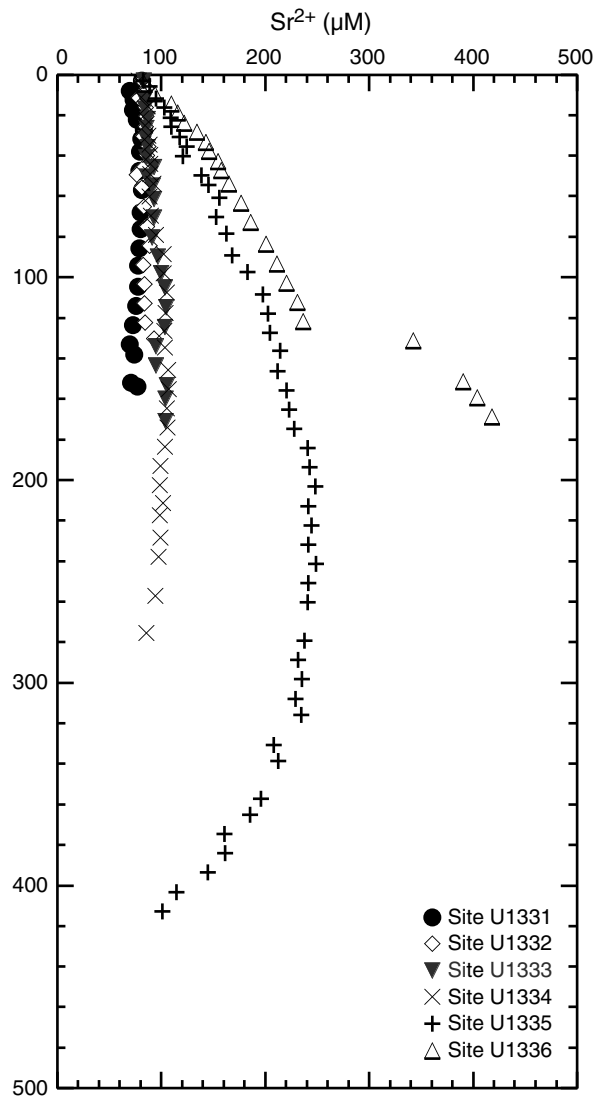
Figure F38. Depth profiles of dissolved lithium in interstitial waters, all Expedition 320 sites. CSF-A = core depth below seafloor, method A.
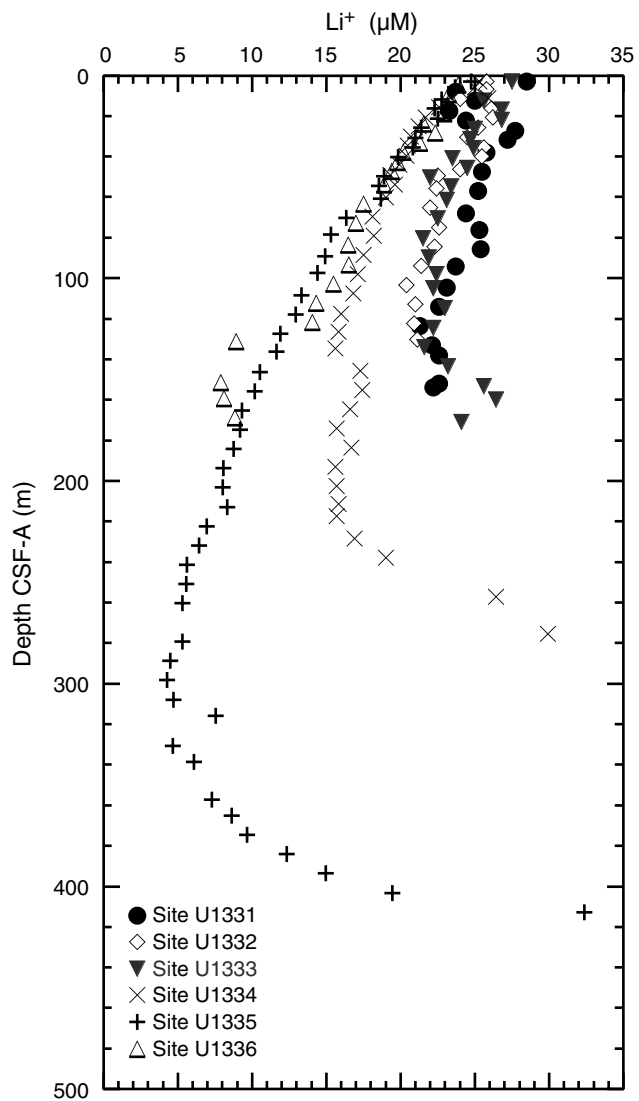
Figure F39. Synthetic seismogram for Site U1331, using core- and downhole log–derived bulk density estimates.
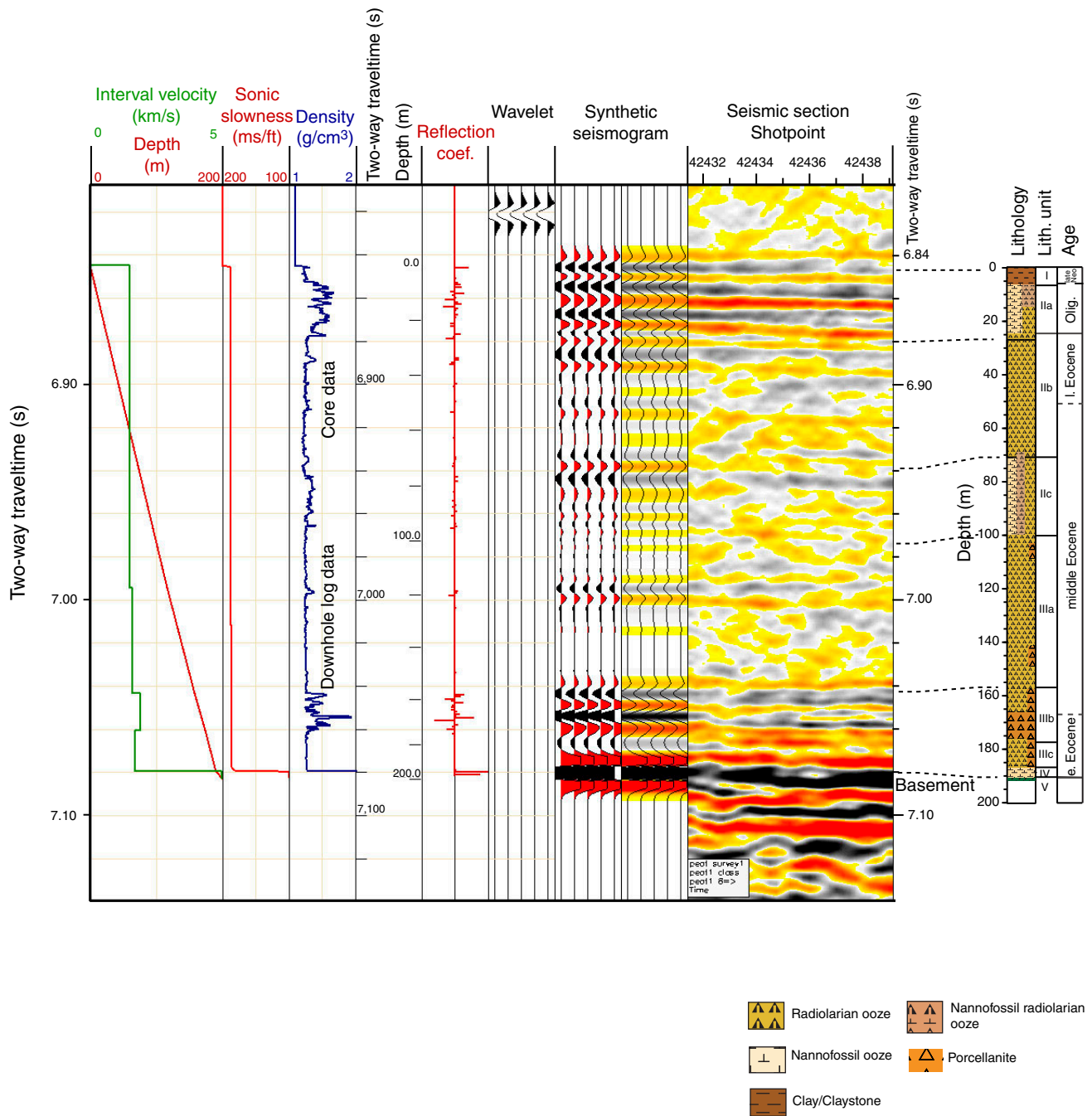
Figure F40. Occurrences of chert and porcellanite at Sites U1331–U1333 and U1336, together with previous ODP Leg 199 sites (1218–1222) (Shipboard Scientific Party, 2004).
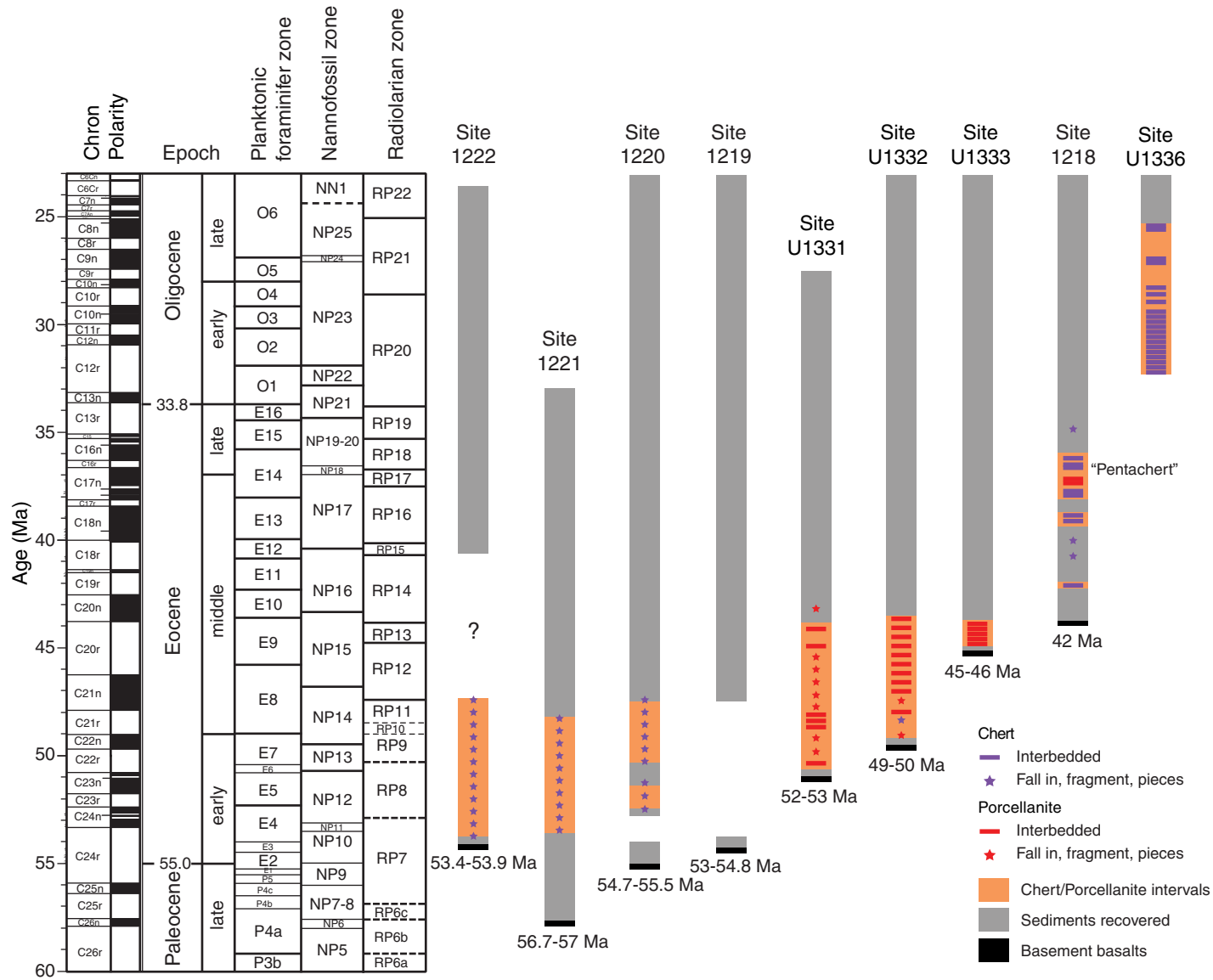
Figure F41. Compilation of geothermal heat flow measurements obtained during Expedition 320 and previous measurements.
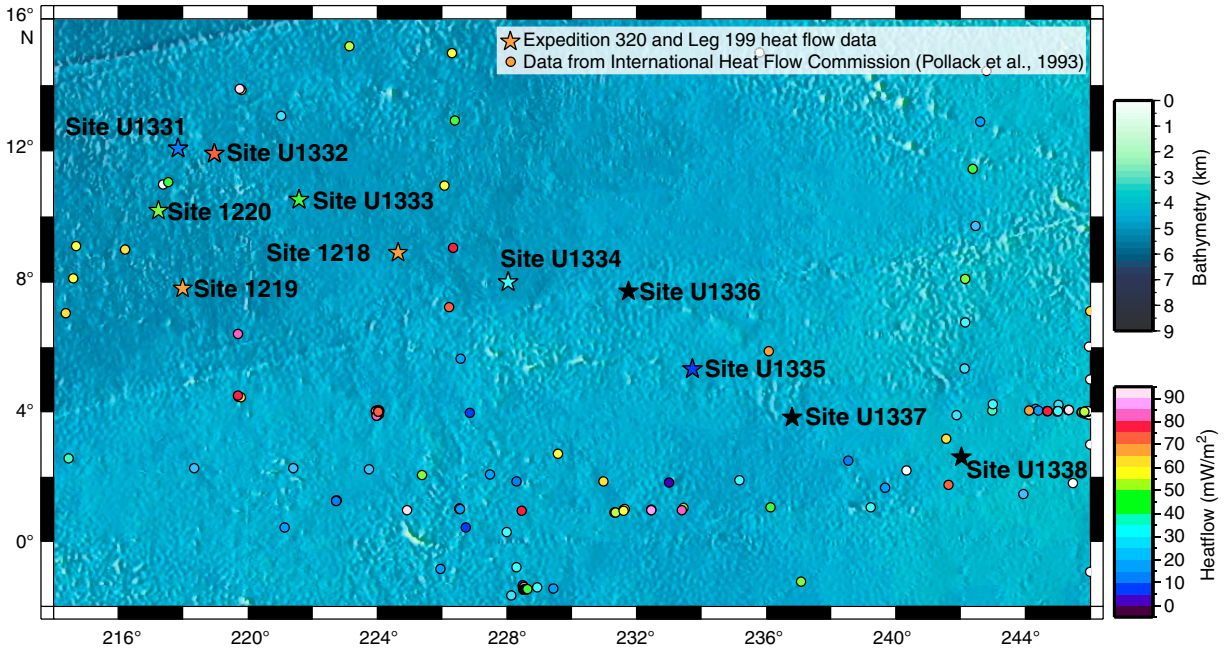
Figure F42. Lithologic summary of Sites U1331 and U1335 indicating the frequency and thickness of gravity flows (turbidites). At Site U1335, planktonic foraminifer Zone O6 is informally divided into an upper and lower part using the base of *Paragloborotalia pseudokugleri.* CSF-A = core depth below seafloor, method A.
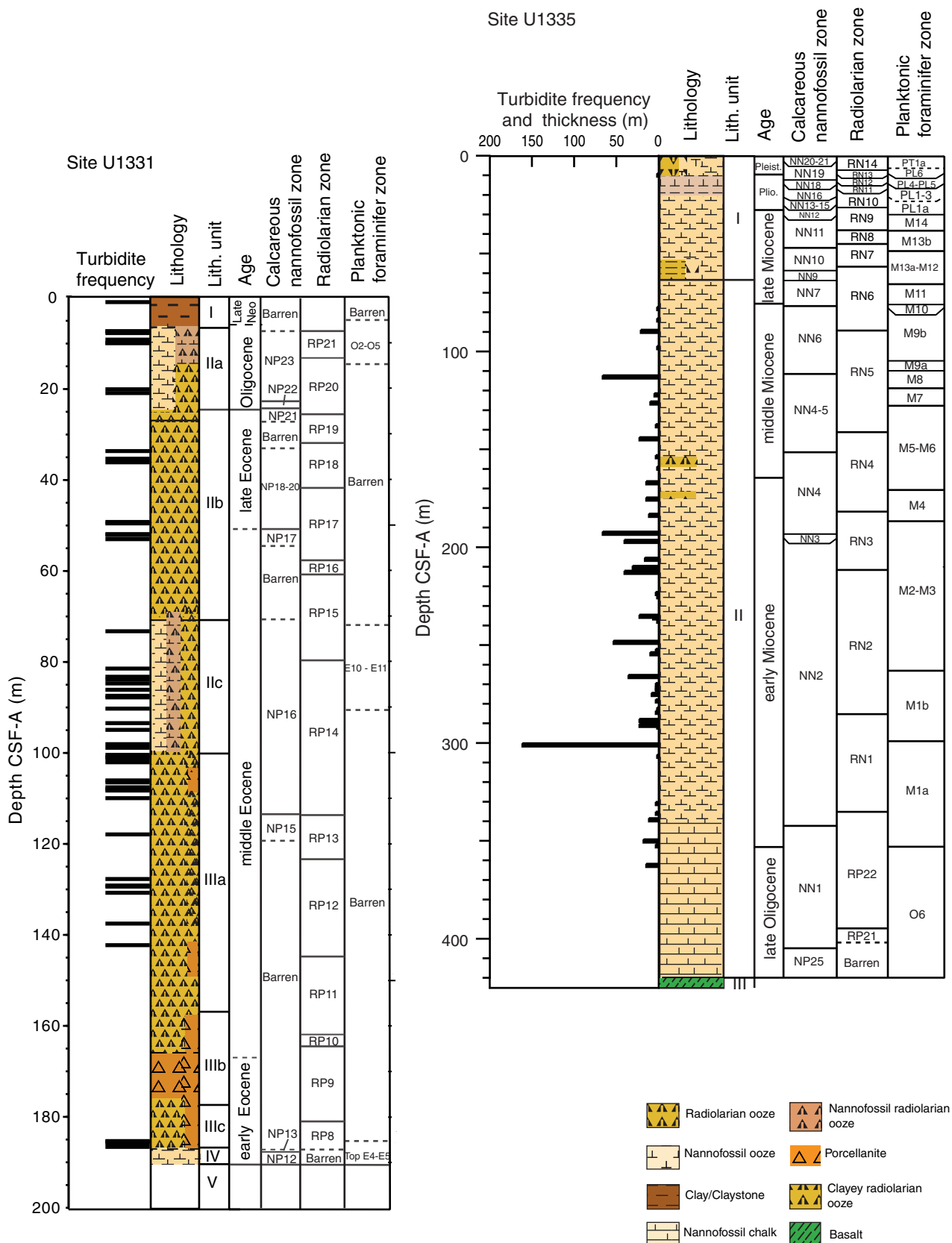
Figure F43. A. ETOPO1 (Amante and Eakins, 2008) bathymetric overview map of Site U1331 and PEAT drilling locations, with previous ODP and DSDP sites. **B.** Swath map bathymetry for Site U1331 region from the AMAT-03 site survey. Black labels = seismic shotpoints, white labels = bathymetric contours. Orange line = seismic Line PEAT1C-sl-8.
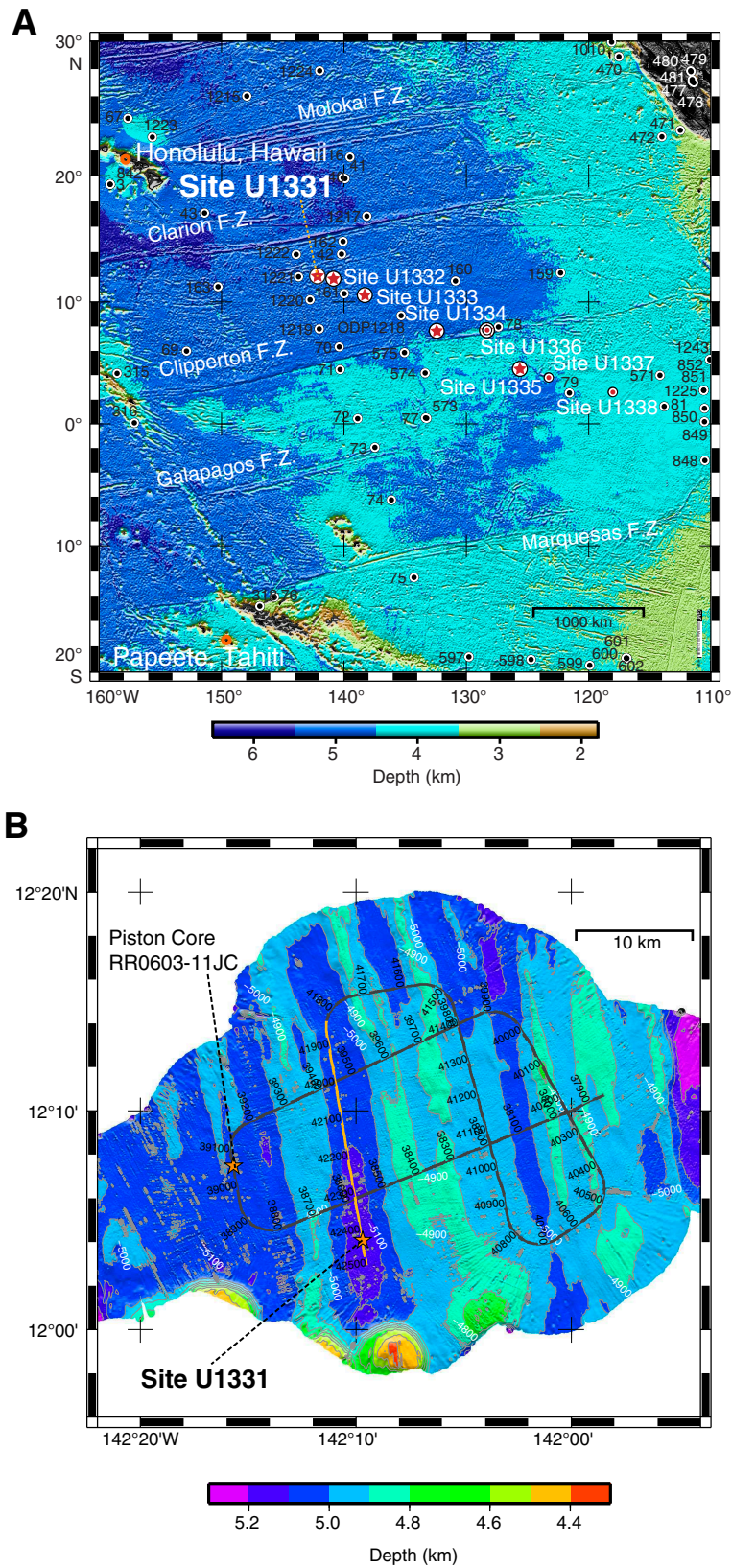
Figure F44. Site U1331 summary. CSF-A = core depth below seafloor, method A.
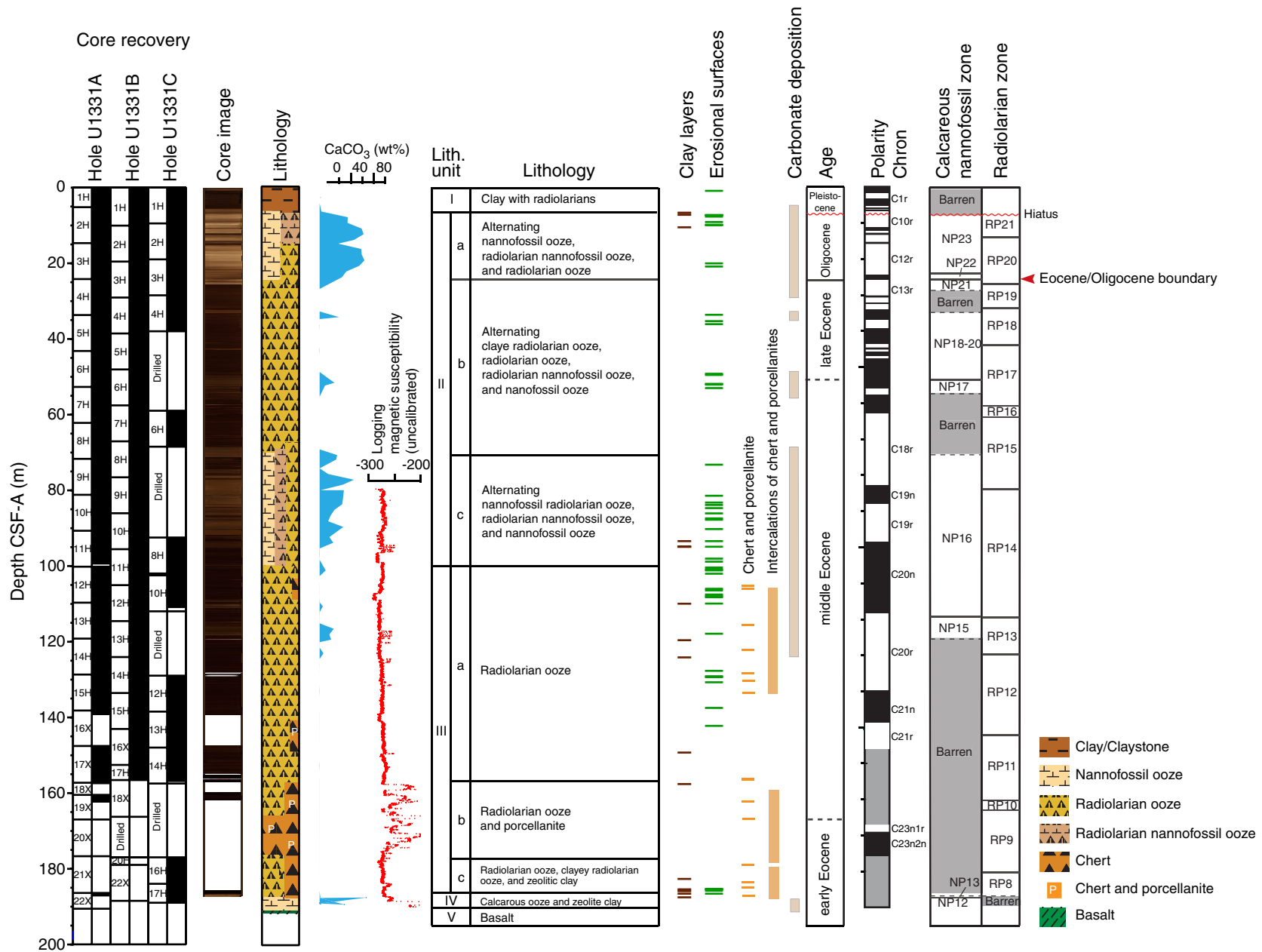
Figure F45. Site U1331 lithologic summary. L* = lightness reflectance value of sediment as defined in the LAB color model. CSF-A = core depth below seafloor, method A.
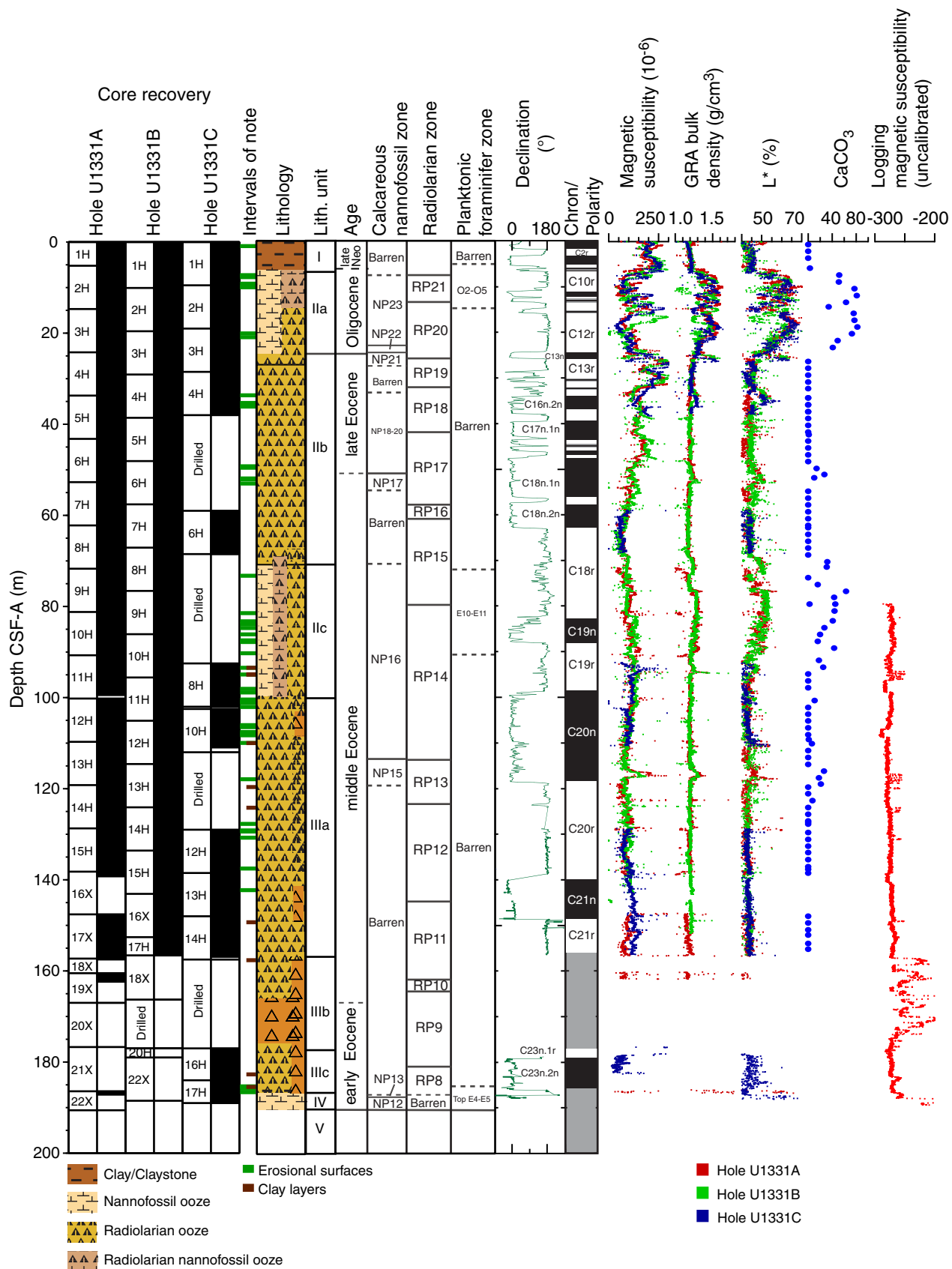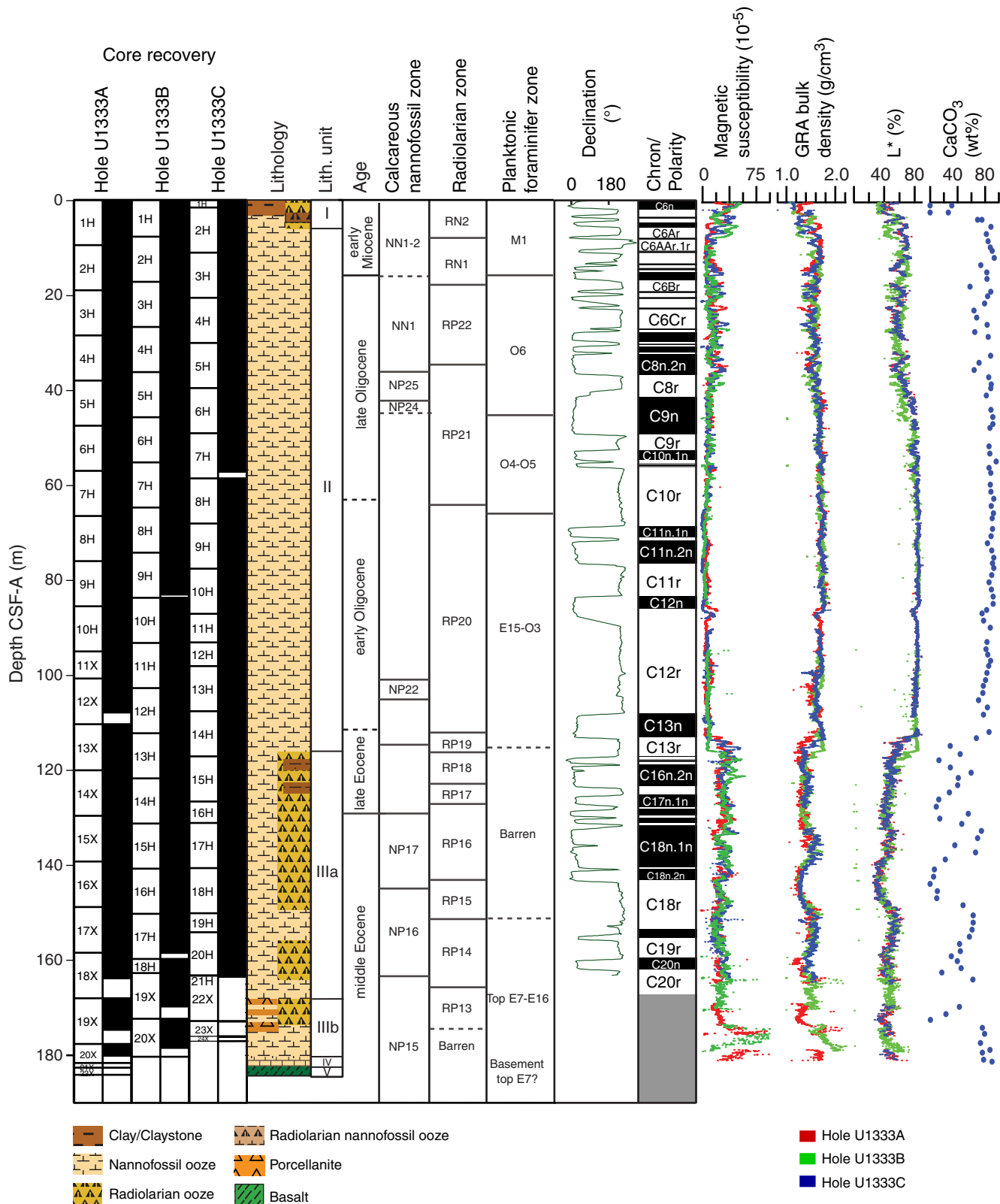
Figure F46. A. ETOPO1 (Amante and Eakins, 2008) bathymetric overview map of Site U1332 and PEAT drilling locations, with previous ODP and DSDP sites. **B.** Swath map bathymetry for Site U1332 region from the AMAT-03 site survey. Black labels = seismic shotpoints, white labels = bathymetric contours. Yellow line = north–south trending survey line for Site U1332.
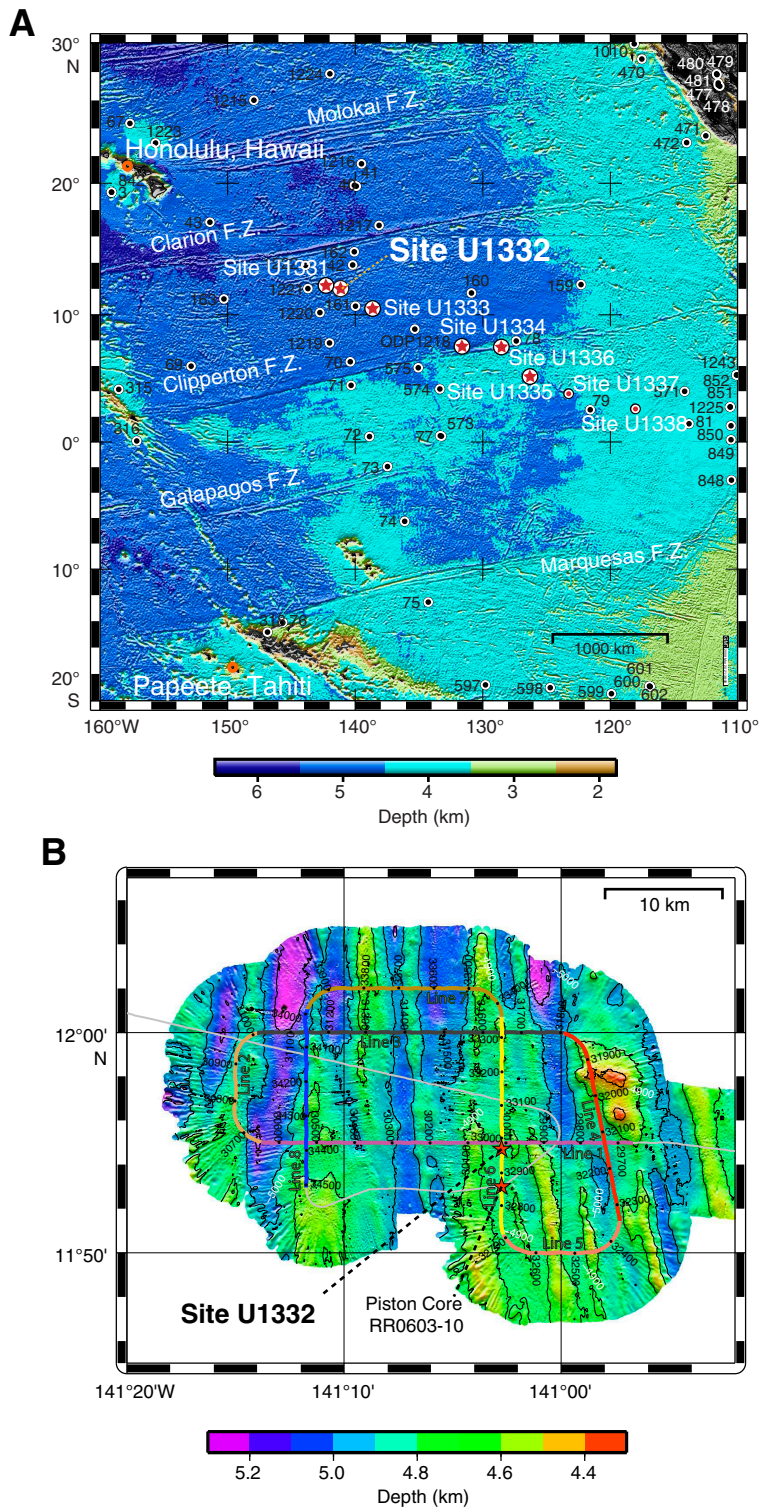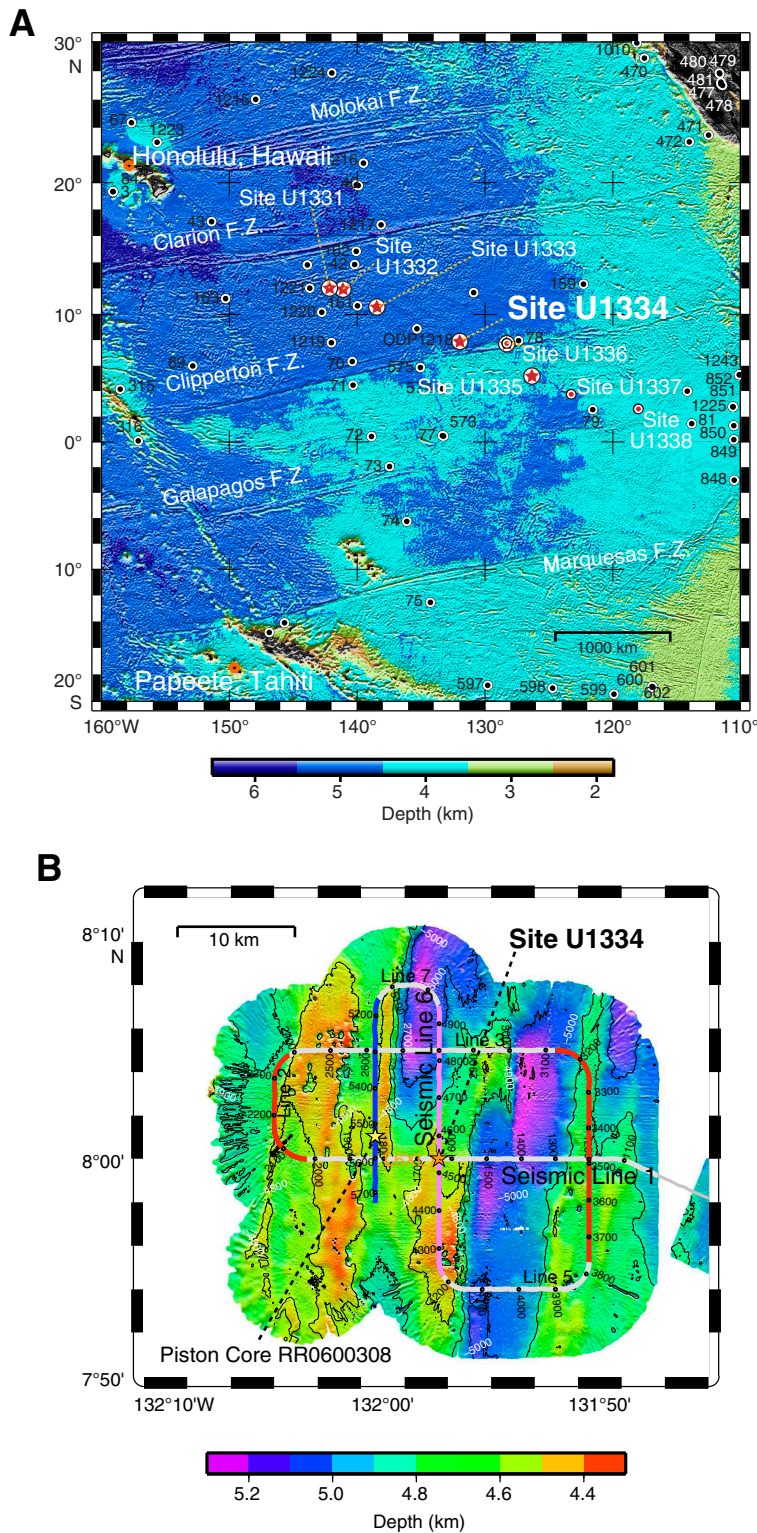
Figure F47. Site U1332 lithologic summary. At Site U1332, planktonic foraminifer Zone O3 is informally divided into an upper and lower part using the top of *Subbotina angiporoides*. A +5 m adjustment is added to the downhole logging magnetic susceptibility depths to convert from wireline log matched depth below seafloor (WMSF) to core depth below seafloor, method A (CSF-A). L* = lightness reflectance value of sediment as defined in the LAB color model. Magnetic susceptibility: green wavy line = slump, red wavy line = hiatus.
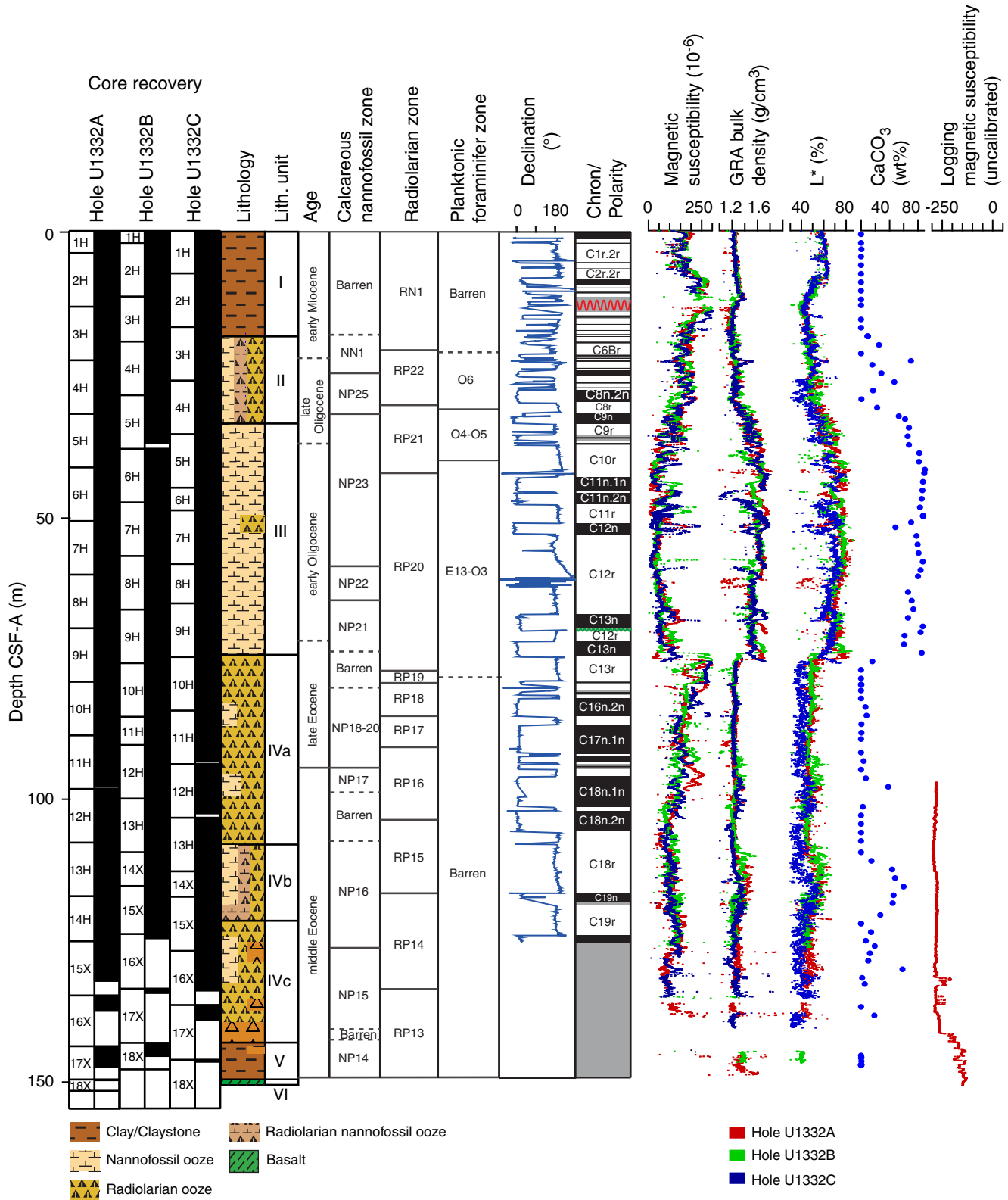
Figure F48. Site U1332 summary. CSF-A = core depth below seafloor, method A.
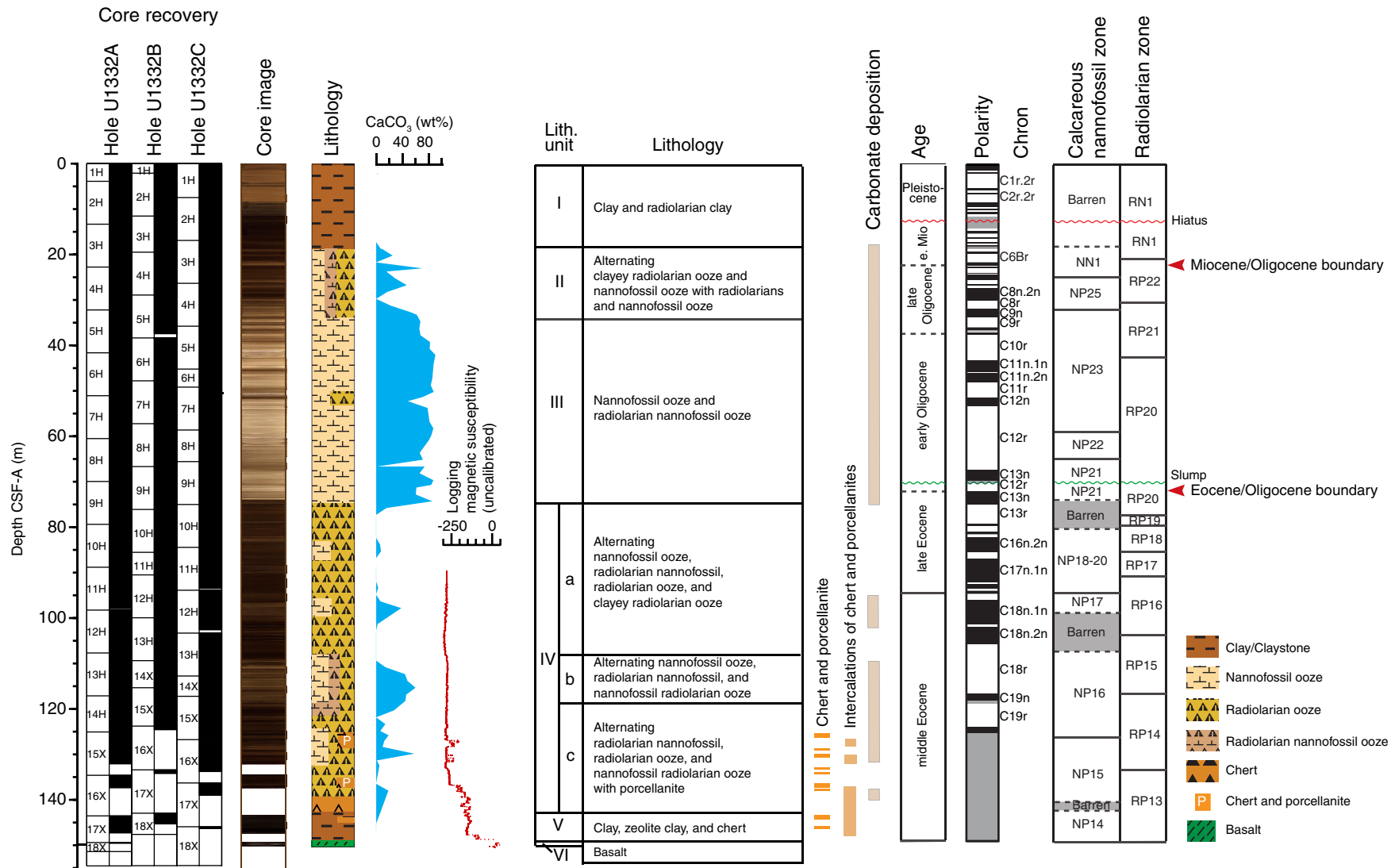
Figure F49. A. ETOPO1 (Amante and Eakins, 2008) bathymetric overview map of Site U1333 and PEAT drilling locations, with previous ODP and DSDP sites. **B.** Swath map bathymetry for Site U1333 region from the AMAT-03 site survey. Black labels = seismic shotpoints, white labels = bathymetric contours. White line = part of the seismic reflection profile across Site U1333.
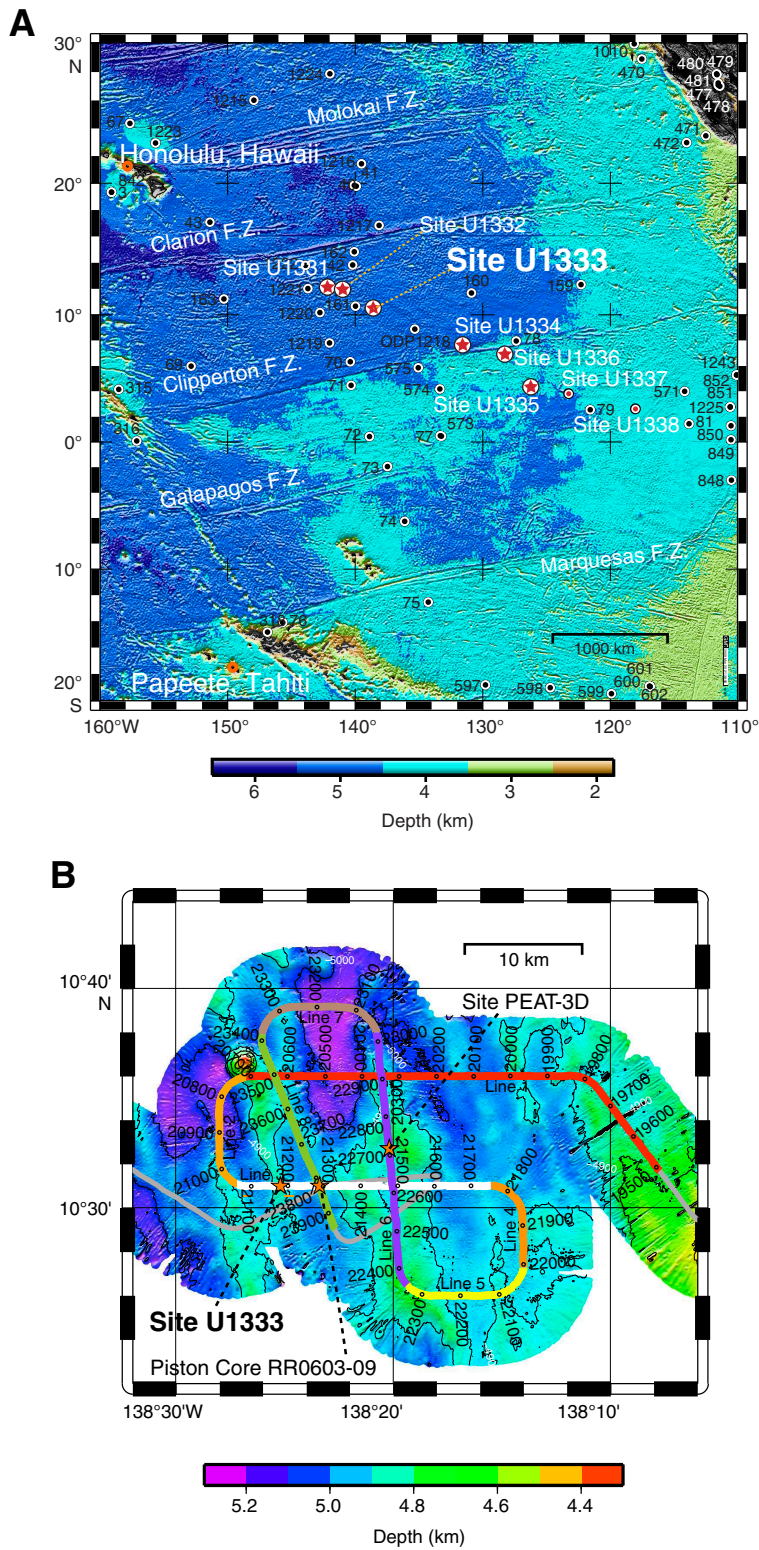
Figure F50. Site U1333 summary. At Site U1333, planktonic foraminifer Zones O3 and O6 are informally divided into an upper and lower part using the top of *Subbotina angiporoides* and base of *Paragloborotalia pseudokugleri,* respectively. CSF-A = core depth below seafloor, method A.
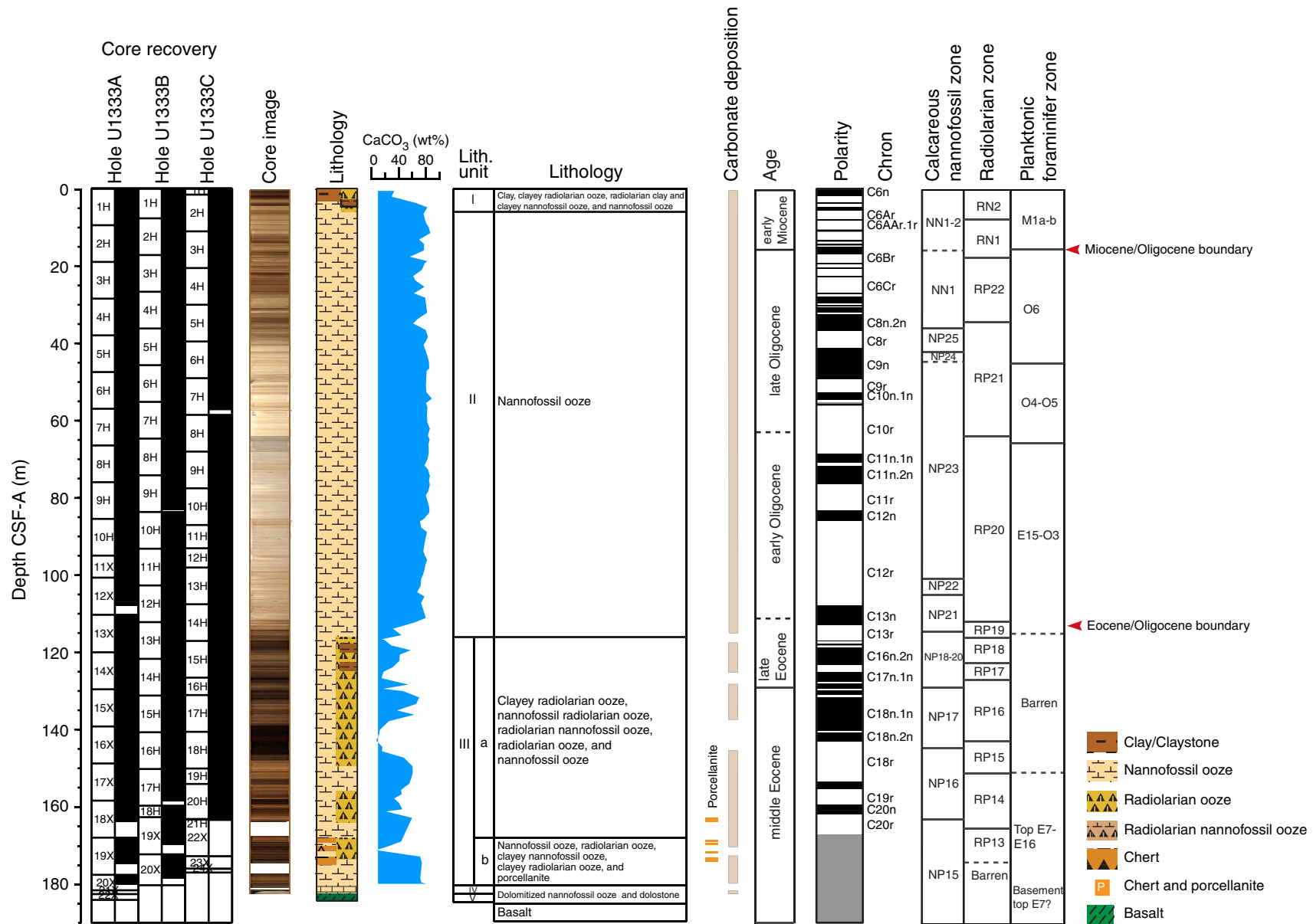
Figure F51. Site U1333 lithologic summary. At Site U1333, planktonic foraminifer Zones O3 and O6 are informally divided into an upper and lower part using the top of *Subbotina angiporoides* and base of *Paragloborotalia pseudokugleri,* respectively. L* = lightness reflectance value of sediment as defined in the LAB color model. CSF-A = core depth below seafloor, method A.
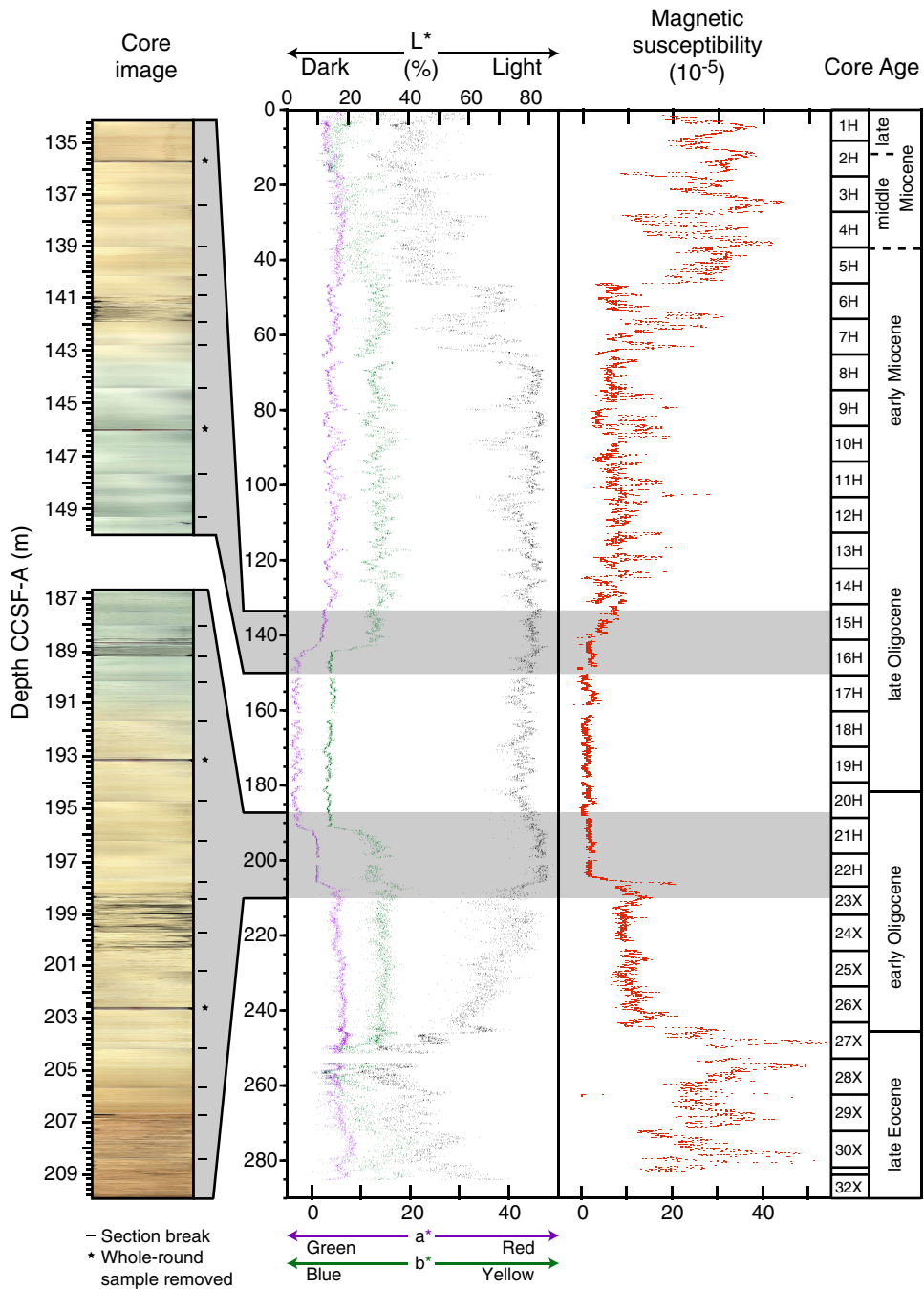
Figure F52. A. ETOPO1 (Amante and Eakins, 2008) bathymetric overview map of Site U1334 and PEAT drilling locations, with previous ODP and DSDP sites. **B.** Swath map bathymetry for Site U1334 region from the AMAT-03 site survey. Black labels = seismic shotpoints, white labels = bathymetric contours. White line = survey Line 1, purple line = survey Line 6.
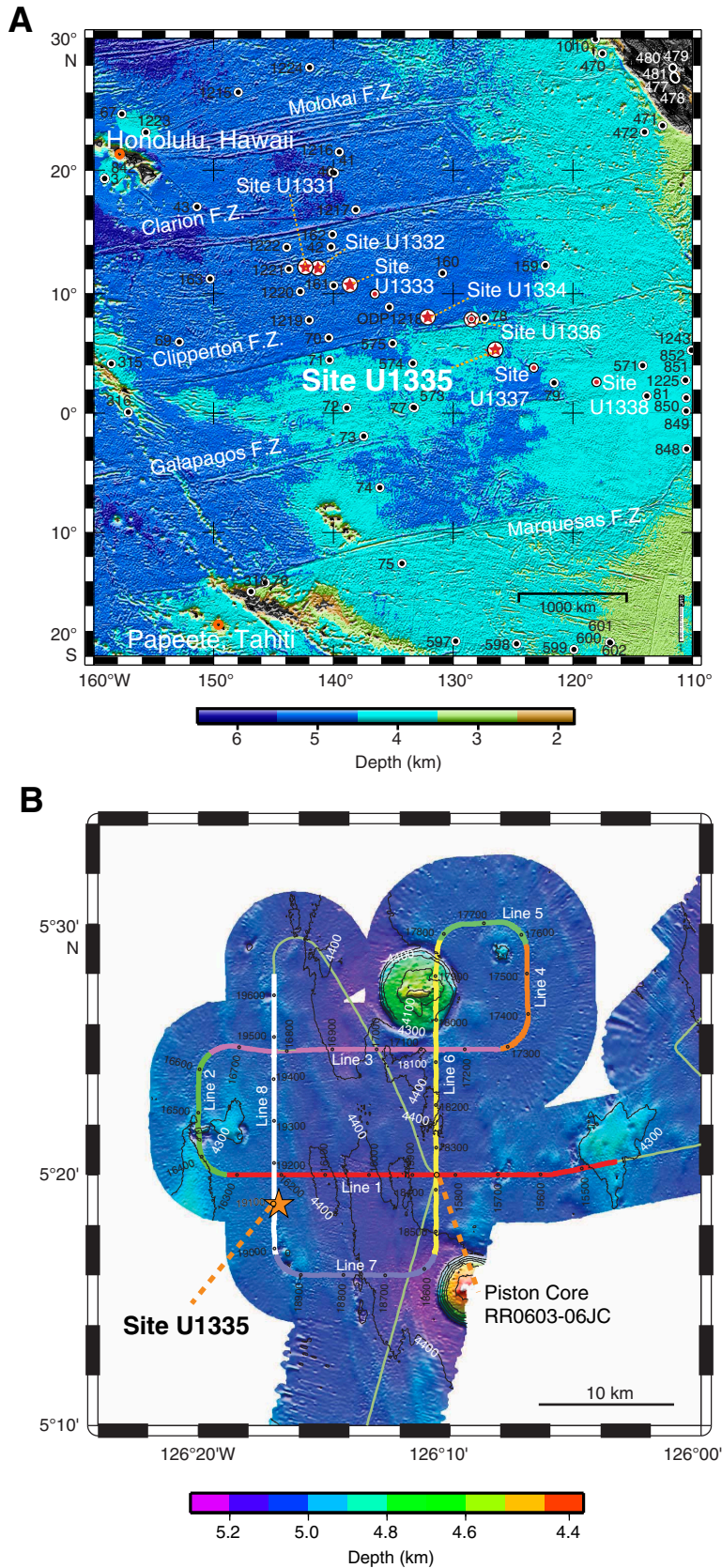
Figure F53. Site U1334 summary. At Site U1334, planktonic foraminifer Zones O2, O3, and O6 are informally divided into an upper and lower part using the base of *Paragloborotalia opima* and top of *Subbotina angiporoides* and the base of *Paragloborotalia pseudokugleri,* respectively. CSF-A = core depth below seafloor, method A.
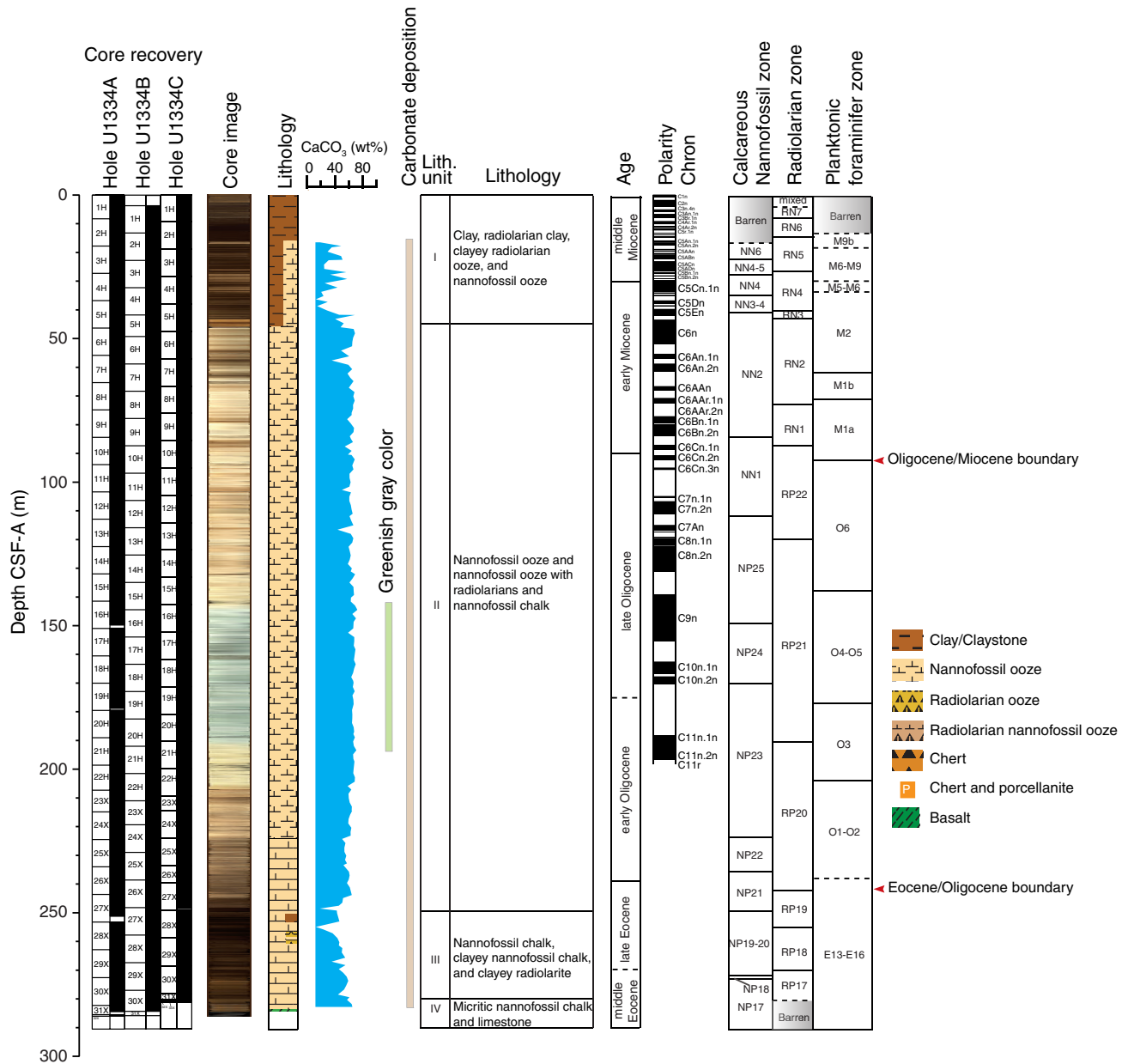
Figure F54. Site U1334 lithologic summary. L*, b* = lightness reflectance value of sediment as defined in the LAB color model. CSF-A = core depth below seafloor, method A.
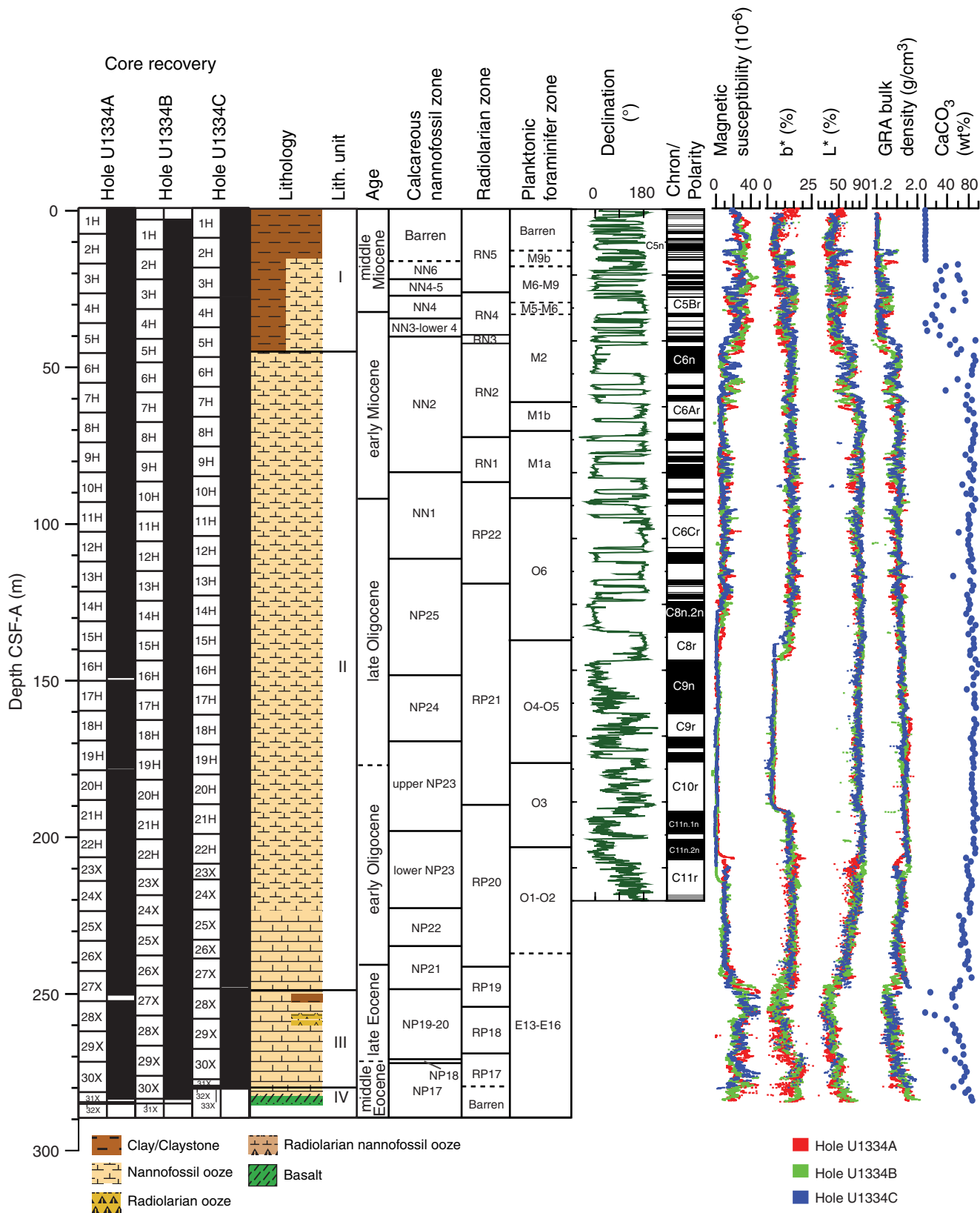
Figure F55. Calcium carbonate (CaCO₃), total carbon (TC), inorganic carbon (IC), and total organic carbon (TOC) determined by normal and acidification methods in sediments from Hole 1334A. CSF-A = core depth below seafloor, method A.
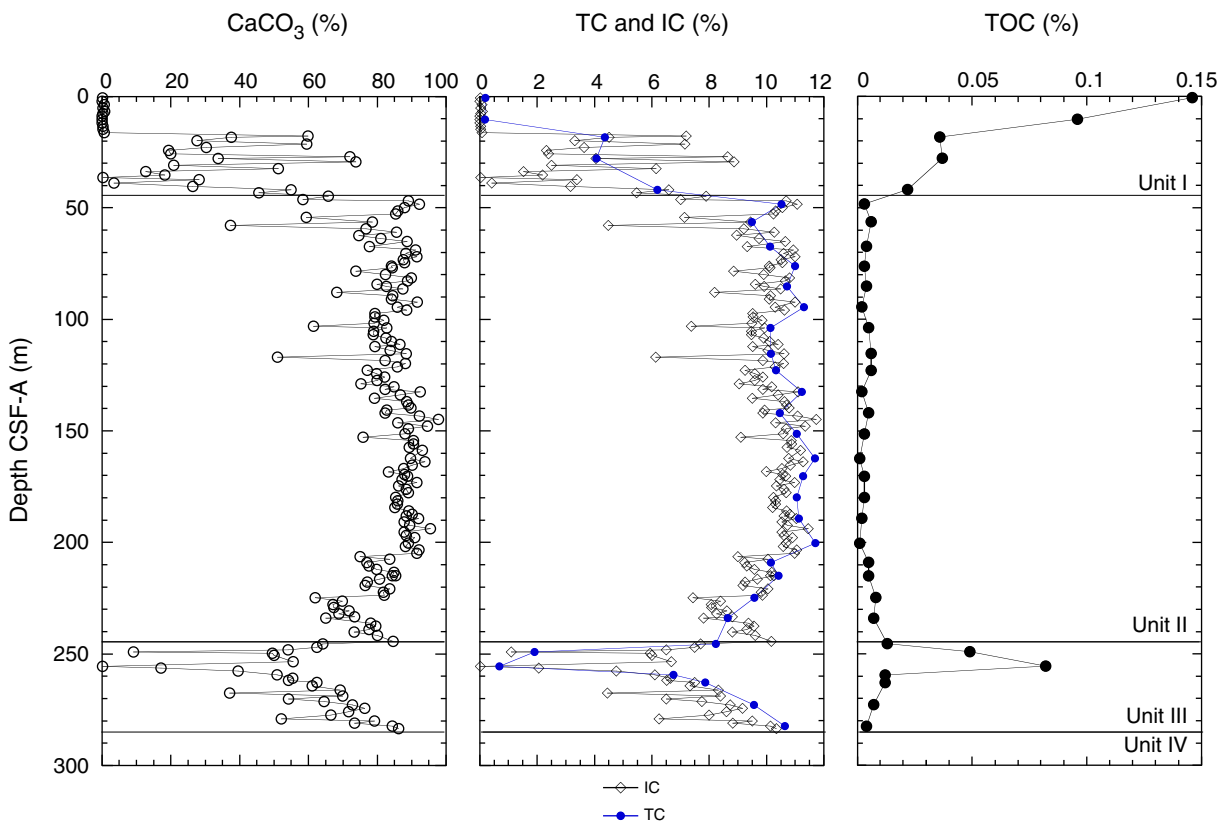
Figure F56. Color reflectance and magnetic susceptibility, Hole U1334A. Line scan images from Cores 320-U1334A-15H through 16H and 21H through 23X highlight observed color changes. L*, a*, b* = lightness reflectance value of sediment as defined in the LAB color model. CCSF-A = composite core depth below seafloor, method A.

Figure F57. A. ETOPO1 (Amante and Eakins, 2008) bathymetric overview map of Site U1335 and PEAT drilling locations, with previous ODP and DSDP sites. **B.** Swath map bathymetry for the Site U1335 region from the AMAT-03 site survey. Black labels = seismic shotpoints, white labels = bathymetric contours. White line = survey Line 8.

Figure F58. Site U1335 summary. At Site U1335, planktonic foraminifer Zone O6 is informally divided into an upper and lower part using the base of *Paragloborotalia pseudokugleri*. CSF-A = core depth below seafloor, method A.
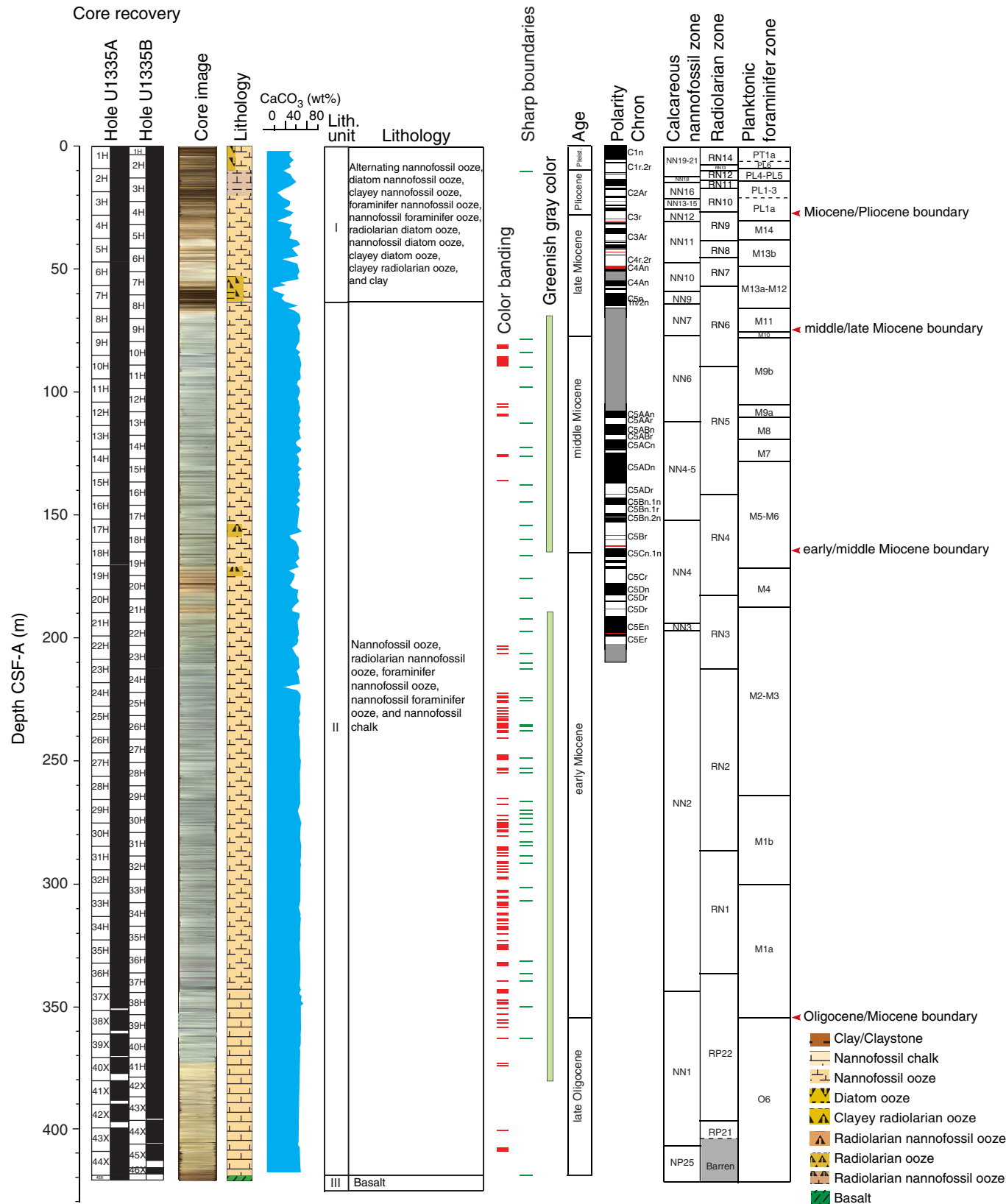
Figure F59. Site U1335 lithologic summary. Magnetic stratigraphy data based on Hole U1335B. At Site U1335, planktonic foraminifer Zone O6 is informally divided into an upper and lower part using the base of *Paragloborotalia pseudokugleri.* Geomagnetic polarity: red interval = possible geomagnetic excursions (cryptochron), gray interval = undetermined interval. L*, b* = lightness reflectance value of sediment as defined in the LAB color model. CSF-A = core depth below seafloor, method A.
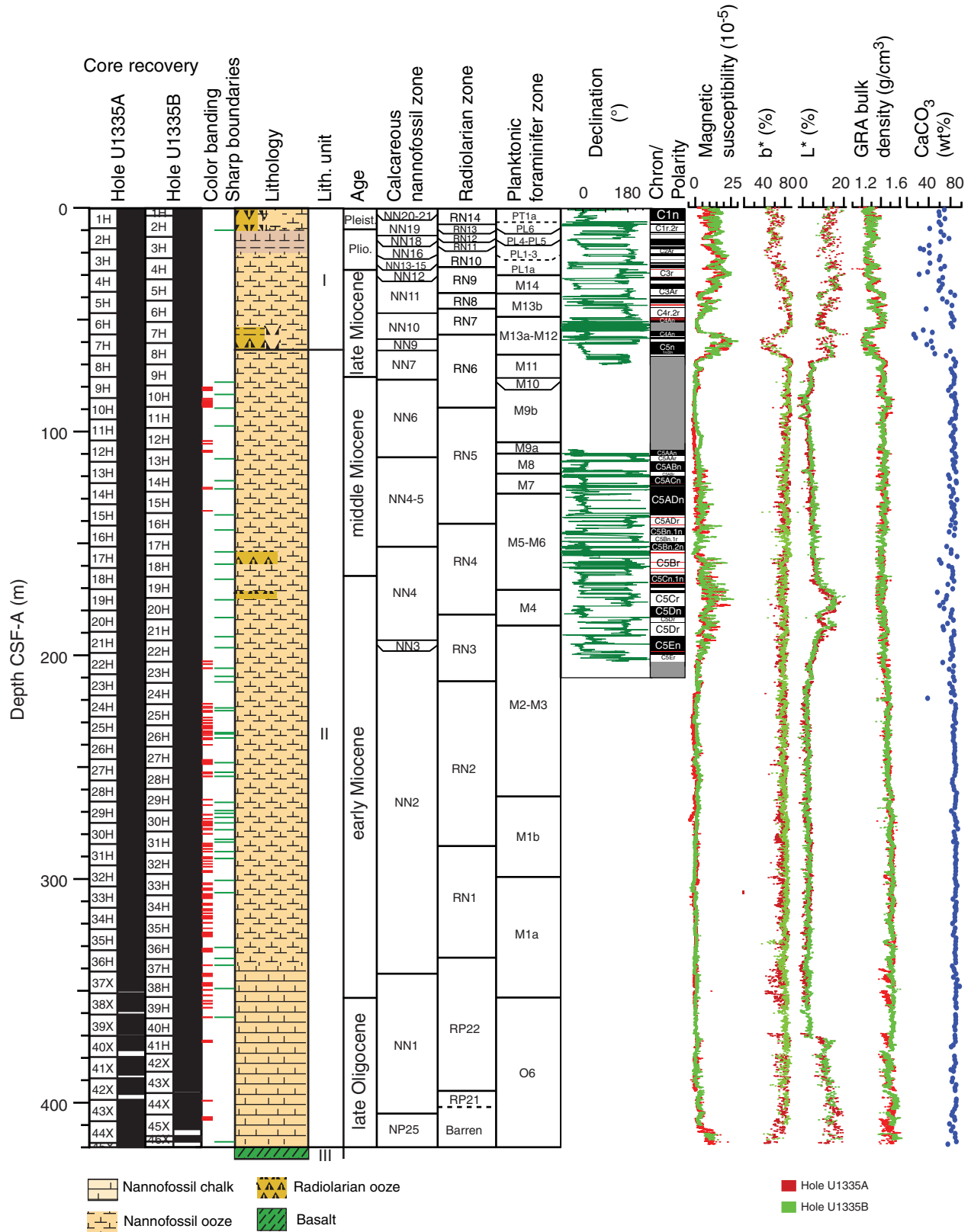
Figure F60. Calcium carbonate (CaCO₃), total carbon (TC), inorganic carbon (IC), and total organic carbon (TOC) determined by normal and acidification methods in sediments from Hole 1335A. CSF-A = core depth below seafloor, method A.
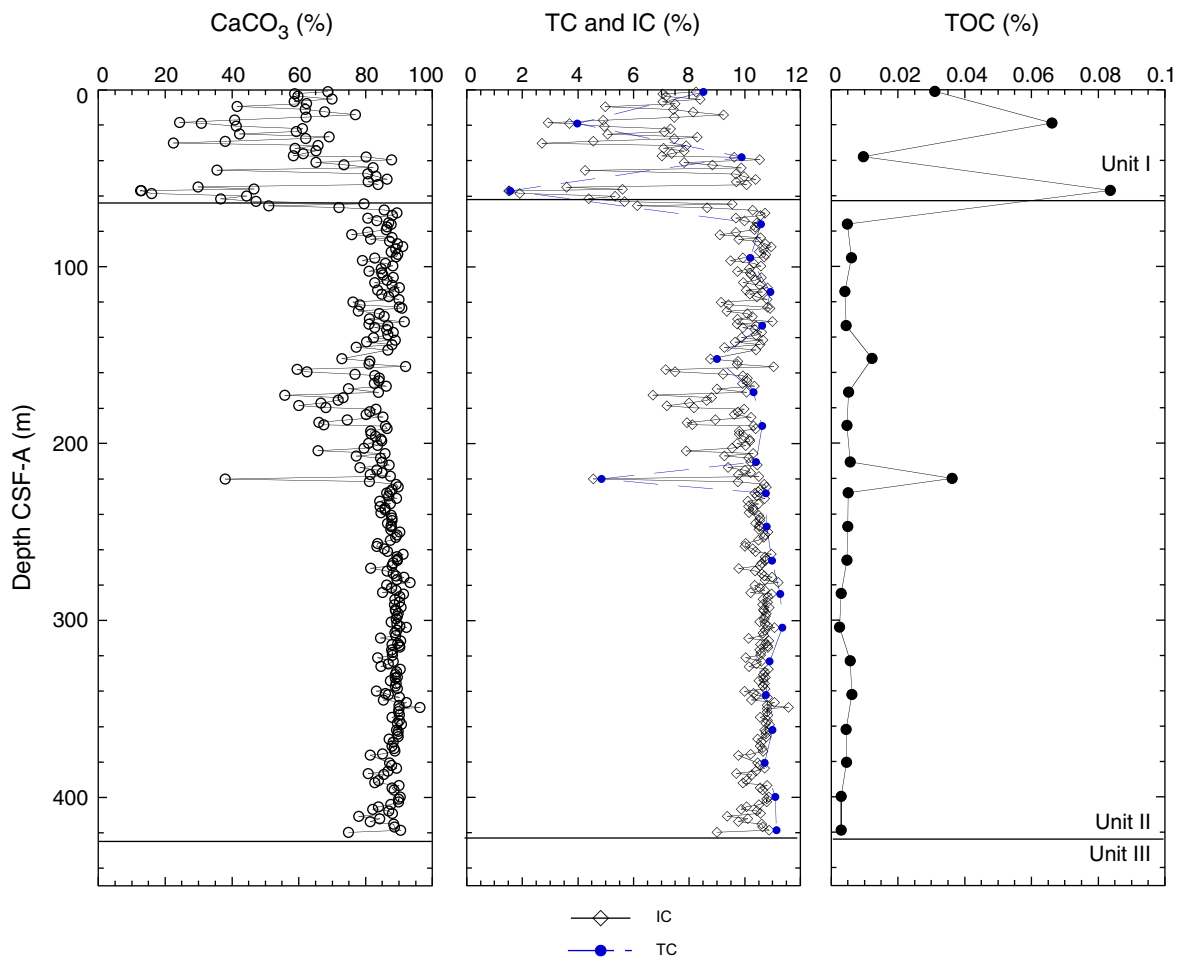
Figure F61. Color reflectance and magnetic susceptibility vs. depth, Hole U1335A. Line scan images from Cores 320-U1335A-7H through 8H, 18H through 22H, and 39X through 45X highlight observed color changes. L*, a*, b* = lightness reflectance value of sediment as defined in the LAB color model. CCSF-A = composite core depth below seafloor, method A.
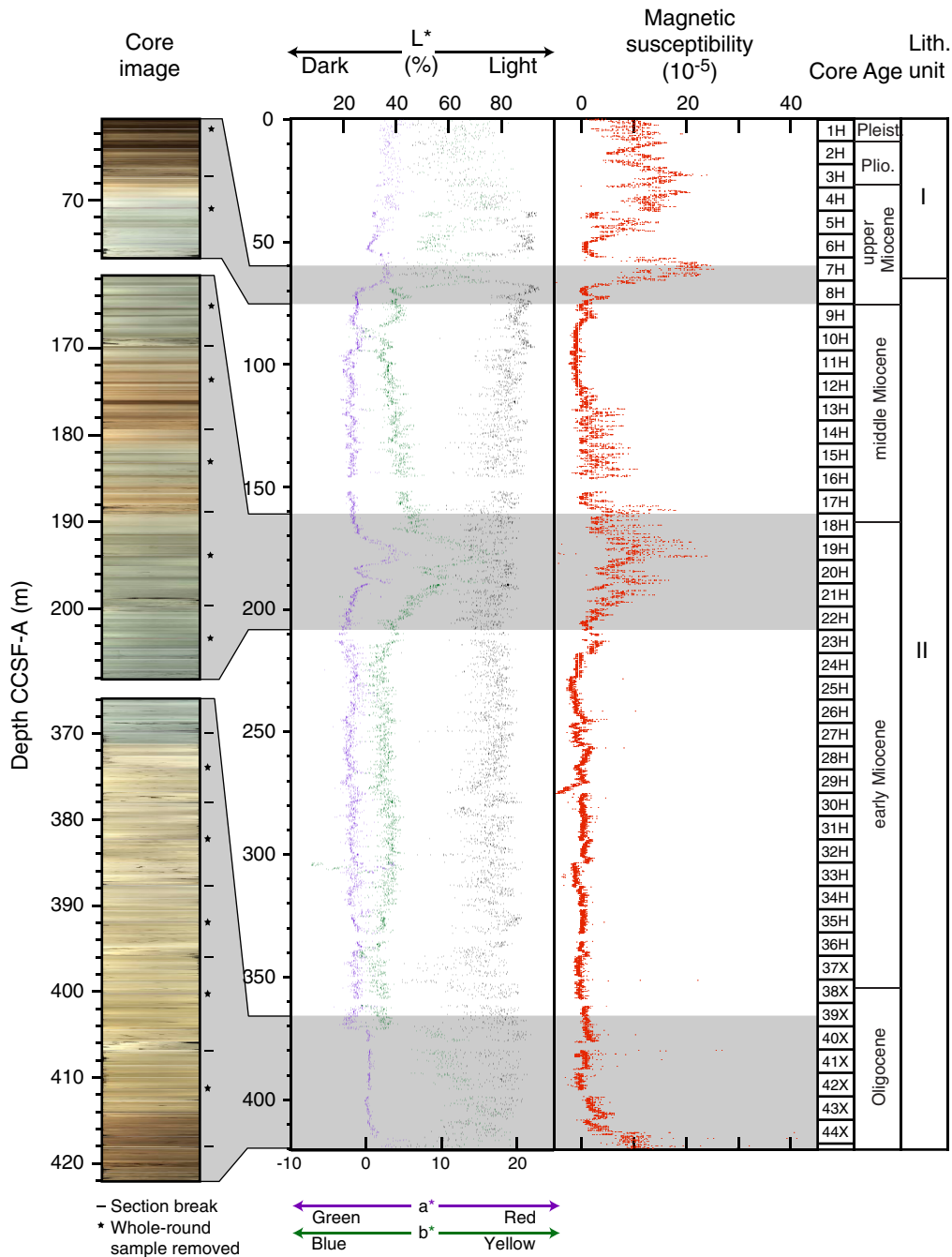
Figure F62. Summary of susceptibility and paleomagnetic results, Hole U1335B. Declinations are shown in sample coordinates (not reoriented to geographical coordinates). CSF-A = core depth below seafloor, method A.
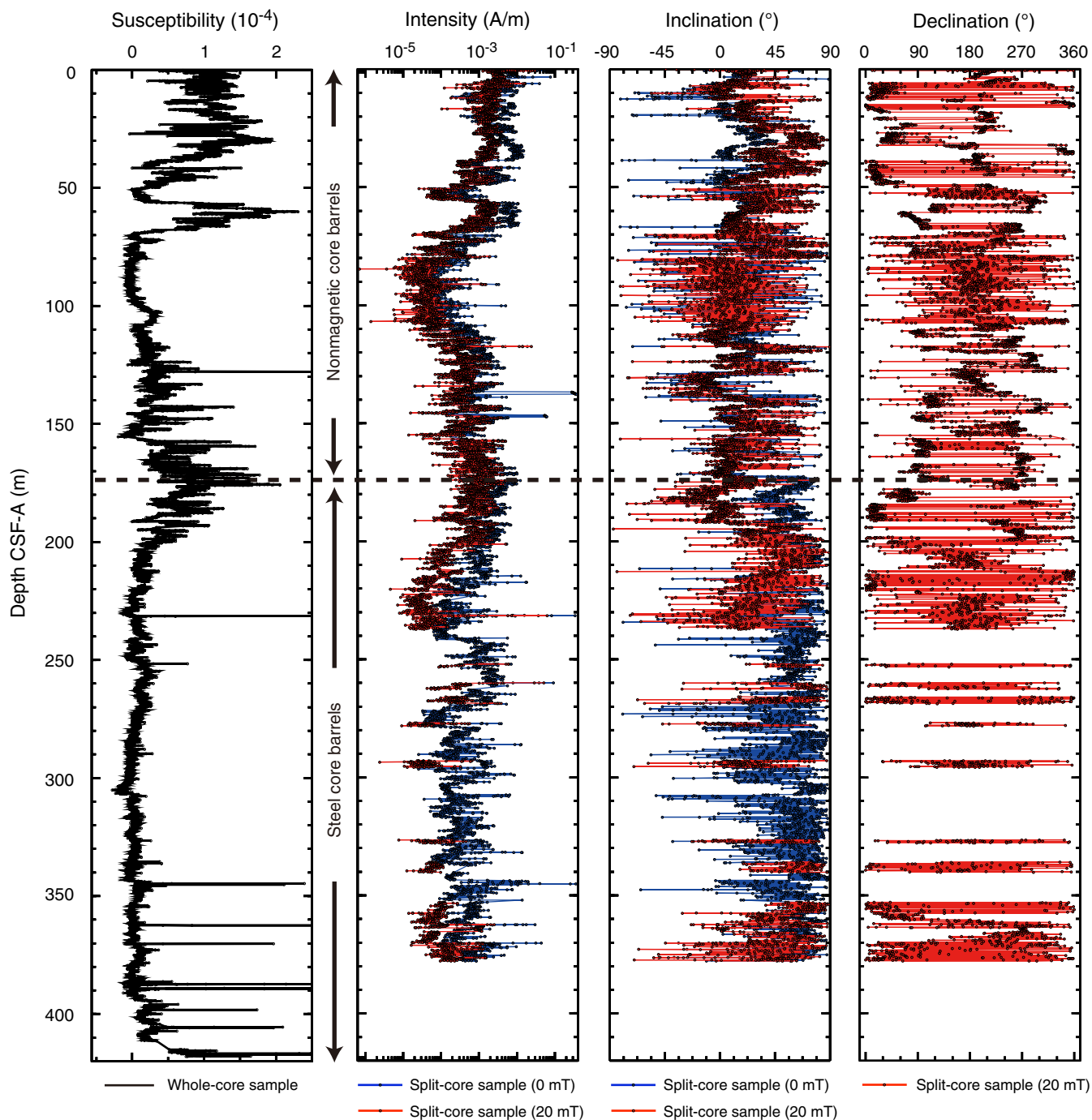
Figure F63. A. ETOPO1 (Amante and Eakins, 2008) bathymetric overview map of Site U1336 and PEAT drilling locations, with previous ODP and DSDP sites. **B.** Swath map bathymetry for Site U1336 region from the AMAT-03 site survey. Black labels = seismic shotpoints, white labels = bathymetric contours. White line = survey Line 6.
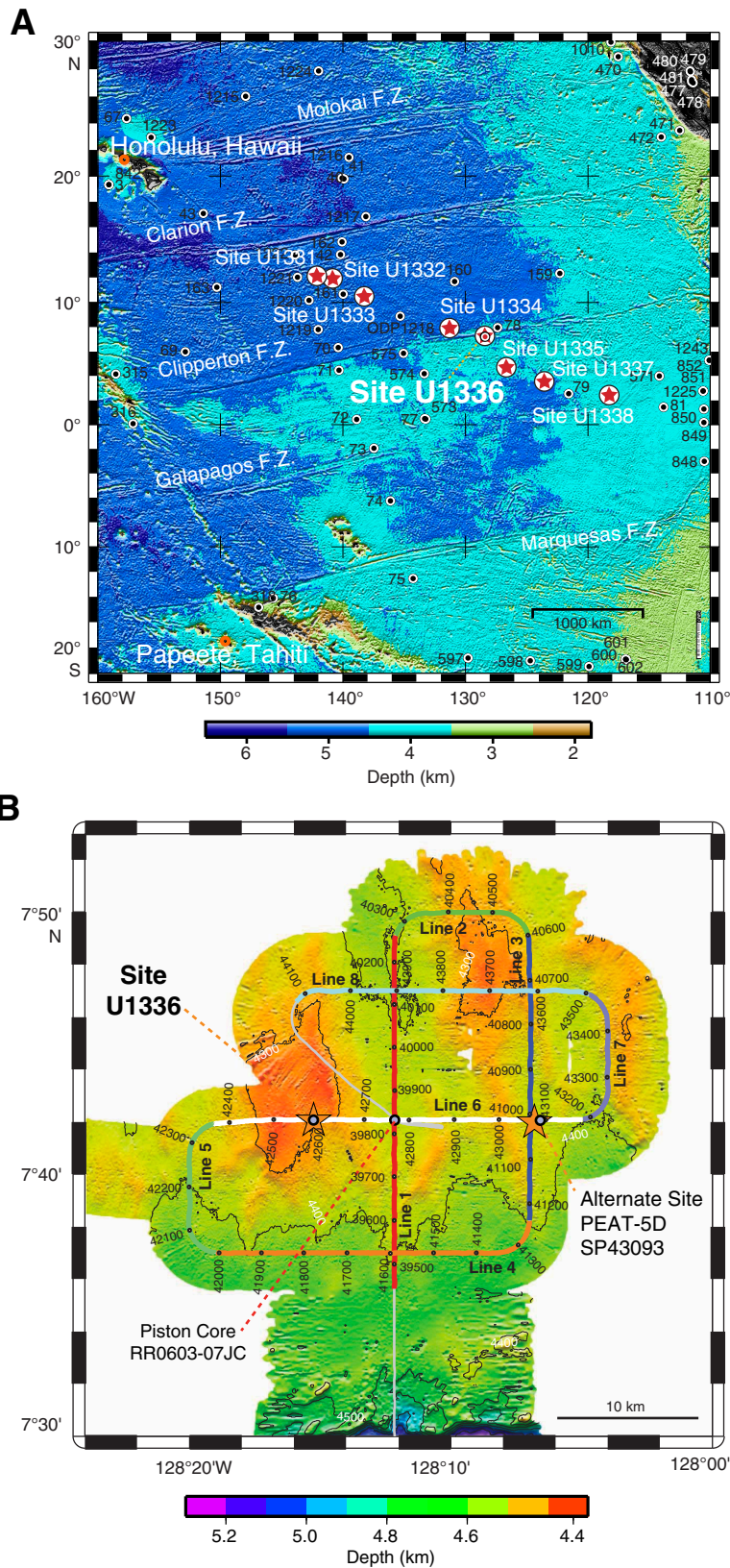
Figure F64. Site U1336 summary. At Site U1336, planktonic foraminifer Zones O6 and M2 are informally divided into an upper and lower part using the base of *Paragloborotalia pseudokugleri* and *Globoquadrina binaiensis,* respectively. CSF-A = core depth below seafloor, method A.
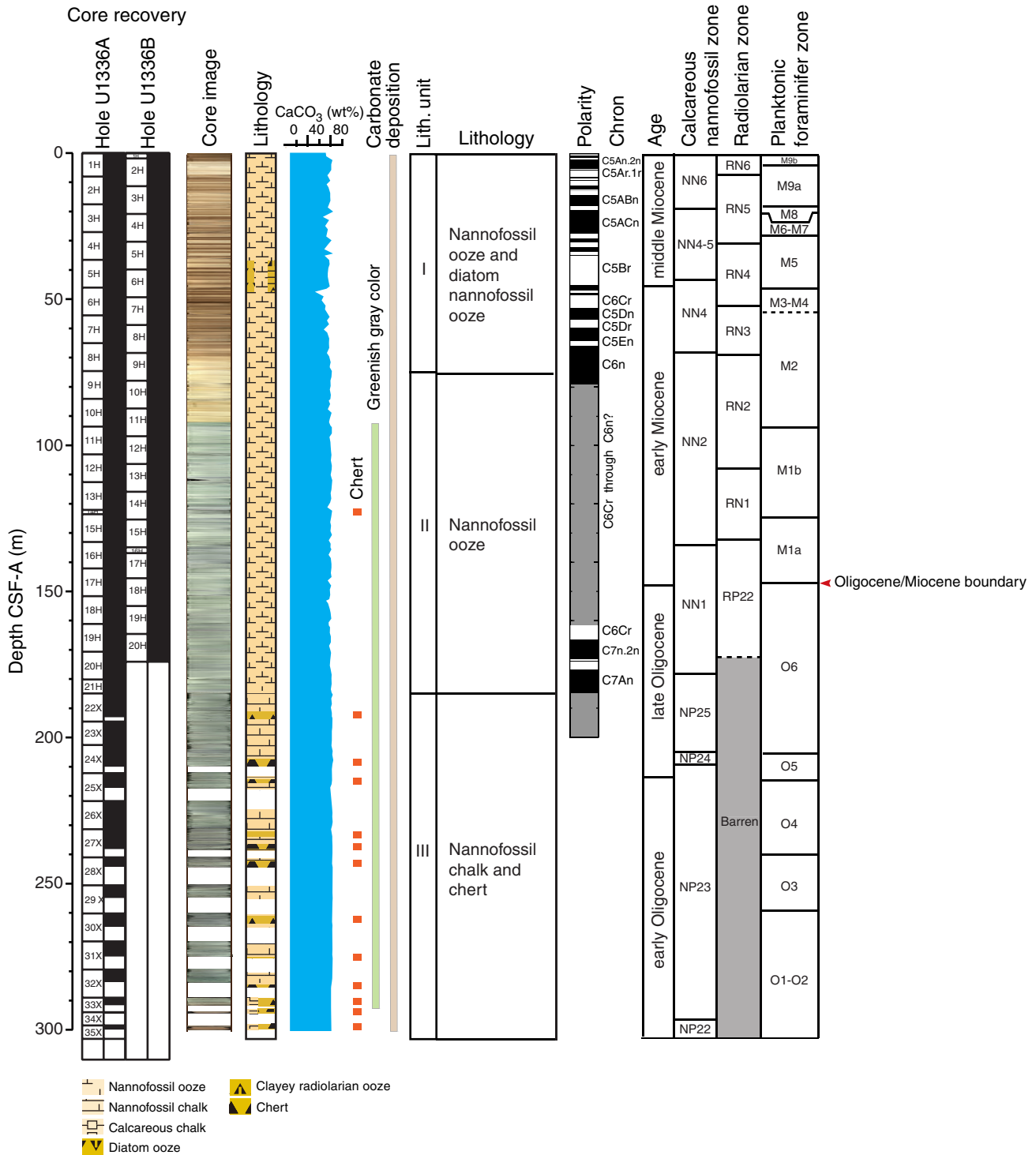
Figure F65. Site U1336 lithologic summary. At Site U1336, planktonic foraminifer Zones O6 and M2 are informally divided into an upper and lower part using the base of *Paragloborotalia pseudokugleri* and *Globoquadrina binaiensis,* respectively. L*, b* = lightness reflectance value of sediment as defined in the LAB color model. CSF-A = core depth below seafloor, method A.